University of Nottingham

UK | CHINA | MALAYSIA

Stiffness and Viscoelasticity of Soft Tissue-Mimicking Hydrogels Regulate Human Monocyte-Derived Macrophage Polarisation

Consuelo Coser, MSci, AFHEA

Thesis submitted to the University of Nottingham for the degree of Doctor of Philosophy

September 2025

To my mom,

Without you nothing would have been possible.

Abstract

The implantation of medical devices often triggers a foreign body response (FBR), a major clinical challenge and leading cause of implant failure. Macrophages are central to this process, as they sense and respond to the mechanical and chemical properties of biomaterials, thereby influencing downstream inflammatory and fibrotic pathways. Existing studies on macrophage-biomaterial interactions are often limited by reliance on non-human or immortalised cell models, the use of stiffness ranges that exceed those of native soft tissues, and the presence of confounding variables. This thesis addresses these gaps by investigating how primary human monocyte-derived macrophages respond to biomaterials with tuneable mechanical properties, with particular emphasis on stiffness and stress relaxation. In the first part of this work, alginate methacrylate (ALMA) hydrogels were optimised to cover a soft tissue-relevant stiffness range (0.25–4.5 kPa) and engineered with EDC/NHS chemistry to introduce surface modifications. While GRGDSP modification had only modest effects on macrophage polarisation, stiffness emerged as the dominant regulator of macrophage phenotype. Increasing stiffness promoted pro-inflammatory activation, with the stiffest hydrogel (ALMA 6% w/v) inducing elevated TNF-α secretion, a higher calprotectin-to-mannose surface marker ratio and pronounced morphological changes that include elongation and spreading. These results demonstrate that even modest variations within the soft tissue–relevant stiffness range are sufficient to modulate macrophage behaviour, priming them toward a pro-inflammatory phenotype. The second part of this work examined viscoelasticity, a mechanical property that has only recently received attention as an independent regulator of cell behaviour. Through a systematic optimisation process in which multiple polyacrylamide

(PAAm) formulations were screened by varying both the total concentration of acrylamide and bisacrylamide and their relative ratios, we identified two formulations - PAAm 15% (acrylamide-to-bisacrylamide ratio 80:1) and PAAm 20% (acrylamide-to-bisacrylamide ratio 300:1) - that exhibited comparable stiffness, porosity, and surface chemistry, but distinct stress relaxation profiles. This enabled the decoupling of viscoelasticity from other factors that could influence macrophage polarisation. PAAm 15% (80:1) exhibited predominantly elastic behaviour, showing minimal stress relaxation, whereas PAAm 20% (300:1) demonstrated pronounced viscoelasticity, with a ~70% reduction in its relaxation modulus, occurring within a biologically relevant timeframe. Macrophages cultured on viscoelastic substrates showed increased spreading and higher eccentricity compared to those on the elastic hydrogel. Further characterisation revealed that the elastic substrate amplified pro-inflammatory responses, with higher calprotectin expression and enhanced secretion of TNF-α and IL-6, whereas anti-inflammatory markers remained unaffected by viscoelasticity, establishing stress relaxation as a key regulator of macrophage phenotype.

Overall, this work demonstrates that macrophage responses are finely tuned by multiple mechanical cues, with stiffness and viscoelasticity exerting distinct and independent effects. By integrating human primary macrophages with biomaterials engineered for specific mechanical properties, this study clarifies conflicting literature results and advances the understanding of immune–biomaterial interactions. Importantly, the findings highlight the need to consider mechanical properties beyond stiffness when designing immunomodulatory biomaterials, offering new strategies to mitigate FBR and improve long-term implant performance.

Publications

Publications Related to This Thesis

Coser C., Ghaemmaghami A. M., Yang J. Soft tissue-mimicking hydrogel stiffness modulates polarisation of human monocyte-derived macrophages. Biomaterials Science 2025, 10.1039/D5BM01187F. DOI: 10.1039/D5BM01187F.

Coser C., di Bari V., Ghaemmaghami A. M., Yang J. Hydrogel Viscoelasticity Regulates Human Monocyte-derived Macrophage Morphology and Phenotype in 2D Culture. (Minor Corrections in Acta Biomaterialia)

Other Publications

Loxley G.A., **Coser C.**, Ghaemmaghami A. M., Yang J. Long-term interleukin-4 release from 3D printable affinity hydrogels promotes M2-like macrophage polarisation in vitro. Biomaterials Science. 2025;13(9):2489-502.

Galbiati A., Zana A., **Coser C.**, Tamborini L., Basilico N., Parapini S., Taramelli D., Conti P. Development of Potent 3-Br-isoxazoline-Based Antimalarial and Antileishmanial Compounds. ACS medicinal chemistry letters 2021, 12 (11), 1726-1732. DOI: 10.1021/acsmedchemlett.1c00354.

Acknowledgements

I would like to begin by expressing my deepest gratitude to the CDT for Transformative Pharmaceutical Technologies for funding my PhD as an international student. The CDT has provided me with an exceptional opportunity to pursue research in a world-leading university and inspiring academic environment that has been fundamental to both my personal and professional growth.

I am profoundly grateful to my supervisors, Dr Jing Yang and Professor Amir M. Ghaemmaghami, for their guidance, mentorship, and encouragement throughout this journey. Their expertise, feedback, and unwavering support have been invaluable in shaping my scientific skills and my approach to independent research. Their guidance has enabled me to navigate challenges and grow as a scientist.

I would also like to extend my sincere thanks to my colleagues and lab mates for their collaboration, insightful discussions, and constant encouragement. In particular, I am deeply grateful to Dr Reem Al Romaihi and Dr Qiran Du for training and teaching me all the basics of cell culture and immunology, and Dr Lisa Kämmerling, whose guidance and expertise as well as her friendship was unvaluable. I would also like to thank Karen Lawler, whose contribution to lab organisation and support for students have gone far beyond expectations. Sharing this journey with a group of motivated and supportive peers has made the lab environment both stimulating and enjoyable, fostering creativity and learning every step of the way.

I would like to acknowledge Dr Hannah Constatin for performing XPS, Nicola Weston for performing ESEM, Dr Long Yang, for performing profilometry, Dr Anna Kotowska for performing ToF-SIMS, and Martin

Roe, for training and supporting me in SEM imaging. I also would like to thank Dr Vincenzo Di Bari for allowing me to use the rheometer located in his lab when the one in the School of Pharmacy was out of order.

On a personal note, I am deeply thankful to my mother and sister, who have been my pillars, always believing in me and standing by my side with unconditional love and support. I am equally grateful to my partner Akhil, whose support and love have sustained me throughout this journey, giving me the strength to never give up. I would also like to honour and remember those who are not here to celebrate this achievement with me: my beloved grandparents, Valentina and Leopoldo. I miss them every day and remain profoundly grateful for the enduring example of resilience, love, and wisdom they have given me, which continues to guide and inspire me in all that I do

Thank you to the colleagues I met through the CDT modules and colloquia. In particular, Graziamarina for being a good friend and my trusted out-of-hours buddy, and Lexie, for being the first student I trained and later becoming a dear friend.

A heartfelt thank you to Angela, Cosimo, and Diego, for being like a second family to me and for their constant support and friendship. Finally, I would like to thank all those who have been part of my life in these last four years and made Nottingham a place to call home: Domenico, Manuela, Enrica, Inas, Fiodor, Ali, and Giuliamaria. To everyone who has shared knowledge, advice, and encouragement along the way, I am grateful and thank you from the bottom of my heart.

Table of Content

List of Abbreviations

2D	Two-Dimensional
3D	Three-Dimensional
AFM	Atomic Force Microscopy
ALMA	Methacrylate Alginate
ANOVA	Anlysis of Variance
APCs	Antigen-Presenting Cells
APS	Ammonium Persulfate
BCR	B-cell Receptor
BIS	N,N'-methylenebis(acrylamide)
BMDMs	Bone Marrow-Derived Macrophages
BPI	Permeability-Increasing Protein
BSA	Bovine Serum Albumin
CB	Chemically Bound
CD	Cluster of Differentiation
CDPs	Common Dendritic Cell Precursors
CLPs	Common Lymphoid Progenitors
cMoPs	Common Monocyte Precursors
CMPs	Common Myeloid Progenitors
DAPI	4′,6-diamidino-2-phenylindole
DCs	Dendritic Cells

DEGDA	Diethylene glycol diacrylate
ECM	ExtraCellular Matrix
EDC	1-ethyl-3-(3-dimethylaminopropyl)carbodiimide
ELISA	Enzyme-Linked Immunosorbent Assay
ESEM	Environmental Scanning Electron Microscopy
FBGCs	Foreign Body Giant Cells
FBR	Foreign Body Reaction
FBS	Foetal Bovine Serum
FWHM	Full Width at Half Maximum
G	α-L-guluronic acid
G’	Storage Modulus
G’’	Loss Modulus
GelMA	Methacrylate Gelatine
GM-CSF	Granulocyte-Macrophage Colony-Stimulating Factor
GMPs	Granulocyte and Macrophage progenitors
HDM	High Degree of Methacrylation
hiPSCs	Human Pluripotent Stem Cells
hMSCs	Human Mesenchymal Stem Cells
HR2	Histamine Receptor 2
IFN	Interferon
IgM	Immunoglobulin M
LAP	phenyl-2,4,6-trimethylbenzoylphosphinate

LDM	Low Degree of Methacrylation
LPS	Lipopolysaccharide
LVE	Linear Viscoelastic
M	β-D-mannuronic acid
MBL	Mannose-Binding Lectin
MCSF-1	Macrophage Colony-Stimulating Factor
MDP	Monocyte-macrophage/Dendritic Cell Precursors
MES	2-(N-Morpholino)ethanesulfonic acid
MHC	Major Histocompatibility Complex
MPO	Myeloperoxidase
MPP	Multipotent Precursor
MR	Mannose Receptor
MSCs	Mesenchymal Stem Cells
MZ	Marginal Zone
N_A	Avogadro's number
NHS	N-hydroxysuccinimide
NK	Natural Killer
PA	Physically Adsorbed
PAAm	Polyacrylamide
PAMPs	Pathogen-Associated Molecular Patterns
PBS	Phosphate-Buffered Saline
PEGDA	poly(ethylene glycol) diacrylate

PMs	Promyelocytes
R	Universal Gas Constant
RGD	Arginine-Glycine-Aspartic acid
RLU	Relative Luminescence Unit
Sa	Arithmetical Mean Height
SD	Standard Deviation
SEM	Scanning Electron Microscopy
SEM	Standard Error of Mean
SPAK	3-sulfopropyl acrylate potassium salt
Sq	Root Mean Square Height
TCP	Tissue Culture plastic
TEGDMA	Tetraethyleneglycol Dimethacrylate
TEMED	N',N',N',N'-Tetramethylethylenediamine
TNF	Tumour Necrosis Factor
ToF-SIMS	Time-of-Flight Secondary Ion Mass Spectrometry
XPS	X-ray photoelectron spectroscopy
β-TCP	β-tricalcium phosphate
η^*	Complex Viscosity
ξ	Mesh Size

List of Figures

List of Table

List of Equations

Chapter 1. Introduction

1.1 Immune System & Response

The immune system is a highly integrated network of lymphoid organs, tissues, cells, humoral factors, and cytokines that collectively function to protect the body against potentially harmful stimuli(1). These include pathogenic microbes, that can be inhaled or swallowed, as well as toxins and allergens(2). Such agents can alter the homeostasis of the host, either through their intrinsic pathogenicity, as in the case of viruses, which are obligate intracellular parasites(3-5) , or through external factors, such as antibiotic exposure or changes in the diet that alter the gut microbiota(6).

The immune systems and its components are generally divided into two main groups: the innate and the adaptive immune systems(7). These differ in their specificity of response, time of activation(8), and the presence of immunological memory, a defining feature of the adaptive immunity(9). Despite the differences between these two branches of the immune system, both innate and adaptive responses are pivotal for protecting the organism and they work in synergy and co-operation to fight pathogens, neutralise toxins and allergens, and maintain the organism in physiological conditions.

1.1.1 Innate Immune System

The innate immune system, also known as nonspecific immune system(10), represents the first line of defence across a wide range of organisms, from vertebrates and invertebrates to plants(11, 12) and even prokaryotes(13). It is characterised by broad, non-specific mechanisms of actions and protective barriers, which can be divided in three different

groups, namely anatomic, physiologic, and phagocytic/endocytic barriers(14) as shown in **Figure 1.1.1.1**.

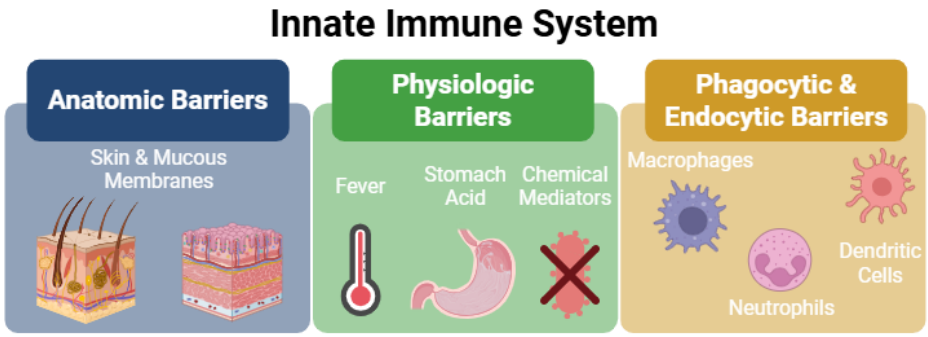

Figure 1.1.1.1 Schematic representation of the innate immune system components, including anatomic, physiologic, and phagocytic/endocytic barriers.

1.1.1.1 Anatomic Barriers

Intact skin(15) and mucous membranes are anatomic barriers that respectively provide mechanical protection and serve as entrapment sites for microbes, that are physically hinder to entry the body. For instance, the colonic mucosa is key for separating the body from the microbes populating the intestine. When its homeostasis is disrupted, bacteria can easily translocate and tigger an inflammatory response(16).

1.1.1.2 Physiologic Barriers

Temperature and pH belong to the physiologic barrier group. High temperature plays a dual role, as it is not only associated with the inhibition of bacteria(17) and viruses(18) reproduction, but it also boosts the activity of immune cells and cytokines(19, 20).

Chemical mediators, like lysozyme and the complement system, represent another sub-type of physiological barriers.

Lysozyme is a mucolytic enzyme involved in the cleavage of β-1,4-glycosid bonds between N-acetyl muramic acid and N-acetyl glucosamine, peptidoglycan that are key components of the bacterial cell wall(21, 22). It can directly affect Gram-positive bacteria as peptidoglycans are found in the outer layer of their membrane. In contrast, Gram-negative bacteria possess an additional external membrane consisting of an inner leaflet made of bilayer phospholipids, and an outer leaflet of lipopolysaccharide(23). This results in the inability of lysozyme to directly access the peptidoglycan layer of Gram-negative bacteria. However, the enzyme becomes effective once the complement and other enzymes disrupt the outer envelope and expose the peptidoglycan layer to degradation(24).

The complement system consists of soluble plasmatic enzymes and membrane receptors involved in a cascade that ultimately leads to the lyses or phagocytosis of microbes(25). This system can follow three distinct pathways: the classical pathway(26), triggered by immunoglobulin M (IgM) and immunocomplexes, the lectin pathway, initiated by mannose-binding lectin (MBL) or ficolins, or the alternative, pathway that spontaneously initiates from the continuous regeneration of C3 component of the system(27, 28).

Histamine is another key player of the physiological barriers. It is defined as “pleiotropic chemical mediator”, owing to its ability to bind four different receptors which activate different signalling pathways(29). Its biological effects include vasodilation and increase of vascular permeability(30), which facilitates the cell migration through the blood vessels, chemotaxis, that enables the recruitment of immune cells(31), and modulation of dendritic cells(32, 33). Interestingly, histamine can also exert anti-inflammatory properties. Binding to histamine receptor 2 (HR2) down-regulates histamine release from

basophils(34) and mast cells and inhibits synthesis of antibodies, cytokine production, and T cell proliferation(35).

Another relevant chemical mediator is represented by the class of interferons (IFNs), which are divided into two big families. Type I IFNs (IFN-α, IFN-β, IFN-ε, IFN-κ, IFN-ω, IFN-δ, IFN-ζ, IFN-τ) are mainly secreted by plasmacytoid dendritic cells, although epithelial cells and neurons can also produce and release them during viral infections(36). Their primary function consists in fighting viral infections by interfering with viral RNA and DNA production and enhancing the recognition of infected cells(1). Additionally, type I IFNs possesses antiproliferative and cytotoxic properties towards tumour cells, and they can also inhibit angiogenesis(37). Type II IFNs, such as IFN-γ, are mainly produced by natural killer (NK) and innate lymphoid type 1 cells. IFN-γ is responsible for T-cell activation and inducing NO production in macrophages(38). NO is toxic on microorganisms and, depending on concentration and exposure time, can inhibit the activation of inflammatory cells. Prolonged high concentrations of NO suppress inflammatory activation of cells, whereas low concentrations determine vasodilatation and neutrophil recruitment(39), favouring a pro-inflammatory response.

1.1.1.3 Phagocytic and endocytic barriers

Phagocytic and endocytic barriers of the innate immune system encompass cells such as macrophages, neutrophils(40), and dendritic cells(41) (DC). These cells can engulf and digesting pathogens, dead cells, and debris, through a process known as phagocytosis, or internalise and decompose foreign molecules found in their environment, through a process known as endocytosis. To initiate these processes, cells need to recognise specific patterns, termed pathogen-associated molecular patterns (PAMPs), which are characteristic of

bacteria and viruses and include lipoproteins, lipopolysaccharide (LPS), flagellin, peptidoglycan, and viral fusion glycoproteins(42).

While macrophages will be discussed in more detail in section 1.1.1.2, neutrophils and dendritic cells are briefly described here.

Neutrophils are white blood cells generated in the bone marrow from hematopoietic stem cells. These progenitors can follow two distinct differentiation pathways to give rise to granulocytes, like neutrophils, or monocytes(43). A defining feature of neutrophils is the presence of granules, which are classified into three groups based on the timing of formation, protein content and functions(44). Primary (or azurophil) granules forms in promyelocytes (PM) and contain potent antimicrobial enzymes that help killing and degrading pathogens, such as myeloperoxidase (MPO), azurocidin, defensins, cathepsin G, and permeability-increasing protein (BPI), as well as proteases that are typically found in lysosomes. Secondary (or specific) granules develop in myelocytes and metamyelocytes and are enriched in enzymes and receptors that help neutrophils in the chemotactic process as well as enzymes that aid in the killing of bacteria, such as lactoferrin and collagenase (45, 46). Tertiary (or gelatinase) granules and secretory vesicles form during the final stages of neutrophil maturation. Tertiary granules mainly contain gelatinase, an enzyme that belongs to the matrix metalloproteinases family and is implicated in degrading and remodelling extracellular matrix (ECM)(47), an essential feature for neutrophil migration. Secretory vesicles have a pivotal role in neutrophil activities as they act as reservoirs of molecules that aid the attachment to the vascular endothelium(48). Neutrophils perform a variety of activities that range from fighting pathogens, through phagocytosis and degranulation, to promoting inflammation by releasing pro-

inflammatory cytokines that recruit other immune cells to the site of interest(49).

DCs are antigen-presenting cells (APCs) whose primary role consists in processing and presenting antigens. Both self and non-self antigens are reduced to epitopes to form complexes with the major histocompatibility complex (MHC) molecules and are then exhibited on the cell surface. Through this mechanism, DCs can crosstalk with T cells, inducing either immune tolerance, when self-epitopes are involved, or a cytotoxic response towards infected cells. They can also engage B cells and macrophages to respectively promote antibody formation and/or cytokine release(41, 50, 51).

1.1.1.3.1 Monocytes

Monocytes are white blood cells that represent ~10% of peripheral leukocytes in the blood(52). Prior to their release in the bloodstream as mature cell, monocytes undergo a well-regulated process of differentiation that starts in the bone marrow. Hematopoietic stem cells generate multipotent progenitor cells (MPPs), which give rise to both the myeloid and lymphoid lineages through differentiation into common myeloid progenitors (CMPs) and common lymphoid progenitors (CLPs). CMPs further differentiate into granulocyte macrophage progenitors (GMPs), which later turns into monocyte-macrophage/dendritic cell precursors (MDPs). These can either result in common dendritic cell precursors (CDPs) or common monocyte precursors (cMoPs). The latter eventually mature into monocytes that are ready to be release into the bloodstream(53), where they circulate with a half-life of approximately three days(54).

Human monocytes are defined as such by the presence of the surface marker cluster of differentiation (CD) 14. Given their heterogeneity

(55), monocytes can be divided into three subsets, depending on the expression of CD16(56). However, it is important to highlight that the functional characterisation of these different monocyte subpopulations has given inconsistent results across studies, particularly regarding the cytokine profiles(57). Classical monocytes are characterised by CD14 only and represent the majority of the circulating monocytes. They are key effectors during infections as they produce high levels of pro-inflammatory cytokines. Intermediate monocytes, which express high levels of both CD14 and CD16, are also responsible for secreting pro-inflammatory cytokines and they seem to be involved in chronic inflammatory diseases. The third subset is represented by nonclassical monocytes, which seem to participate in inflammation, tissue repair and healing processes(58).

The main role of monocytes is to act as reservoir of immune cells, contributing both for homeostasis and inflammatory purposes. They can leave the circulation and reach tissues where an inflammatory response is needed. Upon entering peripheral tissues, monocytes can differentiate into macrophages or DCs, depending on the local microenvironment and stimuli they are subjected to(59, 60).

1.1.1.3.2 Macrophage

Macrophages can be broadly classified as tissue-resident macrophages or monocyte-derived macrophages, depending on their origin. Tissue-resident macrophages are a heterogeneous population that comprehend all macrophages found in peripheral tissues, where they behave like sentinels providing the first line of defence(61). Examples include microglia in the central nervous system, Kupffer cell in the liver, Langerhans cells in the epidermis, and osteoclasts, in the bones. Unlike monocyte-derived macrophages, these subset of macrophages do not derive nor depend on the HSCs in the bone marrow for replenishment.

In fact, tissue-resident macrophages are also capable of self-renewal through local proliferation, thereby maintaining homeostasis independently(62). They originate from the yolk sac and foetal liver during the embryonic and foetal stages of the pregnancy and they differentiate into the specific tissue-phenotype with the onset of organogenesis(63-65).

Monocyte-derived macrophages originate from circulating monocytes, which migrate into tissues through the bloodstream in response to stimuli. Their differentiation is driven by the microenvironmental cues(66), leading to different activation states (**Figure 1.1.1.3.2.1**).

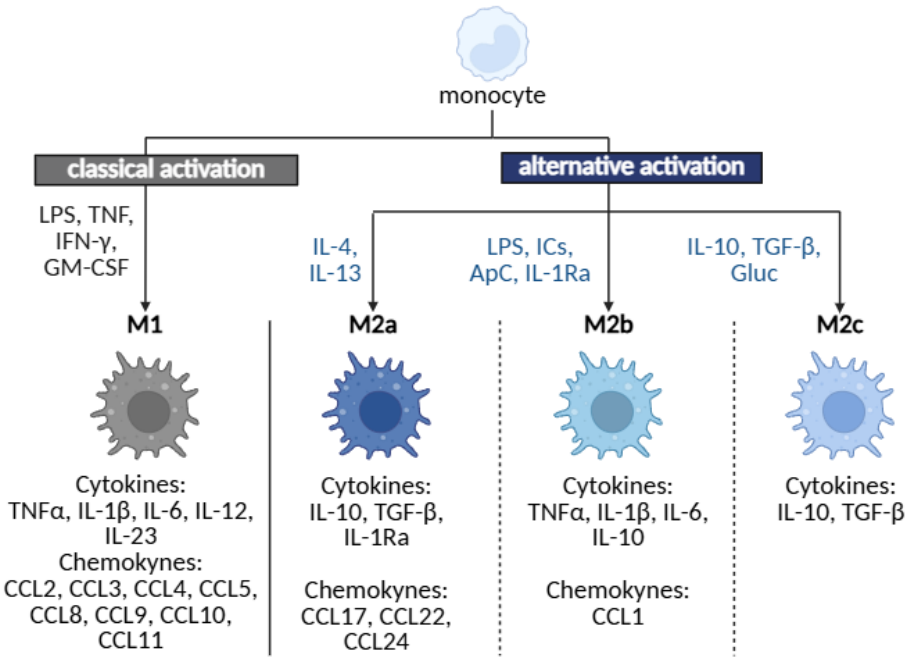

Figure 1.1.1.3.2.1 Schematic showing macrophage polarisation pathways. Monocytes differentiate into macrophages through classical or alternative activation routes, depending on the stimuli.

Classically activated macrophages, known as M1 phenotype, are induced by LPS, IFN-γ, and granulocyte-macrophage colony-stimulating factor (GMCSF). They are pro-inflammatory cells that

produce and release pro-inflammatory cytokines, reactive nitrogen and oxygen intermediates(67), enzymes and acid molecules(68). Conversely, the alternative activation route leads to M2 phenotype that is described to have anti-inflammatory properties as it releases factors like IL-10, matrix metalloproteinases(69), and growth factors(70), supporting tissue repair and remodelling. Although macrophages have traditionally been classified as either M1 or M2, it is now recognised that they exist along a continuum of activation states(71), with M1 and M2 representing the prototypical pro- and anti-inflammatory extremes of this spectrum(72). For example, based on surface marker receptors, cytokine profiles, and specialised immune effector functions(73), four different subsets of M2 macrophages have been recently characterised, with M2a and M2c playing a role in anti-inflammatory, wound healing, tissue repair, and matrix remodelling activities(74).

A third macrophage phenotype, termed naïve or M0 macrophages, represents non-activated macrophages that can be generated *ex vivo* by stimulation with macrophage colony-stimulating factor 1 (MCSF-1) only(75). They are characterised by phagocytic and pathogen detection abilities but they need to polarise towards M1 or M2 phenotype to acquire their full effector function(76).

An important feature of macrophages is their high plasticity, allowing them to shift their phenotype in response to stimuli and environmental cues(77). As a result, the same population of cells can participate both in the induction and resolution of inflammation, depending on the microenvironment they are surrounded by(78).

1.1.2 Adaptive Immune System

The adaptive immune system complements the innate immunity by offering the ability to recognise a virtually unlimited array of antigens.

Unlike the innate immune response, which is evolutionarily conserved across species(79), the adaptive immune system is unique to vertebrates and represents a later evolutionary innovation(80). It provides highly specific immunological defence through the generation of antigen receptors and precise discrimination between self and non-self, thereby supporting a highly specific, more effective, and long-term protection. A defining feature of the adaptive immune system is immunological memory, which is the ability to recall past encounters with antigens, recognise them, and respond more rapidly and effectively upon re-exposure(81, 82). Adaptive immune responses require longer time to develop as it involves the following consequential steps: recognition of specific antigens, evaluation of antigens, whether they are self or non-self, and development of an antigen specific response(2, 14, 83). Key players of the adaptive immunity are two types of lymphocytes known as B cells and T cells(84), as shown in **Figure 1.1.2.1**.

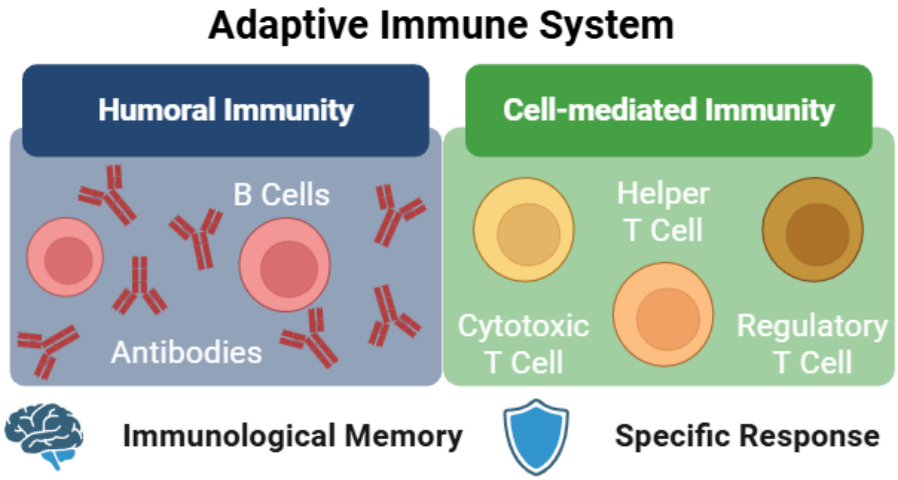

Figure 1.1.2.1 Schematic of adaptive immune response components, encompassing both humoral and cell-mediated immunity and key features.

Both B and T cells originate from the CLPs in the bone marrow but subsequently commit to distinct developmental lineages(85). B cells

continue to mature within the bone marrow through a multi-step process involving several rearrangements and expression of the heavy and light chains genes of immunoglobulins, until complete IgM molecules are expressed and participate in forming the B cell receptors (BCR), that are found on the cell surface. These genetic rearrangements allow the immune system to generate millions of unique antigen receptors, enabling the body to respond to an immense variety of threats(86, 87). Immature B cells then undergo positive and negative selection processes that build up for central tolerance(88-90) and migrate to the spleen, where they complete their maturation process, becoming mature (or naïve) B cells; they are characterised by the expression of both IgM and IgD(91, 92). Mature B cells are divided into three major subsets according to their anatomical localisation(93). Marginal zone (MZ) B cells and B1 cells are activated by T cell-independent antigens (TI antigens), such as lipopolysaccharide and bacterial antigens, following the secretion of antibodies. Conversely, follicular B cells are mainly involved in responding to antigens that elicit helper T cells, known as T cell-dependent antigen. Following antigen binding, the BCR-antigen complex is internalised, processed and involved to form a complex with MHC II, which is essential to promote the activation of helper T cells(94-97).

On the contrary, CLPs committed to the T-lineage migrate to the thymus, where they undergo maturation involving positive and negative selection. This process is essential to reach self-tolerance and leads to mature (or naïve) T cells(98). Mature T cells can be divided into two classes: $CD4^+$ helper and $CD8^+$ cytotoxic T cells(99). After leaving the thymus, they enter lymph nodes and undergo priming, a process where T cells interact with peptide-MHC complexes on APCs, which triggers a downstream process that leads to their activation. Helper T cells can differentiate into two different effector subsets: Th1 and Th2. Th1 cells

are responsible to promote cell-mediated immunity against pathogens by secreting interferon-γ (IFNγ) and tumour necrosis factor α (TNF-α), which promote phagocytic cell recruitment and activation. Th2 cells, by contrast, support the humoral response against extracellular organisms by releasing IL-4, IL-5, IL-10, and IL-13, which stimulate B cells to produce antibodies against extracellular pathogens(100). Upon activation, cytotoxic T cells directly eliminate infected or transformed cells using mechanisms such as perforin-mediated pore formation and the release of lytic enzymes that induce apoptosis in cancerous or virus-infected cells(101, 102). Overall, the adaptive immune system provides a powerful and flexible, defence system that not only eliminates harmful pathogens but also learns from past encounters to protect the host more efficiently upon re-exposure. Its ability to adapt and evolve makes it indispensable for long-term immunity.

There is growing evidence that the adaptive immune system also plays a significant role in modulating biomaterial responses(103, 104). T cells can be recruited to the implant site either directly, through recognition of antigens presented by antigen-presenting cells (APCs), or indirectly, via the cytokine milieu established during the early stages of inflammation(105, 106). Activated $CD4^+$ T helper subsets, for example, can influence the polarisation state of macrophages: Th1 cells promote pro-inflammatory M1-like phenotypes via secretion of IFN-γ, whereas Th2 cells support M2-like, pro-healing macrophage phenotypes through the release of IL-4 and IL-13(107). Additionally, Th17 cells have also been implicated in fibrotic responses, as their signature cytokine IL-17 stimulates fibroblast proliferation and collagen deposition, contributing to encapsulation of biomaterials(108). In addition, regulatory T cells may serve a counter-regulatory role by dampening local inflammation and limiting fibrosis, although their exact involvement in the FBR is still under investigation(109).

The adaptive immune system therefore can be seen as an active modulator of the response to biomaterials, bridging early inflammation with chronic outcomes. The interplay between T cells and macrophages can critically shape the quality of the fibrotic capsule, the persistence of inflammation, and the fate of implants.

1.1.3 Foreign Body Reaction

Every time a host is exposed to a non-self component the immune system perceives a potential danger and acts to protect the organism from it. When an implant is introduced into the body, both innate and adaptive immune system respond to it through a series of subsequent phases that ultimately lead to fibrous encapsulation (**Figure 1.1.3.1**), as it is perceived as foreign material(110, 111).

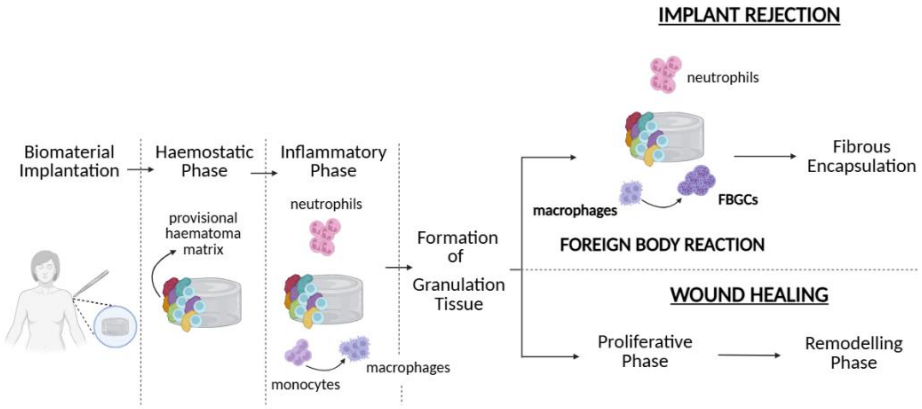

Figure 1.1.3.1 **Overview of the immune response to biomaterial implantation, showing key phases of wound healing and the foreign body reaction leading to either tissue repair or fibrous encapsulation.**

To insert an implant into the body, surgery is needed. This creates an injury in the tissues that surround the implant, triggering the start of the wound healing process. Serum proteins that escape the circulation through damaged blood vessels create a wound clot, known as early

provisional matrix, to stop the bleeding(112). In the presence of an implant, part of those proteins together with blood cells are adsorbed on the surface of the implant, generating what is known as late provisional hematoma matrix(113), made of fibrin, inflammatory mediators, platelets and endothelial cells(114). This blood-material interaction follows the principle of the Vroman effect, according to which protein adsorption is governed by mobility, affinity, concentration and molecular weight of blood proteins(115). Given these variables, the composition of the provisional hematoma matrix can vary over time and across different implanted materials, leading to differences in the immune response(116). These initial events involving protein adsorption represent a pivotal step as they also involve the release of mitogens, chemo-attractants, cytokines, and growth factors, which are all essential for the recruitment of immune cells and the wound healing process(112, 117). Members of the complement system and non-specific antibodies are also involved and provide recognition sites for immune cells, which otherwise have poor ability to bind directly to biomaterial surfaces(77).

The haemostatic phase is followed by the inflammatory phase, which begins as an acute response, characterised mainly by the presence of polymorphonuclear leukocytes(118). If unresolved within the first week, the inflammation evolves to a chronic state, characterised by a persistent leukocytes and monocytes infiltration at the implant site 2-5 weeks after the surgery. Neutrophils and mast cells are the first immune cells to reach the implant site. Neutrophils are involved in removing debris and pathogens through phagocytosis and the release of proteolytic enzymes and reactive oxygen species(119), while mast cells release histamine and serotonin to induce vasodilatation and extravasation of cells from the bloodstream(120). Other types of cells involved in this phase are tissue-resident macrophages(65) and circulating monocytes that later

differentiate into macrophages, as described in section 1.1.1.3.2. These scavenger cells phagocyte dead cells and damaged tissues, and attempt to engulf the implant, which can resist to this action due to its size and physicochemical properties(112). As inflammation persists, granulation tissue generates, characterised by the generation of small blood vessels by vascular endothelial cells, and infiltration of macrophages and fibroblasts (111, 121-123).

A normal wound healing process would further progress with the proliferative and remodelling phases(124, 125). These two processes temporarily overlap, and involve the formation of collagenous ECM, that provides mechanical and architectural support. Through this network, fibroblasts can later migrate and transform it into a scar tissue. In the resolution phase, which comes last, fibroblast undergo apoptosis and healthy conditions of the tissue are restored(126, 127).

When a biomaterial is implanted, however, this physiological wound healing trajectory is altered, giving rise to the foreign body reaction (FBR). FBR is generally characterised by elements of granulation tissue and foreign body giant cells (FBGCs); the precise composition in terms of cell population will depend on the form of the implant and its surface properties and topography(114). FBGCs, which are a sub-type of multinucleated giant cells, are generated from the membrane fusion of pro-inflammatory macrophages when the size of the foreign body exceeds their phagocytic capabilities(128-130). Similarly to their precursors, FBGCs, as bigger cells in size, attempt to digest the biomaterial through phagocytosis, but their phagocytic efficacy is worse compared to macrophages(68, 131).

Ultimately, the immune response ends with the formation of a fibrous encapsulation that walls the implant off the body. The intent is to isolate a “non-self” material when macrophages and FBGCs fail in their attempt

to remove it through phagocytosis and biodegradation(132-134). Although this is a natural immune response that aims to protect the body from harmful pathogens and anything that can compromise the host's wellbeing, FBR can severely jeopardise functionalities of implants and their therapeutic outcomes.

1.2 Biomaterials

The use of materials for medical applications dates to prehistoric times. Ancient civilisations, including the Egyptians, Mayans, Chinese, and populations in Africa and India, developed rudimental biomaterials for wound healing, dental and cranial repairs(135). Biomaterials are natural or synthetic substances, used alone or in combinations, to treat, augment, or replace tissues, organs, or bodily functions to maintain or improve the quality of life of the individual(136, 137). Based on their chemistries and properties, biomaterials can be divided into three main classes: metals, ceramics and polymers.

1.2.1 Metals

Biomedical metals are mainly known for their remarkable mechanical properties, such as strength, resistance, elasticity and ductility(138). These features make them particularly suitable for repairing or replacing damaged bone tissue, as they are capable to withstand load-bearing applications(139). Their performance is influenced by morphological characteristics, physicochemical structure, and surface properties(140). The main limitations associated to this type of biomaterials are the high specific weight and corrosion(135). Titanium, tantalum, cobalt-chromium, magnesium, iron, zinc, steel, and their alloys are the most frequently used metals.

Titanium and its alloys are considered the gold standard for biomedical implants. The implementation of bioactive coatings has also enhanced their effects on promoting cell adhesion, proliferation, and differentiation, particularly in bone regeneration(141). Given the structure similarity with human bones, tantalum represents a good alternative to titanium in the treatment of bone defects. It is also known for promoting osteogenic differentiation, cell adhesion, and for regulating the osteogenic differentiation-related signalling(142). Cobalt-chromium alloys are also frequently used for bone regeneration applications due to their ability to stimulate osteoblastic cells, thereby supporting implant integration and the effectiveness of stem cell therapy in orthopaedic applications(143). An impactful limitation of these materials is related to the release of metal ions, that can lead to inflammation, long term-implant failure, and in severe cases, life-threatening toxicity, such as cardiomyopathy, peripheral neuropathy, vision loss, and chronic respiratory disease(144).

Magnesium alloys offer an additional advantage because they can be completely reabsorbed, meaning that a second surgery will not be needed for their removal upon fracture healing. To achieve the desired balance between mechanical support and corrosion rate, two different strategies can be put in place, such as varying the alloy composition or applying a coating material(145).

The use of metals to treat medical conditions is not limited to implants for bone regeneration. For example, gold nanoparticles have gained interest as for their potential in drug delivery(146) and gene therapy(147).

In summary, metals offer a versatile platform for regenerative medicine, with ongoing research focused on optimising their properties and

applications to expand their potential across a broad range of clinical contexts.

1.2.2 Ceramic

Ceramics are inorganic materials made of metallic and non-metallic atoms, interacting mainly via ionic bonds. Their structure can be crystalline, non-crystalline, or a mixture of both. Ceramics are known for their hardness, which is comparable to natural bones, as well as for their high resistance to loads and corrosion, and greater durability than metals and polymers *in vivo*. However, their major limitations reside in low resistance for tensile loads and susceptibility to brittle fractures. Owing to these properties, they are widely used in dental and orthopaedic applications for wound healing and tissue engineering(135).

One of the most used ceramics in regenerative medicine is β-tricalcium phosphate (β-TCP) due to its synthetic nature, osteoconduction, osteoinduction, and cell-mediated resorption properties. It can also be exploited as a drug delivery carrier for locally releasing growth factors(148).

Alumina is another clinically relevant ceramic, particularly in orthopaedic and dental implants, due to its high compressive strength and chemical inertness. Advances in new generations of this material have improved its density, purity, and grain size, significantly enhancing mechanical performance(149).

More recently, ceramics have been combined with three-dimensional (3D) printing technologies to obtain customised porous scaffolds that mimic natural bone architecture. These porous structures facilitate vascularisation and nutrient diffusion, enhancing tissue integration and healing outcomes(150).

Overall, ceramics offer a diverse and adaptable platform for the development of next-generation scaffolds and implants in regenerative medicine, particularly for the orthopaedic dental, and craniofacial fields.

1.2.3 Polymers

Polymers represent the third class of biomaterials and, among all, they are considered the most versatile as they are easy to process and sterilise, they have a long shelf life, and their physical and chemical properties are tuneable(138). Polymers are macromolecules made of repeating units, known as monomers, that are arranged in long chains wherein they are connected through covalent bonds. They can be classified as homopolymers or heteropolymers based on the identical or different nature of the monomers. Polymer structure can be linear or branched, depending on whether side chains depart from the main backbone. Polymers can be either synthetic or natural.

Synthetic polymers are artificially produced in laboratories. They play a central role in modern medicine due to their tuneable mechanical and degradation properties, mechanical robustness, and versatility across a wide range of therapeutic and diagnostic applications. Additionally, they are characterised by higher reproducibility and purity compared to natural polymers, which is a major advantage when using them for medical applications(151). However, their main limitation lies in the reduced ability to interact with cells(152).

Thanks to their physicochemical properties, polymers are widely used to coat surfaces, making them an attractive tool for antifungal, antiviral(153) and antibacterial(154) purposes. They can also be used as matrixes to encapsulate antiviral or antibacterial drugs to enhance their delivery and therapeutic outcome. For example, VivaGel® consists of a benzylhydramine-amide-lysine core with functional groups capable of

binding genital herpes and HIV, preventing them from infecting cells(155). Zwitterionic polymers have shown to resist bacterial adhesion by forming a stable hydration layer. Recent studies on poly (sulfobetaine methacrylate) and poly (carboxybetaine methacrylate) have shown a significant reduction in the biofilm formation(156). In tissue engineering, biodegradable synthetic polymers like poly(ε-caprolactone), poly (glycerol sebacate), poly (lactic-co-glycolic acid), polyurethane, and poly(l-lactide) have been fabricated as nanofibres for myocardial regeneration, with surface modifications to better mimic the natural structures(157). Similarly, tuneable mechanical properties, porosity, controllable degradation, and ease of fabrication make synthetic polymers such as polyanhydrides, polypropylene fumarate, polycaprolactones, polyphosphazenes, polylactide, and polyglycolide good candidates for bone tissue engineering(150).

Natural polymers are synthesised through biological processes and can be naturally found in the environment. This class includes macromolecules with different chemistries and functions, such as starch, wool, proteins, DNA, cellulose, polysaccharides, glycosaminoglycans, and many more. Their advantages reside in the fact they are readily available and have low cost. However, the main limitations can be summarised as high variability across batches due to the natural sources, limited mechanical strength, high sterilisation costs, and unwanted reactions given by impurities(152).

1.2.3.1 Hydrogels

Due to their physicochemical similarity to the ECM, hydrogels have become pivotal in biomedical applications such as drug delivery, tissue engineering, and regenerative medicine. Hydrogels are a specific type of polymeric network characterised by high affinity to water, which is

incorporated inside their 3D structure due to the presence of highly hydrophilic groups in the polymeric chains. They are formed through a process called gelation, that involved the cross-linking of polymeric chains in the presence of water, which remains entrapped in the forming network. Depending on their chemical structure, gelation can happen through physical interactions, chemical reactions, or a mixture of both.

Physical hydrogels generate through weak interactions between polymer chains, including ionic forces, Van der Waals interactions, polyelectrolyte complexation, stereocomplexation, and hydrophobic forces. The crosslinking is generally induced by changes in intermolecular forces, that can be induced by variations in ionic strength, heat, light, pH, pressure, sound, electric field or due to the presence of certain molecules(158). Due to the weak nature of the forces involved, these hydrogels have a short lifespan, and they are highly sensitive to changes in the surrounding environment, making the control over their mechanical properties a big challenge(159). Chitosan-based hydrogels are an example of physical hydrogels. The amino groups, protonated at acidic pH, can establish ionic interactions with negatively charged molecules and anions across different chains. Hydrogen bonds involving the hydroxylic can further contribute in stabilising the 3D-network(160). Given the mechanism that leads to the hydrogel formation for these systems, an increase in pH above 6 results in a reduction in the ability of forming the network(161).

To increase stability of physical hydrogels, dual crosslinking strategies have been explored. For example, the work on a hydrogel made of calcium-crosslinked xanthan gum and hydrophobically associated polyacrylamide showed improved mechanical properties and high thermal and environmental stability, making it a promising material for load-bearing and durable applications(162).

Chemically crosslinked hydrogels are an alternative to better control properties like swelling, degradation rate, and mechanical strength. They form via covalent bonds induced through the addition of small molecules or by polymer-polymer conjugation(163). Polyacrylate gels are an example of chemically crosslinked gel formed through the establishment of covalent bonds using small molecules, like diethylene glycol diacrylate (DEGDA), poly(ethylene glycol) diacrylate (PEGDA), and N,N'-methylenebis(acrylamide) (BIS), tetraethyleneglycol dimethacrylate (TEGDMA). To further increase the robustness of hydrogels, macro cross-linkers, such as silica and graphene, can also be introduced. However, their big sizes might lead to uneven cross-linking within the network. Therefore, tuning the crosslinker size and concentration is essential to achieve the desired mechanical properties. Acrylated polyethylene glycol is an example of cross-linker that integrates the advantages of both small molecular cross-linkers, as it generates a uniform system, and macro cross-linkers, with numerous physical entanglements(164). A major limitation of chemically crosslinked hydrogels lies in the potential toxicity of residual unreacted crosslinkers.

The polymer-polymer conjugation strategy can take place when the chains are chemically modified with cross-reactive groups. For example, Hiemstra C. et al. developed hydrogels by mixing vinyl sulfone-functionalised dextrans and mercaptopoly(ethylene glycol), that formed the network through Michael type addition(165). With this approach, *in situ* formation of the hydrogel can be achieved. However, a big effort in chemically modify the polymers is needed and potentially toxic materials can be generated(163). Most covalent crosslinking happens via radical reactions. Ionic initiators need to form ions to start the polymeric reaction. Redox initiators rely on a redox reaction to generate

active species(166, 167). Photoinitiators are light-sensitive molecules that generates radical species upon exposure to UV or visible light(168). Thermal initiators are sensitive to changes in temperature and generates radicals due to a change in temperature(169). More recently, enzymatic crosslinking has gained attentions as it exploits physiological enzymes, such as transglutaminase, tyrosinase, phosphopantetheinyl transferase, lysyl oxidase, plasma amine oxidase, phosphatases, thermolysin, β-lactamase and phosphatase/kinase, and peroxidases to induce gelation. These systems have the advantages of allowing *in situ* polymerisation at physiological conditions, avoiding invasive procedures, as well as mild polymerisation conditions, and no use of initiators, that can potentially show toxicity(170).

1.2.3.1.1 Alginates and Methacrylate Alginates (ALMA)

Alginates are natural polymers found and obtained from the cell wall of brown algae and certain bacteria. They are anionic polysaccharides made of α-L-guluronic (G) acid and β-D-mannuronic (M) acid, linked through 1,4-glycosidic bonds. Depending on the source, this copolymer may vary in terms of G and M composition, sequences of M and G blocks and degree of polymerisation(171). There are many advantages related to the use of alginates, such as low cost and toxicity(172), but also they are characterised by a structure that can be easily modified by introducing new moieties on either hydroxylic or carboxylic groups, which are reactive functional groups. In addition to these, alginates have been widely used as excipients for a variety of purposes in different types of formulations, like suspending agent, tablet binder and controlled-release matrix(173). They also find applications in the tissue engineering and regenerative medicine fields. In fact, they can be used to obtain hydrogel-based wound dressings(174) and for cell encapsulation given their mild gelation conditions and low toxicity. For

examples, it has already been shown the pancreatic islet encapsulation in alginate-based hydrogels to treat type 1 diabetes(175).

Despite these several advantages that come with using alginates, there are notable drawbacks that needs to be addressed and overcome. Given that alginates are extracted from natural sources, chances of contaminations are high. Initially, endotoxins were considered the main cause of immune activation. However, even alginates with undetectable endotoxins have been shown to elicit the immune response. This indicates that the material itself can contribute to immunogenicity, highlighting the need for further modifications to enhance its immune compatibility(176). Another major limitation is the gelation process. Alginate forms their 3D network through ionic-crosslinking, a process that follows the egg-box model, in which guluronate carboxylic groups on two adjacent antiparallel chains coordinate divalent cations(177). Because the most common gelation agents, such as $CaCl_2$, are highly soluble in water, the reaction rate is very difficult to control. This can potentially affect the uniformity and strength of the hydrogel: the higher the gelation rate, the lower the uniformity and mechanical integrity. Another significant disadvantage is the poor long-term stability as divalent cations can be exchanged with monovalent cations that are found in higher concentrations in body fluids, leading to the disintegration of the network. Lastly, the release of Ca^{2+} from the hydrogel could also promote haemostasis.

The introduction of methacrylic moieties into the alginate polymeric chains can overcome the limitations as methacrylate alginate (ALMA) hydrogels can be obtained through photo-crosslinking(172). The main advantages lie in obtaining hydrogels with higher structural stability(178) due to the formation of covalent bonds between polymeric

chains and in the opportunity to tune mechanical properties, based on the polymer concentration and degree of methacrylation(179).

1.2.3.1.2 Polyacrylamide Gels (PAAm)

Polyacrylamide hydrogelgels are versatile synthetic materials widely used in mechanobiology to investigate how cells sense and respond to mechanical cues from their environment. They are formed by the copolymerisation of acrylamide and N,N'-methylenebisacrylamide (BIS) monomers, which can be initiated in the presence of a catalyst, such as N',N',N',N′-tetramethylenediamine (TEMED), and an initiator, such as ammonium persulfate (APS). By adjusting the total concentration (T) of acrylamide and BIS, which is the crosslinking agent, as well as the ratio between these two components, it is possible to precisely control the stiffness and viscoelastic properties of the resulting gel. This tuneability makes polyacrylamide gels an ideal platform for mechanobiology studies, allowing researchers to mimic mechanical properties of a wide range of tissues, both soft and hard, only by changing the composition of the components(180-183).

Unlike naturally derived matrices, polyacrylamide gels are biologically inert, meaning they do not provide intrinsic biochemical cues for cell attachment(184). This makes them highly versatile as they can be selectively functionalised on the surface with adhesion proteins such as fibronectin, collagen, or RGD-containing peptides, offering the possibility to control the attachment motifs density that are presented to cells(185). The main drawback of this material resides in the toxicity of acrylamide and BIS as monomers, which can affect the nervous system(186, 187) and the kidneys(188). Although the polymerised gel is considered nontoxic and safe for cell culture(189), the inherent toxicity of the monomers restricts its use to applications requiring cell

encapsulation, as it is crucial that cells are added to the system before the gelation process starts.

As the field of mechanobiology continues to grow, polyacrylamide gels remain indispensable tools due to their reproducibility, chemical versatility, and ability to model physiologically relevant stiffness ranges and viscoelastic properties. They are also being integrated into organ-on-chip systems(190) and 3D culture platforms(180) to explore more complex biomechanical environments. Overall, polyacrylamide gels offer a robust and customisable platform for dissecting the biophysical interactions between cells and their microenvironment, making them essential for advancing our understanding of the cellular mechano-transduction.

1.2.4 Design of Immunomodulatory Hydrogels

A critical area of interest is the immunomodulatory potential of hydrogels. Understanding how they interact with the immune system to promote tissue integration while reducing phenomena that lead to implant rejection is crucial. Efforts have moved towards mimicking the native tissue environment, providing cells with mechanical and chemical cues that support regeneration and maintain tissue-specific functions. This biomimetic approach aims to recreate the feature of the tissue surrounding the implant site. The emergence of 3D bioprinting has significantly advanced this strategy, enabling precise scaffold fabrication with enhanced reproducibility and closely replicating the native properties of the targeted tissues(191). However, matching tissue properties is not always necessary and, in some cases, may be less important than endowing the scaffold with specific characteristics that actively modulate the host response. Biomaterial properties such as stiffness and viscoelasticity can be strategically tailored to influence cellular behaviour, protein adsorption, and immune cell recruitment. By

optimizing mechanical and chemical properties, it is possible to limit inflammation and reduce FBR. This perspective shifts the design rationale from purely mimicry of tissue to active control of the host-material interaction, obtaining immunomodulatory platforms that guide healing and long-term implant success.

The potential of hydrogels to influence the immune response arises from their tuneable physical and chemical properties, as well as the possibility to encapsulate bioactive molecules and living cells to drive immune cell behaviour within their network (**Figure 1.2.4.1**)

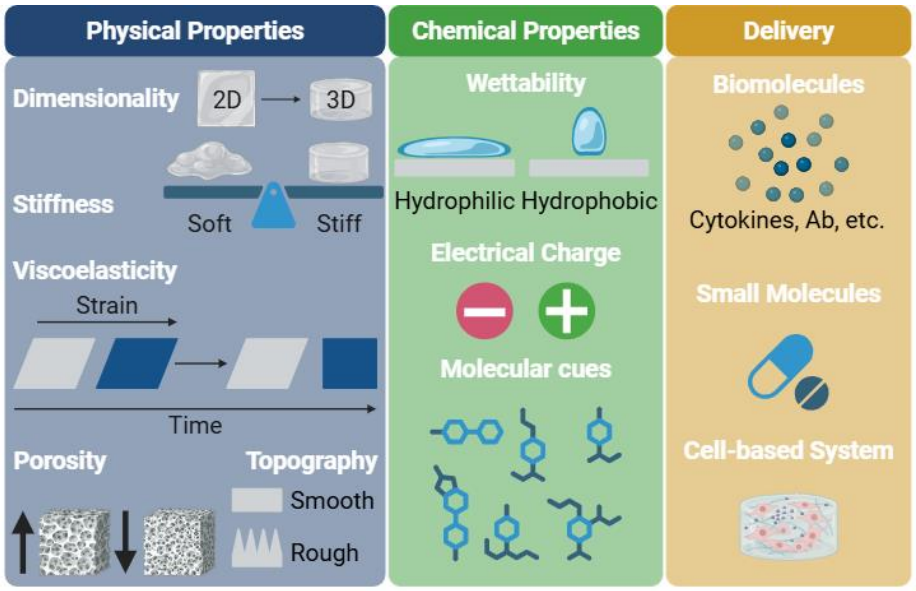

Figure 1.2.4.1 Overview of key hydrogel design parameters and strategies to tune material properties for regulating immune cell behaviour.

1.2.4.1 Physical properties

One of the fundamental physical parameters influencing immune cell response is the dimensionality of the environment. *In vitro* studies are traditionally conducted on two-dimensional (2D) surfaces, which do not

accurately reflect the *in vivo* architecture of tissues. Three-dimensional (3D) environment, such as hydrogels, more closely replicate the complexity of ECM and offer an alternative which better represent physiologically relevant conditions. It has been shown that immune cells exhibit distinct morphological and functional phenotypes when cultured in 3D environment compared to 2D substrates(192). For example, DCs tend to exhibit a more elongated morphology and higher expression of surface markers and cytokines when cultured on a 2D substrate. When they are found in a 3D environment, marker expression and cytokine profile seems to be driven by collagen matrix density(193). Similarly, monocyte differentiation and macrophage polarisation are also affected by dimensionality. For example, THP-1 cells spontaneously differentiate into macrophages when cultured in a 3D environment, whereas additional stimuli need to be provided in a 2D system(194, 195).

Beyond dimensionality, stiffness is another physical property that plays a critical role in shaping the immune response(196). By tuning the crosslinking density or polymer concentration, it is possible to obtain hydrogel characterised by a wide range of stiffnesses. Numerous studies have focused on the role of stiffness in driving the immune response, with a particular focus on macrophages. Despite the extensive research in this field, the effect of stiffness is still unclear as findings across studies have often shown contradictory results. Several studies showed that an increase in stiffness leads to a pro-inflammatory response(197-199), while others demonstrate that soft gels promote M1-like phenotype(200-202). These inconsistencies highlight the complexity of mechanotrasduction pathways and the need of more studies to ultimately determine the ideal stiffness for the rational design of immunomodulatory biomaterials.

Viscoelasticity is a property that has garnered growing interest in recent studies. Viscoelastic materials exhibit both solid- and fluid-like behaviour, leading to a decrease in relaxation modulus (G(t)) under constant strain. This energy-dissipative behaviour arises from the material's viscous component(203), with loosely crosslinked networks showing faster relaxation due to their more liquid-like (or viscous) character. Several studies have shown how viscoelasticity affects different cell types and their behaviour. In human pluripotent stem cells (hiPSCs) alginates with fast stress relaxation supported hiPSC survival, proliferation, polarisation and lumen formation structures, whereas slow relaxation induced apoptosis(204). Human mesenchymal stem cells (hMSCs) on highly viscoelastic hydrogels exhibited increased proliferation, spread area and differentiation, particularly towards smooth muscle cell commitment(205, 206). Skeletal muscle satellite cells(207) and myoblasts(208) also displayed enhanced viability, spreading and proliferation on stress-relaxing hydrogels. In fibroblasts, high viscoelasticity promoted cell spreading and focal adhesion maturation, counteracting the stiffening effect of elastic substrates(209). Migration and myofibroblastic differentiation were also affected(210). A study on breast epithelial cells revealed that viscoelasticity regulated cell spreading, adhesion, mechano-transduction, and migration(211). Hepatocellular carcinoma cells showed faster spreading, larger area, greater motility, and multiple protrusions on viscoelastic substrates, oppositely to healthy hepatocytes(212, 213). Similarly, adenocarcinoma and fibrosarcoma cells migrated effectively on fast-relaxing hydrogels(214). The effect of viscoelasticity on immune cells, particularly macrophages, remains poorly understood, and addressing this gap is a central focus of this thesis.

Another mechanical property that influences immune cells is porosity. The architecture of the hydrogel network determines the pore size and

network density, influencing the extent to which immune cells can infiltrate the material, the diffusion of nutrients and signalling molecules like cytokines. Highly porous hydrogels facilitate immune cell infiltration, enabling cell–cell communication, whereas tightly crosslinked hydrogels with small pores can physically block immune cell penetration. For instance, a work that focused on the interplay between elasticity and pore size showed how a reduced pore size in alginate hydrogel effectively delayed the diffusion of proteins and limited the infiltration of TNF-α, contributing to an "immunoprotective" microenvironment that supported mesenchymal stem cells (MSCs) viability and function(215).

Topography also plays a crucial role in driving the material-cell interactions. Advances in micro- and nanofabrication have enabled the design of surfaces with precise topographical features(216). Luu T.U. et al. showed how surface topography can be strategically used to modulate macrophage behaviour and promote a pro-healing immune response. Micro- and nanopatterned grooves on titanium surfaces were prepared with sizes ranging from 150 nm to 50 μm. Primary murine macrophages showed a pro-healing phenotype when cultured on groove sizes ranging from 400 nm to 5 μm in width, with an increased secretion of the anti-inflammatory cytokine IL-10(217). These findings demonstrate that surface geometry can direct macrophage polarisation, offering a promising strategy for the design of immunomodulatory biomaterials. It is important to highlight that surface topography directly affects protein adsorption patterns, thereby influencing the formation of the provisional haematoma matrix, cell attachment and the downstream of signalling pathways of immune cells(218).

1.2.4.2 Chemical properties

In addition to physical properties, the chemistry of hydrogels also plays a vital role in eliciting immune response.

One of the most studied chemical properties is wettability, which determines the interaction of a material with water and biological fluids. Hydrophilic surfaces, characterised by chemical groups that interact well with water such as hydroxylic or charged groups, tendo to resist nonspecific protein adsorption. Several studies have shown that hydrophilic surfaces favour anti-inflammatory macrophage activation, partly by modulating integrin-mediated signalling pathways. In contrast, hydrophobic surfaces, which tend to repel water, seem to promote a pro-inflammatory response that eventually leads to fibrous capsule formation(219, 220). By fine-tuning the balance of hydrophilicity and hydrophobicity, hydrogel surfaces can be optimised to either suppress or promote the activation of immune system.

Electric properties are also implicated in the immune system activation. Conductive hydrogels, which incorporate components such as polypyrrole or graphene oxide, have traditionally been explored in neural and cardiac applications, but recent studies have shown that these materials can also influence immune cell functions. Macrophages as well as T and B lymphocytes are electrically responsive cells and conductive hydrogels can modulate ion flux across cell membranes, influencing their polarisation status, cytokine secretion profiles, phagocytic behaviour, migration, and differentiation(221).

The presentation of molecular cues on the hydrogel surface can be another option to regulate the immune response. Hydrogels can be chemically modified to display ligands, peptides, or epitopes that engage specific receptors on immune cells. For example, the presence of

integrin-binding motifs like arginine-glycine-aspartate (RGD) sequence enhance cell adhesion, with focal adhesions acting as a bridge between the extracellular environment and the cytoskeleton. The presence of binding motifs onto the material surface is essential to promote cell attachment and have subsequent mechano-transduction. By changing the density of these pro-attachment sequences, differences in the cell–matrix interactions can be achieved, and these will be translated into different immune responses(222).

Hydrogels can be also functionalised with a variety of chemical cues that are known to modulate cell behaviour. For example, using a combinatorial approach, Vegas A. et al. developed a library of chemically modified alginate hydrogels and observed that three triazole-containing variants significantly reduced the inflammatory responses and fibrosis in non-human primates. These modifications appear to modulate macrophage activity, disrupting fibrotic processes and enhancing long-term implant biocompatibility(223).

It is important to highlight that chemistry plays a critical role in modulating cell-biomaterial also because it directly affects the adsorption of proteins from serum or culture media onto the substrate surface(224). The amount, composition, and conformation of the adsorbed protein layer vary depending on the material's chemical properties, and this layer critically determines the presentation of adhesive motifs to cells. Variations in this protein layer directly influence how integrins engage with the substrate, thereby modulating the formation of focal adhesion complexes. These integrin-based adhesion sites act as central mechano-transduction bridges between the extracellular environment and the cytoskeleton(225), ultimately regulating downstream signalling cascades that control cell adhesion, spreading, migration, and differentiation. Importantly, these effects can

occur independently of the bulk mechanical properties of the material: even substrates with comparable stiffness may elicit distinct cellular responses if their surface chemistry drives differential protein adsorption.

1.2.4.3 Delivery of Immunomodulatory Molecules

Perhaps the most versatile immunomodulatory strategy is the use of hydrogels as reservoir for delivering bioactive molecules. Cytokines and chemokines are among the most potent immune regulators and can be loaded into hydrogels for sustained and localised release. Depending on the system, the controlled release can be achieved through various mechanisms, such as tuning mechanical features like porosity and swelling, exploiting affinity interactions between the active molecules and hydrogel components, covalent bonding with cleavable linkers, or stimuli-responsive systems that degrades and release the active ingredient(195, 226).

Our work on 3-sulfopropyl acrylate potassium salt (SPAK)–poly(ethylene glycol) diacrylate (PEGDA) hydrogels is an example of how the combination of advanced manufacturing techniques with delivery of biologics can control macrophage polarisation. In particular, the sustained release of IL-4 up to day 53 was able to promote M2-like macrophage polarisation *in vitro*, representing a novel model of long-term immunomodulation using anti-inflammatory cytokine release(227).

Small molecule immunomodulators such as dexamethasone and rapamycin can also be encapsulated in hydrogels for prolonged release. These drugs act on key immune signalling pathways, offering an effective strategy to modulate inflammation and promote tolerance. In a recent work, a thermo-responsive system, made of poloxamer 407 and

hyaluronic acid was developed. It enabled the sustained release of rapamycin that promoted the polarisation of synovial macrophages from the pro-inflammatory M1 to the anti-inflammatory M2 phenotype. This shift reduced levels of inflammatory cytokines, like TNF-α, IL-1β, and IL-6, and increased IL-10, leading to decreased joint inflammation and delayed cartilage degeneration(228). Another successful example of immunomodulation through the delivery of a small molecule is represented by a work on sustained release of dexamethasone. The study showed how the molecule promoted osteogenic differentiation while simultaneously suppressing pro-inflammatory M1 macrophage activity, highlighting the therapeutic potential of drug-releasing scaffolds to coordinate inflammation and osteogenesis for bone repair(75).

Cell-based delivery systems represent a frontier in immunomodulation. Hydrogels can encapsulate living cells engineered to secrete immunoregulatory factors. The hydrogel matrix provides a protective environment for these cells, maintains their viability, and confines their action to the local tissue. For example, a study on MSCs encapsulated in alginate hydrogel showed an improved *in vivo* survival and *in situ* retention, that determined a higher expression of CD39+CD73+ in a collagen-induced arthritis model. Overall, this study highlighted the potential of hydrogel-based MSCs delivery in treating autoimmune diseases, like rheumatoid arthritis(229).

In summary, hydrogels represent a powerful and versatile platform for potentially modulate and drive the immune response. Through manipulation of their physical properties as well as their chemical features, hydrogels can be finely tuned to direct immune cell behaviours.

As the field evolves, a growing emphasis is placed on the integration of multiple immunomodulatory strategies within a single hydrogel

platform. By simultaneously tuning physical properties, surface chemistry, and bioactive molecule delivery, researchers can create multifunctional systems that control and drive immune responses. These advances are paving the way for innovative therapies across a range of clinical applications, from regenerative medicine and transplantation to cancer immunotherapy and the treatment of chronic inflammatory diseases.

1.3 Knowledge Gap

Despite extensive research into the role of mechanical properties in regulating macrophage responses, important knowledge gaps remain. Studies investigating stiffness-driven macrophage polarisation have produced contradictory findings, and most have relied on murine cells or immortalised cell lines, limiting their translational relevance to human biology. Moreover, the stiffness ranges examined often exceed those characteristics of native soft tissues. Furthermore, the contribution of viscoelasticity, an essential feature of living tissues and hydrogels, has only recently gained attention. However, most available studies lack systematic characterisation of biologically relevant relaxation timescales, or introduce concomitant changes in chemistry or stiffness, thereby confounding interpretation of the biological responses observed.

1.4 Aim and Objectives

In this context, the novelty of this work lies in systematically investigating the effects of physiologically relevant stiffness and viscoelasticity on primary human monocyte-derived macrophages, using ALMA and PAAm hydrogels as well-established platforms for mechanosensing studies. This project aims to advance the understanding on how physical and chemical properties of hydrogels can be engineered to modulate human monocyte differentiation and macrophage

polarisation to ultimately develop immunomodulatory biomaterials with reduced FBR. To build a deeper understanding of the roles of stiffness and viscoelasticity, the study focused on three main objectives:

1. To develop and optimise a reproducible hydrogel platform with tuneable stiffness and chemical properties within the physiologically relevant range of soft tissues.
2. To design a hydrogel platform with controlled stress relaxation while maintaining comparable chemistry and stiffness across formulations.
3. To investigate how subtle variations in stiffness and distinct stress relaxation profiles influence monocyte differentiation and macrophage polarisation using a combination of morphological, molecular, and functional assays.

Chapter 2. Materials & Methods

2.1 Materials

Alginate Methacrylate (degree of methacrylation: low 10% - 20%, high 20% - 40%), 2-Hydroxy-4′-(2hydroxyethoxy)-2-methylpropiophenone (Irgacure D-2959), 3-(Trimethoxysilyl)propyl methacrylate, toluene, acrylamide solution (40%), N,N′-Methylenebisacrylamide solution (2%), ammonium persulfate, N,N,N′,N′-Tetramethyl ethylenediamine, PBS, Tween20, RPMI-1640, foetal bovine serum (FBS), Penicillin-Streptomycin, L-Glutamine, Glycine, Trypan blue solution, Macrophage Colony-Stimulating Factor (MCSF), Granulocyte-Macrophage Colony-Stimulating Factor (GM-CSF), Interferon-γ (IFN-γ), Human recombinant IL-4, and goat serum were purchased from Sigma Aldrich. Sulfuric Acid 1N, Anti-human calprotectin mouse immunoglobulin G1, TMB substrate kit, and LIVE/DEAD Viability Kit, Pierce™ Chromogenic Endotoxin Quant Kit were supplied by Thermo Scientific, UK. ToxiLight™ Non-Destructive Cytotoxicity BioAssay Kit and 100% lysis Control set were purchased from Lonza. Buffy coats were obtained from healthy donors (National Blood Service, Sheffield, UK) after obtaining informed written consent and following ethics committee approval (Research Ethics Committee, Faculty of Medicine and Health Sciences, University of Nottingham). Ficoll-Plaque PREMIUM sterile solution was purchased by cytiva. LS columns, Pre-separation filters (30 mm), and CD14 MicroBeads UltraPure human were bought from Miltenyi Biotec. Anti-human CD206 (MR) rabbit IgG1 primary antibody was provided by Abcam. Phalloidin-iFluor 594 was supplied by AAT Bioquest, Stratech. 4,6-diamidino-2-phenylindole (DAPI), UltraPure EDTA (0.5M, pH 8), AlexaFluor 488 goat anti-mouse IgG (H + L), and Texas Red-X goat anti-rabbit IgG (H + L) were

purchased from Invitrogen. DuoSet® ELISA kits (TNF-α, IL-6, IL-10, CCL18) were purchased from Biotechne®|R&D systems.

2.2 Methods

2.2.1 Coverslips Silanisation

Coverslips were functionalised as previously described with some modifications(230). Plasma cleaning (O_2 100%, 10 min) was performed on glass coverslips (d = 16 mm), which were subsequently silanised with 3-(Trimethoxysilyl)propyl methacrylate (2% v/v) in dry toluene for 24h. The reaction was carried out under argon atmosphere. Coverslips were washed with fresh toluene (x2), acetone (x3), and dried under vacuum for 7 days prior to use.

2.2.2 Preparation of ALMA Hydrogels

To fabricate ALMA hydrogel, Irgacure D-2959 aqueous solution (0.5% w/v) was prepared and subsequently added to alginate methacrylate powder. ALMA solutions (2%, 4%, and 6% w/v) were stirred overnight and underwent photo-crosslinking with UV light (365 nm) for 10 minutes. Samples that were used for the rheological characterisation were prepared as discs (2 mm, r = 1.06 cm). Samples that were used for cell culture were prepared as thin film on silanised coverslips by creating a “sandwich” system with glass slides.

2.2.3 Preparation of PAAm Gels

PAAm hydrogels were formulated in PBS from base solutions of acrylamide 40% w/v and bisacrylamide 2% w/v. After stirring them to achieve the desired concentration, solutions were degassed through sonication under vacuum for 15 minutes. Crosslinking was initiated by

a mixture of ammonium persulfate and tetramethylethylenediamine (0.01%; 3:1). The gels were allowed to crosslink under argon with oxygen concentration below 2000 ppm for 30 minutes. Samples that were used for the rheological characterisation were prepared as discs (2 mm, r = 1.06 cm). Samples that were used for cell culture were prepared as thin film on silanised coverslips by creating a "sandwich" system with glass slides.

2.2.4 Sterilisation of ALMA and PAAm Hydrogels

UV-sterilisation (260 nm) was performed for 40 minutes and samples were then left in Penicillin-Streptomycin (10x) overnight. Samples were washed 5 times with sterile PBS and incubated with RPMI-1640 (FBS 10% v/v, penicillin-streptomycin 1% v/v, L-Glutamine 1% v/v) for 24 hours prior cell seeding.

2.2.5 *In Vitro* Hydrogel Swelling

Hydrogels were immersed in 15 mL PBS at 37 °C and weighed multiple times over a 6-day period. The swollen weight was expressed as a percentage increase from the initial hydrogel weight, recorded immediately after UV photo-crosslinking.

$$\text{Swelling } \% = \left[\frac{W_t - W_0}{W_0}\right] \cdot 100 \qquad \text{Equation 1}$$

2.2.6 Detachment Test

ALMA hydrogels were prepared in 48-well plate (h=2 mm) as described in paragraph 1. PBS (400 μl) was added to each well and attachment/detachment of the hydrogels to the bottom of the well plate was visually assessed every 24 hours for 6 days.

2.2.7 Scanning Electron Microscopy

Hydrogels were frozen overnight at −80 °C and subsequently freeze-dried for 24h (ModulyoD). Each sample was mounted on an aluminium stub using conductive carbon adhesive tape and sputter-coated with gold under argon atmosphere for 40 seconds at a current of 30 mA. Samples were placed in a FEI XL30 SEM under high vacuum and the working distance was optimised for each sample. Hydrogels were imaged at 10 kV(227).

2.2.8 Environmental Scanning Electron Microscopy

Hydrogels were prepared and left equilibrating in PBS for at least 24 h prior the analysis. Samples were placed in a FEI Quanta 650 ESEM and images were captured using an optimised working distance for each sample at 5-10 kV, while humidity was kept between 88.9 - 96.3%.

2.2.9 Optical Profilometry

Surface roughness of hydrated ALMA hydrogels was measured using an optical profilometer. Gels were equilibrated in PBS, blotted to remove excess liquid, and mounted on the stage. Scans were acquired in with a 50× objective over a 340 × 261 μm² area, with 3 regions per sample to account for heterogeneity. Arithmetical mean height (Sa) and root mean square height (Sq) were extracted from topography maps using the instrument's analysis software (Zeta 3D Analysis).

2.2.10 Mechanical Characterisation

Rheological measurements were performed with Anton-Paar rheometer, equipped with a 25 N load cell. Discs of ALMA and PAAm hydrogels were prepared ahead the measurements and incubated in PBS until they

reach the equilibrium swelling. Amplitude sweeps was carried out at a constant frequency of 1 Hz, between 1% and 1000% of shear strain. Frequency sweep was conducted within the linear viscoelastic (LVE) range, at a constant shear strain of 5% for ALMA and 3% for PAAm; storage and loss moduli were extrapolated at frequency 1 Hz. Stress relaxation was performed within the LVE range, at a constant shear strain of 5% for ALMA and 3% for PAAm; relaxation modulus was recorded for 1000 s and expressed as a percentage decrease from the initial relaxation modulus.

2.2.11 Mesh Size Measurement

Rubber elasticity theory was used to calculate mesh size of ALMA hydrogels. The crosslinking density ρ_x ($mol \cdot m^{-3}$) is determined from the storage modulus (G′, Pa), the universal gas constant (R, $J \cdot mol^{-1} \cdot K^{-1}$), and the absolute temperature (T, K), as shown in

$$\rho_x = \frac{G'}{RT} \qquad \text{Equation 2}$$

The mesh size ξ (m) is then calculated from the crosslinking density (ρ_x) and Avogadro's number N_A, according to Equation 2(231).

$$\xi = \sqrt[3]{\frac{6}{\pi \rho_x N_A}} \qquad \text{Equation 3}$$

2.2.12 Surface modification of ALMA Hydrogel

ALMA hydrogel was prepared as described in section 2.2.2. Surface modification was performed by adding EDC (0.05M) and NHS (0.025M) in MES Buffer (pH 4.7) on the hydrogel surface for 5min, 15min, 1h, 2h. Protein solutions were prepared in PBS (1% w/v BSA, 15 μM IgG, 20 μM GRGDSP) and added for 1h, 2h, 6h, 8h, 24h after

removing EDC-NHS solution. Surface-modified ALMA hydrogels were washed with distilled water to remove unreacted reagents.

2.2.13 Time-of-Flight Secondary Ion Mass Spectrometry (ToF SIMS)

Analysis was conducted by using a ToF-SIMS V instrument (IONTOF, GmbH). For surface analysis, a Bi_3^+ beam energy of 25 keV and a pulsed target current of ~0.3 pA were employed. A 500 μm × 500 μm region was analysed with pixel density 256 × 256. Low energy electron flood gun was used for charge compensation.

2.2.14 X-Ray Photoelectron Spectroscopy (XPS)

All samples were mounted onto stainless steel stubs using carbon sticky tabs. X-ray Photoelectron Spectroscopy (XPS) was conducted using a Kratos Axis Ultra DLD with a monochromatic Al X-ray source (1486.6 eV, 15 kV, 10 mA). Wide and high-resolution scans were conducted in addition to the measurement C 1s for calibration: charge corrected to 284.8 eV. Parameters for wide scan acquisition were as follows: 160 eV of pass energy, step size of 0.5 eV, and 1200s of scan time. Parameters for high resolution scan acquisition were as follows: 20 eV of pass energy, step size of 0.1 eV, and 1200s of scan time. Binding energies were measured over a range of 0–1300 eV. All spectra were analysed in CasaXPS constraining the Full Width at Half Maximum (FWHM) to the same value for all deconvoluted spectral peaks for the same element.

2.2.15 Monocyte Isolation and Differentiation

Buffy coats from healthy donors were obtained from the National Blood Service (Sheffield, UK) following ethics committee approval (2009/D055). Monocytes were isolated through positive selection

(CD14 magnetic beads), using MACS magnetic cell separation system. Isolated monocytes were prepared to a cell density of 1 x 10^6 cell/mL in RPMI-1640 medium (10% FBS, 1% L-glutamine, 1% streptomycin and penicillin, 10 ng/ml MCSF) and seeded on ALMA hydrogel. To ensure cells were only seeded on the hydrogels, non-cultured-treated plates were used, and media was changed after 24h to remove floating monocytes. Cells were incubated in a humidified incubator maintained at 37 °C and 5% CO_2 for 6 days (37 °C, 5% CO_2) until differentiation was completed; fresh media was added on day 3. Media was supplemented with MCSF (10 ng/ml) on day 1 and 3 to induce the differentiation into naïve macrophages. As a reference, monocytes were also cultured on tissue culture plastic at the same cell density and conditions(232). For M1 polarisation, media was supplemented with GM-CSF (50 ng/mL) and IFN-γ (20 ng/mL) on day 0 and 3. For M2 polarisation, media was supplemented with MCSF (50 ng/mL) and IL-4 (20 ng/mL) on day 0 and 3.

2.2.16 Live/Dead Viability Assay

On Day 6, media was removed, and macrophages were incubated with PBS containing a mixture of green-fluorescent calcein-AM (1:2000) and red-fluorescent ethidium homodimer-1 (1:500) for 30 minutes at 37 °C and 5% CO_2. Cells were imaged using an Olympus IX51 fluorescence microscope, with 10x objective.

2.2.17 ToxiLight Assay

20 µL of culture supernatant was collected and added to a white assay plate. 100 µL of adenylate kinase detection reagent was added and incubated at room temperature (RT) for 5 minutes. Luminescence was read using a plate reader (Promega GloMax® explorer). A negative (M0

macrophages cultured on TCP) and positive (M0 macrophages cultured on TCP and lysed after 6 days of culture using the Toxilight™ 100% lysis reagent) were included.

2.2.18 AlamarBlue Assay

AlamarBlue reagent was added directly to the culture medium at a final concentration of 10% (v/v), and plates were incubated at 37 °C in a humidified atmosphere with 5% CO_2, protected from light, for 3 hours. Fluorescence was measured at 560 nm excitation and 590 nm emission using a plate reader. Wells containing only PAAm gels in media and alamarBlue without cells were used as blanks, and macrophages seeded on tissue culture plastic (TCP) served as control. Fluorescence values were blank-subtracted and expressed as percentage of control.

2.2.19 Endotoxin Quantification Assay

ALMA 6% and PAAm 30% (19:1) hydrogels were incubated with PBS (1.5 ml) in humidified incubator maintained at 37°C and 5% CO_2 for 6 days (37 °C, 5% CO_2) to simulate cell culture conditions. Endotoxin standard solutions (0.1-0.01 EU/ml) and samples (50 µL) were added to 96-well plate and incubated with amoebocyte lysate solution (50 µL) for 25 minutes at 37 °C. Chromogenic substrate solution (100 ml) was added and incubated for 6 minutes at 37 °C. Acetic acid 25% v/v (50 µL) was added as stop solution and absorbance was read at 405 nm using a plate reader (Promega GloMax® explorer). The endotoxin concentration in each condition was calculated using a 4 point standard curve (**Figure S1**).

2.2.20 Immunostaining of Macrophages

Macrophages were fixed by incubation in paraformaldehyde 4% v/v (in PBS) for 15 min on day 1, day 3, and day 6. On Day 1 and 3, cells were

washed 3 times with 0.2% Tween-20 in PBS (0.2% v/v) followed by a blocking step with BSA (3% w/v) and glycine (1%) in PBS. Cells were washed 3 times with 0.2% Tween-20 in PBS and incubated with Phalloidin-iFluor 647 (1:1000) and DAPI (1:5000) in PBS (BSA 1% w/v) for 1 hour at RT. On day 6, cells were washed 3 times with 0.2% Tween-20 in PBS and two blocking steps were subsequently performed, firstly with BSA (3% w/v) and glycine (1%) in PBS, then with goat serum (5%) in PBS. Macrophages were washed 3 times with 0.2% Tween-20 in PBS and incubated with anti-human calprotectin mouse immunoglobulin G1 (IgG1) antibody (2 mg/ml) and anti-human CD206 (MR) rabbit IgG1 primary antibody (1 mg/ml) overnight at 4 °C. Cells were washed 3 times with 0.2% Tween-20 in PBS and incubated with AlexaFluor-488 goat anti-mouse IgG (8 mg/ml) and Rhodamine Red goat anti-rabbit IgG secondary antibody (8 mg/ml) for 1 hour at RT. Cells were further incubated with Phalloidin-iFluor 594 (1:1000) and DAPI (1:5000) in PBS (BSA 1% w/v) for 1 hour at RT. Cells were washed 3 times with PBS and imaged using a Leica TCS SPE confocal microscope(233). Image analysis was performed using CellProfiler software (http://www.cellprofiler.org/) to quantify the cell number, the eccentricity, the cell area, and the fluorescent signal corresponding to calprotectin and mannose receptor markers.

2.2.21 Enzyme-linked Immunosorbent Assay (ELISA)

For TNF-α, IL-6, IL-10, and CCL18, 384-plates were coated with 25 µL capture antibody (TNF-α: 4 µg/ml, IL-6, IL-10, and CCL18: 2 µg/ml) overnight on a rocker at RT. ELISA plates were washed 3 times with PBS containing 0.05% tween-20 (100 µL) and blocked with 75 µL BSA 1% w/v for 1 hour at RT. Supernatant was thawed and brought to RT.

Plates were washed 3 times with PBS containing 0.05% tween-20 (100 µL) and incubated with 25 µL supernatant and standard solutions (TNF-α: 1000-15.6 pg/ml, IL-6: 600-9.38 pg/ml, IL-10: 2000-31.2 pg/ml, and CCL18: 500-7.81 pg/ml) for 2 hours on a rocker at RT. Plates were washed 3 times with PBS containing 0.05% tween-20 (100 µL) and incubated with 25 µL detection antibody (TNF-α, IL-6, and IL-10: 50 ng/ml, CCL18: 100 ng/mL) for 2 hours on a rocker at RT. Plates were washed 3 times with PBS containing 0.05% tween-20 (100 µL) and incubated with 25 µL streptavidin-HRP conjugate (40-fold diluted) for 20 minutes while protected from light on a rocker at RT. Plates were washed 3 times with PBS containing 0.05% tween-20 (100 µL) and incubated with 25 µL TMB substrate for 20 minutes while protected from light on a rocker at RT. Sulfuric acid 1N (12.5 µL) was added as stop solution and absorbance was read at 450 nm and 570 nm using a plate reader (Promega GloMax® explorer). The cytokine concentration in each condition was calculated using a 7 point standard curve (**Figure S2A-D**).

2.2.22 Statistical Analysis

Hydrogel characterisation data is presented as mean ± standard deviation (SD) with each experimental condition tested in triplicate. Mechanical property and endotoxin data is presented as mean ± standard deviation of three experimental repeats (n = 3) per condition. Cell culture data is presented as mean ± standard error of mean (SEM) from three independent experiments (N = 3), each with three experimental repeats (n = 3) per condition. Statistical analysis was carried out in GraphPad PRISM 9.0. One-way ANOVA was performed to determine significant differences between experimental conditions ($\alpha = 0.05$). Tukey's post hoc test was performed for pair-wise comparisons. Pairs without significant differences were labelled as ns or not labelled. Pairs

with significant differences were labelled as *$p \leq 0.05$, **$p < 0.01$, ***$p < 0.001$ and ****$p < 0.0001$.

Chapter 3. Development of a Tuneable ALMA Hydrogel Platform to Mimic the Stiffness of Soft Tissues

3.1 Abstract

This chapter describes the systematic development, optimisation, and characterisation of alginate methacrylate (ALMA) hydrogels with tuneable stiffness and surface chemistry, aimed at investigating macrophage responses on substrates with mechanical properties mimicking a physiologically relevant range of soft tissue mechanics. ALMA hydrogels were prepared with varying polymer concentrations (2–6% w/v) and degrees of methacrylation (10–40%) to generate materials within a physiologically relevant stiffness rage to mimic soft tissues. Photoinitiator selection was optimised, with Irgacure-2959 at 0.5% w/v yielding stable hydrogels. Rheological characterisation revealed that stiffness increased with polymer concentration and degree of methacrylation, whereas photoinitiator concentration had negligible effects, demonstrating that network density predominantly governs mechanical properties. Surface functionalisation with proteins and small peptides was achieved via EDC/NHS chemistry, with covalent coupling verified by ToF-SIMS and XPS. Sterility was ensured through UV irradiation (260 nm) combined with antibiotic treatment, and sample preparation suitable for cell culture was optimised until obtaining thin hydrogel films on silanised coverslips. Collectively, this first chapter establishes a reproducible and versatile ALMA hydrogel platform with finely controlled mechanical and chemical properties, providing a robust basis for future cell-biomaterial mechanotrasduction studies.

3.2 Introduction

Hydrogels are widely used as biomimetic platforms because their intrinsic mechanical, chemical, and surface properties critically influence cellular behaviour, including adhesion, proliferation, differentiation, and immunological responses. Macrophages, as key immune cells, are particularly sensitive to changes in their microenvironment, making the design of biomaterials that modulate their polarisation and phenotype a rational strategy to minimise FBR and promote tissue integration.

This chapter is based on the hypothesis that the mechanical and chemical properties of ALMA hydrogels can be precisely tuned. Specifically, increasing polymer concentration and degree of methacrylation as well as type and concentration of photoinitiators are expected to produce stiffer gels. Additionally, functionalising the hydrogel surface with the GRGDSP peptide is further hypothesised to promote integrin-mediated macrophage adhesion and polarisation toward a pro-regenerative phenotype, supporting tissue integration and reducing inflammatory responses. The objectives are to optimise ALMA hydrogel formulations by varying polymer concentration, degree of methacrylation, photoinitiator type and concentration, to characterise mechanical properties of different ALMA formulations, their swelling behaviour and network stability. Other objectives are to functionalise and characterise ALMA hydrogel surfaces before and after conjugation with GRGDSP peptide.

This chapter presents the development, optimisation, and characterisation of ALMA hydrogels with tuneable mechanical properties and surface chemistry, establishing a physiologically relevant soft-tissue platform to investigate macrophage-biomaterial interactions.

ALMA hydrogels were systematically prepared with varying polymer concentrations (2-6% w/v) and degrees of methacrylation (10-40%) to cover a broad range of mechanical stiffness, more specifically from ~50 Pa to ~4.5 kPa. Photoinitiator selection was optimised, comparing Irgacure-2959 and lithium phenyl-2,4,6-trimethylbenzoylphosphinate (LAP) across multiple concentrations. Irgacure-2959 at 0.5% w/v was identified as optimal, yielding stable hydrogels with controlled swelling and structural integrity, whereas LAP-based hydrogels exhibited excessive swelling and network collapse within the first 24 hours. Rheological analysis revealed that stiffness increased with polymer concentration and methacrylation degree, while photoinitiator concentration had negligible impact.

Surface chemistry was tailored through functionalisation with the integrin-binding peptide GRGDSP. This short peptide was selected because it is widely used in the literature to functionalise polymers to promote cell attachment on substrates that do not naturally contain adhesion motifs(234). The RGD motif plays a pivotal role in cell adhesion, as it represents the minimal active sequence capable of binding to integrins, a superfamily of receptors through which cells mediate their attachment. Integrins are heterodimers composed of α and β subunits, with the binding site located at the N-terminus of the β subunit, which interacts directly with RGD peptides(235, 236). Peptides containing the RGD sequence are particularly useful because they retain functionality during biomaterial processing and sterilization, which often denatures full-length proteins. Moreover, synthetic peptides like GRGDSP lower the risk of immune reactions typical of proteins from xenograft sources, are easy to synthesise, and can be displayed on materials' surface with a better control over density and orientation(237). Directing interactions between cells and biomaterials toward wound-healing responses is essential to minimise FBR and

promote tissue integration. Beyond promoting cell adhesion, this biomimetic peptide has also been shown to prevent cell apoptosis, aid tissue regeneration(238), and reduce the release of pro-inflammatory cytokines in macrophage cultures(239). Covalent conjugation was performed and optimised via EDC/NHS chemistry, and the success of the reaction was confirmed through ToF-SIMS and XPS analyses. ALMA hydrogel surfaces presenting varying densities of GRGDSP were achieved by testing different peptide solution with GRGDSP concentrations ranging from 0.01 μM to 200 μM. Sterility and long-term stability were ensured through UV irradiation (260 nm) combined with antibiotic treatment for 24 hours, and covalent attachment to silanised coverslips prevented hydrogel detachment and floating during cell culture.

Overall, this chapter establishes a reproducible, versatile ALMA hydrogel platform with precisely controlled mechanical and chemical properties, providing a physiologically relevant system to investigate how stiffness and surface functionalisation influence human macrophage differentiation and polarisation in soft tissue-mimicking environments.

3.3 Results

Different variables were considered in preparing ALMA to achieve a variety of mechanical properties, including polymer concentration (2%, 3%, 4%, 6% w/v), degree of methacrylation (low: 10–20%, high: 30–40%), type of photoinitiator (Irgacure-2959 and lithium phenyl-2,4,6-trimethylbenzoylphosphinate (LAP)), and photoinitiator concentration (0.1%, 0.5%, and 1% w/v). The weight increase of hydrogels was determined gravimetrically by recording the initial dry weight (W_0) prior to immersion in PBS and the weight at each time point (W_t).

Initially, the two different photoinitiators, LAP and Irgacure-2959, were tested in the preparation of LDM ALMA 3% to identify the most suitable concentration. *In vitro* swelling (**Figure 3.3.1A**) demonstrated that Irgacure-2959 produced the most stable hydrogels, reaching the equilibrium swelling within 24 hours and remained intact for at least 6 days, thereby meeting the requirements for subsequent *in vitro* studies with macrophages. In contrast, hydrogels made with LAP nearly doubled in weight within 2 hours (**Figure 3.3.1B**) due to excessive water uptake, leading to structural weakening and eventual transition into a liquid state after 24 hours only. This instability rendered LAP-based hydrogels unsuitable for further mechanical characterisation and cell culture.

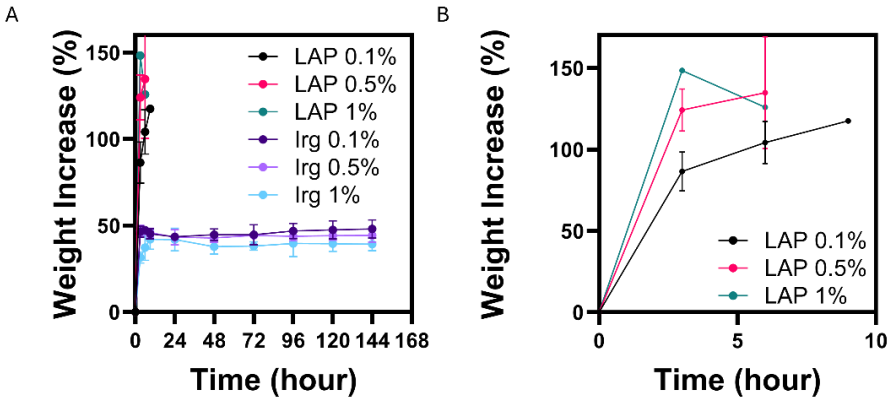

Figure 3.3.1 *In vitro* swelling of ALMA 3% prepared with Irgacure-2959 or LAP at different concentrations. (A) Comparison of LAP and Irgacure-2959 across 6 days. **(B)** Zoomed-in view of LAP during the first 24 hours. Data is presented as mean of triplicates ± SD (n=3).

On this basis, Irgacure-2959 was selected as the most suitable photoinitiator and subsequent studies with ALMA hydrogels of varying compositions were carried out to investigate how polymer and

photoinitiator concentrations as wells as ALMA degree of methacrylation influenced mechanical properties beyond swelling.

Given that stiffness is a critical physical cue influencing macrophage differentiation and phenotype(198, 240, 241), rheological properties of ALMA hydrogels were evaluated. The limit of the linear viscoelastic (LVE) region was first determined through amplitude sweep performed at a constant frequency of 1 Hz, a timescale relevant to cellular traction forces(205). The LVE region corresponds to the shear strain (γ %) range within which the hydrogel exhibits predominantly elastic (or solid-like) behaviour, with minimal viscous contributions. Mechanical properties of ALMA hydrogels were characterised at the equilibrium swelling to mimic cell conditions and ensure biological relevance. LVE regions of LDM and HDM ALMA hydrogels at 2% and 3%, prepared with Irgacure-2959 at concentrations ranging from 0.1% to 1% w/v, were established through amplitude sweeps (**Figure 3.3.2**). All the compositions exhibited a solid-like behaviours at strains below 10%.

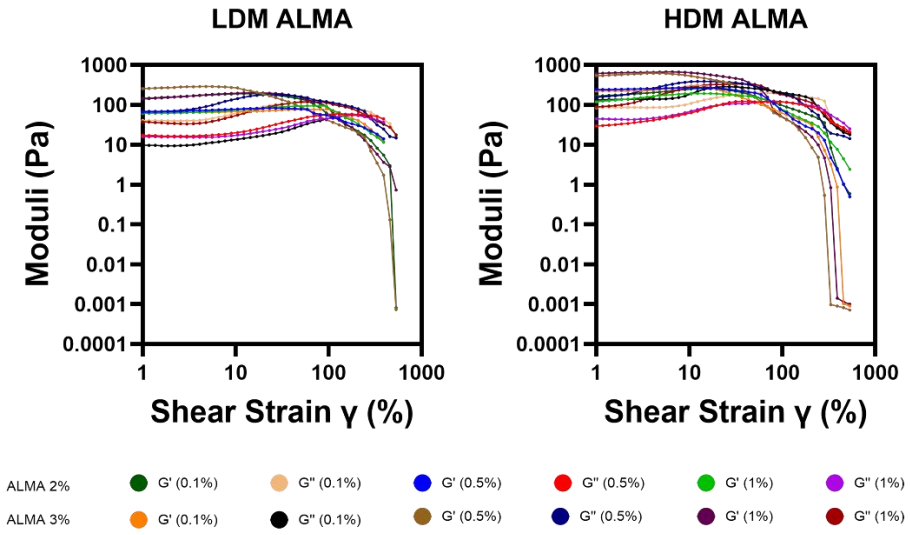

Figure 3.3.2 Amplitude Sweeps of LDM and HDM ALMA Hydrogels at 2% and 3% w/v obtained with Irgacure-2959 at

different concentrations. Data is presented as mean of triplicates ± SD (n=3).

For accurate determination of the storage (G′) and loss (G″) moduli, frequency sweep was performed within the LVE region, at a strain of 3%. The storage modulus (G′) reflects the elastic energy stored by the material and is an indicator of stiffness, while the loss modulus (G″) represents the viscous dissipation of energy. **Figures 3.3.3A** shows frequency sweep data of ALMA hydrogels with two degrees of methacrylation (low and high), two polymer concentrations (2% and 3%), and three concentrations of Irgacure-2959, to assess how these parameters influenced G′ and G″.

Across all conditions, G′ (squares) consistently exceeded G″ (triangles), confirming that all hydrogel formulations behaved predominantly as elastic solids rather than viscous fluids, as expected within the LVE region. G′ values, directly correlated with stiffness, were extrapolated at 1 Hz by linear regression and are summarised in **Figure 3.3.3B**. When comparing formulations with the same degree of methacrylation and polymer concentration but varying photoinitiator concentration, no significant changes in G′ were observed. In contrast, increasing ALMA concentration led to a clear rise in G′ in both LDM and HDM hydrogels, consistent with the formation of a denser polymer network.

These findings demonstrate that hydrogel stiffness is governed primarily by ALMA concentration and degree of methacrylation, while photoinitiator concentration does not exert a significant influence. This

highlights the tunability of ALMA hydrogels, allowing precise modulation of mechanical properties for targeted applications.

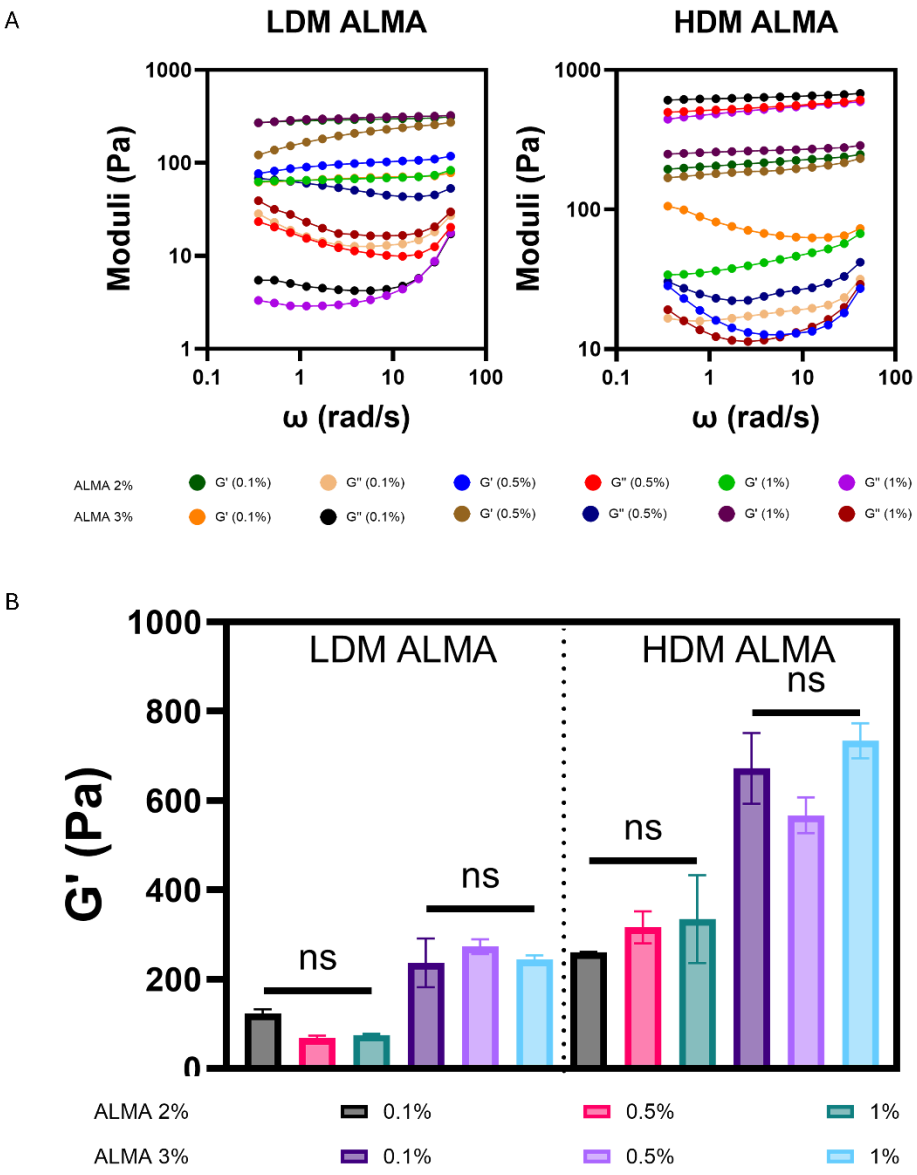

Figure 3.3.3 Rheological characterisation of ALMA Hydrogels. (A) Frequency sweeps and **(B)** extrapolate storage moduli (G') of ALMA 2% and 3% with varying concentration of Irgacure-2959. Frequency sweep was performed within LVE region (1% strain) and G' were extrapolated at 1 Hz. Data is presented as mean of triplicates ± SD (n=3).

Based on these initial results, the concentration of Irgacure-2959 was set at 0.5% w/v, as this represented the best compromise between sample preparation time and maximising the mechanical properties of the hydrogels. To further expand the achievable stiffness range, formulations with increasing ALMA concentrations were investigated, up to 6% w/v. Higher concentrations could not be tested due to solubility limitations of the polymer. Amplitude sweeps (**Figure 3.3.4A** and **Figure 3.3.4B**) were carried out to define the linear viscoelastic (LVE) region. All compositions showed to have a solid-like behaviour up to shear strain ~10%. To determine storage moduli of these compositions,

frequency sweeps (**Figure 3.3.4C-D**) was performed at 3% strain, value that falls within LVE of all the compositions characterised.

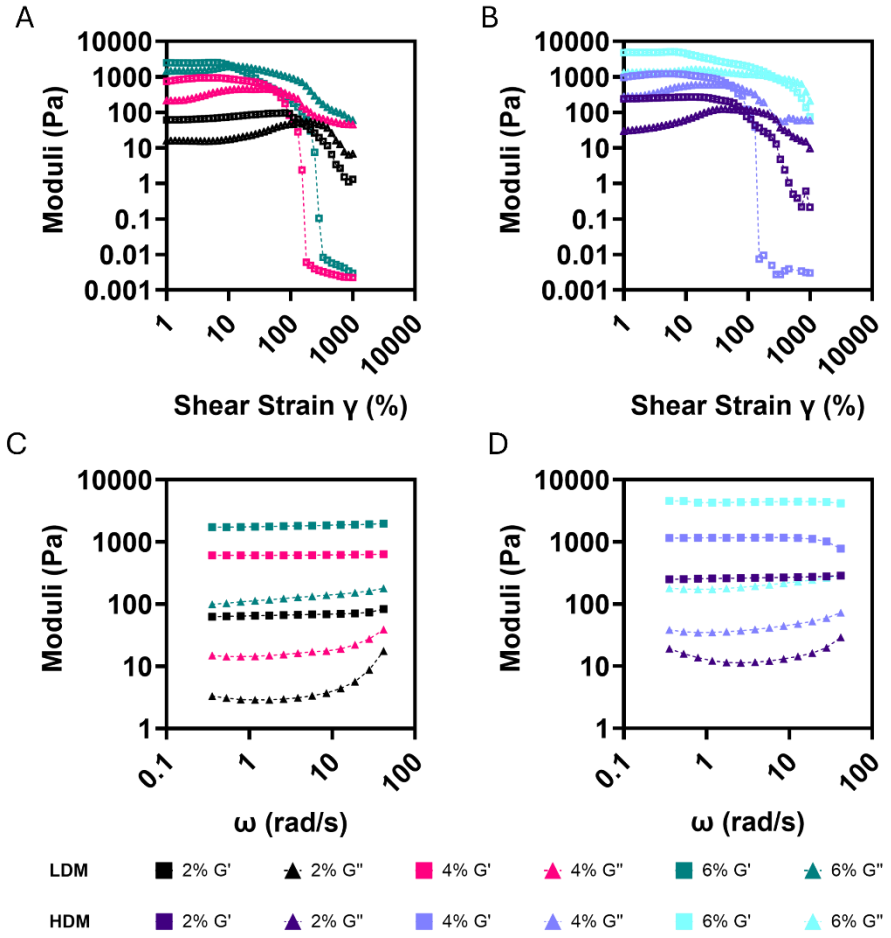

Figure 3.3.4 Mechanical characterisation of ALMA hydrogels. (A, B) Amplitude sweeps and **(C, D)** frequency sweeps of LDM and HDM ALMA hydrogels with concentrations ranging from 2% to 6% w/v. Frequency sweeps was performed at 3% strain. Data is presented as mean of triplicates ± SD (n=3).

G' values were extrapolated from the frequency sweeps at the biologically relevant value of at 1 Hz. Statistical analysis was performed to assess how variations in ALMA concentration and degree of methacrylation influenced the storage modulus, and thus the stiffness of

the different hydrogel compositions. No significant differences in G' were observed between 2% and 4% ALMA hydrogels, irrespective of the degree of methacrylation. Similarly, hydrogels with the same ALMA concentration but different degree of methacrylation did not differ significantly in stiffness at concentrations below 6% w/v. These results were encouraging for the subsequent viscoelasticity studies that will be discussed in Chapter 5. In contrast, HDM ALMA 6% hydrogels exhibited a markedly higher G' modulus (4426.6 Pa) compared to all other formulations, including LDM ALMA 6%, characterised by a lower degree of methacrylation (**Figure 3.3.5**).

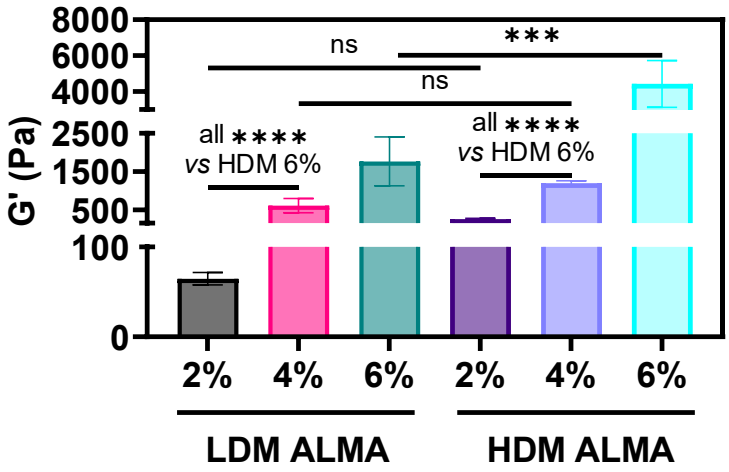

Figure 3.3.5 Storage Moduli of LDM and HDM ALMA Hydrogels. Data is presented as mean of triplicates ± SD (n=3).

Chemistry is another factor known to influence cell behaviour(220, 224, 242). ALMA hydrogels, owing to the presence of hydroxylic and carboxylic groups, offer the advantage of easy chemical modification, enabling functionalisation with a wide range of molecules, including immunomodulatory moieties and biomolecules. To establish a reliable method for surface modification of ALMA hydrogels, bovine serum albumin (BSA), a commonly used model protein, was employed to demonstrate the effectiveness of the conjugation strategy. The

modification, as shown in the schematic in **Figure 3.3.6**, followed a two-step procedure: (i) activation of carboxylic groups to NHS-esters in acidic conditions (MES buffer, 5 minutes), followed by (ii) protein conjugation in basic conditions (PBS buffer, 24 hours). This approach was adapted from established protocols employing EDC-NHS and EDC-Sulfo-NHS chemistry(243-245).

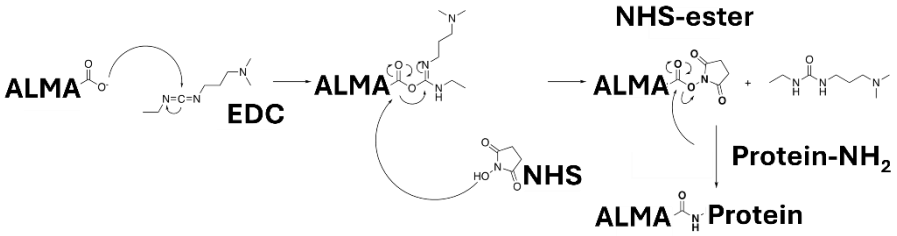

Figure 3.3.6 Reaction scheme for the surface modification of ALMA hydrogels.

To determine whether BSA was covalently bound rather than merely adsorbed, X-ray Photoelectron Spectroscopy (XPS) analysis was performed. ALMA hydrogels incubated with BSA in the absence of carboxylic activation (PA), as well as unmodified ALMA hydrogels (ALMA), were included as controls (**Figure 3.3.7A**). Quantification of N 1s peaks (**Figure 3.3.7B**), which originate exclusively from BSA since ALMA lacks nitrogen, did not reveal a statistically significant increase in nitrogen content for covalently modified samples compared to the ALMA with physically adsorbed BSA, although the average nitrogen signal appeared to be higher.

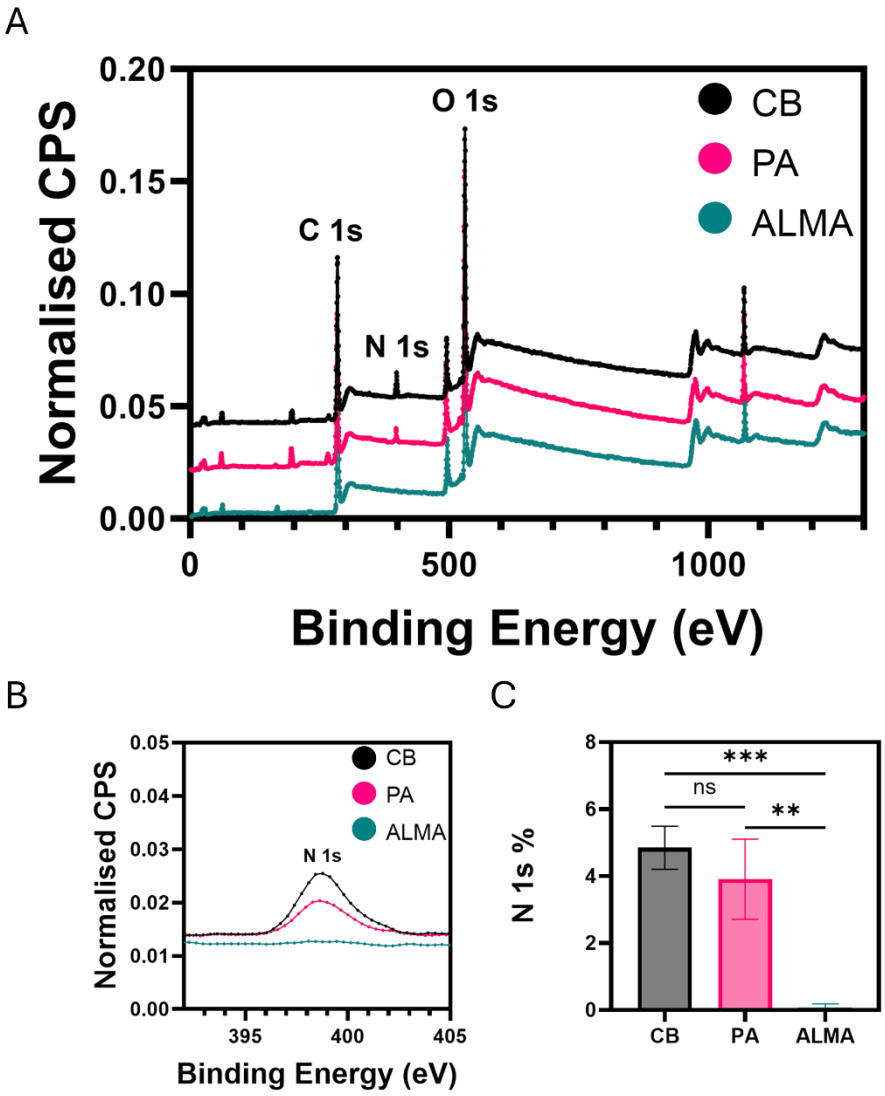

Figure 3.3.7 Surface analysis of modified and unmodified ALMA hydrogels (A) XPS wide-scan spectra and **(B)** enlarged N 1s peaks extracted from the wide-scan spectra, used to evaluate protein content on modified (CB) ALMA hydrogels. ALMA with adsorbed BSA (PA) and unmodified ALMA (ALMA) were used as controls. **(C)** Quantification of the integrated N 1s peak areas. Data is presented as mean of triplicates ± SD (n=3).

To investigate whether the conjugation was actually unsuccessful, Time-of-Flight Secondary Ion Mass Spectrometry (ToF-SIMS), a highly sensitive surface analytical technique, was also performed. **Figure 3.3.8A** presents ToF-SIMS spectra, which provide the chemical fingerprint of detected fragments, confirming the presence of BSA-specific signals compared to the controls. Corresponding ToF-SIMS images of the samples' surface analysed are shown in **Figure 3.3.8B-D**, showing clear differences across the surfaces of different ALMA hydrogels.

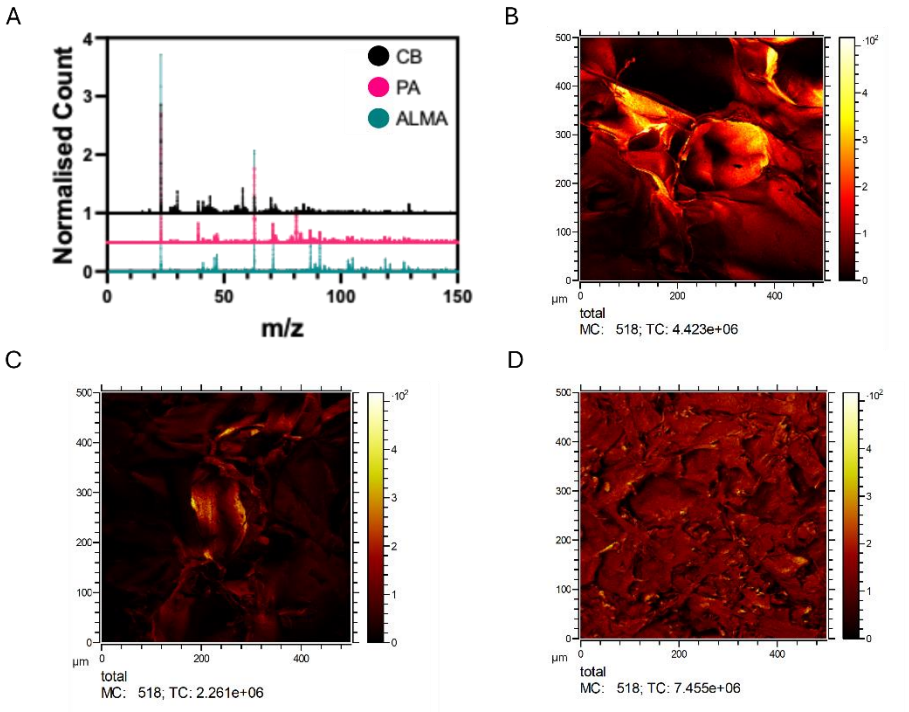

Figure 3.3.8 Surface analysis of modified and unmodified ALMA hydrogels by using ToF-SIMS. (A) Representative spectra of covalently BSA-modified ALMA hydrogels (CB), ALMA hydrogels with physically adsorbed BSA (PA), and unmodified ALMA hydrogels. Total ion images of **(B)** covalently BSA-modified ALMA, **(C)** ALMA with physically adsorbed BSA, and **(D)** unmodified ALMA hydrogels.

As shown in **Figure 3.3.9A–D**, both the peaks of representative BSA fragment ions and the corresponding surface images, which provide spatial and qualitative information on their localisation and relative abundances, revealed clear differences between ALMA hydrogels subjected to carboxylic activation followed by BSA conjugation and the control samples. These results further confirm the successful covalent attachment of BSA to ALMA surface, as evidenced by significantly higher peaks attributable exclusively to BSA-derived fragments, since ALMA does not inherently contain nitrogen atoms.

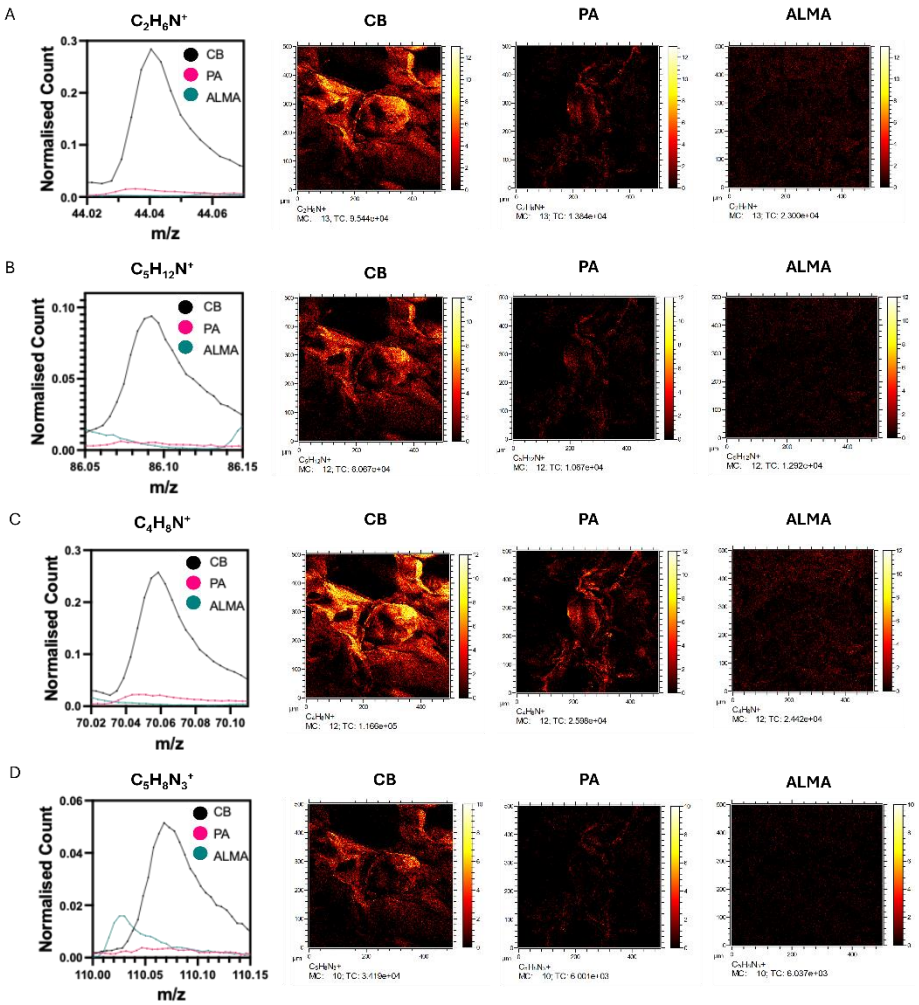

Figure 3.3.9 Enlarged peaks from the ToF-SIMS spectra used to assess BSA conjugation. (A) C2H6N+, **(B)** C5H12N+, **(C)** C4H8N+,

and **(D)** $C_5H_8N_3^+$ spectra and images of BSA-modified ALMA hydrogels (CB), ALMA hydrogels with physically adsorbed BSA (PA), and unmodified ALMA hydrogels.

Both ToF-SIMS and XPS demonstrated that the amount of BSA present on ALMA hydrogels subjected to carboxylic activation was greater than on samples where BSA was only adsorbed. This indicates that the protein was covalently conjugated to the hydrogel surface. Nevertheless, quantitative analysis of the XPS data did not reveal a statistically significant difference in the percentage of N 1s between hydrogels with chemically bound BSA (CB) and those with physically adsorbed BSA (PA), which may be attributed to suboptimal reaction conditions.

To achieve higher protein conjugation, the chemical reaction underwent an optimisation process in which key parameters were taken into consideration. Specifically, the activation time of carboxylic acids to NHS-esters and the conjugation time of the protein were optimised, and different reaction times were explored. ALMA hydrogels were subjected to surface modification using activation times ranging from 5 minutes to 2 hours, followed by 24 hours of BSA conjugation. XPS was performed to determine whether the amount of conjugated BSA was affected by this parameter (**Figure 3.3.10A,B**). An activation time of 15 minutes proved to be optimal, as it resulted in a significantly greater amount of conjugated BSA compared to activation for 5 or 60 minutes (**Figure 3.3.10C**). Moreover, the 15-minute activation condition showed the most pronounced difference in N 1s content relative to hydrogels with physically adsorbed BSA.

The superior performance observed with 15 minutes of activation can be attributed to the balance between efficient NHS-ester formation and the stability of these reactive intermediates. At shorter activation times (e.g. 5 minutes), the conversion of carboxylic groups to NHS-esters is

likely incomplete, leading to fewer available reactive sites for protein attachment. In contrast, at prolonged activation times (e.g. 60 minutes or longer), hydrolysis of NHS-esters becomes more prominent, decreasing their reactivity and thereby limiting effective protein coupling. Thus, the 15-minute activation period provided the optimal compromise, ensuring sufficient generation of reactive sites while minimising their premature hydrolysis, which ultimately translated into

the highest degree of BSA conjugation as reflected by the XPS N 1s signal.

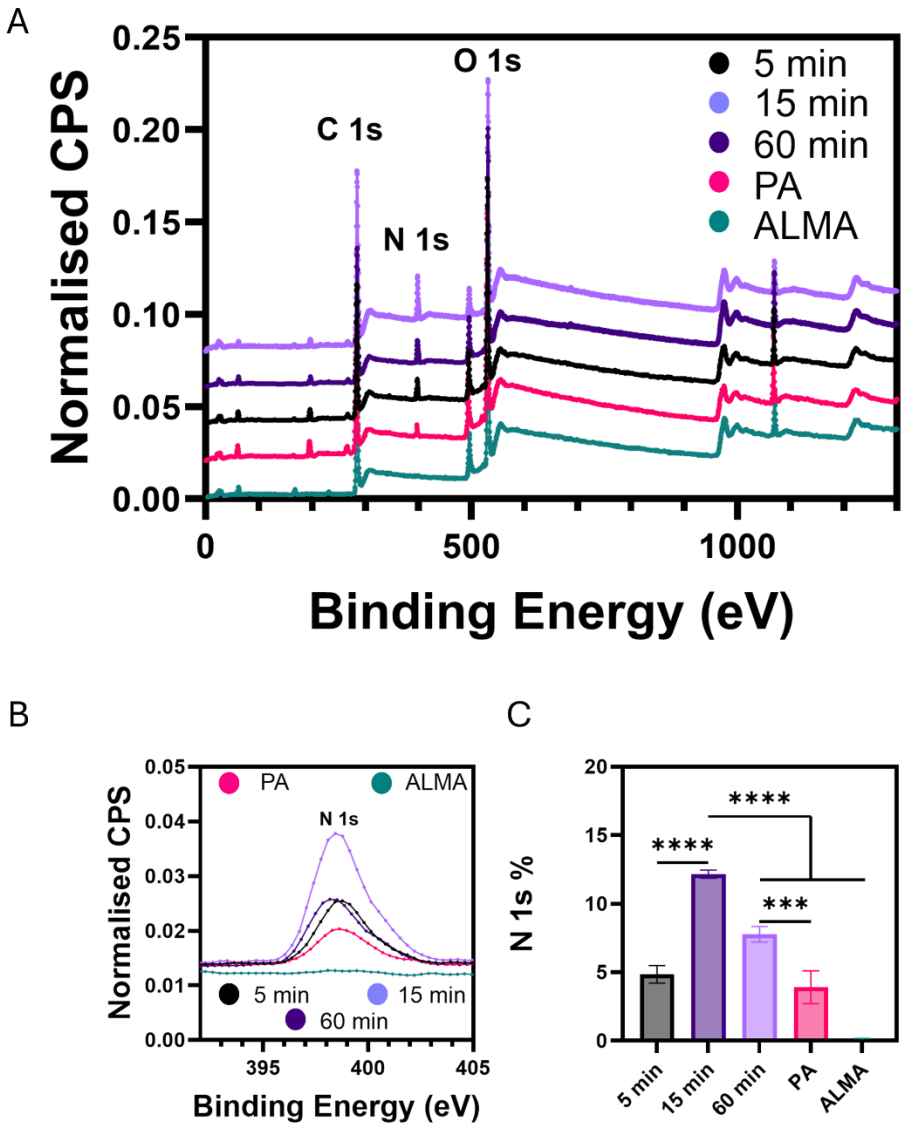

Figure 3.3.10 Surface analysis of ALMA hydrogels for carboxylic activation optimisation (A) XPS wide-scan spectra and **(B)** enlarged N 1s peaks extracted from the wide-scan spectra, used to evaluate protein content of chemically modified ALMA hydrogels after different carboxylic activation times, ranging from 5 minutes to 1 hour (ALMA). **(C)** Quantitative analysis of N 1s % on ALMA hydrogel surface

performed on XPS wide scan spectra. Data is presented as mean of triplicates ± SD (n=3).

As for the activation of the carboxylic groups, the optimal protein conjugation time was investigated by considering reaction times ranging from 1 to 24 hours. As shown in **Figure 3.3.11A** and **B**, N 1s peaks increased with longer conjugation times. Specifically, BSA conjugation rose from approximately 5% to 7% when the conjugation time was extended from 2 to 6 hours and reached about 12% after 24 hours (**Figure 3.3.11C**), representing the optimal time to achieve the highest protein conjugation. This finding suggests that shorter conjugation times are insufficient for complete reaction of the available NHS-esters,

whereas extending the process to 24 hours allows for more efficient utilisation of reactive sites, thereby maximising protein immobilisation.

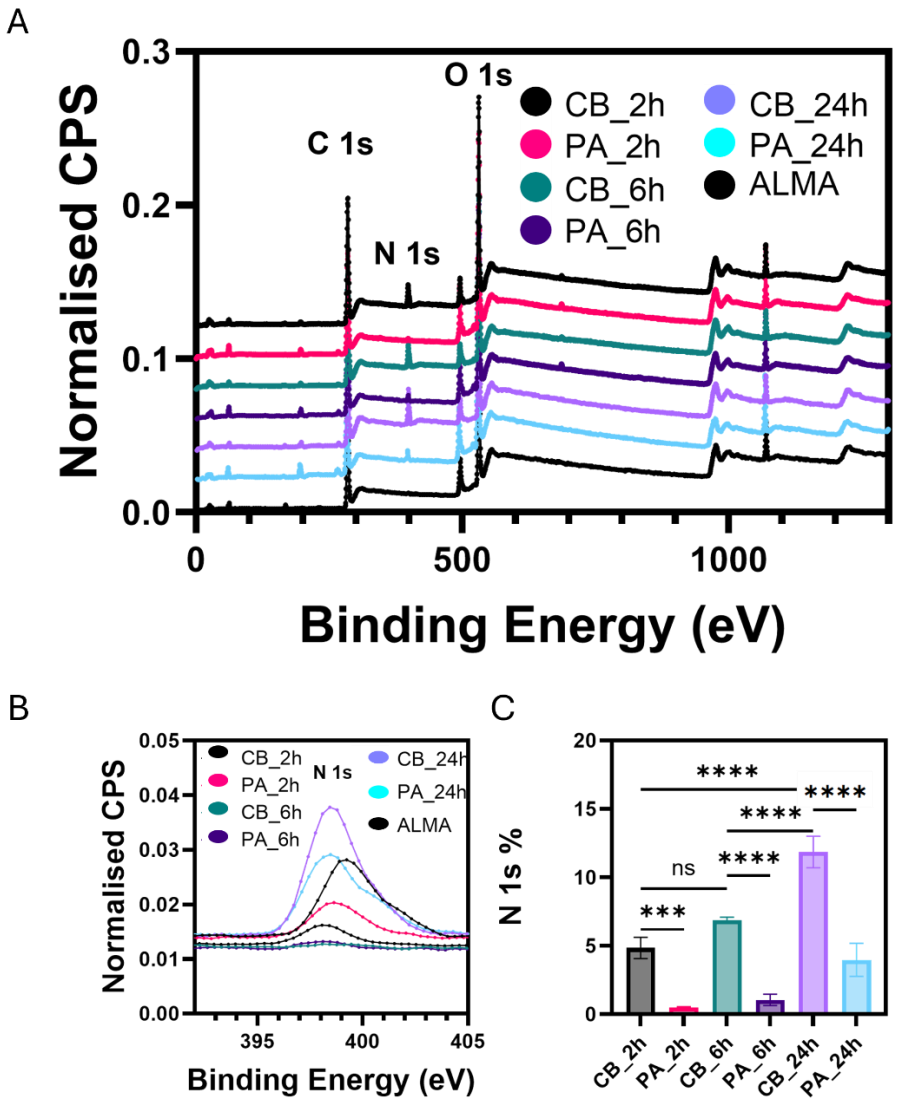

Figure 3.3.11 Surface analysis of ALMA hydrogels for carboxylic activation optimisation (A) XPS wide-scan spectra and **(B)** enlarged N 1s peaks extracted from the wide-scan spectra, used to evaluate protein content of chemically modified ALMA hydrogels after different conjugation times, ranging from 2 to 24 hours. **(C)** Quantitative analysis

of N 1s % on ALMA hydrogel surface performed on XPS wide scan spectra. Data is presented as mean of triplicates ± SD (n=3).

Overall, this optimisation process demonstrated that the optimal conditions for protein immobilisation involved a carboxylic activation time of 15 minutes and a conjugation time of 24 hours, as a significant increase in the N 1s percentage was observed when the conjugation period was extended from 2 to 24 hours, whereas no significant difference was detected between 2 and 6 hours.

Modified and unmodified ALMA hydrogels were qualitatively characterised for their topography and porosity using Scanning Electron Microscopy (SEM), by imaging both their surface and cross-sectional morphology. Samples with chemically bound (CB) and physically adsorbed (PA) BSA exhibited relatively homogeneous surfaces with evenly distributed ripples, whereas unmodified ALMA hydrogels displayed a more porous and irregular surface morphology (**Figure 3.3.12**). The cross-sections of all samples appeared highly porous, which is consistent with the removal of water from the three-dimensional network during the freeze-drying process.

The differences observed in surface morphology may be attributed to the presence of BSA at the hydrogel interface. In CB and PA samples, protein coverage could have smoothed out the underlying surface irregularities of the ALMA network, giving rise to a more homogeneous topography with evenly distributed ripples. In contrast, the unmodified ALMA hydrogels lacked this protein layer, and their surface appeared

more porous and irregular, reflecting the intrinsic microstructure of the polymeric network(246, 247).

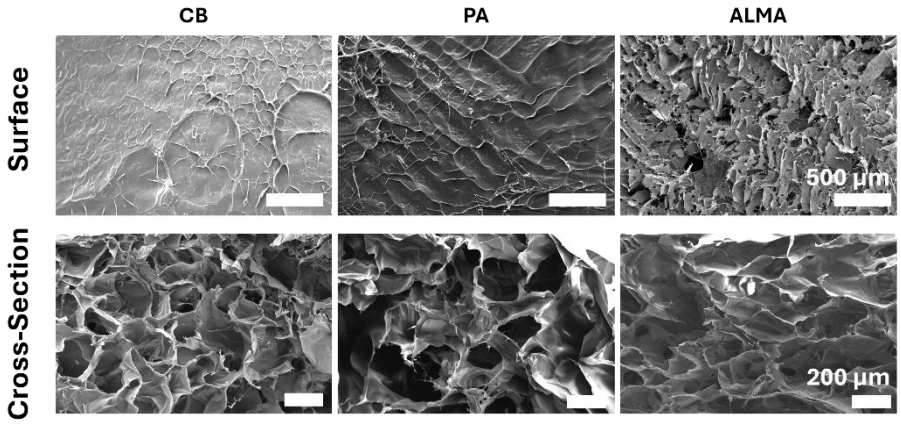

Figure 3.3.12 SEM analysis of ALMA hydrogels. Surface and cross-sectional images of covalently BSA-modified (CB), physically adsorbed-BSA (PA), and unmodified ALMA hydrogels.

To demonstrate the versatility of the ALMA hydrogel platform, surface modification was extended to immunoglobulin G (IgG, ~150 kDa) and GRGDSP (0.659 kDa), respectively a protein significantly larger and a peptide significantly shorter than BSA (~66.5 kDa). This experiment aimed to verify that molecules of different molecular sizes could be efficiently conjugated to the hydrogel surface, highlighting the adaptability of the conjugation strategy. Demonstrating this versatility was important, as it establishes the potential of ALMA hydrogel platform to present a wide range of bioactive cues - from small peptides to larger proteins - that can be tailored to modulate macrophage adhesion, differentiation, and polarisation in a controlled manner, providing value both within this thesis and for future applications. Successful immobilisation of both GRGDSP and IgG would confirm that ALMA hydrogels can serve as a flexible platform for functionalisation with a wide range of proteins, making them suitable for diverse biomedical applications.

IgG from bovine serum was used as a model antibody and optimal activation and conjugation times were applied to carry out the modification. XPS was performed to quantify N 1s % on the hydrogel surface (**Figure 3.3.13A** and **B**), which proved to be significantly higher in samples that underwent the carboxylic activation and IgG conjugation (CB) compared to hydrogels wherein IgG was only physically absorbed (PA) (**Figure 3.3.13C**).

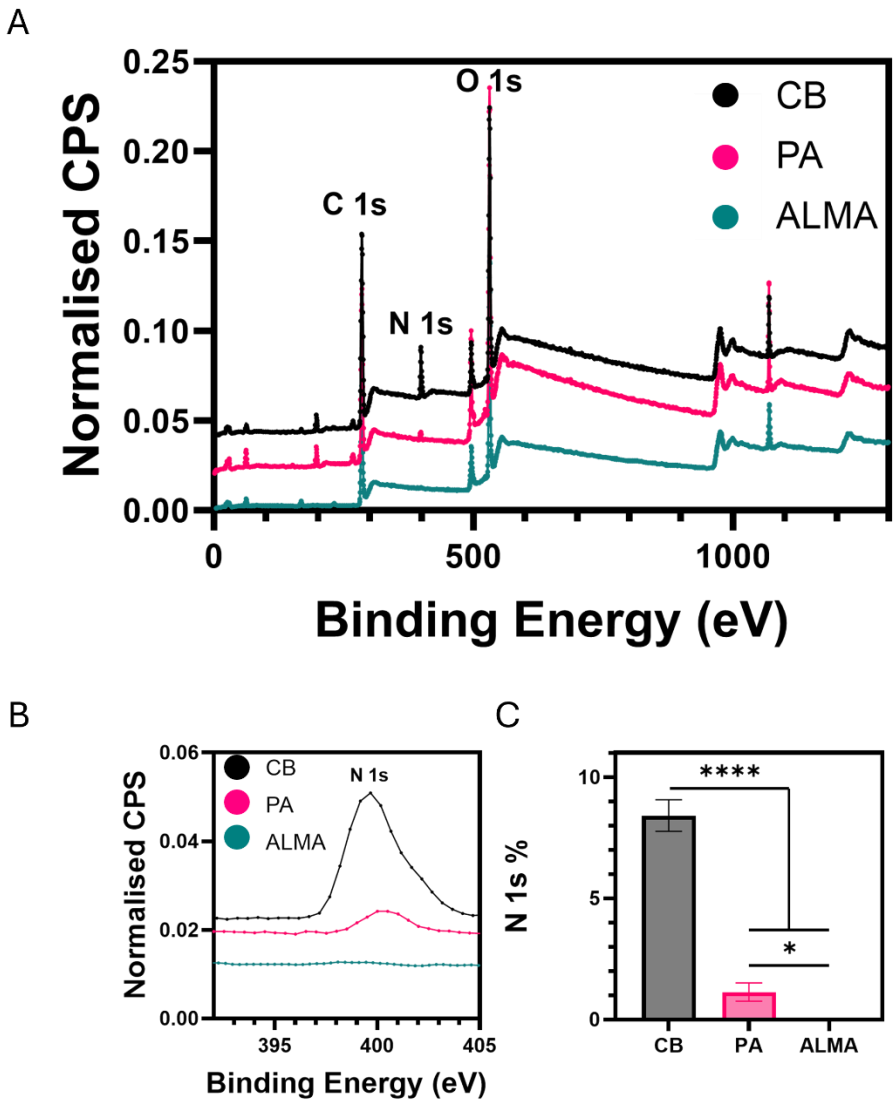

Figure 3.3.13 Surface analysis of ALMA hydrogels (A) XPS wide-scan spectra and **(B)** enlarged N 1s peaks extracted from the wide-scan

spectra, used to evaluate protein content of chemically modified ALMA hydrogels with IgG from bovine serum. **(C)** Quantitative analysis of N 1s % on ALMA hydrogel surface performed on XPS wide scan spectra. Data is presented as mean of triplicates ± SD (n=3).

Given the multifunctional properties of GRGDSP, a range of GRGDSP solutions (0.01–200 μM) were tested to optimise the conjugation step and achieve different densities of this peptide on ALMA surface. The density and spatial distribution of RGD motifs are critical for effective integrin binding. Efficient cell adhesion depends not only on the presence but also on the availability, surface display, spacing, and clustering of pro-attachment motifs. High peptide densities may enhance adhesion but can also lead to steric hindrance or improper orientation, whereas low densities may reduce binding efficiency. Surface chemistry, hydrogel stiffness, and topography can further modulate how GRGDSP interacts with cells, influencing adhesion strength, focal adhesion formation, and downstream signalling pathways. XPS analysis, with N 1s peaks serving as indicators of peptide conjugation on the ALMA surface (**Figure 3.3.14A** and **B**) showed maximal peptide immobilisation when using a concentration of 20 μM (**Figure 3.3.14C**). Increasing the concentration beyond this point did not enhance conjugation, likely due to saturation of available carboxylic groups at 20 μM, or steric hindrance, whereby excess peptide may adopt conformations that restrict access to reactive sites. Based on these findings, all subsequent GRGDSP-functionalised ALMA hydrogels were prepared using 20 μM peptide solution.

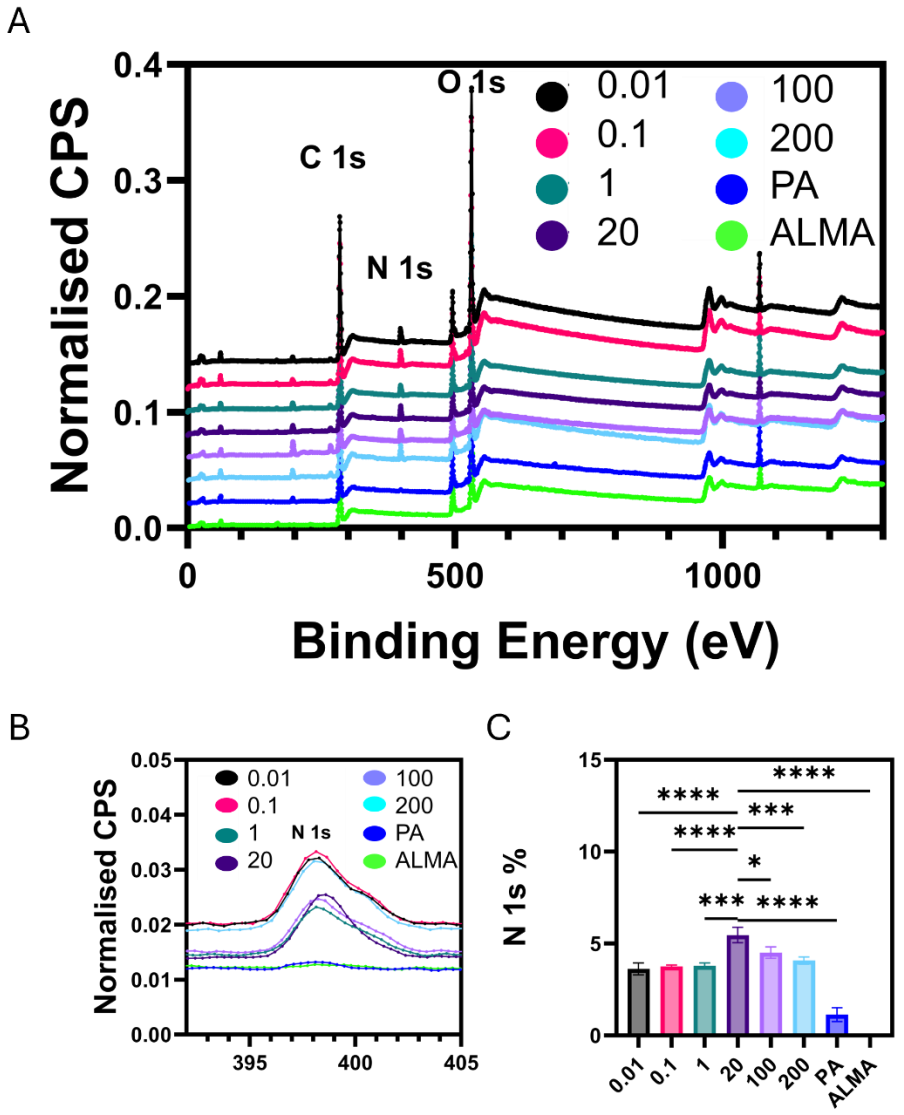

Figure 3.3.14 Surface analysis of GRGDSP-modified ALMA hydrogels. (A) XPS wide-scan spectra and **(B)** enlarged N 1s peaks extracted from the wide-scan spectra, used to evaluate GRGDSP conjugation to ALMA hydrogel surfaces using solutions at different concentrations. **(C)** Quantitative analysis of N 1s % on ALMA hydrogel surface performed on XPS wide scan spectra. Data is presented as mean of triplicates ± SD (n=3).

To analyse the non-specific protein adsorption coming from the environment, we performed XPS on GRGDSP-modified and

unmodified samples before and after incubation with complete media containing 10% (v/v) foetal bovine serum (FBS). All synthetic RGD-containing peptides have been shown to exhibit lower potency compared to the natural protein fibronectin(248), therefore, it is important that GRGDSP-modified ALMA hydrogels possess a reduced capacity for non-specific protein adsorption. Fibronectin, a ubiquitous glycoprotein highly involved in fibrosis(249), binds to integrins and can compete with synthetic peptides for cell attachment. Consequently, GRGDSP must be present at sufficient density on the hydrogel surface to outcompete fibronectin and exert its intended biological effect.

N 1s % attributed solely to GRGDSP (**Figure 3.3.15A**) and to GRGDSP with adsorbed proteins (**Figure 3.3.15B**) were determined for each condition. The contribution of GRGDSP alone was subtracted from the total N 1s signals to calculate the amount of proteins adsorbed onto the different hydrogel surfaces (**Figure 3.3.15C**). GRGDSP-modified hydrogels (CB) demonstrated significantly lower protein adsorption compared to the controls.

The reduced protein adsorption observed on CB_GRGDSP hydrogels can be attributed to the presence of a dense, covalently immobilised layer of GRGDSP on the hydrogel surface. This peptide layer likely occupies available reactive sites and sterically hinders non-specific binding of serum proteins, effectively limiting adsorption. In contrast, hydrogels with physically adsorbed GRGDSP (PA) or unmodified ALMA lack a stable, covalently attached peptide layer, allowing more serum proteins to interact with and adhere to the surface. Another possible explanation for reduced protein adsorption on the GRGDSP-modified ALMA lies in the zwitterionic nature of this small peptide. The presence of GRGDSP may attract water molecules through hydrogen bonding and ionic solvation, thereby strengthening the hydration layer

and further reducing non-specific protein adsorption(175, 250, 251). Additionally, the presence of a hydration layer can increase the energy barrier for protein adsorption, making it more difficult for proteins to displace water molecules and adhere to the surface. This mechanism is particularly effective in preventing biofouling, as it hinders the initial adhesion of proteins that could lead to subsequent cell attachment and biofilm formation(252, 253).

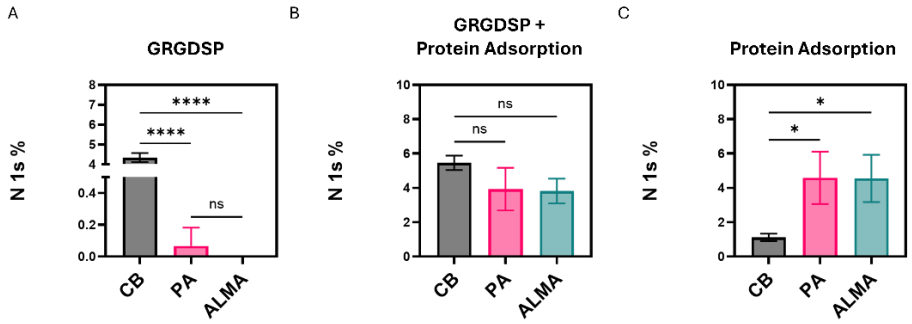

Figure 3.3.15 Quantitative analysis of N 1s content on ALMA hydrogels. N 1s % of chemically bound (CB) and physically adsorbed (PA) GRGDSP, as well as unmodified ALMA hydrogels, incubated **(A)** or not incubated **(B)** for 24 hours in complete media containing 10% (v/v) FBS. **(C)** N 1s % attributed solely to proteins adsorbed on the hydrogel surfaces. Data is presented as mean of triplicates ± SD (n=3).

It was also possible to establish the thickness of the protein layer on different ALMA hydrogels by using Equation 4 from Ray S. et al(254).

$$d_{N\ (1s)} = -L_{N(1s)} cos\theta ln\ (1 - \frac{[N]-[N]_0}{[N]_0-[N]_\infty}) \qquad \text{Equation 4}$$

Where L = electron attenuation length (3.02 nm), cos(θ) = 1, [N] = measured nitrogen fraction on surfaces of samples that were incubated in complete media, $[N]_\infty$ = atomic fraction of nitrogen in the pure protein (15%), $[N]_0$ = measured nitrogen fraction on surfaces of samples that were not incubated in complete media.

As shown in **Figure 3.3.16**, the thickness of adsorbed protein on GRGDSP-modified hydrogels (CB) was reduced by approximately 3-fold compared to both unmodified ALMA hydrogels (ALMA) and hydrogels with physically adsorbed GRGDSP (PA), further confirming that covalent surface modification significantly decreases non-specific protein adsorption.

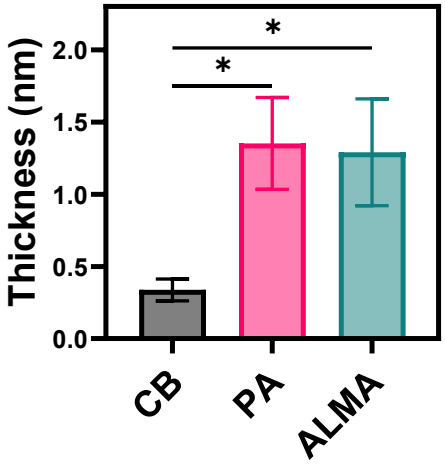

Figure 3.3.16 Thickness of the protein layer adsorbed on ALMA hydrogels. Protein thickness on CB, PA, and unmodified ALMA hydrogels after 24 hours of incubation in complete media containing FBS 10% (v/v). N 1s percentages were used to calculate protein layer thickness according to Equation 4. Data is presented as mean of triplicates ± SD (n=3).

To conduct cell culture studies, it was important to assess whether ALMA hydrogels did not detach from the bottom of the well plate within 6 days, which corresponded to the period cell were cultured.

ALMA hydrogels were prepared at different concentrations and degree of methacrylation, and their attachment was assessed every 24 hours for 6 days. Despite the composition, ALMA hydrogels started detaching from day 4, as show in **Figure 3.3.17**

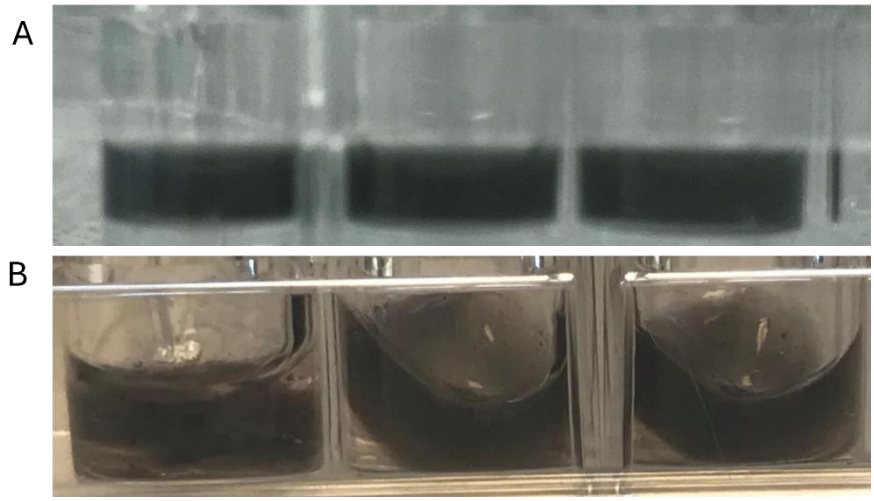

Figure 3.3.17 Representative images of ALMA hydrogels before and after media incubation. Photographs of ALMA hydrogels **(A)** before and **(B)** after 4 days of incubation in complete media in a 96-well plate, illustrating hydrogel detachment and stability over time.

To overcome this limitation, coverslips were functionalised by silanisation with 3-(Trimethoxysilyl)propyl methacrylate(230). The methacrylic moieties introduced on the glass surface enabled covalent conjugation of the hydrogel. Upon exposure to UV light, a radical polymerisation reaction was initiated, leading to the formation of the three-dimensional hydrogel network and covalent bonds between the methacrylic groups of the hydrogel and those on the coverslip, as shown in the schematic represented in **Figure 3.3.18**.

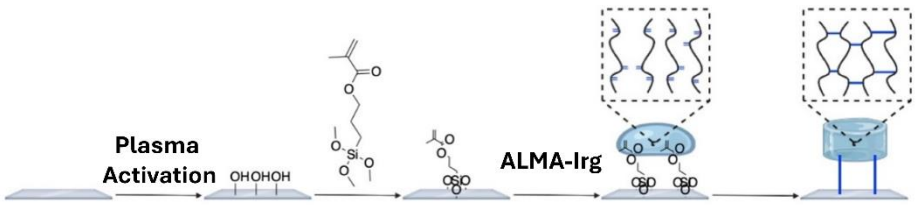

Figure 3.3.18 Coverslip silanisation and ALMA hydrogel formation. Schematic illustration of coverslip functionalisation with 3-

(Trimethoxysilyl)propyl methacrylate and subsequent covalent conjugation of ALMA hydrogel through photo-polymerisation.

An additional consideration was the need to sterilise ALMA hydrogels. Because neither ALMA nor Irgacure-2959 were supplied in sterile form, several preparation methods were taken into consideration to reliably generate sterile hydrogels. Filtration of the ALMA–Irgacure-2959 solution was initially investigated. To evaluate this approach, LDM ALMA 2% w/v solutions were filtered, and hydrogels were subsequently prepared in 96-well plates (**Figure 3.3.19A**) and incubated in PBS for 6 days. As shown in **Figure 3.3.19B**, the hydrogels dissolved over the observed period, suggesting that filtration reduced ALMA concentration and compromised the formation of a stable and reproducible 3D network.

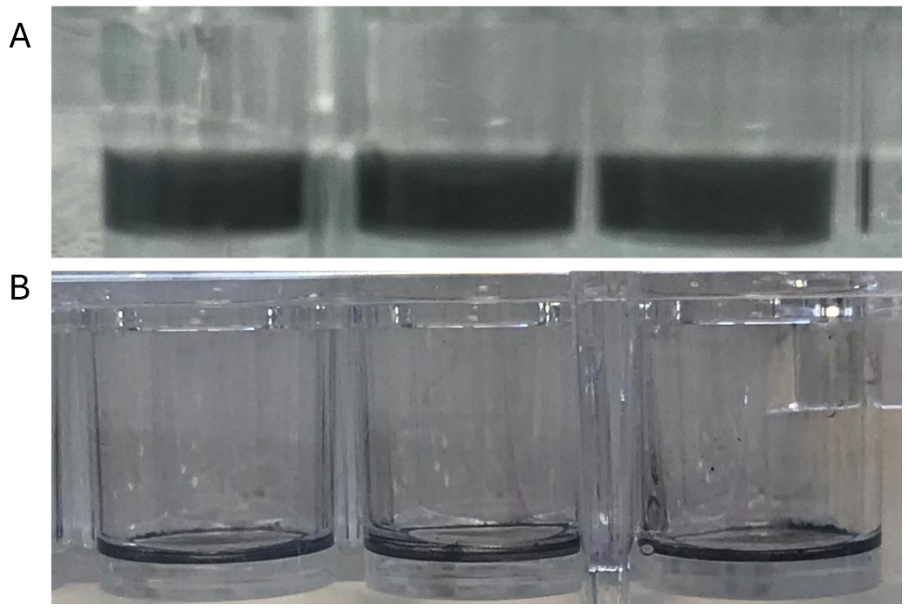

Figure 3.3.19 Photographs of hydrogels prepared from filtered ALMA–Irgacure solutions (A) before and (B) after PBS incubation, demonstrating the negative outcome of this sterilisation method.

Since direct production of sterile ALMA hydrogels was not feasible, an alternative sterilisation method was developed. Hydrogels were first prepared and then exposed to UV light (260 nm) for 40 minutes. Following UV treatment, the hydrogels were incubated with a 10% solution of penicillin and streptomycin for 24 hours. After this incubation, the hydrogels were washed five times with PBS to completely remove residual antibiotics, preventing any potential effects on subsequent cell responses. This combined sterilisation strategy was chosen to ensure hydrogel sterility while preserving the structural and mechanical integrity of the hydrogel network. UV irradiation effectively inactivates microorganisms on the hydrogel surface without introducing chemical residues, while the subsequent incubation with antibiotics ensures elimination of any remaining contaminating bacteria.

3.4 Discussion

The performance of hydrogels as substrate to study the cell-material interactions critically depends on their structural integrity, mechanical properties, and surface functionality. To address these factors, a systematic evaluation of ALMA hydrogels was undertaken, beginning with the choice of photoinitiator. LAP proved to be an unsuitable photoinitiator as the hydrogels exhibited excessive swelling and poor structural stability, ultimately transitioning to a liquid state within 24 hours. In contrast, Irgacure-2959 yielded stable hydrogels across all tested concentrations (0.1%–1% w/v), which reached equilibrium swelling within 24 hours and maintained stability for at least 6 days. Accordingly, Irgacure-2959 was selected as the optimal photoinitiator.

Rheological characterisation then revealed how composition influenced hydrogel mechanics. Amplitude and frequency sweeps demonstrate that the storage modulus (G′) - a direct indicator of hydrogel stiffness -

increased with polymer concentration but remained unaffected by changes in the photoinitiator concentration. These results confirmed that stiffness is governed primarily by polymer concentration. A pronounced increase in G′ was observed at 6% w/v ALMA in HDM hydrogels compared to the other formulations, indicating the formation of a denser and more robust network. Interestingly, below this threshold, the degree of methacrylation, namely the crosslinking density, did not markedly influence stiffness, when comparing hydrogels of equal ALMA concentration, providing flexibility for future studies investigating the effect of viscoelasticity on human macrophages.

The versatility of ALMA hydrogels was further demonstrated through successful surface functionalisation. BSA was initially used as a model protein to validate the conjugation chemistry, due to its low cost and high availability. Carboxylic groups on the hydrogel surface were activated with EDC/NHS, enabling covalent binding of BSA. Optimisation identified an activation time of 15 minutes and a conjugation time of 24 hours as optimal, as confirmed by XPS analysis. The same strategy was successfully extended to bovine serum IgG, as a model antibody, and to GRGDSP, a short peptide, thereby demonstrating its applicability across molecules of widely different molecular weights.

GRGDSP, a biomimetic peptide known to promote cell adhesion and modulate immune responses, was efficiently immobilised under the optimised conjugation conditions, with maximal attachment achieved at 20 μM peptide solution. This concentration was identified as optimal, likely due to limitations in available reactive groups and steric hindrance at higher peptide concentrations. Importantly, GRGDSP-modified hydrogels exhibited an anti-fouling behaviour, with significantly reduced non-specific protein adsorption compared to unmodified

ALMA hydrogels. This feature is critical for immunomodulatory biomaterials, as it is more likely that cell–substrate interactions are driven primarily by the intended biofunctionalisation rather than random protein deposition.

To enable long-term cell culture, ALMA hydrogels were covalently anchored to silanised coverslips bearing methacrylic groups, preventing detachment and floating while culturing cells. This strategy ensured mechanical stability and minimised disturbance of the system. Sterilisation challenges were also addressed: conventional filtration compromised reproducibility of the hydrogel composition and was therefore replaced with a two-step procedure involving UV irradiation followed by antibiotic incubation. This approach preserved hydrogel properties while ensuring sterility and reproducibility of the mechanical properties, a prerequisite for downstream biological studies.

3.5 Conclusion

This chapter demonstrated that ALMA hydrogels with finely tuneable mechanical and chemical properties can be reliably fabricated for mechanotrasduction studies with macrophages. Hydrogels with different stiffnesses, ranging from ~50 Pa to ~4.5 kPa, were obtained by adjusting polymer concentration and degree of methacrylation, while photoinitiator type and concentration were optimised to achieve consistent crosslinking and mechanical reproducibility. Surface functionalisation of ALMA hydrogels with different proteins and peptides, including BSA, bovine IgG, and GRGDSP, was successfully achieved and optimised. GRGDSP-modified hydrogels were prepared using solutions at concentrations ranging from 0.01 μM to 200 μM, creating a well-defined platform to investigate how differences in ligand densities affect macrophage adhesion and polarisation. This chapter

establishes a robust and reproducible platform for fabricating ALMA hydrogels with precisely controlled mechanical properties and surface chemistry, enabling the production of stable, cell-compatible hydrogels. Collectively, these findings lay the foundation for Chapter 4, where the effects of surface chemistry and stiffness on monocyte-derived macrophages will be investigated.

Chapter 4. Soft Tissue-Mimicking Hydrogel Stiffness Modulates Polarisation of Human Monocyte-derived Macrophages

4.1 Abstract

Minimising the foreign body response (FBR) to implants remains an unmet clinical challenge. The mechanical properties of biomaterials, particularly stiffness, have been shown to influence macrophage activation and FBR. However, current literature on the effects of material stiffness on macrophage activation presents conflicting results. These inconsistencies may stem from the use of cell lines or murine primary cells, which do not fully represent the behaviour of primary human monocyte-derived macrophages. Additionally, many previous studies have focused on stiffness values that fall outside the physiological range of soft tissues. In this study, we investigated how variations in stiffness affect the activation status of human monocyte-derived macrophages using alginate methacrylate (ALMA) hydrogels. The hydrogel stiffness was tuned within a physiologically relevant range (0.25 – 4.5 kPa) to mimic the mechanical properties of soft tissues. We found that increasing hydrogel stiffness consistently upregulated pro-inflammatory markers. Specifically, the stiffest hydrogel (ALMA 6% w/v) induced higher secretion of TNF-α and increased the calprotectin-to-mannose surface maker ratio, both hallmarks of inflammatory macrophages. Moreover, macrophages cultured on stiffer hydrogels exhibited a more elongated morphology and greater spreading. These findings provide new insight into how small changes in stiffness, within

a soft tissue-relevant range, can modulate the inflammatory behaviour of human macrophages. Our results, together with findings from the literature, suggest that the contradictory data on the effects of stiffness on macrophages may be attributed to other factors, such as viscoelasticity, surface chemistry, and protein absorption, which warrant further investigation.

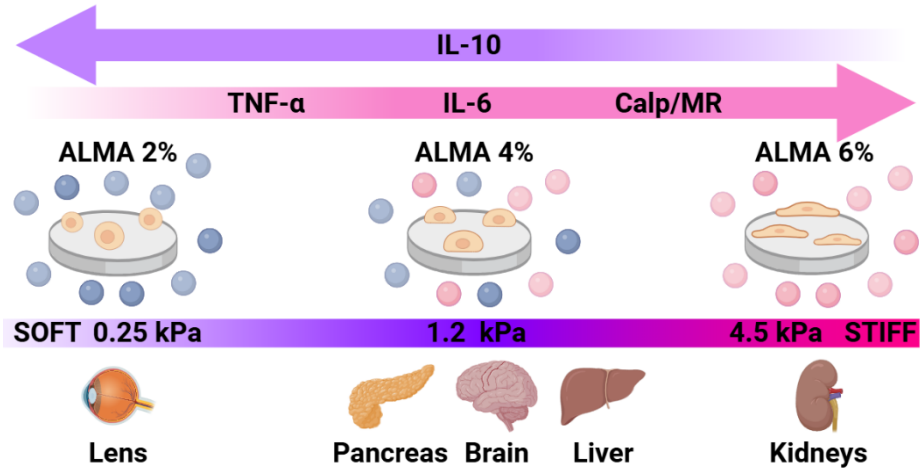

Figure 4.1.1 Schematic showing the effect of hydrogel stiffness on macrophage morphology and phenotype.

4.2 Introduction

Both chemical and mechanical properties of biomaterials contribute to directing macrophage polarisation(196, 255). Importantly, cells do not interact directly with the material itself, but more specifically with binding motifs present at the material surface, which may arise from the material's intrinsic composition or from adsorbed proteins derived from serum or culture medium(224, 256-260). Through integrin-based adhesion complexes, which couple the extracellular environment to the cytoskeleton(225), variations in chemistry and protein adsorption can alter adhesion strength and activate distinct mechanotrasduction

pathways. These processes ultimately affect gene expression and macrophage function, as shown in previous studies(256, 257, 259).

Beyond chemistry, stiffness is another key feature that has demonstrated to deeply affect cellular activities. In the context of macrophages, several studies have reported that stiffer substrates promote M1 polarisation. For example, in a study using RAW 264.7 cells, a mouse macrophage cell line, M1 polarisation was significantly reduced on the polyethylene glycol (PEG) hydrogel with a lower modulus (130 kPa), compared to stiffer hydrogels (240 kPa and 840 kPa). Additionally, when these gels were tested *in vivo*, the softest hydrogel resulted in the thinnest layer of macrophages at the implant site(197). Similarly, a study using polyacrylamide hydrogels showed that the stiff gel (323 kPa) drove THP-1-derived macrophages towards a pro-inflammatory phenotype with impaired phagocytosis, while soft (11 kPa) and medium (88 kPa) gels induced an anti-inflammatory and highly phagocytic phenotype(198). In another work, methacrylate gelatine (GelMA) hydrogels with different stiffnesses (2, 10 and 29 kPa) were tested using primary mouse bone marrow-derived macrophages. The stiffer hydrogel induced a pro-inflammatory phenotype, increased cell spreading and promoted a more severe *in vivo* inflammatory response(199). In contrast, the softer GelMA supported greater cell infiltration but resulted in thinner fibrotic capsule formation. Furthermore, another study examined the response of primary mouse bone marrow-derived macrophages on soft (0.3 kPa) and stiff (230 kPa) polyacrylamide hydrogels, showing that soft substrates induced less pro-inflammatory mediators than stiff ones(261).

Conversely, other studies have reported opposite trends, highlighting the complexity of macrophage responses to substrate stiffness. One work on polyacrylamide gels, with stiffnesses ranging from 2.55 kPa to 63.53

kPa, showed that the low-stiffness gel promoted M1 polarisation in mouse bone marrow-derived macrophages, whereas the intermediate stiffness gel induced an anti-inflammatory phenotype(200). In another study using RGD-coated soft polyvinyl alcohol gels, the softest gel (0.56 kPa) induced a stronger inflammation compared to medium (13.42 kPa) and high stiffness (56.25 kPa) gels in both RAW264.7 cells and mouse bone marrow-derived macrophages. *In vivo* experiment in C57BL/6 mice further showed that softer gels produced a thicker fibrous capsule(201). Similarly, poly(D,L-lactide-co-caprolactone) scaffolds with low stiffness (< 5 kPa) drove NR8383 cells, a semi-adherent rat alveolar macrophage cell line, towards M1 polarisation and chronic inflammation *in vivo*, whereas stiffer scaffolds (> 40 kPa) induced M2 polarisation, tissue formation and remodelling in a rat subcutaneous model(202). Another study examining stiffness from 6 kPa (soft) to 16 kPa (stiff) showed that increasing matrix stiffness enhanced M2 macrophage polarisation in THP-1 cells(262). Additional evidence includes a study using fibronectin-coated polyacrylamide gels (1, 20, and 150 kPa) with murine primary bone marrow-derived macrophages and RAW264.7 cells, which found a pro-inflammatory response on the softest gel(263). Similarly, collagen-coated polyacrylamide gels (1 and 10 kPa) in a mouse tumour model demonstrated that increased matrix stiffness led to the accumulation of M2-like macrophages(264).

Only a limited number of studies have investigated the effects of stiffness on human primary macrophages. One study showed that increasing the stiffness of collagen/alginate hydrogels (0.1 – 20 kPa) promoted M2-like polarisation(265). Similarly, another work using RGD-modified PEG-based gels found that stiffer (10.3 kPa) substrates drove macrophages towards an anti-inflammatory phenotype(266). In a separate study, human monocyte-derived macrophages cultured on fibronectin-coated polyacrylamide gels (1 to 280 kPa) exhibited greater

cell spreading and enhanced formation of actin fibres with increasing stiffness, although their phagocytic capacity was not affected. Surface markers or cytokine profiling were not quantified in their study(241).

Despite extensive research in this field, the effect of substrate chemistry and stiffness on macrophages is still unclear as findings across studies have often been contradictory. Additionally, most works have predominantly relied on cell lines or murine primary cells, with limited investigation using primary human monocyte-derived macrophages. These models have significant limitations due to both interspecies differences(267-270) and the differences between primary cells and cell lines(271, 272), potentially compromising the translatability of findings to human biology. Another limitation is the use of stiffness ranges that do not reflect the mechanical properties of native soft tissues, which are usually the intended targets in regenerative medicine applications involving hydrogels. Tissues such as the brain, fat, pancreas, kidneys, and liver typically exhibit a Young's modulus below 10 kPa(273). For example, the stiffness of different pancreatic regions ranges between 1.15 ± 0.17 kPa and 2.09 ± 0.33(274, 275). In pathological conditions, such as pancreatic ductal adenocarcinoma(276) and chronic pancreatitis(277), the stiffness increases to approximately 2.89 - 4.3 kPa, reaching values as high as 5.8 kPa in long-term chronic pancreatitis.

To have a better understanding on how both surface chemistry and stiffness affect macrophage polarisation, we investigated the activation status of human monocyte-derived macrophages on methacrylate alginate (ALMA) hydrogels with mechanical properties mimicking soft tissues. Alginate-based hydrogels due to their low cost, low toxicity, abundance, and ease of chemical modification(172-175) have been explored in the context of immunomodulatory biomaterials(223). Mechanical tuneability and chemical versatility make ALMA a valuable

material for investigating macrophage responses in the context of FBR. However, despite extensive research, an alginate-based material that fully prevent FBR have yet to be achieved, representing a key barrier to a successful clinical translation. We hypothesised that substrate stiffness within physiologically relevant soft tissue ranges influences macrophage polarisation, and that these responses differ from those observed in murine models and cell lines. We further hypothesised that variations in the density of molecular cues modulate the immune response by altering cell-material interactions. Accordingly, this chapter aims to investigate the combined effects of mechanical properties and surface chemistry on macrophage activation and polarisation, using an array of biological techniques, to inform the design of immunomodulatory biomaterials for mitigating the foreign body reaction.

The mechanical properties of the hydrogels were determined using rheological testing. Monocytes were isolated from healthy blood donors and cultured on ALMA hydrogels for 6 days. Macrophage phenotype was assessed using a combination of techniques, including morphological evaluation, surface marker expression and cytokine profiling. We observed that increasing hydrogel stiffness promoted a pro-inflammatory macrophage phenotype, as evidenced by elevated TNF-α secretion, an increased calprotectin-to-mannose receptor ratio, and a more elongated cell morphology.

4.3 Results

Among all the different compositions characterised in the previous chapter, HDM ALMA Hydrogel 4% was selected given its storage modulus (G') ~1.2 kPa, which reflects the mechanical properties of a variety of soft tissues, including thyroid (1.3 kPa), pancreas (1.1 kPa),

lung (1.5 kPa), adipose tissue (1.6 kPa), liver (2 kPa), and brain (1 kPa)(273). Hydrogels were prepared directly in 96-well plates, either surface-modified with GRGDSP or unmodified, and subsequently sterilised. For the modification, ALMA hydrogels were incubated with GRGDSP solutions at two concentrations, resulting in distinct degrees of substitution: CB_1, obtained with 1 μM GRGDSP solution, and CB_20, obtained with 20 μM GRGDSP solution. As shown in chapter 3, CB_20 yielded the highest level of GRGDSP conjugation, whereas CB_1 resulted in a comparatively lower but still markedly greater amount of GRGDSP conjugation than that achieved through simple adsorption. Monocytes from healthy donors were isolated and seeded at a cell density of 1 x 10^6 cells/mL. Monocytes were cultured on hydrogels for 6 days with the addition of MCSF (10 ng/mL) at day 0 and day 3 to stimulate the differentiation into naïve macrophages. Hydrogels were incubated with media for 24 hours prior cell seeding to allow them to reach equilibrium swelling.

Images of cells cultured on hydrogels were taken on day 1 and day 6 to monitor their morphology (**Figure 4.3.1A**). As shown in the zoomed-in images in **Figure 4.3.1B**, cells cultured ALMA hydrogels formed some clusters since day 1.

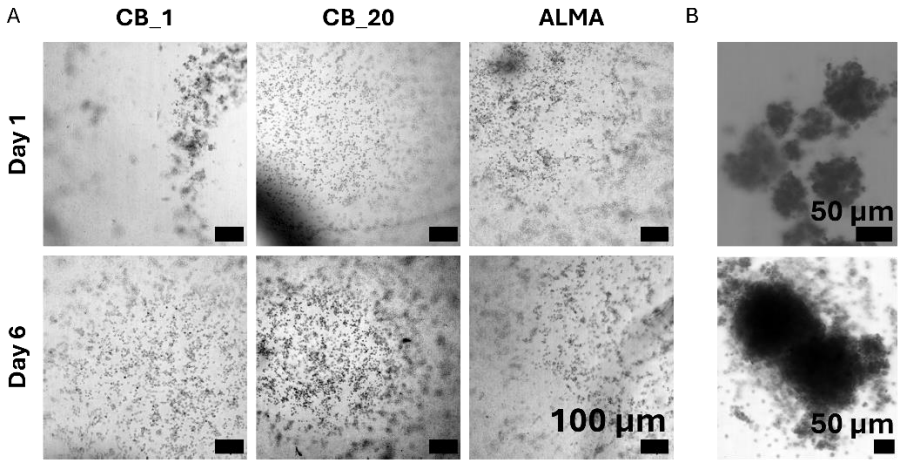

Figure 4.3.1 Human macrophages on different ALMA hydrogels. (A) Representative images of monocytes (day 1) and macrophages (day 6) cultured on GRGDSP-modified and unmodified ALMA hydrogels Scale bar: 50 μm. **(B)** Zoomed-in images of macrophage clusters at day 6.

A Live/Dead assay (**Figure 4.3.2A**) was performed to assess the toxicity of modified and unmodified ALMA hydrogels. The data showed that macrophages remained viable after 6 days of culture even though areas with dead cells could be seen. Given the poor quality of images, mainly due to sample thickness, cell viability was also assessed via ToxiLight assay performed on day 1 and day 6 (**Figure 4.3.2B**). On day 1, no significant cytotoxicity was detected in either modified or unmodified ALMA hydrogels, as luminescence values were comparable to the live control (M0 (Live), monocytes cultured on TCP). In contrast, the positive control (M0 (Dead), lysed cells) displayed a clear increase in luminescence, reflecting membrane permeability and cell death. By day 6, macrophages cultured on both hydrogel conditions still exhibited significantly lower toxicity than the M0 (Dead) control. However, ATP levels increased ~2-fold across all cells cultured on hydrogels compared to day 1 and were significantly higher than those measured in macrophages cultured on TCP at day 6 (M0 (Live)). Notably, both M1- and M2-polarised macrophages also displayed higher luminescence signals, comparable to cells cultured on unmodified and modified ALMA hydrogels. This suggests that the apparent cytotoxic effect may not be a direct consequence of material toxicity but rather linked to cell behaviour, namely the acquisition of specific macrophage phenotypes is associated with altered metabolic activity and increased luminescence signals. Another potential explanation is cell clustering: uneven attachment and heterogeneous seeding density across the hydrogel

surface could have determined local differences in nutrient availability and accumulation of metabolic by-products, resulting in stress for cells.

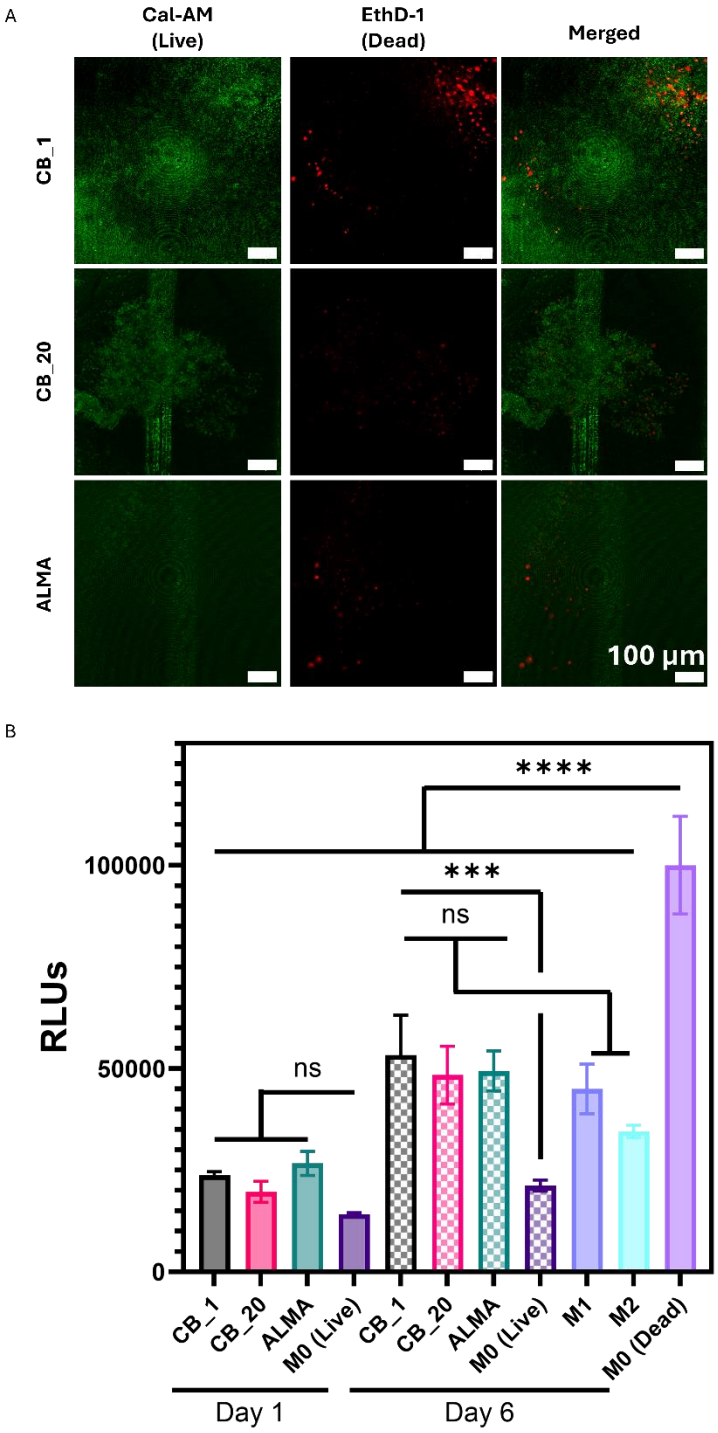

Figure 4.3.2 Human primary macrophage viability on ALMA hydrogels. (A) Fluorescent microscopy images of macrophages stained for Calcein-AM (green – live cells) and Ethidium homodimer-1 (red – dead cells) at day 6. Scale bar: 100 µm. **(B)** Cytotoxicity of surface modified ALMA hydrogel (CB_1 and CB_20) and unmodified ALMA hydrogel (ALMA) on monocytes at day 1 and on macrophages at day 6. Positive control consisted in cells cultured on tissue culture plastic that were lysed. M0, M1, and M2 cultured on TCP were used as live controls. Data is presented as mean of triplicates of three independent experiments ± SEM (n=3, N=3).

To assess the phenotype of macrophages cultured on different ALMA hydrogels, the expression of calprotectin (pro-inflammatory marker) and mannose receptor (MR) (anti-inflammatory marker) as well as the release of two pro- (TNF-α, IL-6) and two anti- (IL-10, CCL18) inflammatory cytokines were quantified, in line with our previous work(278). As a preliminary step, the suitability of these markers was validated by analysing M0, M1, and M2 macrophages, which were obtained though monocyte differentiation on TCP through cytokine stimulation. Marker expression was quantified using immunostaining combined with automated image analysis. Fluorescence microscopy images were acquired in the blue (nuclei), green (calprotectin), and red (MR) channels to identify marker-positive cells (**Figure 4.3.3A**). To ensure comparability across conditions, gain and exposure settings were calibrated to the sample with the highest fluorescence intensity and kept constant throughout imaging acquisition. The total number of cells per image was first quantified and found not to be significantly different across images and samples, confirming that marker expression could be reliably compared between samples and donors (**Figure 4.3.3B**).

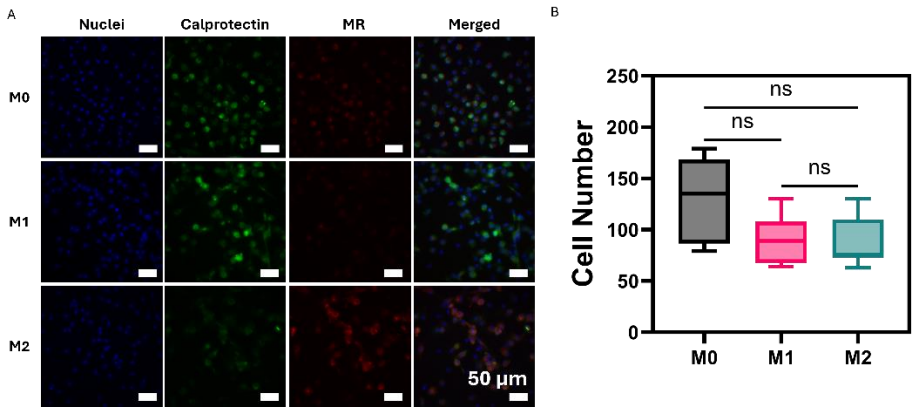

Figure 4.3.3 Human macrophage polarisation characterised by surface markers on TCP. (A) Confocal microscopy images of macrophages stained for pro- (calprotectin – green) and anti- (mannose receptor – red) inflammatory surface markers at day 6. Scale bar: 50 µm. **(B)** Quantification of cell numbers cultured on TCP for 6 days and differentiated into M0, M1 and M2 phenotypes. Data is presented as mean of triplicates of three independent experiments ± SEM (n=3, N=3).

Quantification of the green (calprotectin) (**Figure 4.3.4A**) and red (MR) (**Figure 4.3.4B**) signals was performed using CellProfiler. Both markers demonstrated their suitability for phenotypic characterisation: calprotectin, the pro-inflammatory marker, was found to be significantly upregulated in M1 macrophages, whereas MR, the anti-inflammatory marker, was significantly increased in M2 macrophages. To account for inter-sample and inter-donor variability, the ratio between calprotectin and MR was calculated, thereby normalising fluorescence values and enabling direct comparison across conditions. This analysis further validated the suitability of these surface markers for phenotypic characterisation as the calprotectin-to-MR ratio was significantly higher in M1 macrophages (ca. 4-fold) compared to M2 macrophages (**Figure 4.3.3C**), in line with the literature.

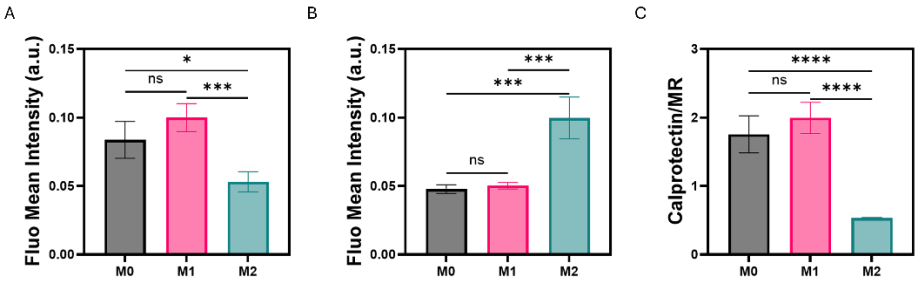

Figure 4.3.4 Surface marker quantification. Quantification of **(A)** calprotectin, as pro-inflammatory **(**M1), and **(B)** mannose receptor, as anti-inflammatory (M2), markers through immunostaining. **(C)** Ratio between calprotectin and mannose receptor expression in naïve (M0), M1, and M2 macrophages. Data is presented as mean of triplicates of three independent experiments ± SEM (n=3, N=3).

Cytokines were quantified by sandwich ELISA to validate their use as markers for macrophage phenotype characterisation (**Figure 4.3.5**). As expected, the pro-inflammatory cytokines TNF-α and IL-6 were significantly elevated in M1 macrophages, while their secretion remained below the detection threshold in both M0 and M2 macrophages. In contrast, the anti-inflammatory cytokines IL-10 and CCL18 were markedly upregulated in M2 macrophages, with levels significantly higher than those observed in M0 and M1. These findings aligned with the established cytokine profiles of classically activated

(M1) and alternatively activated (M2) macrophages, thereby confirming the suitability of these markers for subsequent phenotypic analyses.

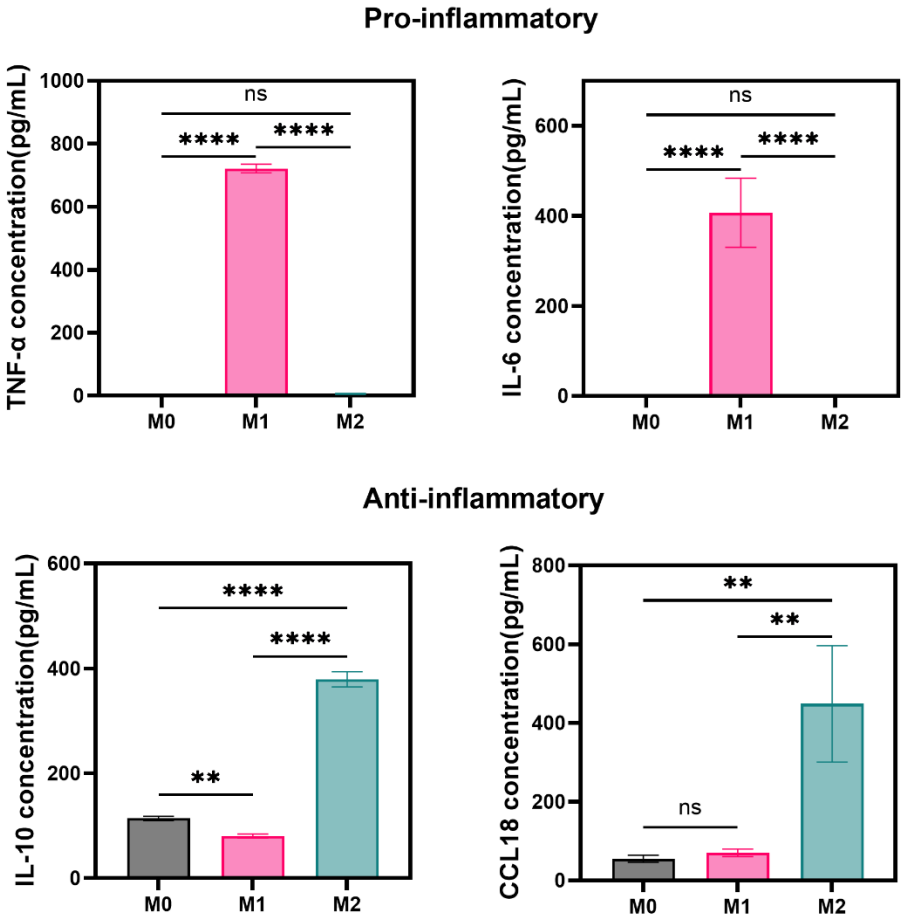

Figure 4.3.5 Quantification of pro- (TNF-α, IL-6) and anti- (IL-10, CCL18) inflammatory cytokines secreted by M0, M1, and M2 macrophages at day 6. Data is presented as mean of triplicates of three independent experiments ± SEM (n=3, N=3).

Macrophages cultured on both modified and unmodified hydrogels were subsequently stained for the same surface markers. However, reliable imaging and fluorescence quantification could not be achieved due to several technical limitations, including strong background interference (also observed in the Live/Dead assay), sample thickness, and

pronounced cell aggregation. These factors hindered the resolution of individual fluorescent signals, rendering accurate detection and quantification of marker expression unfeasible. Optimisation of sample preparation was therefore required to enable reliable characterisation via immunostaining and imaging.

Despite these limitations, to investigate whether surface modifications of the hydrogels influenced macrophage phenotype, culture supernatants were collected on day 6 and analysed to determine the cytokine profile. A shown in **Figure 4.3.6**, TNF-α secretion was significantly reduced in macrophages cultured on the hydrogel with higher GRGDSP conjugation (CB_20) compared to those cultured on the unmodified hydrogel (ALMA). In contrast, no significant change was observed for macrophages on the hydrogel with lower GRGDSP (CB_1). Similarly for IL-10, secretion was significantly higher in macrophages cultured on unmodified ALMA compared to both modified hydrogels, suggesting greater macrophage activation in the absence of GRGDSP modification. Although no statistically significant difference was detected between CB_1 and CB_20, IL-10 release was slightly elevated and TNF-α was lower in macrophages cultured on CB_20, indicating a potential anti-

inflammatory trend associated with higher GRGDSP conjugation on ALMA hydrogel surface.

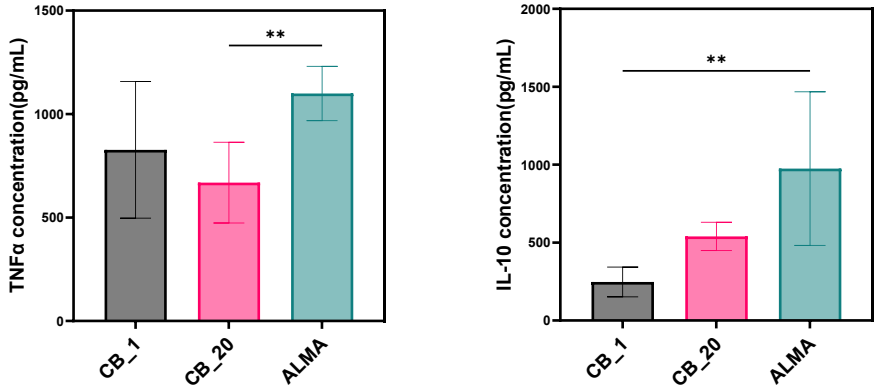

Figure 4.3.6 Quantification of pro- (TNF-α) and anti- (IL-10) inflammatory cytokines secreted by macrophages at day 6. Data is presented as mean of triplicates of three independent experiments ± SEM (n=3, N=2).

Based on the initial findings, surface modification with higher GRGDSP conjugation was selected as the most promising modified ALMA formulation for investigating the interplay between surface chemistry and stiffness. Hydrogels of varying stiffness (ALMA 2%, 4%, and 6%) were prepared in both unmodified and surface-modified forms (CB_ALMA), with a reduced thickness of 500 µm (compared to the previous 1 mm) to facilitate imaging. Monocytes were seeded and cultured for 6 days to allow full differentiation. On day 6, samples were stained for pro- and anti-inflammatory surface markers, and supernatants were collected for cytokine analysis by sandwich ELISA (TNF-α, IL-6, IL-10, and CCL18).

Despite the reduced thickness, cells still could not be imaged at magnifications higher than 10x, preventing single cell individuation and reliable surface marker quantification. CCL18 levels remained below

the detection threshold and were therefore excluded from further analysis.

For the other cytokines, as shown in **Figure 4.3.7**, a consistent pattern emerged among modified and unmodified hydrogels with stiffness being the dominant factor that influenced macrophage cytokine secretion. When comparing hydrogels of the same stiffness (identical ALMA %) but different surface chemistries (unmodified ALMA vs. CB_ALMA), no significant differences in cytokine release were observed. In contrast, when comparing hydrogels of the same surface chemistry but different stiffnesses, cytokine secretion progressively decreased as ALMA concentration (and thus stiffness) increased. This trend was evident for both pro- and anti-inflammatory cytokines.

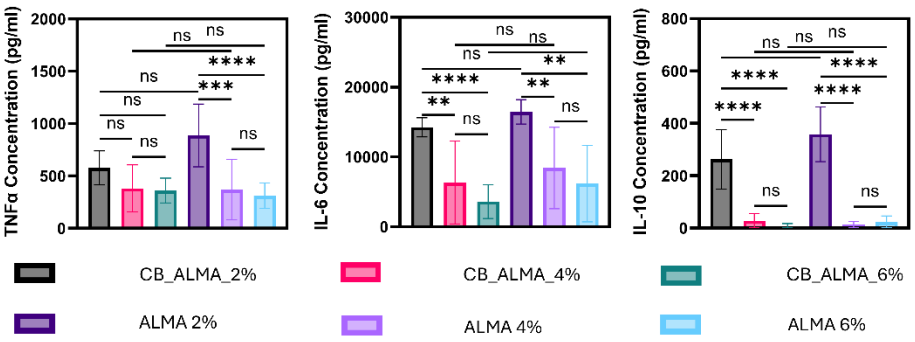

Figure 4.3.7 Quantification of pro- (TNF-α, IL-6) and anti- (IL-10) inflammatory cytokines secreted by macrophages at day 6. Data is presented as mean of triplicates of three independent experiments ± SEM (n=3, N=2).

Together, these results indicate that, while GRGDSP surface modification may exert subtle effects under the tested conditions, hydrogel stiffness plays a more decisive role than surface chemistry in regulating macrophage polarisation, with stiffer matrices generally suppressing macrophage activation and cytokine release. On the basis of these preliminary findings, the study proceeded to investigate

mechanical properties, focusing primarily on the impact of hydrogel stiffness on macrophage responses.

Before proceeding with the study, it was necessary to optimise sample preparation, as imaging at sufficiently high magnification to resolve individual cells and quantify their fluorescent signals was not feasible. Furthermore, hydrogels prepared directly in well plates were observed to adopt a "U"-shaped profile after swelling (**Figure 4.3.8**), likely resulting from capillary forces acting on the gels and inducing meniscus formation.

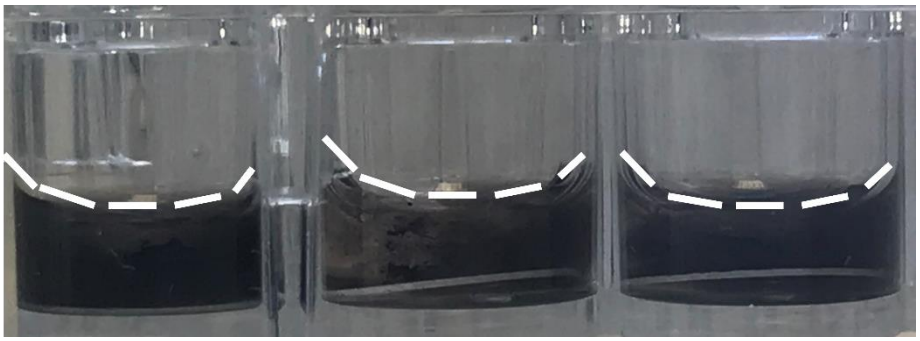

Figure 4.3.8 Example of ALMA hydrogels directly prepared in 96-well plates.

Substrate geometry has been reported to significantly influence cell behaviour and immune response(279, 280). Additionally, macrophages were observed to form clusters, which may have been the result of the non-flat surface and the presence of a central depression. It was therefore essential to establish a preparation method that yielded thin, flat hydrogels, enabling cell imaging and eliminating substrate geometry as a confounding factor, while ensuring stiffness remained the sole variable across samples.

The first attempt involved placing different volumes of ALMA–Irgacure 2959 solution onto a glass slide, which was then covered with silanised coverslips. The system was exposed to UV light until complete

polymerisation, after which the coverslip bearing the hydrogel was removed using tweezers (**Figure 4.3.9**). While this method successfully produced films of ALMA hydrogel on silanised coverslips, it presented significant limitations. The thickness could not be controlled and, in samples with very thin films, the hydrogel often acted as a glue between the coverslip and the glass slide, resulting in sample breakage during detachment.

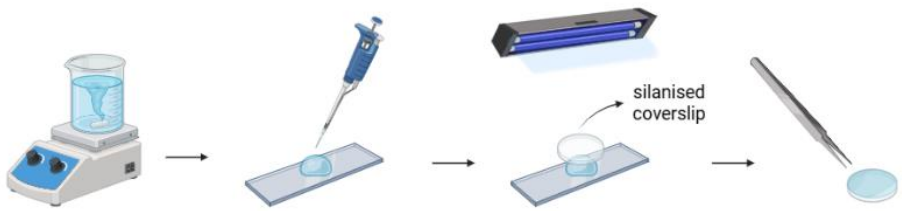

Figure 4.3.9 Schematic representation of the first attempt to obtain a thin film of ALMA hydrogel on silanised coverslips.

We next attempted a "sandwich" set-up by using adhesive tape on a glass slide to define specific hydrogel thicknesses. In the first approach, the silanised coverslip was placed onto the taped glass slide, and the ALMA solution was dispensed into the narrow gap between the coverslip and the glass slide. However, this method was unsuccessful given the high viscosities of ALMA solutions that did not allow to penetrate within the extremely restricted space (**Figure 4.3.10A**). A second approach was then tested, in which ALMA solutions was first dispensed onto the glass slide, followed by placing the silanised coverslip on top to spread the solution evenly (**Figure 4.3.10B)**. This method successfully produced flat hydrogels with controlled thickness, providing a more reliable preparation strategy.

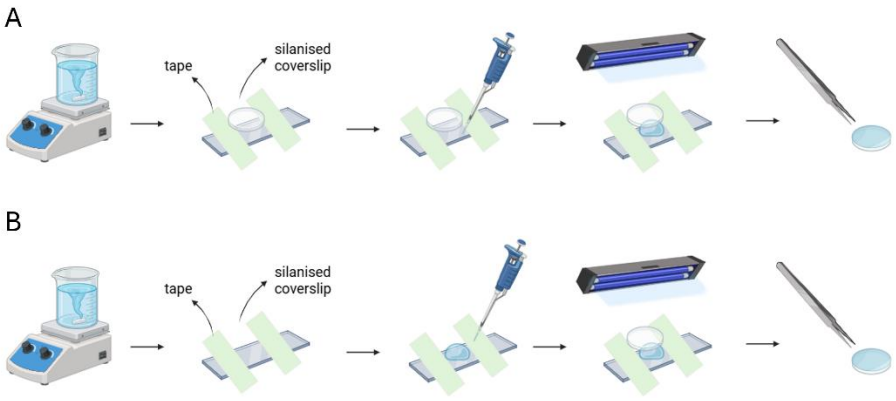

Figure 4.3.10 Schematic representation of the "sandwich" method used to prepare thin ALMA hydrogel films on silanised coverslips. **(A)** Approach in which ALMA solution was dispensed into the gap between the coverslip and the glass slide. **(B)** Approach in which ALMA solution was dispensed directly onto the glass slide before placing the silanised coverslip on top.

To evaluate the reliability and consistency of this method, a strategy for thickness assessment was developed. Samples were prepared using either one or three layers of tape (**Figure 4.3.11A**), and the theoretical hydrogel thickness was estimated with a calliper by measuring the combined thickness of the tape layers. Hydrogels were then fabricated, and their actual thickness was measured using confocal microscopy coupled with image analysis. For this purpose, the glass slide was marked with a black cross and the silanised coverslip with a green dot, providing clear reference points for the top and bottom boundaries of the hydrogel sample (**Figure 4.3.11B**).

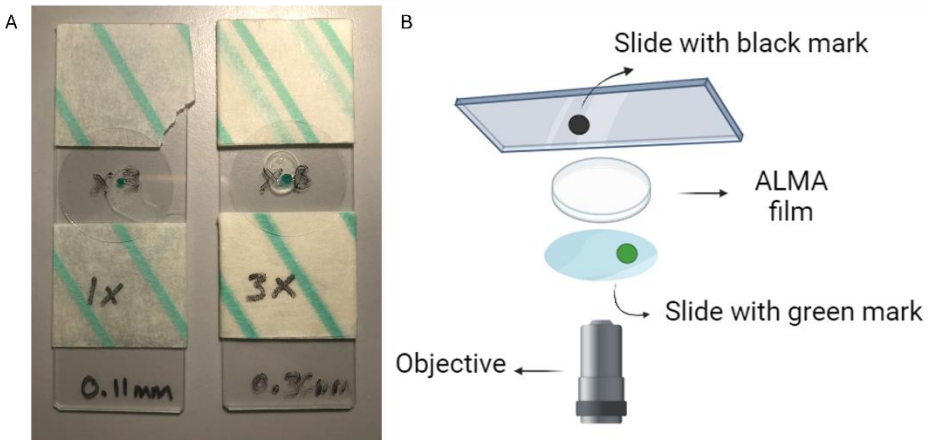

Figure 4.3.11 Assessment of ALMA hydrogel thickness using the "sandwich" method. (A) Example of the sandwich system used to obtained hydrogels with different thicknesses, using one and three layers of tape. **(B)** Schematic representing the set-up used to measure the thickness of hydrogels using confocal microscopy.

Based on calliper measurements of the tape layers, the hydrogels were expected to reach thicknesses of approximately ~110 µm (1x – one tape layer) and 360 µm (3x - three tape layers). As shown in **Figure 4.3.12**, the measured values were in close agreement with these predictions. Specifically, the sample prepared with a single tape layer (1x) exhibited a thickness of ~160 µm, while the sample prepared with three tape layers (3x) showed a thickness of ~300 µm. These results suggest that this

hydrogel preparation method is both reliable and adaptable, allowing the fabrication of samples with customised thicknesses as required.

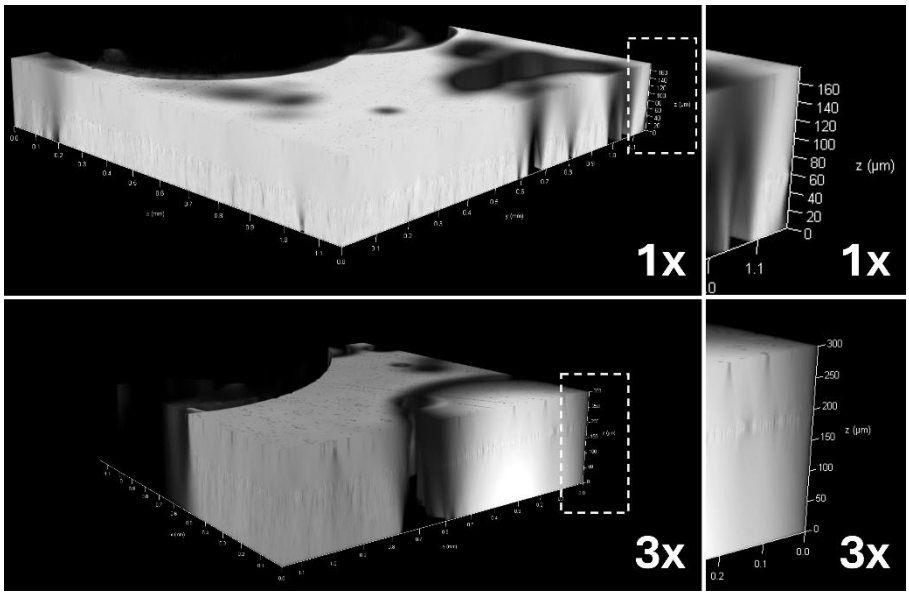

Figure 4.3.12 Representative confocal images of hydrogel samples prepared using the "sandwich" method, illustrating different thicknesses obtained by varying the number of tape layers.

The main limitation of this method was the tape being in direct contact with ALMA solution. This raised the concern that small molecules may leach from the tape into the hydrogel precursor solution, introducing potential sources of variability that could influence macrophage behaviour. To address this issue, the set-up was modified by repositioning the tape at the edges of the glass slide and adding an additional glass slide to support the silanised coverslip. ALMA solution was dispensed onto the coverslip and overlaid with another glass slide, thereby avoiding direct contact between the hydrogel and the tape as shown in **Figure 4.3.13**.

Figure 4.3.13 Schematic representation of the optimised "sandwich" method for producing ALMA hydrogel films with controlled thickness on silanised coverslips.

To prevent the formation of "U"-shaped hydrogels caused by swelling, larger well plates were employed. Thin hydrogel films were prepared using the optimised sandwich method on coverslips sized for 24-well plates and subsequently placed into 12-well plates, providing sufficient space to avoid constraints on the gels. Following sterilisation, the hydrogels were pre-incubated in complete medium for 24 hours to allow protein adsorption, a critical step for promoting cell attachment. Importantly, non-treated well plates were used to ensure that cells adhered exclusively to the hydrogel surface. 24 hours after seeding, the culture medium was replaced to remove non-adherent monocytes, thereby reducing the risk of apoptotic signals interfering with the differentiation and polarisation of the attached cells.

With the optimised preparation method in place to obtain flat and reproducible hydrogel films, we next applied this set-up to investigate how hydrogel stiffness influences macrophage polarisation. Specifically, three formulations of HDM ALMA hydrogels (2%, 4%, and 6%) were selected and further characterised.

In vitro swelling (**Figure 4.3.14B**) showed that all three hydrogel compositions reached equilibrium in less than 24 hours, with ALMA 4% and 6% exhibiting a similar weight increase of 20%. The composition with 2% methacrylate alginate showed a higher swelling, reflecting the lower concentration of the polymer involved in forming the 3D network.

To quantitatively determine the mesh size, the rubber elasticity theory was applied to relate the storage modulus (G') measure via amplitude sweeps to the network crosslinking density(231, 281, 282). Increasing ALMA concentration led to significantly smaller mesh sizes, showing an inverse correlation with stiffness (**Figure 4.3.14C**). This observation is consistent with the fact that higher polymer concentrations yield stiffer hydrogels by forming denser crosslinked networks, which reduces both void space and the swelling capacity(283). Environmental scanning electron microscopy (ESEM) images (**Figure 4.3.14D**) were collected to characterise the surface of hydrogels at different ALMA concentrations in their native hydrated state. To complement ESEM observations, we further characterised surface topography using optical profilometry. Profilometry of hydrated gels provided quantitative roughness parameters, including the arithmetical mean height (Sa) and root mean square height (Sq). Roughness was higher for ALMA 2% (Sa = 41.6 nm; Sq = 53.4 nm) compared with ALMA 4% (Sa = 26.2 nm; Sq = 33.4 nm) and 6% (Sa = 24.3 nm; Sq = 30.7 nm), while no significant differences were observed between the 4% and 6% hydrogels (**Figure**

4.3.14E). Both ESEM and profilometry indicated that surface smoothness increased with polymer concentration.

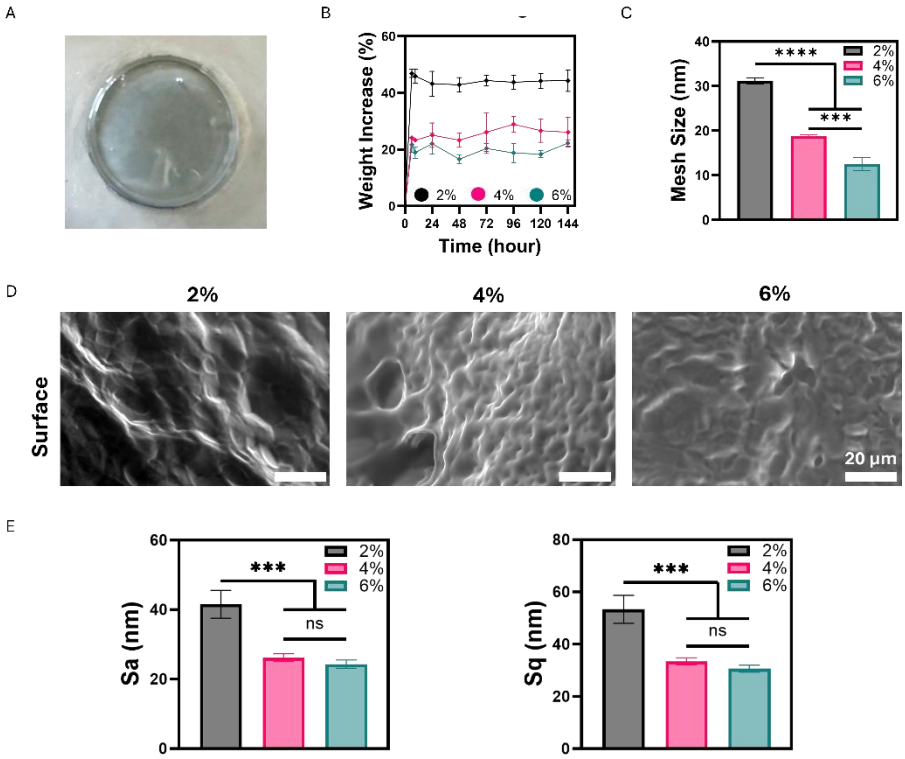

Figure 4.3.14 Swelling, mesh size and surface morphology of ALMA hydrogels. (A) Gross view of an ALMA hydrogel disc **(B)** Swelling equilibrium and **(C)** mesh size of ALMA hydrogels at 2%, 4%, and 6% w/v calculated by using the rheological data and the rubber elasticity theory **(D)** Representative environmental scanning electron microscopy (ESEM) images of the hydrogel surfaces. **(E)** Quantification of arithmetical mean height (Sa) and root mean square height (Sq) using optical profilometry for ALMA hydrogels at 2%, 4%, and 6% w/v. Data is presented as mean of triplicates ± SD (n=3).

Protein adsorption and surface chemistry were assessed by XPS (**Figure 4.3.15A**). Analysis of the integrated N 1s peaks (**Figure 4.3.15B**), which arise exclusively from adsorbed proteins as ALMA lacks nitrogen, showed no significant differences in nitrogen content among the

compositions (**Figure 4.3.15C**), indicating comparable protein adsorption across all formulations. Similarly, the quantification of C 1s (**Figure 4.3.15D**) and O 1s (**Figure 4.3.15E**) peaks revealed no detectable changes in surface functional groups with increasing polymer concentration. It is important to note that XPS provides only elemental composition and relative abundance of elements and cannot determine the identity, conformation, or orientation of the adsorbed proteins. Complementary approaches, such as mass spectrometry, would be required to fully characterise the adsorbed protein layer.

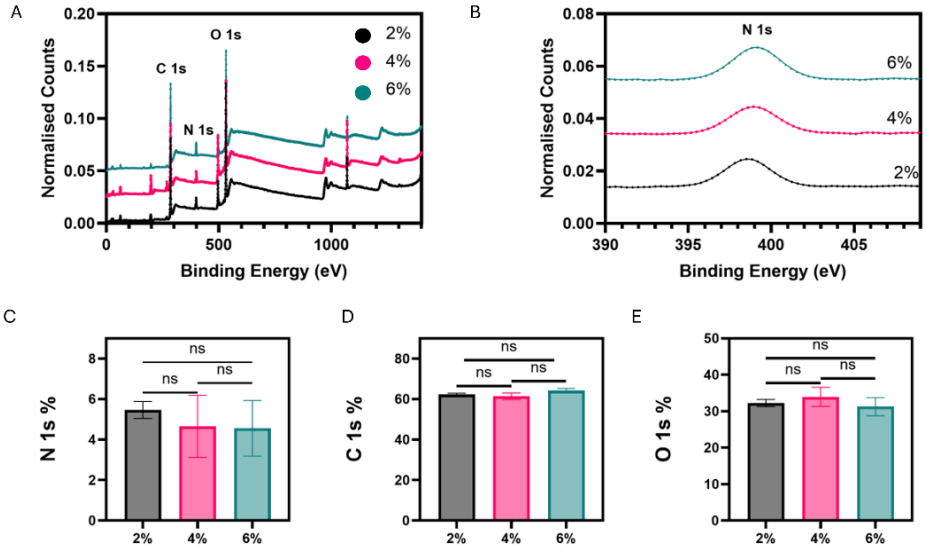

Figure 4.3.15 Surface characterisation of ALMA hydrogels. (A) XPS wide-scan spectra of ALMA hydrogels at 2%, 4%, and 6% following 24-hour incubation in culture medium. **(B)** Enlarged N 1s peaks from the wide-scan spectra used to quantify protein adsorption. Quantification of **(C)** N 1s, **(D)** C 1s, and **(E)** O 1s peaks. Data is presented as mean of triplicates ± SD (n=3).

The storage (G') and loss (G'') moduli (**Figure 4.3.16A**) were extrapolated at 1 Hz from frequency sweeps that were shown in Chapter 3. While ALMA 2% and 4% did not show a significant difference in

their G' (257.9 Pa and 1195.7 Pa, respectively) and G'' values (33.8 Pa and 35.2Pa, respectively), the ALMA 6% hydrogel exhibited significantly higher moduli (G' value of 4426.6 Pa and G'' value of 175.3 Pa) compared to the two softer hydrogels. Together, these three compositions span stiffness values across the physiologically relevant range of soft tissues – from very soft tissues, such as the lens (0.2–0.8 kPa), to intermediate tissues, including the thyroid (1.3 kPa), pancreas (1.1 kPa), lung (1.5 kPa), adipose tissue (1.6 kPa), liver (2 kPa), and brain (1 kPa), and to relatively stiffer organs such as the kidney (4–5 kPa)(273) – thus enabling investigation of cell responses across a representative mechanical spectrum. Complex viscosity was also determined (**Figure 4.3.16B**), and stress relaxation (**Figure 4.3.16C**) was investigated as many studies have shown the effect of viscoelasticity on cell responses(284-286). All three hydrogels showed similar stress relaxation profiles, confirming that observed differences in macrophage activation status were due to stiffness rather than viscoelasticity.

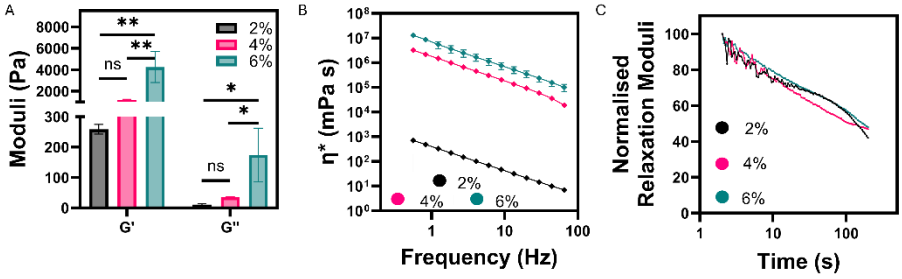

Figure 4.3.16 Rheological characterisation of methacrylate alginate. **(A)** storage (G') and loss (G'') moduli, **(B)** complex viscosity, and **(C)** normalised stress relaxation of ALMA hydrogels. Stress relaxation was performed within LVE region (5% strain). Data is presented as mean of triplicates ± SD (n=3).

Rheological measurements reflect the bulk properties of a material and may not accurately capture the local mechanical environment at the material's surface. To obtain local stiffness measurements, atomic force microscopy (AFM) was attempted, but reliable data could not be acquired due to technical challenges. The extreme softness of the substrates used in this study posed a major challenge, as capillary forces dominated the measurements and interfered with reliable characterization(287, 288), effectively pulling the tip toward the surface and confounding the true tip-sample interactions. Another critical limitation was tip contamination. The AFM tip often penetrated through the hydrogel surface, dislodging fragments that subsequently adhered to the tip and rendering subsequent measurements unreliable. Another factor that prevented reliable AFM analysis was gel breakage during measurement, which caused the probe to directly contact the underlying glass substrate. This was evident from the probe-sample interaction curve overlapping with the calibration curve, indicating that the tip was primarily detecting the glass rather than the hydrogel layer (data not available).

To provide an overview of the experimental strategy used to investigate macrophage responses to hydrogel stiffness, a schematic representation is shown in **Figure 4.3.17**.

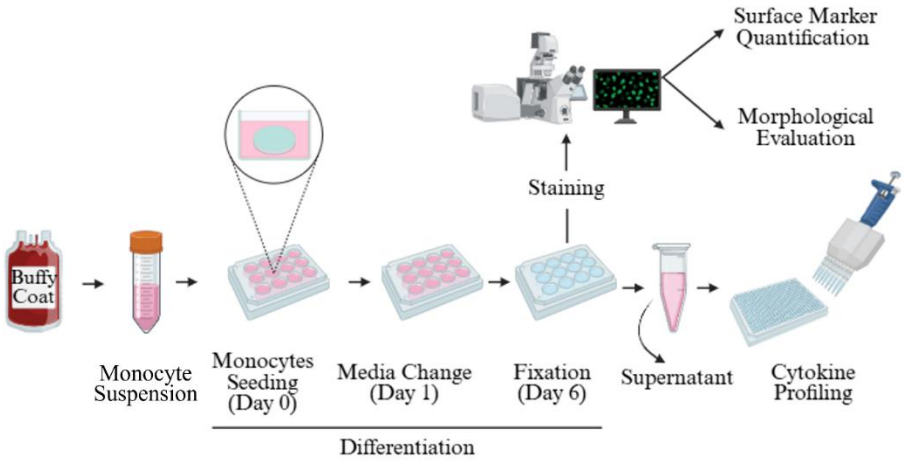

Figure 4.3.17 Overview of the experimental workflow. Monocyte isolation from healthy blood donor, differentiation and characterisation of morphology, surface markers and cytokine profiling of macrophages.

A Live/Dead assay (**Figure 4.3.18A**) was performed to assess the toxicity of ALMA hydrogels. The data showed that macrophages remained viable after 6 days of culture across all hydrogels, suggesting comparable biocompatibility. The high cell viability was also supported by the ToxiLight assay which showed no significant differences in metabolic activity between macrophages cultured on the hydrogels and those cultured on TCP controls (**Figure 4.3.18B**). Together, these results demonstrated the suitability of ALMA hydrogels as biocompatible substrates for macrophage differentiation and culture.

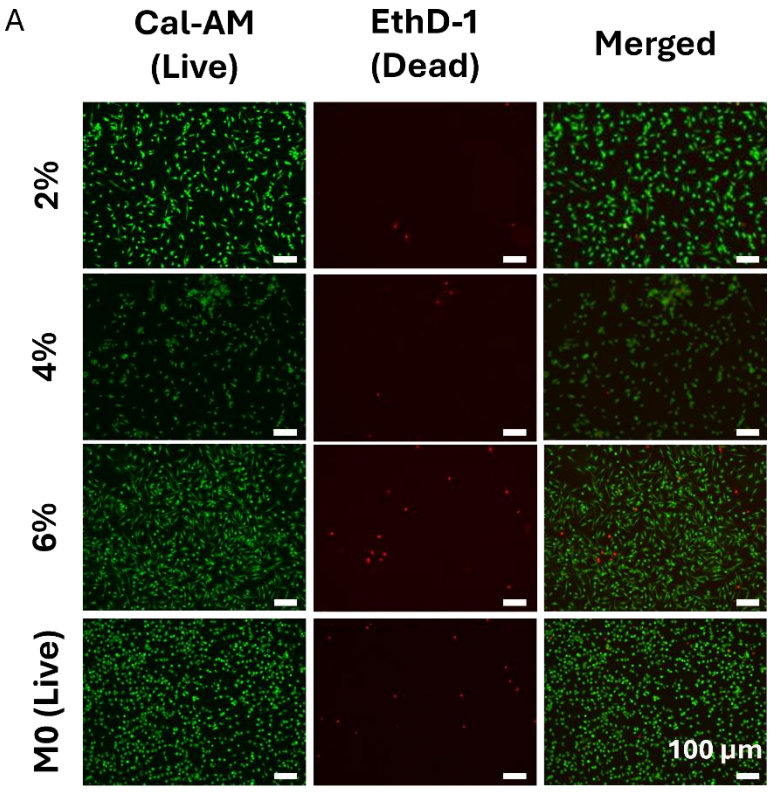
A
Cal-AM (Live)
EthD-1 (Dead)
Merged
2%
4%
6%
M0 (Live)
100 µm

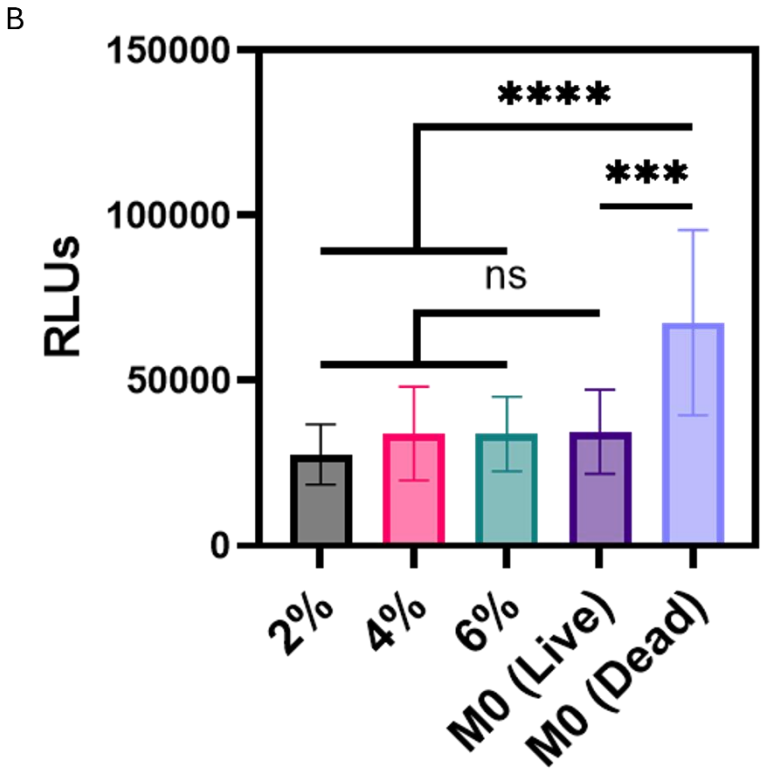
B
RLUs
150000
100000
50000
0
****
***
ns
2%
4%
6%
M0 (Live)
M0 (Dead)

Figure 4.3.18 Human primary macrophage viability on methacrylate alginate. (A) Fluorescent microscopy images of macrophages stained for Calcein-AM (green – live cells) and Ethidium homodimer-1 (red – dead cells) at day 6. Scale bar: 100 μm. **(B)** ToxiLight assay on macrophages cultured for 6 days on ALMA 2%, 4%, and 6%. Positive control (M0 (Dead)) is purposely lysed macrophages. M0 macrophages cultured on tissue culture plastic (M0 (Live)) were used as negative controls. Data is presented as mean of triplicates of three independent experiments ± SEM (n=3, N=3).

The expression levels of calprotectin (pro-inflammation marker) and mannose receptor (anti-inflammatory markers) were quantified by immunofluorescent staining and image analysis, in line with our previous works(278) (**Figure 4.3.19A**). To ensure cross-sample comparisons, the number of imaged cells was quantified across the different hydrogels. No significant differences in cell number were detected (**Figure 4.3.19B**). The calprotectin-to-mannose expression ratio was used as a surrogate for assessing the macrophage activation status (**Figure 4.3.19C**). There was no significant difference in the calprotectin-to-MR ratio between macrophages cultured on ALMA 2% and 4%. Macrophages cultured on 2% and 4% ALMA expressed more MR relative to calprotectin as the ratios were below one. In contrast, calprotectin was expressed significantly more (ca. 6-fold) in macrophages that were cultured on ALMA 6%. This suggested that a significant increase in the storage modulus (G') promoted a shift towards a more pro-inflammatory, M1-like phenotype.

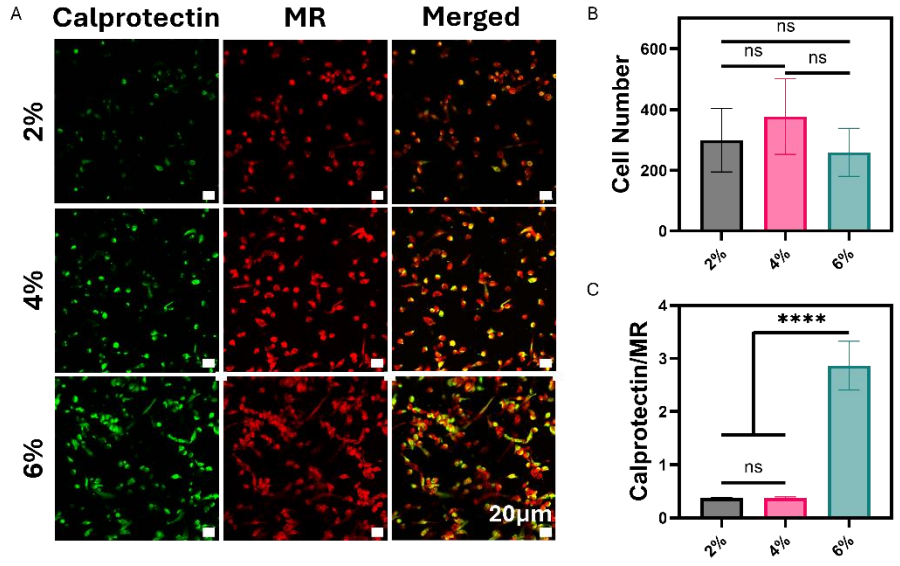

Figure 4.3.19 Human macrophage polarisation characterised by surface markers on different ALMA hydrogels. (A) Confocal microscopy images of macrophages stained for pro- (calprotectin – green) and anti- (mannose receptor – red) inflammatory surface markers at day 6. Scale bar: 20 µm. **(B)** Quantification of cell numbers cultured on ALMA hydrogels at day 6 **(C)** Ratio between calprotectin and MR fluorescent signals. Data is presented as mean of triplicates of three independent experiments ± SEM (n=3, N=3).

To further characterise macrophage activation in response to different stiffnesses, monocytes were stained for nuclei and F-actin to monitor their morphology over the 6-day culture period. As shown in **Figure 4.3.20A** and **4.3.20B**, cells cultured on ALMA 6% presented a more elongated morphology starting from day 3, in contrast to those on the softer hydrogels, which maintained a rounder shape. To quantitatively compare cell morphologies, parameters including cell eccentricity and area were measured. Eccentricity was used to quantify cell elongation, where a value of zero corresponds to a perfect circle and one to a line. On day 6, macrophages on the stiffest ALMA hydrogel (ALMA 6%)

displayed significantly higher eccentricity (~0.8) compared to those on the softest hydrogel (ALMA 2%), which showed eccentricity values below 0.75 (**Figure 4.3.20C**). Similarly, the cell area was significantly larger on the stiffest hydrogel (~197 μm^2) than on the softest substrate (~120 μm^2), suggesting decreased cell interaction with the softer materials (**Figure 4.3.20D)**.

Interestingly, cells located near the edge of the disk-shaped hydrogels consistently exhibited much greater spreading compared to those resided on more central regions (**Figure 4.3.20E**). This phenomenon was observed for all the three ALMA concentrations. The spreading appeared to be unidirectional towards the edge, evidenced by the cell lamellipodia distribution. This unexpected edge-related cell morphology might be due to a higher local stiffness near the perimeter, potentially caused by increased water evaporation near the edge during hydrogel preparation. However, the local stiffness and composition will need further characterisation in future studies to elucidate the underlying mechanisms.

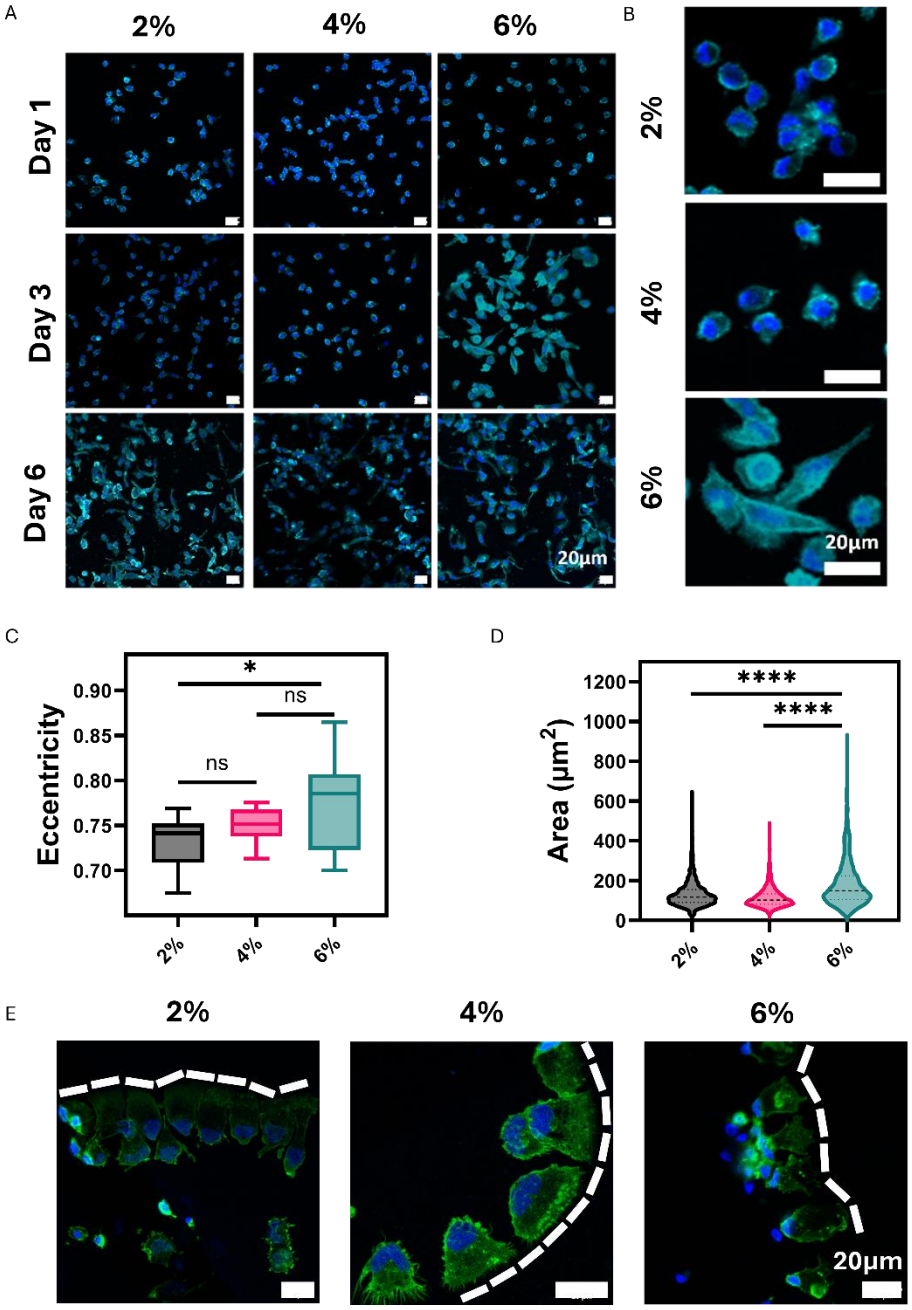

Figure 4.3.20 Human macrophage morphology on different alginates (A) Confocal microscopy images of monocyte (day 1 and 3) and macrophages (day 6) stained for nuclei (DAPI – blue) and F-actin (Phalloidin – cyan) at day 1, day 3, and day 6. Scale bar: 20 µm. **(B)** Zoomed-in confocal microscopy images representative of macrophage morphology at day 3. Scale bar: 20 µm. **(C)** Quantification of

eccentricity and **(D)** area of macrophages at day 6. **(E)** Representative morphologies of macrophages adhered close to the edge of the disk-shaped ALMA hydrogels. White dashed lines represent the edges. Scale bar: 20 μm. Data is presented as mean of triplicates of three independent experiments ± SEM (n=3, N=3).

To further determine the phenotype of macrophages on different ALMA hydrogels, pro- (TNF-α, IL-6) and anti- (IL-10, CCL18) inflammatory cytokines were quantified by using sandwich ELISA (**Figure 4.3.21**). TNF-α secreted from macrophages cultured on ALMA 6% was significantly higher compared to cells on ALMA 2% and 4%, suggesting a shift towards a pro-inflammatory phenotype on the stiffer substrate. Although no significant difference was observed for IL-6, a trend of increasing secretion with increasing stiffness was observed. In terms of anti-inflammatory cytokines, IL-10 secretion was significantly higher from macrophages cultured on the softest ALMA 2%. Although no significant difference was observed for CCL18 release, a decreasing trend with increasing stiffness was observed. Overall, the cytokine profile supported the observation that stiffer hydrogels induced a pro-inflammatory phenotype, whereas softer substrates showed an anti-inflammatory activation status.

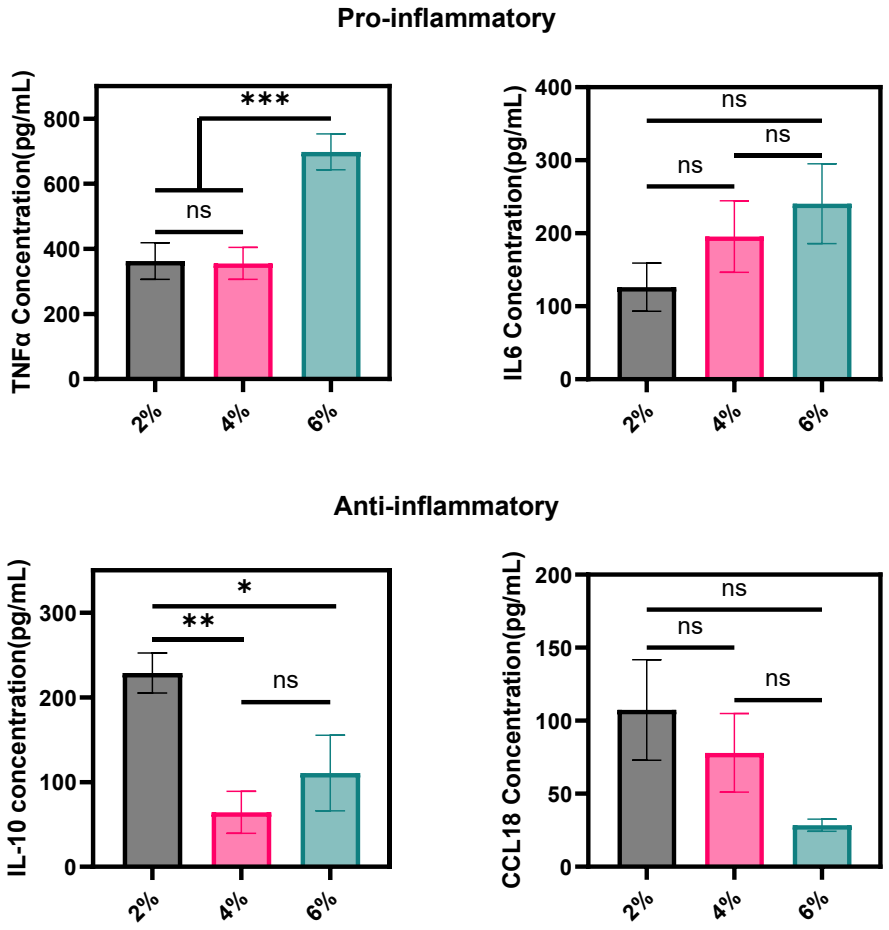

Figure 4.3.21 Quantification of pro- (TNF-α, IL-6) and anti- (IL-10, CCL18) inflammatory cytokines secreted by macrophages at day 6. Data is presented as mean of triplicates of three independent experiments ± SEM (n=3, N=3).

It is known that high endotoxin levels can induce pro-inflammatory polarisation in macrophages(289). To exclude the possibility that changes in cell behaviour were a consequence of high endotoxin levels, ALMA 6% was prepared and incubated in PBS, simulating the cell culture conditions. After 6 days, endotoxins were quantified and data showed that their level was below the accepted limit of 0.1 EU/mL for *in vitro* immunogenicity assays, which excluded the possibility of the

influence of endotoxins on macrophage activation status (**Figure 4.3.22**).

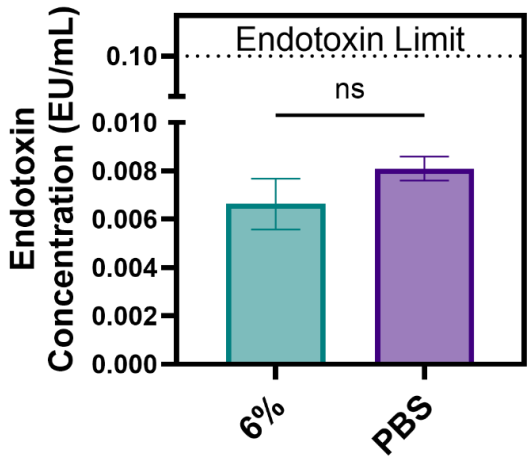

Figure 4.3.22 Endotoxin quantification at day 6 in the supernatant of ALMA 6% sample. Sterile PBS was used as a control. Data is presented as mean of triplicates ± SD (n=3).

4.4 Discussion

Cells and their activities are strongly influenced by the geometry of the substrates to which they adhere(290). In this study, the final results differed from the preliminary data, where increasing stiffness of ALMA hydrogels was associated with reduced cytokine release. However, extensive optimizations in sample preparation were performed which altered the hydrogel geometry, shifting from U-shaped hydrogels to flat surfaces, which likely contributed to the differences observed.

Firstly, differences in effective cell density must be considered. In the early experiments, when hydrogels were directly prepared in the well-plate, macrophages tended to aggregate. We initially hypothesised that this was driven either by the softness of the substrate or by the "U" shape assumed by the hydrogel, which forced cells to accumulate in the central hollow rather than distribute evenly. Our data indicate that cell clustering

was not linked to substrate softness as ALMA 2%, used to mimic lens' stiffness, is characterised by a very low G' (~258 Pa), and cell aggregation was not observed when the hydrogels were prepared with the optimised sandwich method. Cell density is known to profoundly influence cellular metabolism and activity by modifying resource availability, waste accumulation, and intercellular signalling. At high density, rapid nutrient and oxygen consumption leads to local depletion and hypoxia, often shifting metabolism towards glycolysis. Concurrently, waste buildup and increased cell-cell contact reinforce changes in signalling pathways and can suppress anabolic fluxes through contact inhibition. Although these effects are cell type-specific, macrophages are no exception. For example, it was shown in a recent study how macrophage culture density significantly influences morphology, phenotype, and inflammatory responses *in vitro*. Increasing density alters cytokine and chemokine secretion across multiple macrophage models, including iPSC-derived macrophages, blood monocyte-derived macrophages, THP-1 cells, and iPSC-derived microglia(291). Consistent with this, the ToxiLight assay suggests a similar density-dependent effect. Macrophages cultured on optimised, flat hydrogels displayed metabolic activity comparable to M0 macrophages cultured on TCP, whereas macrophages cultured on the same U-shaped hydrogel showed a significant increase in luminescence, indicating altered metabolic behaviour and membrane permeability.

The conflicting reports on macrophage responses to substrate stiffness, along with the relatively high stiffness ranges commonly investigated in the literature, prompted us to study human macrophages on soft hydrogels. We prepared hydrogels with different mechanical properties by varying ALMA concentrations from 2% to 6% w/v. Our results showed that even a modest increase (in absolute value) from ~0.25 kPa to ~4.5 kPa led to significant changes in human monocyte-derived

macrophages. Our results demonstrated that cells cultured on the stiffest substrate (ALMA 6%, ~4.5 kPa) showed a more elongated morphology as early as day 3. This feature was also associated with a higher calprotectin-to-mannose receptor expression ratio, and a significant increase in pro-inflammatory cytokine release, particularly TNF-α. A stiffness-dependent increase in IL-6 was also observed when moving from soft (ALMA 2%) to stiff (ALMA 6%) hydrogels.

The stiffness-dependent trend observed in our study aligns with several previous reports in which increased stiffness promoted a shift towards M1-like macrophage phenotype. Blakney et al. reported increased TNF-α, IL-1β, and IL-6 expression in macrophages cultured on stiff PEG gels (840 kPa)(197), while Sridharan et al. found greater cell spreading and upregulation of two pro-inflammatory chemokines, such as CXCL11 and CCL20, on stiff polyacrylamide gels (323 kPa)(198). In both studies, softer gels (> 11 kPa) promoted an anti-inflammatory phenotype. Similarly, Zhuang et al. showed that increasing GelMA stiffness (2–29 kPa) enhanced inflammatory signalling and M1 polarisation(199). Our findings are also consistent with those of Previtera et al., who showed reduced pro-inflammatory mediator release on soft gels (0.3 kPa) compared to stiff ones (230 kPa)(261). Although these reported findings align with our data, it is important to note that most of the previously defined “soft” substrates are still 2–3 orders of magnitude stiffer than our ALMA 2% hydrogel (~0.25 kPa), with the exception of the soft gel used by Previtera et al. These reported soft hydrogels are even at least 2-fold stiffer than our stiffest gel (ALMA 6%, ~4.5 kPa). Notably, our findings extend and expand the existing knowledge by demonstrating that stiffness-driven M1 activation is not limited to high-stiffness substrates (>10 kPa) but can also arise within the low-kilopascal range. This is particularly relevant in the context of soft tissues, both in healthy and fibrotic conditions. For example, in the

liver and brain, stiffness can increase from 0.3-1 kPa under healthy conditions to >25 kPa during fibrosis(292, 293). These results highlight the need for comparative studies which focus on the low-kPa range to elucidate how subtle changes in the mechanical properties of soft tissues influence macrophage behaviour.

Several studied reported an opposite trend to what we and others observed, showing a pro-inflammatory phenotype associated with softer gels(201, 202, 262-264). Such discrepancies might depend on other factors than stiffness alone. In fact, stiffness is not the only mechanical property of hydrogels. Viscoelasticity is another key feature(294) and changing the degree of crosslinking in a 3D polymer network can alter the viscoelastic properties of hydrogels(295-297). Viscoelasticity has been shown to modulate mechano-sensitive molecular pathways in various cell types(286), such as fibroblasts and cancer cells(297), hepatocytes(298), and human induced pluripotent stem cells(204). Kalashnikov N. et al. have directly addressed how viscoelastic cues modulate THP-1 macrophage morphology and functions, revealing that more viscous substrates induce a rounder morphology and a reduced phagocytic activity(284). Despite this, studies examining the role of viscoelasticity in macrophage behaviour remain scarce. Further research is needed to elucidate how viscoelastic properties affect macrophages, particularly in the context of FBR.

Another factor that may explain the divergent results is the source of macrophages used in different studies(299). It is worth noting that most studies used murine bone marrow-derived macrophages, RAW264.7 cells(201) or NR8383 rat alveolar macrophages(202), all of which may exhibit different sensitivities and responses to mechanical cues compared to human macrophages. Only a few studies have used primary monocyte-derived macrophages, and interestingly they showed trends

opposite to ours. Guenther et al. showed that increased stiffness led to a M2-like phenotype, with macrophages on stiffer substrates expressing higher levels of CD206 and MMP13(265). However, their study involved coculture with cancer cells, introducing additional variables such as tumour-macrophage crosstalk that can independently affect macrophage phenotype. Furthermore, the use of a 3D culture system in their study adds complexity, as dimensionality is also known to impact macrophage behaviour(195). Similarly, Scott et al. reported that human macrophages cultured on stiffer RGD-modified-PEG-based gels (10.3 kPa) displayed a shift towards an anti-inflammatory phenotype(266). Adlerz et al. also studied human monocyte-derived macrophages on fibronectin-coated polyacrylamide gels of varying stiffness(241). While their findings addressed morphological changes, they did not include key phenotypic indicators such as surface marker expression or cytokine secretion, making it difficult to determine whether substrate stiffness promoted a pro- or anti-inflammatory state.

Surface chemistry plays a critical role in modulating cell-biomaterial interactions, primarily by influencing the adsorption of proteins from serum or culture media onto the substrate surface(224). The amount, composition, and conformation of the adsorbed protein layer vary depending on the material's chemical properties, and this layer critically determines the presentation of adhesive motifs to cells. Hydrogels can also be functionalised with peptides, such as RGD-containing sequences(266), or extracellular matrix proteins, such as fibronectin or collagen(241, 263) that favour cell attachment, promoting a stronger integrin engagement compared to unmodified hydrogels, which rely solely on non-specifically adsorbed proteins. These variations directly affect how integrins engage with the substrate, as integrin-based adhesion complexes serve as key mechano-transduction bridges between the extracellular environment and the cytoskeleton(225). As a

result, variations in protein adsorption and differences in surface densities of binding motifs can influence cell adhesion and mechano-transduction pathways, independently from the mechanical properties of the gels. Ultimately, these changes can affect gene expression and functional responses in cells, including macrophages, as demonstrated in previous studies(222, 256, 257, 259). This may partly explain the divergent polarisation outcomes observed across different studies using hydrogels with comparable stiffness but different surface chemistries.

Other features, such as surface roughness and mesh size, can influence macrophage responses, as previously reported in the literature(300, 301). However, our data indicate that their contribution is minimal in our system, with stiffness emerging as the dominant factor shaping cellular behaviour. For example, although ALMA 4% and 6% exhibited comparable roughness but different stiffnesses, macrophages cultured on ALMA 6% displayed significantly higher calprotectin/MR ratio, greater spreading, and increased TNF-α release. These effects can therefore be attributed primarily to stiffness, as topographical differences were negligible. Conversely, while ALMA 2% and 4% hydrogels differed significantly in both roughness and mesh sizes, their storage moduli (G') were not significantly different, and macrophage responses - including calprotectin/MR ratio, eccentricity, cell spreading, and TNF-α, IL-6, and CCL18 release - remained largely similar. Taken together, these findings suggest that nanoscale variations in roughness and mesh size exert little influence on macrophage behaviour in this system, whereas stiffness consistently acts as the key mechanical determinant of macrophage phenotype.

4.5 Conclusions

In this chapter, we investigated the relative contributions of substrate chemistry and stiffness to macrophage polarisation. Initial experiments examined the role of surface chemistry through conjugation of the pro-adhesive peptide GRGDSP. Both modified and unmodified hydrogels supported high cell viability, confirming absence of toxicity. Cytokine profiling indicated that GRGDSP reduced pro-inflammatory signalling (TNF-α), while its effects on anti-inflammatory responses (IL-10) were modest. These findings suggest that surface chemistry can influence macrophage activity but does not serve as the primary determinant of polarisation in this system. Following an extensive optimisation of the sample preparation method, the focus shifted more on the mechanical properties. We show that the stiffness of ALMA hydrogels significantly influences the behaviour of human primary macrophages. Specifically, stiffer hydrogels (~4.5 kPa) promoted a pro-inflammatory phenotype. This was evidenced by the elongated morphology observed on the stiffest hydrogel (ALMA 6%) and a higher calprotectin-to-mannose receptor ratio, indicating a stiffness-dependent, mechano-sensitive shift in macrophage behaviour. These findings were further supported by cytokine profiling, which showed an elevated secretion of TNF-α and IL-6 on stiffer hydrogels compared to softer substrates (~258 Pa). Importantly, this pro-inflammatory response was observed even within the range of soft tissue-relevant stiffness, highlighting the sensitivity of macrophages to subtle mechanical variations. Future studies should explore additional material properties such as viscoelasticity, surface chemistry, and protein adsorption to further elucidate the complex interactions between biomaterial mechanics and macrophage polarisation. A deeper understanding of how biomechanical properties

interface with surface chemistry and protein presentation will guide the rational design of immunomodulatory biomaterials.

Chapter 5. Hydrogel Viscoelasticity Regulates Human Monocyte-derived Macrophage Phenotype

5.1 Abstract

Macrophages are a key cell type in the foreign body reaction (FBR), playing a central role in inflammation and fibrotic encapsulation of implants. However, the influence of viscoelasticity of biomaterials on these immune cells remains poorly understood. Here, we investigated how viscoelasticity of biomaterials modulates human monocyte-derive macrophage responses. Polyacrylamide (PAAm) hydrogels with comparable storage moduli, mesh size, and chemistry but distinct viscoelasticities were prepared by tuning monomer (acrylamide) and crosslinker (bisacrylamide) concentrations. PAAm hydrogels prepared at 15% with an acrylamide-to-bisacrylamide ratio of 80:1 (15% (80:1)) displayed a solid-like, elastic behaviour, with minimal stress relaxation. In contrast, PAAm hydrogels prepared at 20% with a 300:1 ratio (20% (300:1)) showed pronounced stress relaxation, ~70% decrease of its modulus within 5 minutes, a biological-relevant timeframe as cells generate and release traction forces with a similar timing. We showed that human peripheral monocyte-derived macrophages cultured on the viscoelastic substrate spread more extensively and displayed higher eccentricity compared to those on the elastic substrates, which had smaller area and were characterised by cluster formation. Phenotype characterisation revealed that elastic hydrogels promoted a pro-inflammatory response, marked by higher calprotectin expression and a significant increase in the secretion of TNF-α and IL-6, while anti-

inflammatory surface marker and cytokines remained unaffected. These findings demonstrate that stress relaxation is a key factor in regulating macrophage phenotype, independent of storage modulus, and should be considered in the rational design of immunomodulatory biomaterials to mitigate FBR.

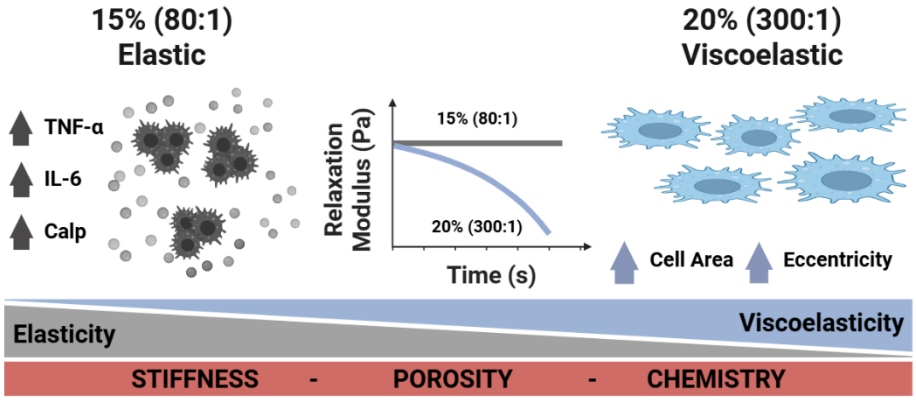

Figure 5.1.1 Schematic showing the effect of hydrogel viscoelasticity on macrophage morphology and phenotype.

5.2 Introduction

The foreign body reaction (FBR), which typically develops around implanted materials, is primarily driven by the host immune response and often leads to immune cell infiltration, formation of giant cells, and fibrous encapsulation. FBR compromises the functionalities and therapeutic outcome of implants and can markedly lower the life quality of affected people(113, 116). Macrophages play a central role in orchestrating FBR, a function underscored by multiple studies employing immune cell knockout models in animals(176, 302), Macrophages can adopt a spectrum of different activation states, with the pro- (M1) and the anti- (M2) inflammatory phenotypes at the opposite ends of this continuum(71, 72, 77), and strategies to mitigate

FBR often aim to promote M2 polarisation to reduce fibrous encapsulation(303, 304).

It is well established that various material properties, including stiffness, viscoelasticity, porosity, surface chemistry, and topography can influence macrophage polarisation, thereby shaping the onset and progression of FBR(195, 196, 255, 305, 306). Adherent cells engage with substrates through integrin-based adhesion complexes and generate contractile forces on the substrates. Through the cytoskeleton, which serves as a mechano-transduction bridge between the extracellular and the internal cellular environment, cells can sense the mechanical cues of the substrates they are attached to(225, 307, 308). Beyond integrins, cells can exploit other pathways to sense materials' mechanical properties, such as the mechanosensitive ion channels(309) PIEZO1(310) and TRPV4(311), which macrophages also utilise.

Most studies on cell–substrate interactions have taken a stiffness-centric approach, focusing on stiffness as the only mechanical property(198, 201, 265) while other important features, including viscoelasticity, remain less explored. Yet, living tissues - including kidneys(312), brain(313), pancreas(314) - as well as structural components like collagen(315) and hydrogel-based biomaterials, display more complex mechanical behaviours that are best described as viscoelastic. These materials show both elastic and viscous responses when deformed. Viscoelasticity can be quantified by storage modulus (G') and loss (G'') moduli which represent the elastic and viscous component, respectively. Viscoelastic materials also show related properties, such as stress relaxation, which described the progressive decrease in stress observed when a constant strain is maintained over time(203). Materials with higher viscoelasticity display greater relative G'' values and enhanced

stress relaxation, i.e. more rapid declining of stress when maintaining a constant strain(286, 316).

Several studies have shown that viscoelasticity affects different cell types and their behaviour. For example, myoblasts cultured on RGD-modified alginate exhibited enhanced spreading and proliferation on viscoelastic hydrogels compared to purely elastic ones(208). Similarly, survival, proliferation, and polarisation of human pluripotent stem cells (hiPSCs) were supported by fast-relaxing ($\tau_{1/2}$ ~ 70 s) alginates, whereas slow-relaxing ($\tau_{1/2}$ ~ 1000) hydrogels induced apoptosis(204). Effects of viscoelasticity have also been reported in human mesenchymal stem cells (hMSCs)(205, 206), skeletal muscle satellite cells(207), fibroblasts(209, 210), breast epithelial cells(211), hepatocellular carcinoma cells, hepatocytes(212, 213), adenocarcinoma and fibrosarcoma cells(214).

Only a very limited number of studies have investigated the effect of viscoelasticity on macrophages. For example, THP-1 macrophages cultured on viscous polyacrylamide (PAAm) gel displayed altered morphology and reduced phagocytosis(284). Similarly, RAW 264.7 cells showed that elastic PAAm hydrogels supported transient lipopolysaccharide (LPS)-treated macrophages activation, while viscoelastic counterparts amplified inflammation under persistent stimulation. These effects were mediated by F-actin dynamics and transcription factors (NF-κB, C/EBPδ, ATF3), highlighting viscoelasticity as a key regulator of immune responses in inflammatory and cancerous contexts(317). In another study, murine bone marrow-derived macrophages (BMDMs) cultured on fast-stress-relaxation PEG-modified alginate hydrogels exhibited higher TGF-β1–mediated macrophage–MSC interactions, a metabolic shift from glycolysis to oxidative phosphorylation, and promoted bone regeneration(285).

Building on these studies, there is scope to further investigate how viscoelasticity shapes macrophage behaviour. Previous works on viscoelasticity-macrophage interactions have relied on cell lines and murine cells, whereas the effect of viscoelasticity on primary human monocyte-derived macrophages remains unexplored. Given their central role in orchestrating the immune response(176), understanding how human macrophages respond to viscoelasticity - thus overcoming the limitations associated with immortalised or cross-species models - is crucial. Such insights would help to develop and design novel implantable biomaterials with improved biocompatibility in humans, while reducing unwanted immunological response, such as FBR.

Additionally, prior studies on viscoelasticity-macrophage interactions lacked characterisation of stress relaxion(210) or the reported rapid stress relaxation (<5 s for both elastic and viscoelastic materials to reach ~30% of their initial moduli). Such fast stress relaxation determined nearly identical profiles after few seconds which are unlikely biologically relevant(211, 317). When cells engage with a substrate via adhesion complexes, they exert and release traction forces between 20 s and 5 minutes(205). Nascent adhesions require up to 2 minutes to mature under sustained tension(318), and, for them to develop into focal adhesions, actin needs to polymerise, a highly dynamic process with filament turn-over times of 10-30 seconds(319). Therefore, materials that relax within 5 s are likely to dissipate forces before effective cell-material interactions and adhesion maturation can occur. To be suitable, substrates should exhibit stress-relaxation dynamics within biologically relevant timescales, allowing cells to sense and respond to these variations. In this work, the viscoelastic composition relaxes by ~70% over in 10 minutes, aligning with the timeframe of adhesion maturation and providing an appropriate platform to probe macrophage responses.

Finally, when designing viscoelastic biomaterials, it is important to minimise changes in composition so that differences in cellular responses can be more confidently attributed to viscoelastic properties rather than to variations in chemistry or other physical features. For example, introducing new chemical components to tune viscoelasticity may alter biological responses, complicating data interpretation. Polyacrylamide (PAAm) hydrogels offers a distinct advantage in this regard as their properties can be optimised by changing the concentration of acrylamide and bisacrylamide as well as the ratio between these two components to achieve the desired modulus and viscoelasticities(183, 205, 320), while minimising the change in chemical composition. Additionally, PAAm gels have been extensively used in the literature to study the influence of mechanical properties on a variety of cell types so that the obtained results can be compared to similar studies(181, 321, 322).

We hypothesised that substrate viscoelasticity regulates macrophage polarisation, and that differences in stress relaxation profiles lead to distinct activation states in human monocyte-derived macrophages. We further hypothesised that macrophage responses to viscoelasticity differ from those reported in murine models and cell lines. Accordingly, the objective of this study was to investigate the effect of viscoelastic properties, independent of major compositional changes, on macrophage activation and polarisation, using morphological assessment, surface marker expression, and cytokine profiling, to inform the design of biomaterials with improved immunomodulatory performance.

To do so, we prepared PAAm gels with similar initial relaxation moduli - within the range soft tissues - but differed in their viscoelastic behaviours, as defined by distinct stress relaxation profiles. The

mechanical properties of the PAAm gels were determined using rheological testing. Monocytes were isolated from healthy blood donors and cultured on PAAm gels for 6 days. Macrophage phenotype was assessed using a combination of techniques, including morphological evaluation, surface marker expression and cytokine profiling. We observed that elastic PAAm promoted a pro-inflammatory macrophage phenotype, as evidenced by elevated TNF-α and IL6 secretion and an increased calprotectin-to-mannose receptor ratio. Significant differences in the cell morphologies were also observed, with macrophages being on the viscous substrate developing a higher area and a more elongated morphology.

5.3 Results

To investigate the influence of viscoelasticity on primary human macrophages, our aim was to engineer two hydrogel formulations with comparable chemical composition and stiffness, while differing specifically in their stress relaxation behaviour when undergoing identical strain conditions, as schematically represented in **Figure 5.3.1**. By adopting this design strategy, we sought to ensure that viscoelasticity would represent the only property varying between the samples, thereby allowing its specific contribution in driving macrophage polarisation to be studied.

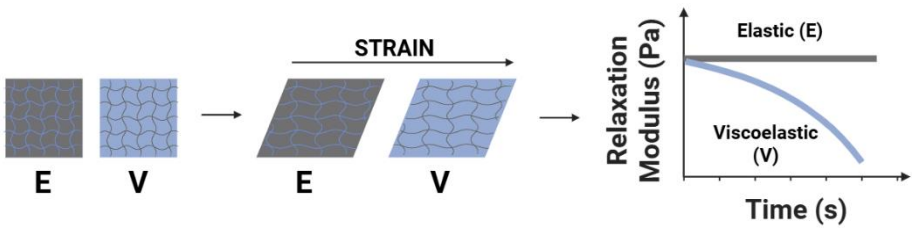

Figure 5.3.1 Schematic illustration of the targeted mechanical properties of the hydrogels designed to isolate and study the effects of viscoelasticity on macrophage behaviour.

Previous studies have demonstrated that changes in the type of crosslinking (ionic vs. covalent) can be used to obtain materials with different stress relaxation properties(297). However, introducing distinct molecules or chemical groups in only one of the formulations to achieve different relaxation properties inevitably alters the chemistry of the hydrogel. This constitutes a big limitation of such approach, as it is well established that material chemistry directly affects cellular behaviour. Consequently, the incorporation of new chemical species to tune stress relaxation introduces an additional variable, making it difficult to disentangle whether observed changes in cell responses are driven by differences in mechanical or chemical properties of the substrates.

Other studies have also shown that variations in crosslinking density or molecular weight of polymers could determine differences in viscoelastic properties(323). Based on this evidence, we selected two pairs of ALMA hydrogel compositions - ALMA 2% and ALMA 4% - that exhibited comparable stiffness but differed in their degree of methacrylation, specifically low (10–20%) and high (20–40%). We hypothesised that these differences in methacrylation would result in distinct stress relaxation behaviours. Contrary to our expectations, the stress relaxation data did not support this hypothesis, as both pairs of ALMA hydrogels showed no significant differences in their relaxation moduli G(t). As shown in **Figure 5.3.2**, the relaxation curves displayed highly similar profiles.

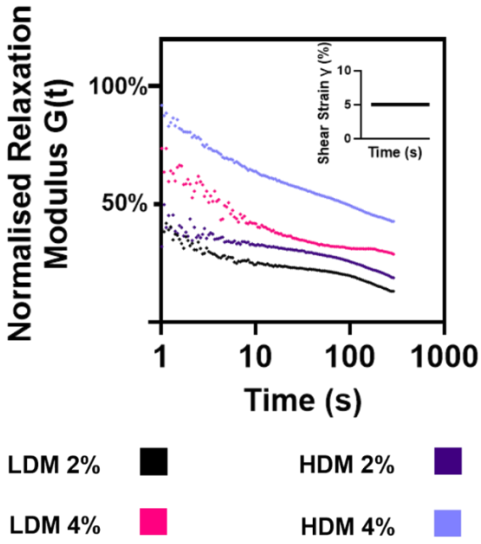

Figure 5.3.2 Normalised stress relaxation curves of ALMA hydrogels (2% and 4% w/v) prepared using low (LDM) and high (HDM) degrees of methacrylation. Data is presented as mean of triplicates ± SD (n=3).

As it was not possible to achieve the desired viscoelastic properties with ALMA hydrogels, we shifted to an alternative material to further investigate the effect of stress relaxation on macrophages. Among the available polymers, polyacrylamide (PAAm) hydrogels were selected. Owing to their well-established mechanical tuneability and chemical versatility, PAAm hydrogels represent an ideal platform, as their properties can be precisely modulated by varying the total concentrations of acrylamide and bisacrylamide, as well as the ratio between these monomers, thereby enabling the generation of substrates with controlled stiffness and viscoelastic behaviour(183, 320, 322).

Based on the work of Cameron A et al(205), we tried to reproduce two PAAm hydrogel formulations with the targeted mechanical properties: PAAm 8% (80:1), prepared with 8% (w/v) acrylamide and 0.1% (w/v) bis-acrylamide, and PAAm 15% (1200:1), prepared with 15% (w/v)

acrylamide and 0.0125% (w/v) bis-acrylamide. The gels were initially synthesised following the methodology reported in their study, which is summarised in the schematic shown **Figure 5.3.3**.

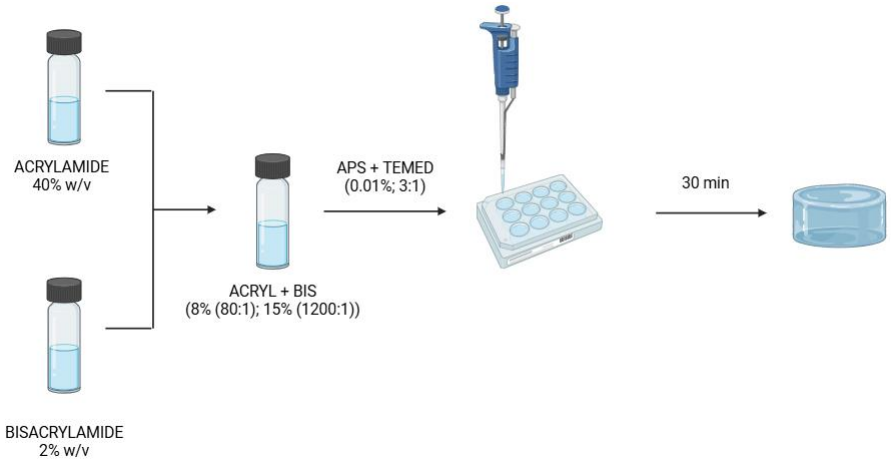

Figure 5.3.3 Schematic illustration of the methodology used for the preparation of PAAm hydrogels: 8% (80:1) and 15% (1200:1).

Stock solutions of acrylamide (40% w/v) and bis-acrylamide (2% w/v) were prepared by dissolving the powders in water overnight. Acrylamide and bis-acrylamide were subsequently mixed, and ammonium persulfate (APS, initiator) together with tetramethylethylenediamine (TEMED, catalyst) were added to initiate polymerisation. After thorough mixing, the solutions were dispensed into 12-well plates and left to crosslink for 30 minutes. Although both formulations underwent partial crosslinking, it was evident that this set-up did not enable complete gelation, limiting the reproducibility of the manufacturing method. The resulting PAAm gels appeared liquid-like, unable to maintain their disk shape, and exhibited a "sticky" consistency (**Figure 5.3.4A**), all features indicative of incomplete crosslinking. This initial visual assessment was corroborated by amplitude sweep tests performed on PAAm 8% (80:1) (**Figure 5.3.4B**) and PAAm 15% (1200:1) (**Figure 5.3.4C**), which confirmed that the materials behaved

as extremely soft gels, with PAAm 15% (1200:1), showing comparable values of G′ and G″.

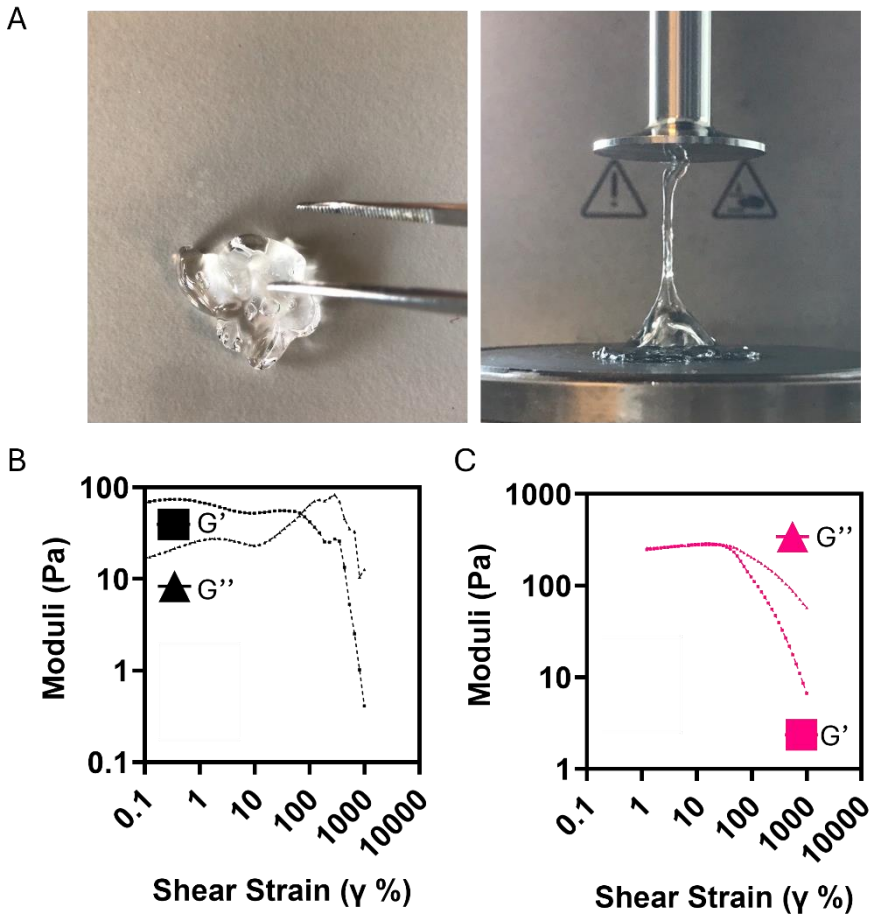

Figure 5.3.4 PAAm hydrogels prepared following the method of Cameron A. et al(205). (A) Representative images of PAAm hydrogels. Amplitude sweeps of PAAm **(B)** 8% (80:1) and **(C)** 15% (1200:1). Data is presented as mean of triplicates (n=3).

Considering that crosslinking occurs through a radical reaction, we carefully examined all the variables that might have negatively influenced the progression of the reaction. A first aspect to consider was the presence of oxygen. Oxygen is a well-known radical scavenger, and due to its high reactivity, it can readily cross-react with free radicals.

This interaction can inhibit the propagation of the chain reaction and ultimately result in incomplete crosslinking(324). Another factor that might have played a role was the type of initiator used. In our system, APS was employed as a thermal initiator, which generates sulfate free radicals upon heating or in the presence of a catalyst, such as TEMED. The efficiency of this process is highly dependent on the surrounding conditions, particularly pH. Since the polymerisation was carried out in water, no buffer system was present to control the pH. As radical polymerisations require a basic environment to proceed efficiently, the presence of protons could have interfered with radical propagation, again resulting in incomplete crosslinking(325). A final variable that we considered was the source and solubility of the monomers. While commercial pre-made solutions of acrylamide and bisacrylamide were available, we prepared stock solutions starting from the powders of both monomers. During this process, we observed that bisacrylamide at 2% w/v was particularly difficult to dissolve. Although the solution appeared clear to the eye, it is possible that the solubility was not complete, which would have resulted in a lower effective concentration of crosslinker.

To develop a consistent and reliable sample preparation method, we systematically investigated how these variables influenced the mechanical properties of the hydrogels. We prepared two PAAm gels at 20% (19:1) and compared gels obtained from the pre-made solutions with those prepared from powder-derived stock solutions. This composition was intentionally chosen as we wanted to ensure that even at relatively high concentrations of acrylamide (19% w/v) and

bisacrylamide (1% w/v), the solubility of bisacrylamide did not have a tangible negative effect on reproducibility.

Mechanical characterisation was performed by amplitude sweeps (**Figure 5.3.5A**), from which complex moduli were calculated as a measure of the hydrogels' mechanical properties (**Figure 5.3.5B**). The results clearly showed that PAAm prepared from pre-made solutions had a complex modulus almost one order of magnitude higher than the corresponding gels obtained from dissolved powders. This large difference can reasonably be attributed to an effectively lower concentration of bisacrylamide due to limited solubility. Visual inspection of the hydrogels supported this interpretation (**Figure 5.3.5C**): the gel prepared from powders appeared opaque white, suggesting incomplete dissolution, while the gel obtained from pre-

made solutions was colourless and transparent, as expected from a homogeneous system.

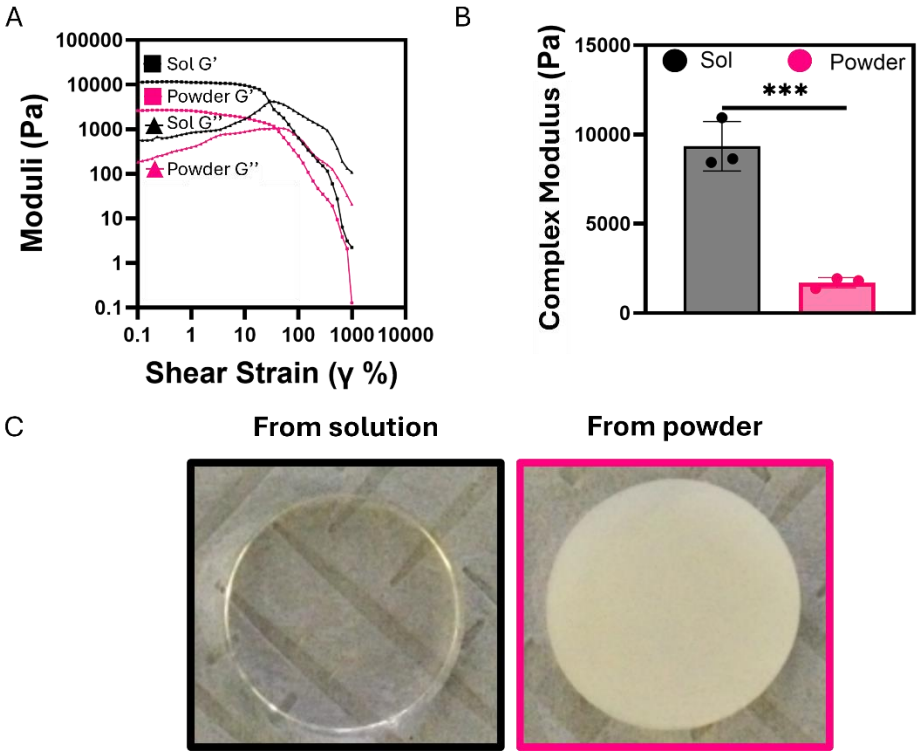

Figure 5.3.5 Comparison of PAAm 20% (19:1) hydrogels prepared from acrylamide and bisacrylamide powders versus pre-made solutions. (A) Amplitude sweep showing storage modulus (G′) and loss modulus (G″) for the two formulations. **(B)** Complex moduli of PAAm 20% hydrogels obtained from the two different starting materials. **(C)** Representative images of the hydrogels, highlighting the opaque appearance of the gel prepared from powders compared to the transparent gel obtained from pre-made solutions.

Once established the solubility of bisacrylamide could compromise the mechanical properties of PAAm gels, pre-made solutions of acrylamide (40% w/v) and bisacrylamide (2% w/v) were used to prepare all

subsequent gels. To further improve reproducibility, all solutions were prepared in PBS to maintain a slightly basic pH.

We then examined other parameters that could influence the mechanical properties of PAAm gels, focusing on the formulations 8% (80:1) and 15% (1200:1). We tested three different degassing methods - nitrogen flushing (N_2), sonication (sonic), and sonication under vacuum (sonic + vac) - to remove dissolved oxygen from the solutions while leaving them to crosslink in air. Amplitude sweeps were performed (**Figure 5.3.6A**), and complex moduli were calculated (**Figure 5.3.6B**). Although no statistically significant differences were observed between samples,

sonication under vacuum appeared to yield hydrogels with higher complex moduli, particularly for PAAm 8% (80:1) (**Figure 5.3.6C**).

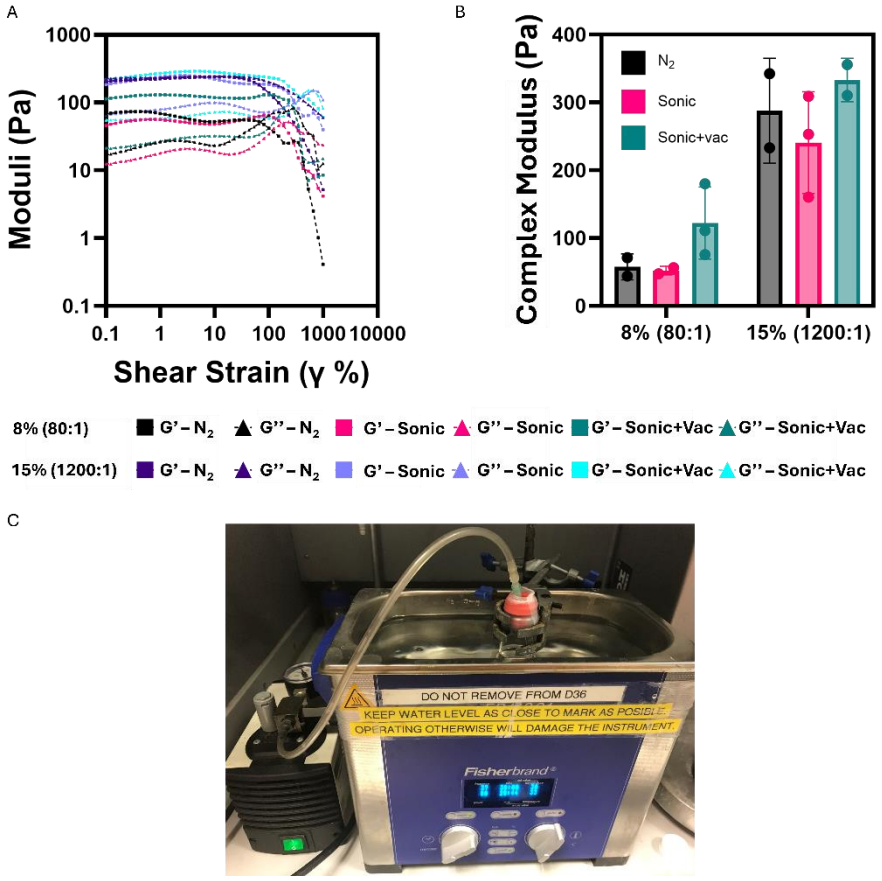

Figure 5.3.6 Rheological characterisation of PAAm hydrogels prepared with different degassing methods. (A) Amplitude sweep showing storage modulus (G′) and loss modulus (G″) as a function of strain. **(B)** Complex moduli derived from Amplitude sweeps. **(C)** Experimental set-up of sonication under vacuum, which provided the most promising results. Data is presented as mean of triplicates ± SD (n=3).

Despite the significant improvements achieved, PAAm 8% (80:1) and 15% (1200:1) still exhibited significantly different complex moduli, as well as storage (G′) and loss (G″) moduli, from the values reported in

the literature. This prompted us to investigate additional variables that might have influenced the crosslinking process and, consequently, the mechanical properties of the gels. We prepared PAAm hydrogels by varying both the type of initiator - either APS with TEMED or Irgacure-2959 - and the atmospheric conditions - the presence or absence of oxygen. Amplitude sweeps of PAAm 8% (80:1) and 15% (1200:1) were performed (**Figure 5.3.7A**), and complex moduli were calculated (**Figure 5.3.7B**).

Among the factors examined, oxygen emerged as the most critical one. When comparing gels prepared with the same initiator under different atmospheric conditions, it became evident that the presence of oxygen had a strongly negative effect on gel formation. Specifically, the complex moduli of both PAAm formulations were significantly higher when crosslinking was performed in an oxygen-free environment, which we achieved using a glove box filled with argon, maintaining oxygen levels below 2000 ppm. Regarding the initiators, APS in combination with TEMED proved to be more effective than Irgacure-2959. Hydrogels prepared with APS consistently exhibited significantly higher

complex moduli compared to those obtained with Irgacure-2959, confirming its suitability for these formulations.

Based on these findings, all subsequent PAAm hydrogels were degassed via sonication under vacuum and prepared in oxygen-free conditions using APS and TEMED.

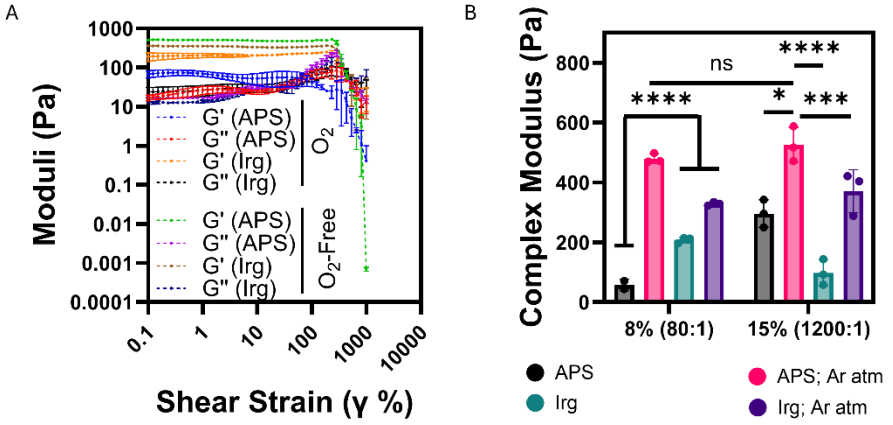

Figure 5.3.7 Rheological characterisation of PAAm hydrogels prepared with different initiators and polymerised either in air or in oxygen-free environment. (A) Amplitude sweeps showing storage modulus (G′) and loss modulus (G″) as a function of strain. **(B)** Complex moduli of the hydrogels, derived from amplitude sweep measurements. Data is presented as mean of triplicates ± SD (n=3).

Given the similarity in the storage modulus curves (**Figure 5.3.8A**) and in the complex moduli (**Figure 5.3.8B**), PAAm 8% (80:1) and 15% (1200:1) were further characterised for their stress relaxation to determine their viscoelastic properties (**Figure 5.3.8C**). To better compare their relaxation rates, the absolute values were normalised by their initial values (**Figure 5.3.8D**), revealing that the two hydrogels had distinct viscoelastic properties, while having comparable stiffnesses. Specifically, PAAm 8% (80:1) displayed predominantly an elastic behaviour, whereas PAAm 15% (1200:1) exhibited a higher

viscoelasticity, with its relaxation modulus decreasing by approximately 80% over the observation period.

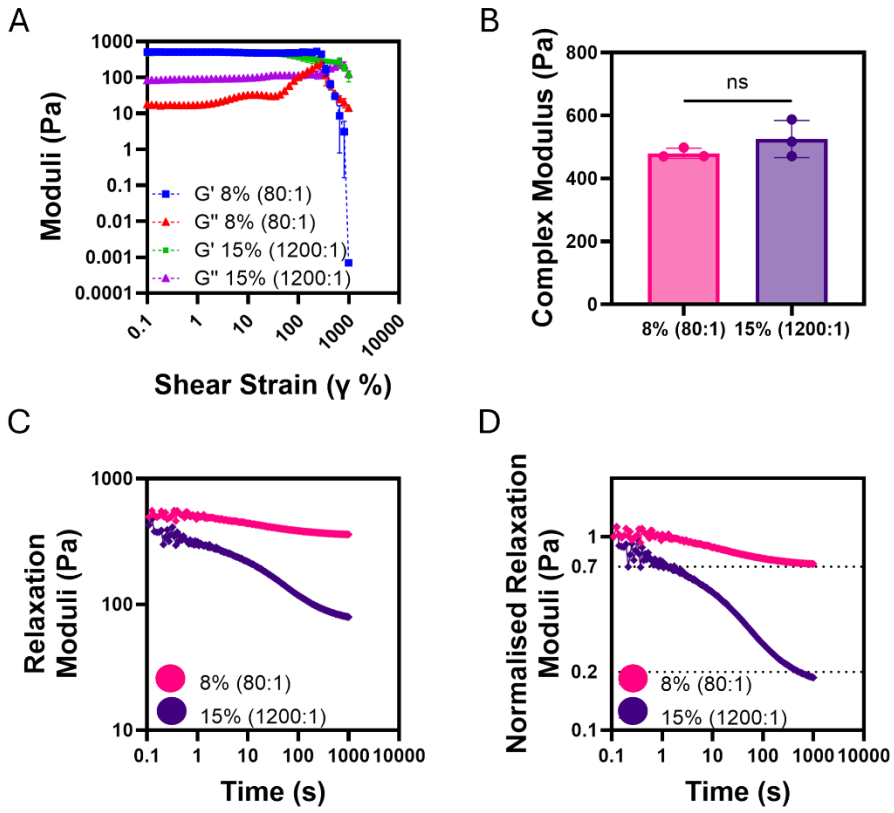

Figure 5.3.8 Rheological characterisation of PAAm 8% (80:1) and 15% (1200:1) hydrogels. (A) Amplitude sweeps showing storage (G′) and loss (G″) moduli as a function of strain. **(B)** Complex moduli derived from amplitude sweep measurements. **(C)** Stress relaxation and **(D)** Normalised stress relaxation curves. Data is presented as mean of triplicates ± SD (n=3).

Given that these two formulations exhibited the desired mechanical properties - comparable stiffness but significantly different stress relaxation - while maintaining only minimal differences in their chemical composition, they were selected as suitable candidates for investigating the effect of viscoelasticity on human primary

macrophages. To generate samples compatible with cell culture, the optimised "sandwich" methodology previously developed for ALMA hydrogels (Chapter 4) was adapted for PAAm hydrogels. The main modification consisted in degassing the precursor solutions and performing the crosslinking reaction under oxygen-free conditions as illustrated in the schematic represented in **Figure 5.3.9**.

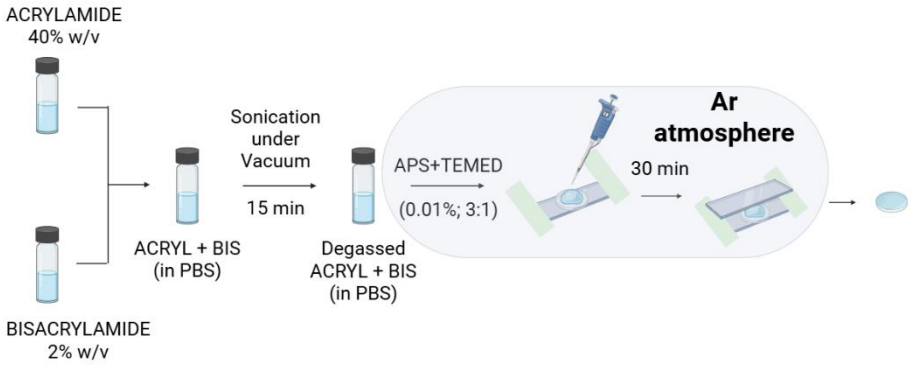

Figure 5.3.9 Schematic representation of the "sandwich" method for producing PAAm hydrogel films with controlled thickness on silanised coverslips.

Samples were thoroughly washed with PBS (x 5) to remove any unreacted monomers that could contribute to cytotoxicity and subsequently sterilised under UV light (260 nm) for 40 minutes. Samples were incubated in penicillin–streptomycin (10x) for 24 hours, and then in complete RPMI medium for a further 24 hours to allow protein adsorption, a critical step to achieve cell attachment since PAAm does not naturally contain pro-attachment motifs. Human monocytes were isolated from buffy coats via positive selection and seeded at a density of 1 x 10^6 cells/mL. Cells were allowed to adhere for 24 hours, after which non-adherent cells were removed by media replacement, and the remaining adherent cells were cultured for 6 days to allow differentiation into macrophages. Cell viability was assessed using both Live/Dead (**Figure 5.3.10A**) and ToxiLight (**Figure 5.3.10B**) assays.

While Live/Dead assay provides a qualitative measure of viability, showing live and dead cells, ToxiLight assay evaluates metabolic activity, which is used a surrogate of cellular health status. Together, these assays confirmed that cells remained viable for 6 days of culture on both PAAm 8% (80:1) and 15% (1200:1) hydrogels, with no significant differences with M0 (Live), macrophages cultured on TCP. These results demonstrate that PAAm hydrogels provide suitable, non-toxic substrates for the differentiation and long-term culture of human macrophages.

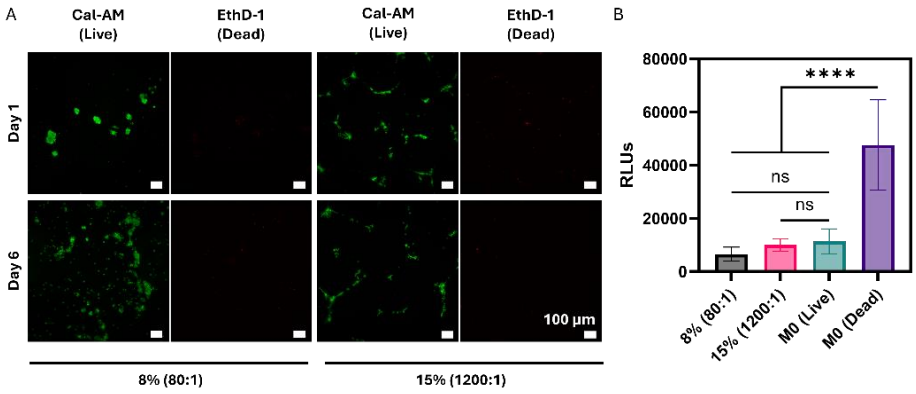

Figure 5.3.10 Human primary macrophage viability on PAAm gels. **(A)** Fluorescent microscopy images of macrophages stained for Calcein-AM (green – live cells) and Ethidium homodimer-1 (red – dead cells) at day 1 and day 6. Scale bar: 100 µm. **(B)** ToxiLight assay on macrophages cultured for 6 days on PAAm 8% (80:1) and 15% (1200:1). Positive control (M0 (Dead)) is purposely lysed macrophages. M0 macrophages cultured on tissue culture plastic (M0 (Live)) were used as negative controls. Data is presented as mean of triplicates of three independent experiments ± SEM (n=3, N=2).

Brightfield imaging revealed that macrophages cultured on PAAm 15% (1200:1) tended to form aggregates, with "filament-like" extensions

emanating from the cell clusters, features that were not observed in macrophages on PAAm 8% (80:1) (**Figure 5.3.11**).

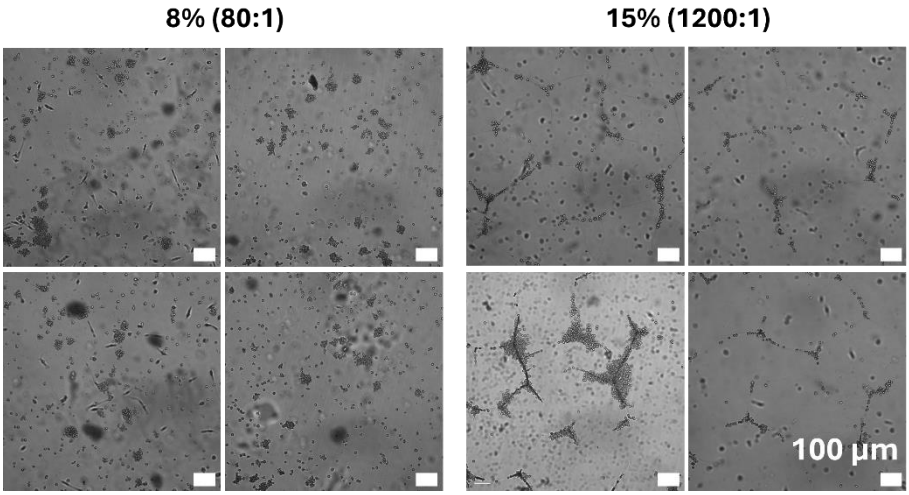

Figure 5.3.11 Representative brightfield images of macrophages on day 6 cultured on PAAm 8% (80:1) and PAAm 15% (1200:1).

To determine whether the filament-like structures were a feature of the material itself or were induced by cellular activity, we compared PAAm 15% (1200:1) samples before and after incubation with media, both in the presence (**Figure 5.3.12A**) and absence (**Figure 5.3.12B**) of cells. Prior to incubation, the hydrogel surface appeared homogeneous. However, after 24 hours, the filamentous structures appeared, resulting in a non-uniform surface. We hypothesised that this phenomenon was a consequence of phase separation happening during the swelling, due to the low concentration of the crosslinking agent. This presented a significant limitation, as consistent material properties across the surface

are essential to attribute biological observations solely to viscoelasticity, which is intended to be the only varying parameter.

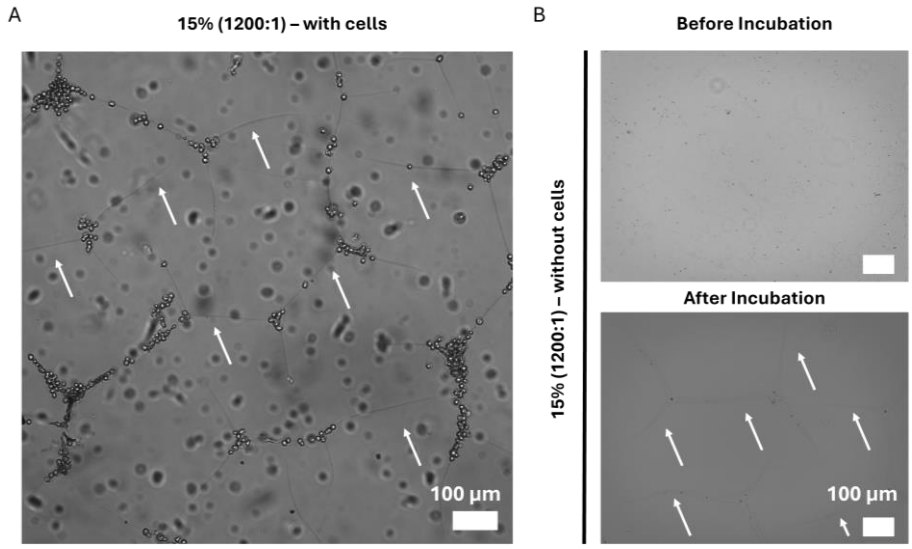

Figure 5.3.12 Representative brightfield images of PAAm 15% (1200:1) hydrogels (A) with and (B) without macrophages, illustrating the formation of the filament-like structures.

Another limitation we observed was the change in the hydrogel texture and mechanical properties after 6 days. As shown in Figure **5.3.13A**, PAAm 15% (1200:1) became a liquid-like material, unable to retain its original shape, whereas PAAm 8% (80:1) (**Figure 5.3.13B**) remained structurally intact. The low BIS content in PAAm 15% (1200:1) resulted in a 4-fold increase in the hydrogel weight, corresponding to approximately 400% swelling (**Figure 5.3.13C**). In contrast, PAAm 8% (80:1) exhibited only ~8% swelling (**Figure 5.3.13D**), which did not compromise the integrity of the 3D network. This difference highlights the critical influence of crosslinking density on hydrogel stability during the culture period and represented a significant limitation for

mechanobiology studies, as uncontrolled swelling compromises the mechanical properties of hydrogels.

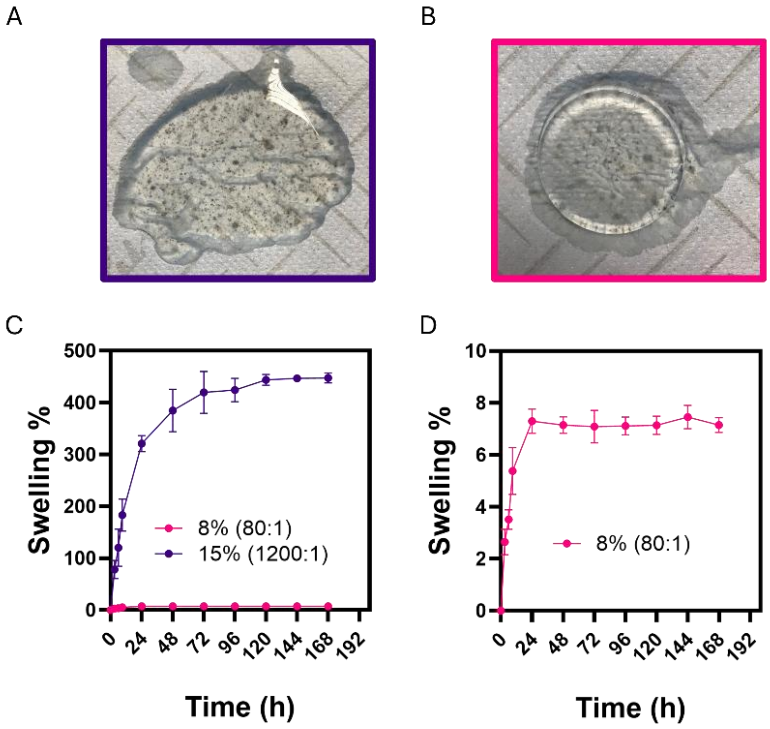

Figure 5.3.13 Swelling behaviour of PAAm 8% (80:1) and 15% (1200:1). (A, B) Representative images of hydrogels after equilibration in PBS. **(C, D)** Swelling of PAAm hydrogels. Data is presented as mean of triplicates ± SD (n=3).

Another aspect requiring optimisation was the stiffness of the PAAm hydrogels. Since the aim was to work with substrates that mimic the mechanical properties of soft tissues, the targeted stiffness range was set between 1 and 2 kPa.

To identify formulations with the desired mechanical properties, a high-throughput screening approach was used. It consisted in preparing several PAAm hydrogels where acrylamide concentrations and

acrylamide-to-bisacrylamide ratios were systematically varied, as reported in **Table 5.3.1**.

Table 5.3.1. Compositions and concentrations of PAAm tested for their mechanical properties.

ID	Comp	Acryl:Bis Ratio					
		19:1	30:1	80:1	300:1	1200:1	100k:1
15%	Acryl (w/v %)	/	14.516	14.815	/	15	/
	BIS (w/v %)		0.484	0.185		0.0125	
20%	Acryl (w/v %)	19	19.355	19.753	19.934	19.983	19.9998
	BIS (w/v %)	1	0.645	0.247	0.066	0.017	0.0002

ID	Comp	Acryl:Bis Ratio				
		80:1	1200:1	2500:1	5000:1	7500:1
30%	Acryl (w/v %)	29.630	29.975	29.988	29.994	29.996
	BIS (w/v %)	0.370	0.025	0.012	0.006	0.004

ID	Comp	Acryl:Bis Ratio			
		10k:1	20k:1	40k:1	100k:1
30%	Acryl (w/v %)	29.997	29.9985	29.99925	29.9997
	BIS (w/v %)	0.003	0.0015	0.00075	0.0003

PAAm hydrogels were allowed to swell for 6 days, after which shape and texture were visually assessed. Samples that became liquid-like and were unable to retain the disc shape were excluded from further characterisation, while those maintaining solid-like properties were further characterised (**Figure 5.3.14A**). For these, amplitude sweeps tests were performed (**Figure S3**) to determine the linear viscoelastic region (LVE) and the complex moduli of all compositions (**Figure 5.3.14B**). When comparing complex moduli across formulations, significant differences were observed between 15% (30:1) and both 15% (80:1) and 15% (1200:1), between 20% (19:10) and both 20% (1200:1) and 20% (100k:1), and between 30% (80:1) and 30% (100k:1). These formulations share similar acrylamide content but differ in BIS concentration, indicating that the crosslinker density is the main factor influencing network architecture and, consequently, mechanical properties. Not all compositions with different total monomer concentrations but identical acrylamide-to-BIS ratios exhibited significant differences in complex moduli. For example, 30% (80:1) showed a markedly higher modulus than 15% (80:1), whereas 15% (30:1) and 20% (30:1) were comparable.

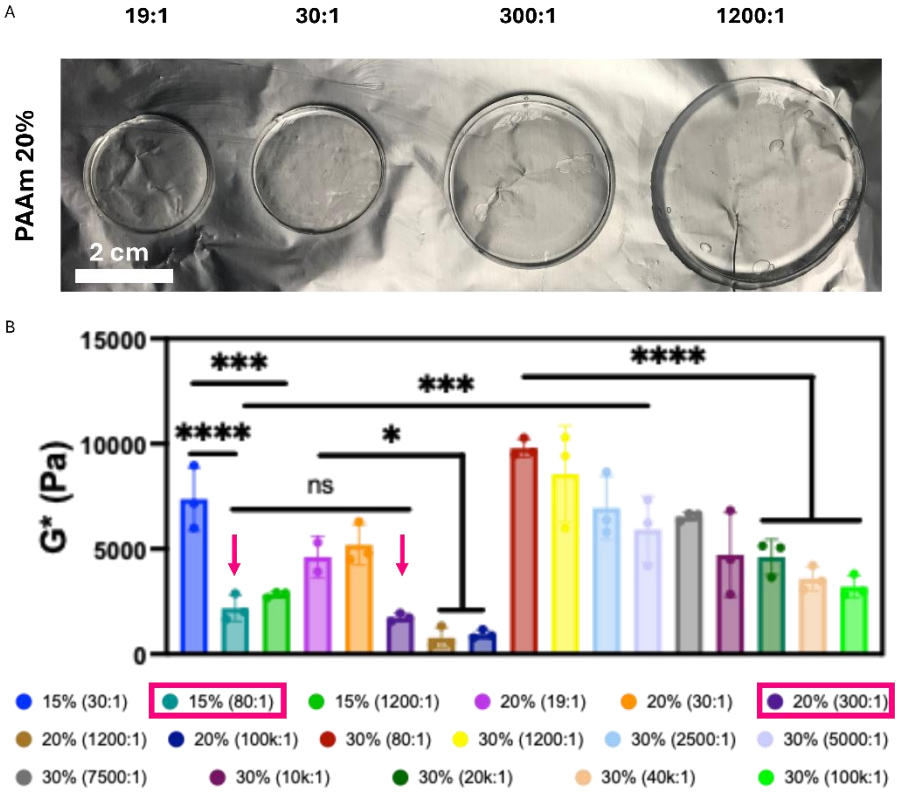

Figure 5.3.14 Characterisation of PAAm hydrogel mechanical properties. (A) Examples of PAAm 20% hydrogels with varying acrylamide:BIS ratios that maintained structural integrity and were selected for mechanical testing. **(B)** Complex moduli of different PAAm hydrogels. Data is presented as mean of triplicates ± SD (n=3).

To assess viscoelastic properties, stress relaxation tests were performed (**Figure 5.3.15A**). Relaxation curves were normalised to their initial relaxation modulus to allow direct comparison between formulations (**Figure 5.3.15B**). Among the tested compositions, 15% (80:1) displayed the most solid-like behaviour, with only ~20% reduction in modulus, whereas 30% (7500:1) exhibited the most pronounced viscoelasticity. However, these two formulations also differed significantly in complex moduli, making them unsuitable for decoupling the effect of stiffness from viscoelasticity. To specifically evaluate this property, it is necessary to compare hydrogels with similar stiffness, namely similar

storage moduli so that their elastic components (G′) are comparable, but they differ in the rate or extent of stress dissipation. This approach ensures that observed cellular responses can solely be attributed to viscoelasticity.

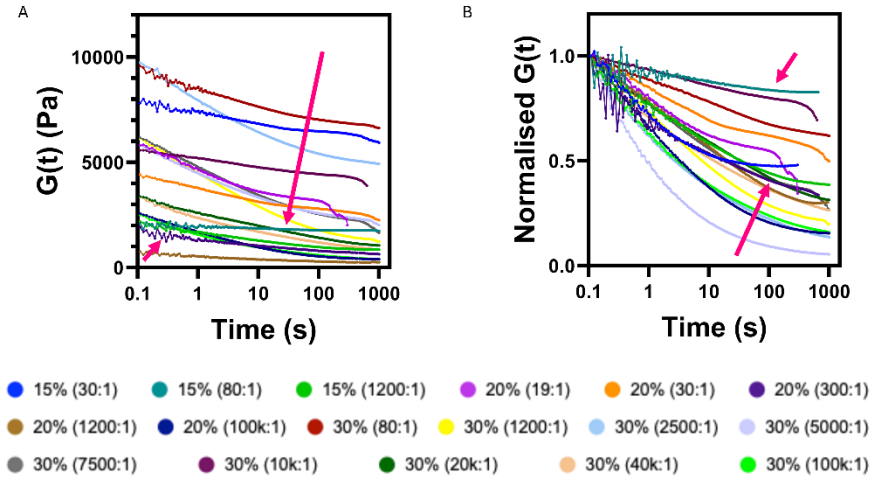

Figure 5.3.15 Stress relaxation behaviour of PAAm hydrogels prepared with different compositions. (A) Absolute relaxation moduli, illustrating differences in relaxation magnitude among the formulations. **(B)** Normalised relaxation moduli, highlighting the relative decay over time. Data is presented as mean of triplicates (n=3).

Among all tested formulations, PAAm 15% (80:1) and 20% (300:1) exhibited similar complex moduli, therefore comparable stiffness, but different relaxation properties, and were selected for further characterisation. To ensure that the mechanical properties were consistent across different preparation batches, the two formulations were re-prepared and fully characterised. Both amplitude (**Figure 5.3.16A**) and frequency sweeps (**Figure 5.3.16B**) showed overlapping storage modulus (G′) curves, while the loss moduli (G″) indicated distinct contributions from the viscous components. To quantify these differences, G′ and G″ were extrapolated from frequency sweeps at 1 Hz, a timescale relevant to cellular traction forces(205). As shown in

Figure 5.3.16C, G′ values were not significantly different, whereas G″ values differed significantly, confirming a difference in the viscous components between the two formulations. Complex viscosity (**Figure 5.3.16D**) was also characterised and showed no significant differences. Stress relaxation was performed at 1% strain for ~15 minutes, parameters that were carefully chosen to simulate what cells undergo in physiological conditions. Cells can take from few seconds(326, 327) to up to 5 minutes(328) to generate and release tractional forces, timeframe that is comprised in our observations. As shown in **Figure 5.3.16E** and **Figure 5.3.16F**, both formulations started with comparable relaxation moduli, confirming similar stiffness, but their relaxation profiles diverged: PAAm 15% (80:1) remained largely elastic, whereas PAAm 20% (300:1) exhibited a ~70% decrease in modulus over the 15-minute observation period.

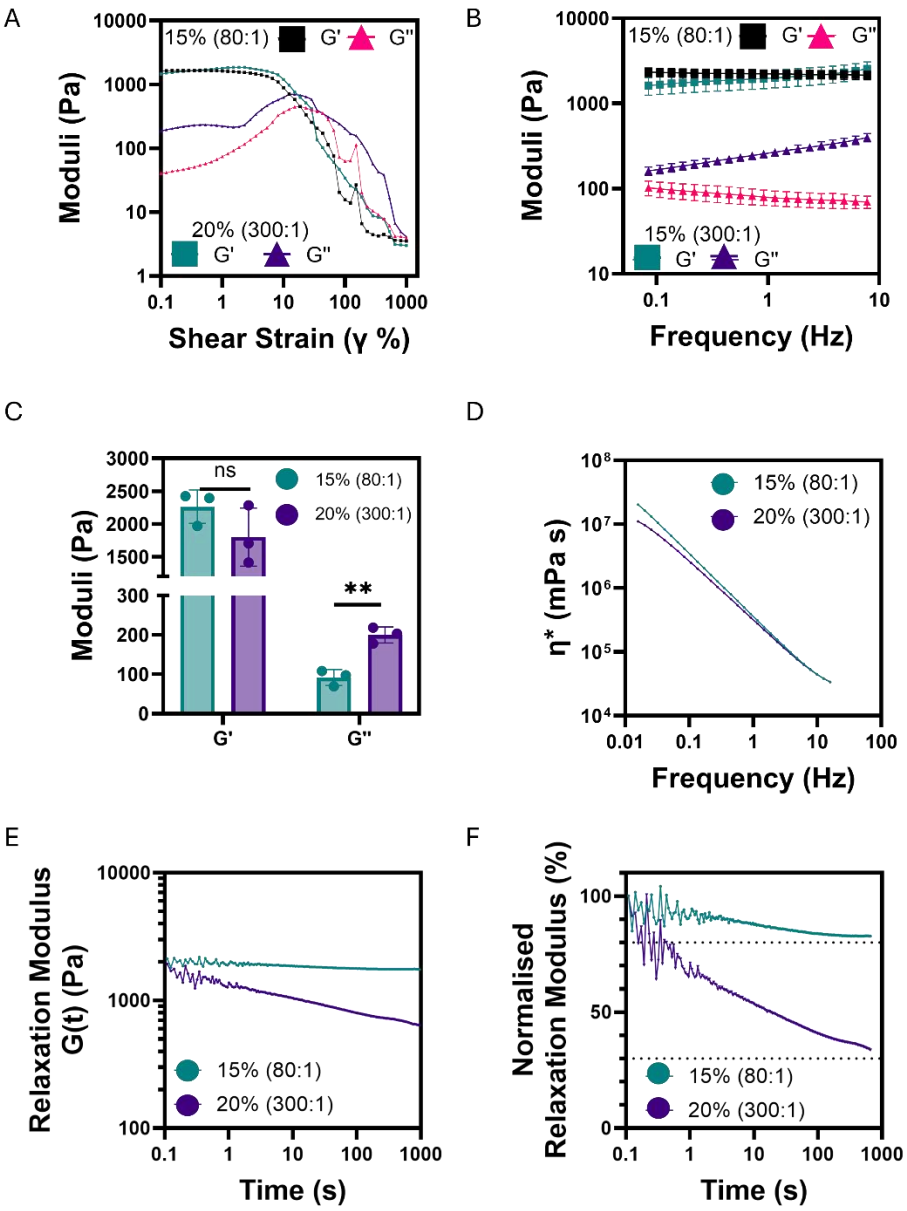

Figure 5.3.16 Rheological characterisation of PAAm 15% (80:1) and 20% (300:1). (A) Amplitude Sweeps, **(B)** Frequency Sweeps, **(C)** storage (G') and loss (G'') moduli, **(D)** complex viscosity, **(E)** absolute and **(F)** normalised stress relaxation of selected PAAm hydrogels. Frequency sweeps and stress relaxation were performed within LVE region (1% strain) with hydrated samples at equilibrium. Data is presented as mean of triplicates ± SD (n=3).

In vitro swelling (**Figure 5.3.17A**) showed that both hydrogels reached equilibrium within 24 hours, consistent with the timeframe during which samples were incubated in media prior to cell seeding. PAAm 20% (300:1) exhibited greater swelling (~20% increase), despite a higher total monomer concentration compared to PAAm 15% (80:1), which swelled by ~10%. We hypothesise that the higher swelling of the viscoelastic PAAm is due to its lower BIS crosslinker content (0.066% w/v) compared to the elastic formulation (0.185% w/v). Despite these differences in swelling, both hydrogels retained a robust 3D network and solid-like properties, preserving their original shape (**Figure 5.3.17B**). To ensure that the two formulations differed only in their stress relaxation behaviour, we also characterised the porosity, surface topography, and chemical composition of PAAm 15% (80:1) and 20% (300:1) hydrogels. Mesh size was estimated using rubber elasticity theory(231) (**Figure 5.3.17C**) while scanning electron microscopy (SEM) was employed to assess network porosity (**Figure 5.3.17D**), a parameter known to influence cellular behaviour(202). Both mesh size quantification and SEM analyses indicated comparable porosity and network architecture.

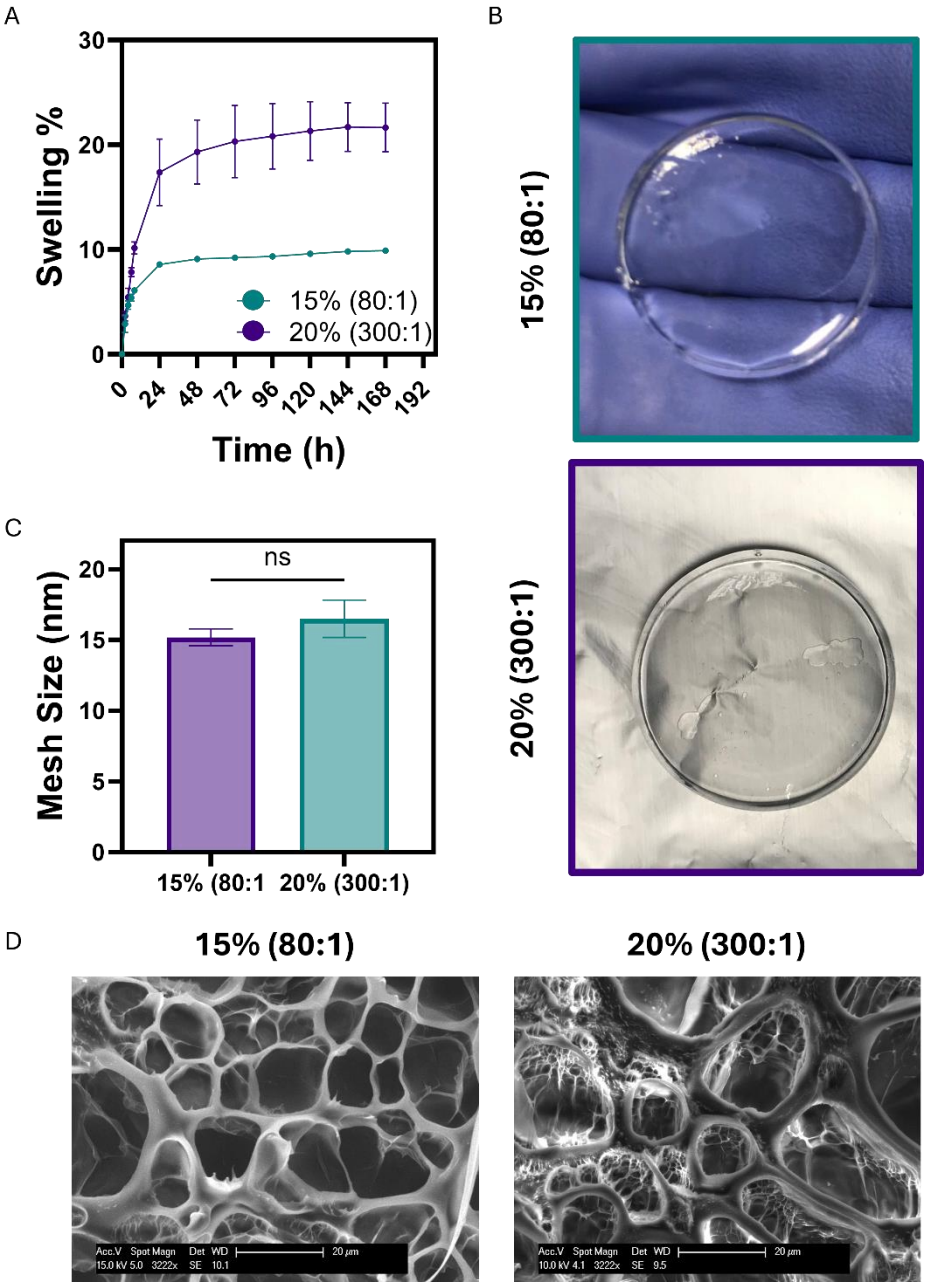

Figure 5.3.17 Swelling, morphology and porosity of PAAm hydrogels. (A) Swelling equilibrium and **(B)** gross view of PAAm 15% (80:1) and PAAm 15% (300:1) discs after reaching the equilibrium swelling. **(C)** Mesh size quantification and **(D)** Scanning electron microscopy of the cross-section of the elastic and viscous PAAm hydrogels. Data is presented as mean of triplicates ± SD (n=3).

Environmental scanning electron microscopy (ESEM) and optical profilometry were performed to characterise the surfaces of PAAm hydrogels. Although ESEM images (**Figure 5.318A**) suggested similar surface features, quantitative roughness analysis revealed significant differences between the two formulations. Specifically, PAAm 15% (80:1) displayed lower surface roughness (Sa = 26.03 nm; Sq = 33.27 nm) compared to PAAm 20% (300:1) (Sa = 40.3 nm; Sq = 50.7 nm) (**Figure 5.318B**).

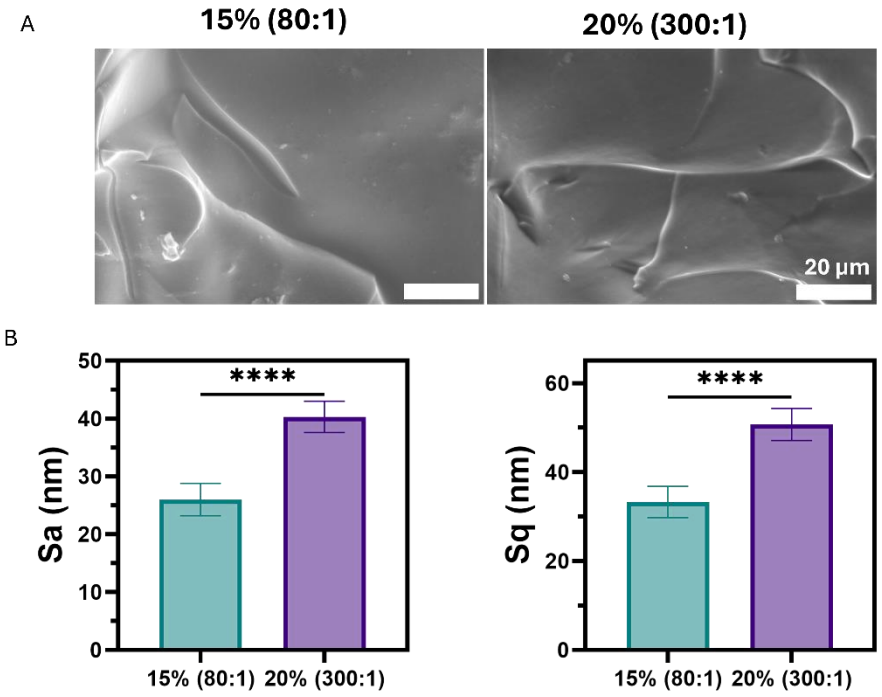

Figure 5.3.18 Topographical characterisation of PAAm hydrogels. **(A)** Representative environmental scanning electron microscopy (ESEM) images of hydrogel surfaces. **(B)** Quantitative analysis of surface roughness parameters, including arithmetical mean height (Sa) and root mean square height (Sq), obtained by optical profilometry. Data is presented as mean of triplicates ± SD (n=3).

The surface chemistry was analysed by XPS (**Figure 5.3.19A**). Quantification of the integrated N 1s, C 1s, and O 1s peaks after 24 hours

of incubation in culture medium (**Figure 5.3.19B-D**) revealed no significant differences between the surfaces of the two hydrogels, indicating comparable protein adsorption and surface chemistry. While XPS reveals the elemental composition and relative abundance of surface species, it does not provide structural information. A deeper characterisation therefore necessitates the use of complementary techniques, like mass spectrometry.

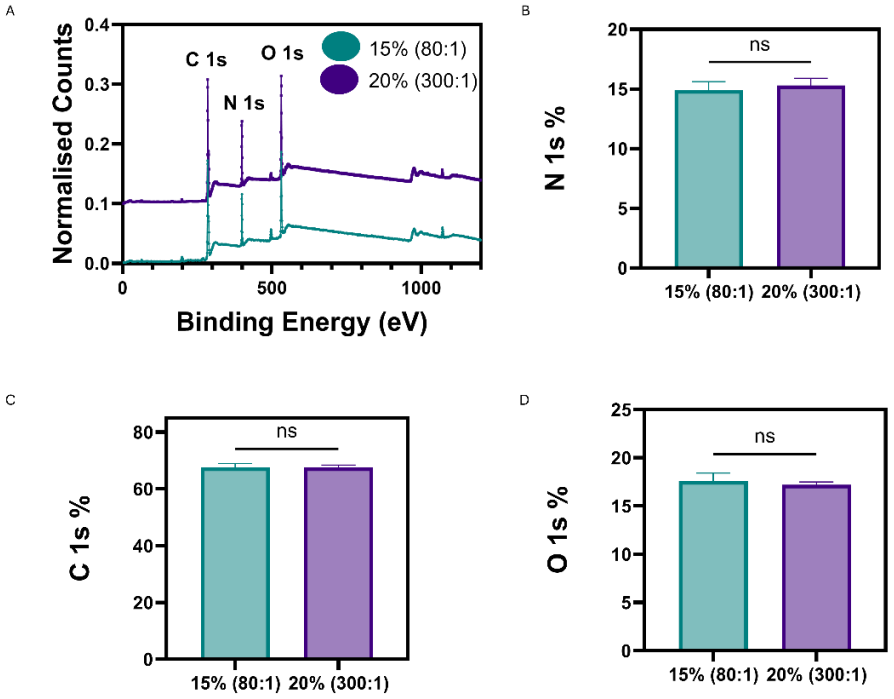

Figure 5.3.19 Chemical characterisation of PAAm hydrogel surfaces. (A) XPS wide-scan spectra of PAAm hydrogels following 24-hour incubation in culture medium with 10% FBS. Quantification of **(B)** N 1s, **(C)** C 1s, and **(D)** O 1s peaks. Data is presented as mean of triplicates ± SD (n=3).

After the mechanical characterisation, PAAm hydrogels were prepared and tested *in vitro* with human monocyte-derived macrophages following the workflow represented in **Figure 5.3.20**.

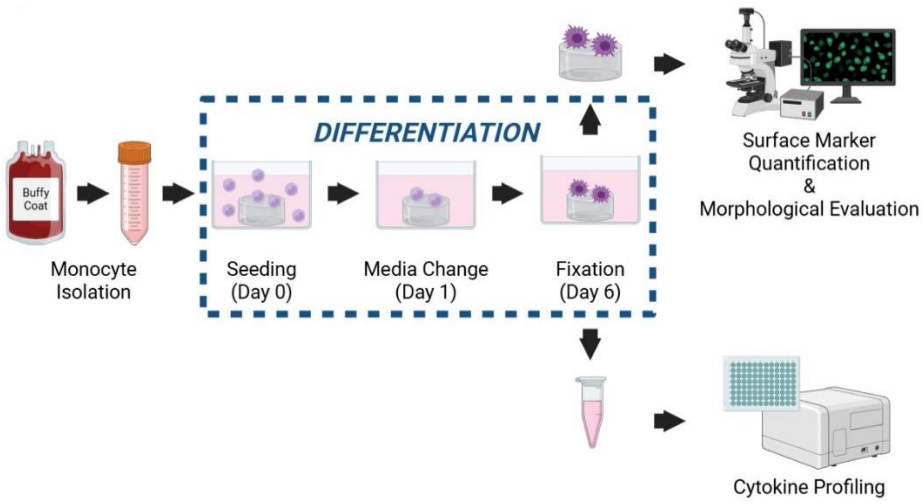

Figure 5.3.20. Schematic of the experimental workflow. Positive selection of monocyte, differentiation and characterisation of morphology, surface markers and cytokine profiling of macrophages.

As shown by the Live/Dead assay at day 6 (**Figure 5.3.21A**), macrophages maintained high viability on both hydrogel formulations, demonstrating good biocompatibility and the absence of cytotoxic effects from residual monomers. These results were further supported by the AlamarBlue assay, which quantitatively confirmed comparable viability between cells cultured on PAAm hydrogels and those on TCP, used as controls (**Figure 5.3.21B**). Together, these findings validate PAAm 15% (80:1) and 20% (300:1) as suitable substrates for macrophage culture.

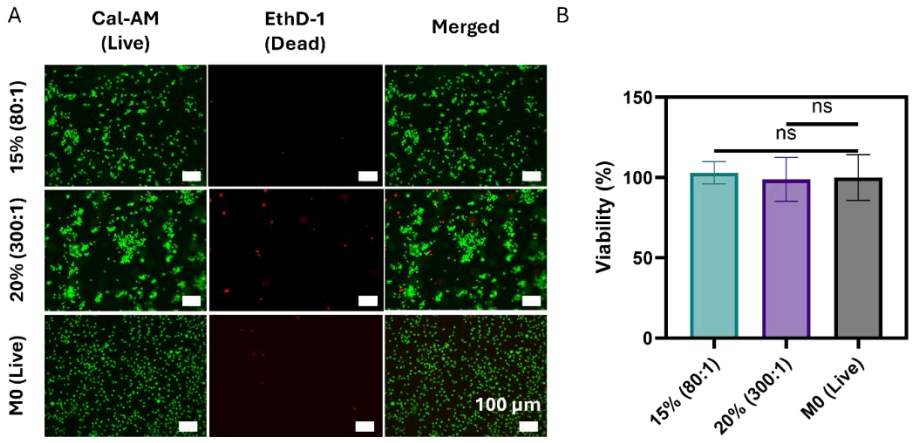

Figure 5.3.21 Human primary macrophage viability on PAAm 15% (80:1) and 20% (300:1) hydrogels. (A) Fluorescent microscopy images of macrophages stained for Calcein-AM (green – live cells) and Ethidium homodimer-1 (red – dead cells) at day 6. Scale bar: 100 µm. **(B)** AlamarBlue assay on macrophages cultured for 6 days. M0 macrophages cultured on tissue culture plastic (M0 (Live)) were used as positive controls. Data is presented as mean of triplicates of three independent experiments ± SEM (n=3, N=3).

To evaluate how hydrogel viscoelasticity influences macrophage activation status, monocytes (Day 1) and macrophages (Day 6) were stained for nuclei and F-actin to monitor morphology over the culture period. By day 6, cells displayed strikingly different shapes depending on the substrate the adhered to. In addition to these morphological differences, cells on the elastic substrate tended to cluster into aggregates, whereas macrophages on the viscoelastic substrate remained more evenly distributed across the hydrogel surface, as shown in **Figure 5.3.22A**. Quantitative analysis performed with an automated software revealed that macrophages on elastic PAAm were less elongated, with an average eccentricity of ~0.71, whereas those on viscoelastic PAAm exhibited greater eccentricity (~0.75; **Figure 5.3.22B**), a parameter that stands for the cell elongation. Cell spreading was markedly enhanced on

the viscoelastic hydrogel, with an average area of ~404 µm², approximately double that of cells on the elastic PAAm (~198 µm²; **Figure 5.3.22C**). These findings indicate that stress-relaxing hydrogels promoted stronger cell–material engagement and more pronounced morphological adaptation, highlighting viscoelasticity as a key determinant of macrophage morphology.

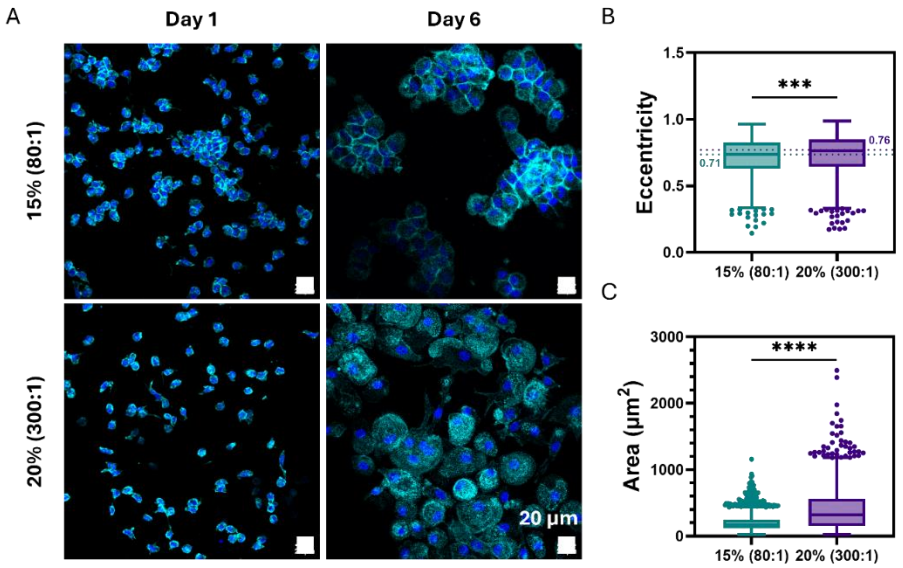

Figure 5.3.22 Human macrophage morphology on different PAAm hydrogels (A) Confocal microscopy images of monocyte (day 1) and macrophages (day 6) stained for nuclei (DAPI – blue) and F-actin (Phalloidin – cyan) at day 1and day 6. Scale bar: 20 µm. Quantification of **(B)** eccentricity and **(C)** area of macrophages at day 6. Data is presented as mean of triplicates of three independent experiments ± SEM (n=3, N=3).

To further characterise macrophage phenotype, expression levels of calprotectin (pro-inflammation marker) and mannose receptor (anti-inflammatory markers) were quantified by immunofluorescent staining. Imaging was performed on the same day for all samples, with green and red channel settings optimised on the brightest samples and kept

consistent throughout acquisition (**Figure 5.3.23A**). Calprotectin (green) and MR (red) fluorescence were quantified (**Figure 5.3.23B**). While MR expression was higher overall, no significant differences were observed between cells cultured on different hydrogels. In contrast, calprotectin was significantly higher in macrophages cultured on the elastic hydrogel (15% (80:1)). To enable donor-independent comparisons for future studies, the calprotectin-to-MR ratio was calculated (**Figure 5.3.23C**). Even though this ratio remained below one, indicating predominance of the anti-inflammatory marker, it was significantly higher in macrophages cultured on the elastic substrate. This suggested that a reduction in the viscous contribution promoted a shift towards a more pro-inflammatory, M1-like, phenotype.

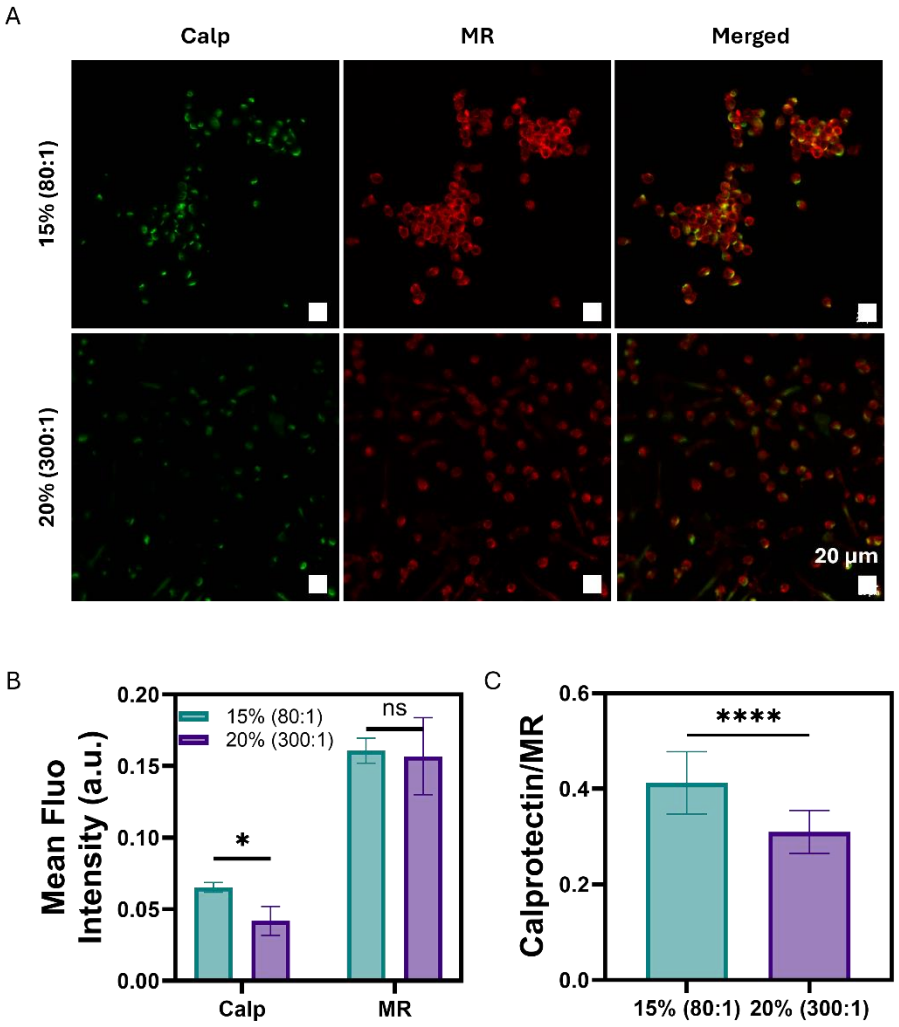

Figure 5.3.23 Human macrophage polarisation characterised by surface markers on different PAAm hydrogels. (A) Confocal microscopy images of macrophages stained for pro- (calprotectin – green) and anti- (mannose receptor – red) inflammatory surface markers at day 6. Scale bar: 20 µm. **(B)** Quantification of mean fluorescence intensity of calprotectin and MR at day 6 **(C)** Ratio between calprotectin and MR fluorescent signals. Data is presented as mean of triplicates of three independent experiments ± SEM (n=3, N=3).

Pro- (TNF-α, IL-6) and anti- (IL-10, CCL18) inflammatory cytokines release by macrophages cultured on PAAm 15% (80:1) and 20% (300:1)

were quantified by using sandwich ELISA (**Figure 5.3.24**) to further characterise macrophage phenotype. TNF-α and IL-6 secreted from cell cultured on PAAm 15% (80:1) were significantly higher compared to cells PAAm 20% (300:1), suggesting a shift towards a pro-inflammatory phenotype of macrophages cultured on the elastic substrate. In terms of anti-inflammatory cytokines, both IL-10 and CCL18 were not significantly different released, meaning that viscoelasticity did not seem to interfere with these anti-inflammatory cytokines. Overall, the cytokine profile supported the observation that elastic hydrogels induced a pro-inflammatory phenotype, whereas viscoelastic substrates showed a lower activation status since both pro- and anti-inflammatory cytokines were released in lower amounts.

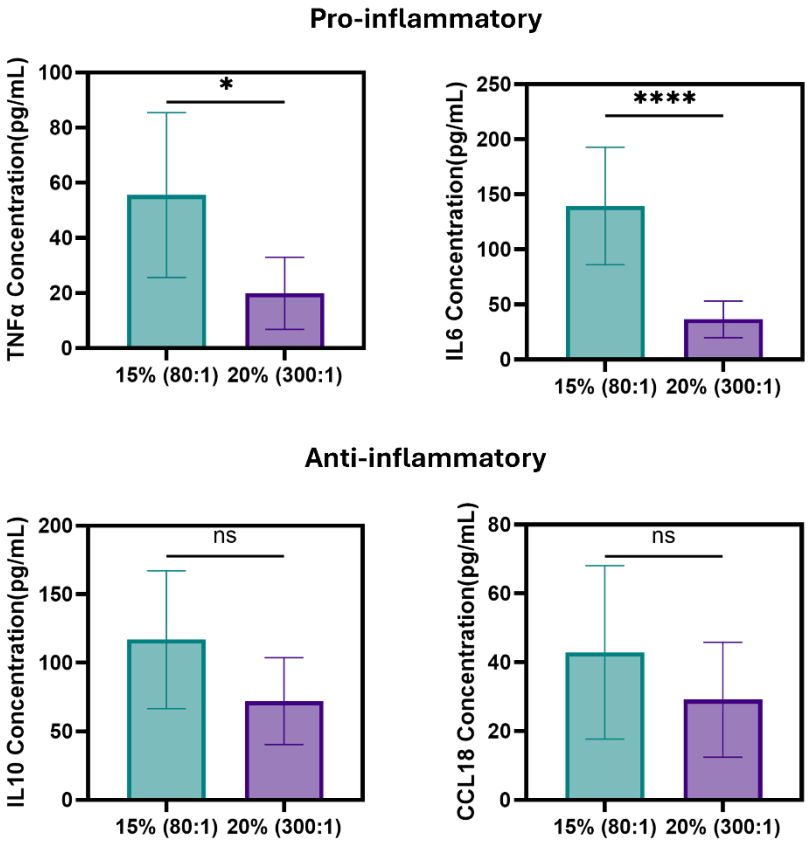

Figure 5.3.24 Quantification of pro- (TNF-α, IL-6) and anti- (IL-10, CCL18) inflammatory cytokines secreted by macrophages at day 6. Data is presented as mean of triplicates of three independent experiments ± SEM (n=3, N=3).

5.4 Discussion

This chapter demonstrate that viscoelasticity, independent of stiffness and chemistry, plays a decisive role in regulating human primary macrophage–material interactions. Compared to previous works on macrophages and viscoelasticity, we used primary human macrophages and specifically investigated how they respond to hydrogel viscoelasticity characterised by significant stress relaxation, which has direct implications for designing implantable materials to minimise the

FBR. We developed two PAAm formulations with similar initial relaxation moduli and chemical compositions, but one is elastic and the other is viscoelastic as shown in their stress relaxation profiles. PAAm 15% (80:1) showed an elastic behaviour, while PAAm 20% (300:1) showed pronounced viscoelastic properties evidenced by enhanced stress relaxation. These two hydrogels had comparable porosity, mesh size, surface chemistry, and protein adsorption, but differed in surface roughness. Although this difference (~14 nm) is on a scale similar to integrin dimensions (~28 nm)(329), it did not alter protein adsorption. Considering the relatively small magnitude of the difference in topography, it is more plausible that the viscoelastic properties of the gels serve as the dominant regulator of macrophage responses, with nanoscale roughness playing only a secondary role. Supporting this interpretation, a recent study on macrophage polarisation showed that surfaces differing by ~12.8 nm in roughness - comparable to our findings - did not induce significant release of TNF-α, IL-1β, arginase, or IL-4 at day 7(330).

Macrophages cultured on the viscoelastic substrate spread more extensively and showed greater eccentricity, indicating enhanced interaction with the substrate. In contrast, cells grown on PAAm 15% (80:1) were smaller and tended to form clusters. Phenotypic characterisation further showed that macrophages on the elastic PAAm adopted a more pro-inflammatory phenotype, with higher calprotectin expression and increased secretion of TNF-α and IL-6, while anti-inflammatory cytokine secretion remained unaffected. Together, these findings demonstrate that stress relaxation alone is sufficient to modulate human macrophage phenotype, with viscoelastic substrates favouring a less inflammatory response and elastic substrates promoting a pro-inflammatory response.

Our work used human monocyte-derived macrophages which have not been used in previous studies on viscoelasticity. Previous studies using immortalised and non-human macrophages have reported outcomes broadly consistent with this present work, with viscoelasticity driving morphology, phagocytosis, and inflammatory responses. However, their translational relevance has remained uncertain due to the limitations of relying on immortalised cell lines or murine cells rather than primary human macrophages(331-333). By working with primary human cells, we directly address this gap and highlight viscoelasticity as a key determinant of macrophage function in contexts relevant to FBR. However, contradictory findings - including and extending beyond macrophage-focused studies - have also been reported. Such variability likely reflects differences in how viscoelasticity was introduced and characterised. In many cases, changes in relaxation were accompanied by differences in chemical composition(209, 214) or in the initial stress values(284, 317, 334), indicating concomitant changes in chemistry or stiffness that complicate the attribution of observed responses solely to viscoelasticity(335, 336). Furthermore, some studies on macrophages(284, 285, 334), as well as on other cell types(205-207, 212, 214, 284, 285, 334), performed rheological characterisation before hydrogels reached equilibrium swelling meaning that the reported mechanical properties may not fully capture the environment experienced by cells. In some studies, there is also the tendency to conflate stress relaxation with storage and loss moduli, or to attribute biological effects to viscoelasticity when stiffness was the parameter that differed(334). To the best of our knowledge, this is the first study to demonstrate that stress relaxation alone modulates phenotype in primary human macrophages, independent of stiffness and chemistry as we compared stress-relaxing and elastic hydrogels with comparable stiffness and chemistry.

In addition to the use of primary human monocyte-derived macrophages, another key contribution of our study is the alignment of hydrogel relaxation dynamics with cellular traction forces. To accurately interpret cell–material interactions, it is important to match hydrogel relaxation timescales with those of cellular traction forces, typically occurring within 20 s to 5 min(205, 328, 337). The molecular clutch model provides an explanation on how integrins and associated proteins interact with actin, producing traction forces that depend on the substrate stiffness(338, 339). Stress relaxation introduces an additional layer of complexity as the viscoelasticity of hydrogels can be seen as a dynamic process of clutch engagement and traction forces generation between cells and the material, involving maturation of protein adhesions, mechanotrasduction and eventually material remodelling(297). Even though actin cytoskeleton reorganisation occurs within seconds(340), cell spreading equilibrates over minutes(341). Hydrogels that relax too quickly (<5 s) fall outside this biologically relevant window. Some studies have also just relied on the quantification of G' and G'' to determine materials' viscoelasticities(210), which do not provide information on stress relaxation under sustained deformation. By engineering hydrogels that diverged in their relaxation profiles specifically within this timescale, we ensured that the observed macrophage responses reflected physiologically meaningful mechanical interactions.

While this study overcomes several limitations of prior work, some challenges remain. First, we relied on a 2D culture model. *In vivo*, macrophages interact with three-dimensional, heterogeneous environments; therefore, extending these findings to 3D systems will be important for future studies. Although PAAm is well-suited to fundamental mechanobiology studies, it is not appropriate for cell encapsulation due to monomer toxicity. Translation of these principles

into biocompatible hydrogel will therefore be required. Moreover, while we demonstrated that viscoelasticity shapes macrophage morphology and cytokine secretion, the molecular pathways linking stress relaxation to polarisation remain unclear. Future work should probe mechanosensitive pathways such as integrin signalling, actin dynamics, and downstream transcription factors to identify how time-dependent mechanics influence inflammatory responses. Finally, our experiments captured early macrophage responses, but the FBR evolves over weeks and involves macrophage fusion, fibroblast recruitment, and fibrotic encapsulation. Long-term studies will be critical to establish how viscoelasticity influences these later stages.

Despite these limitations, our findings contribute tangibly to the advance of our understanding on macrophage-materials interactions, particularly with material viscoelasticity. By demonstrating that stress relaxation directs human macrophage phenotype, we have helped establishing viscoelasticity as a design principle for immunomodulatory biomaterials. Specifically, hydrogels engineered with relaxation timescales comparable to the kinetics of cellular traction forces may dampen macrophage-driven inflammation and reduce implant-associated FBR.

5.5 Conclusion

In conclusion, our study demonstrates that hydrogel viscoelasticity, independent of stiffness and chemistry, is a critical regulator of human macrophage behaviour. By comparing two polyacrylamide formulations with matched stiffness but distinct stress-relaxation profiles, we show that viscoelastic substrates promote greater macrophage spreading and elongation, while elastic hydrogels elicit a more pro-inflammatory phenotype, characterised by elevated calprotectin expression and

increased TNF-α and IL-6 secretion. These findings highlight that time-dependent stress relaxation, rather than static stiffness or chemical composition, governs macrophage responses. Importantly, our approach overcomes common confounders in prior studies, including differences in chemistry, mechanical testing conditions, and non-physiological relaxation timescales, providing a biologically relevant assessment of cell–material interactions. By using primary human macrophages, our results offer translational insight into designing implantable materials that minimise the foreign body reaction, emphasising the necessity of incorporating viscoelastic properties alongside stiffness in biomaterial design strategies.

Chapter 6. Conclusions & Future Work

6.1 Final Discussion & Conclusions

The work presented in this thesis set out to understand how hydrogel mechanical properties can be designed to modulate macrophage behaviour, with the broader goal of identifying strategies to minimise the FBR. In contrast to much of the existing literature, which has predominantly investigated biomaterial-immune interactions on relatively stiff substrates, this thesis provides a systematic analysis of how variations in stiffness within soft tissue-relevant ranges, together with viscoelastic properties tuned to biological timescales, regulate human macrophage responses. A central theme that emerges from this work is that macrophage phenotype is not determined by a single property, but multiple features can affect monocyte differentiation and macrophage polarisation. The inconsistencies reported in the literature regarding macrophage responses to hydrogel mechanical and chemical properties can be largely attributed to simultaneous changes in multiple experimental variables. Material chemistry can deeply influence protein adsorption and integrin engagement, thereby affecting downstream signalling. Even minor chemical modifications can substantially change the overall material chemistry. For example, adjusting mechanics through ionic versus covalent crosslinking inherently alters the chemical environment sensed by cells but it is often overlooked. Mechanical properties are often summarised as stiffness, while important factors such as viscoelasticity and complex viscosity are frequently not considered. Cell source is another critical factor. Many studies use murine cells or immortalised cell lines, which differ from human monocyte-derived macrophages in integrin expression,

mechanosensitivity, and cytokine profiles, limiting the translational relevance of the findings. Ligand presentation and surface density of pro-attachment motifs vary widely across studies, influencing adhesion strength and downstream signalling. Without careful control of these parameters, differences in macrophage responses may be mistakenly attributed to mechanical cues.

By systematically disentangling these parameters and working with primary human macrophages, this work brings new insights for the design of immunomodulatory biomaterials, while also exposing limitations and challenges that must be addressed to achieve clinical translation.

The first part of this work, discussed in Chapter 3, focused on optimising ALMA hydrogel preparation to ensure reproducible and stable systems for biological studies. Rheological studies revealed that stiffness was primarily determined by polymer concentration, whereas the degree of methacrylation significantly affected mechanical properties at ALMA concentrations above 6% w/v. Moreover, the optimisation demonstrated the versatility of ALMA hydrogels for surface functionalisation via EDC/NHS chemistry, enabling covalent conjugation of proteins and peptides. Together, these methodological refinements established a reliable platform for studying the effect of surface chemistry and stiffness on human monocyte-derived macrophages.

Initial experiments, presented in Chapter 4, examined the effect of surface chemistry by functionalising ALMA hydrogels with varying degrees of GRGDSP substitution. Although higher levels of GRGDSP functionalisation appeared to reduce pro-inflammatory responses, comparison between modified and unmodified ALMA hydrogels of different stiffnesses revealed that stiffness exerted a more dominant

influence on macrophage polarisation, with stiffer matrices generally suppressing activation and cytokine release. We hypothesise that, although GRGDSP-modified hydrogels exhibited significantly reduced protein adsorption, the residual adsorption remained sufficient to mask the effects of the chemical modification and was therefore insufficient to drive macrophage responses.

After optimising sample preparation for cell culture, three HDM ALMA formulations (2%, 4%, and 6%) were selected to investigate the effect of stiffness. These compositions spanned a stiffness range of ~0.25 to ~4.5 kPa, reflecting the mechanical properties of various soft tissues such as lens (0.2–0.8 kPa), thyroid (1.3 kPa), pancreas (1.1 kPa), lung (1.5 kPa), adipose tissue (1.6 kPa), liver (2 kPa), brain (1 kPa), and kidney (4–5 kPa)(273). Even modest increases in stiffness produced striking differences in macrophage morphology, marker expression, and cytokine secretion. On the stiffest substrates, macrophages adopted a more elongated morphology, exhibited higher calprotectin-to-mannose receptor ratios, and secreted increased levels of TNF-α and IL-6, indicative of a pro-inflammatory phenotype. These findings are significant because much of the existing literature defined “soft” hydrogels at stiffnesses that remain substantially higher than those of many physiological tissues. Beyond extending the knowledge of stiffness-driven immune modulation, these insights carry translational importance for biomaterial design in soft tissue environments, where even small increases in modulus may be sufficient to activate inflammatory pathways.

While stiffness is a potent regulator of macrophage function, it is not sufficient on its own to fully explain cell–material interactions and must be considered alongside other mechanical properties. For this reason, Chapter 5 investigated viscoelasticity as an independent regulator of

macrophage behaviour. To isolate this variable, PAAm hydrogels were engineered with comparable chemistries and stiffness but distinct stress relaxation profiles. Macrophages cultured on viscoelastic substrates spread more extensively and exhibited reduced activation compared to those on elastic substrates, which displayed a more M1-like phenotype, characterised by elevated calprotectin expression and increased secretion of TNF-α and IL-6. These findings demonstrate that stress relaxation alone is sufficient to alter macrophage polarisation. Importantly, the relaxation timescales were tuned to fall within the biologically relevant window of cellular traction forces (20 s to 5 min), thereby avoiding artefacts associated with materials that relax too quickly or too slowly. This rigorous approach helps resolve inconsistencies in the existing literature, where variations in stiffness, chemistry, or non-physiological conditions have often confounded interpretation. Collectively, the results provide clear evidence that viscoelasticity, independent of stiffness or chemistry, can modulate human macrophage phenotype. The use of primary human macrophages further strengthens the translational relevance of these findings, in contrast to much of the prior work that relied on murine or immortalised cells, which do not accurately capture human immune responses.

Taken together, the results presented in this thesis demonstrate that macrophage responses are governed by a nuanced interplay between mechanical and chemical properties. Within a single hydrogel system, modulation of surface chemistry through variations in pro-adhesive ligand density, in the absence of changes in mechanical properties, did not significantly alter macrophage phenotype. While this suggests that mechanical cues may dominate, chemical properties cannot be completely disregarded. When comparing ALMA 4% and PAAm 20% (300:1) hydrogels, biomaterials with comparable mechanical properties

but completely different chemistries, macrophages exhibited different degrees of elongation, indicating that chemical features also contribute to how cells engage with and respond to biomaterials. Notably, macrophages cultured on ALMA hydrogels showed higher release of both pro- and anti-inflammatory cytokines, reflecting an overall heightened immune activation compared to PAAm. A key distinguishing factor between these materials is ionic charge, which is negative in ALMA and neutral in PAAm. This difference can influence protein adsorption and the formation of the cell-material interface, thereby modulating integrin binding and adhesion strength, and ultimately affecting cell morphology and activation. Collectively, these findings emphasise that, although mechanics may act as the primary driver, chemical properties define the context in which cells sense and respond to mechanical cues. These insights highlight the importance of simultaneously tuning mechanical and chemical parameters when designing biomaterials to achieve predictable and controlled immunomodulatory outcomes, with softer, viscoelastic, and more chemically inert substrates appearing to elicit a comparatively reduced immune response.

Despite these advances, limitations of the present work must be acknowledged. The experiments were all conducted in 2D systems, whereas macrophages *in vivo* interact with three-dimensional, heterogeneous environments. Findings from 2D studies on substrate mechanics offer important guidance and serve as a fast and cost-effective in understanding the fundamentals behind more complex systems. While 2D analysis offers high speed and simplicity, moving towards 3D systems will be essential to fully capture how viscoelasticity and stiffness shape immune responses in tissue-like contexts. By applying the mechanical insights from this work, 3D scaffolds can be

designed with the understanding that stiffer and more elastic gels promote macrophage elongation and pro-inflammatory activation, highlighting the importance of carefully tuning stiffness and viscoelasticity to regulate inflammatory responses in soft tissue applications. Furthermore, our studies focused on early macrophage responses, but the FBR unfolds over weeks and involves additional processes such as macrophage fusion, fibroblast recruitment, and fibrotic encapsulation. Whether the modulatory effects of viscoelasticity observed here persist during these later stages remains to be determined. Material choice also presented a limitation. Since ALMA hydrogels with varying degrees of methacrylation did not exhibit differences in stress relaxation, the study of viscoelasticity was conducted using PAAm hydrogels. Although PAAm is highly tuneable and well suited for fundamental mechanobiology studies, it is unsuitable for cell encapsulation or clinical application due to monomer toxicity. Therefore, translating these principles into biocompatible and clinically relevant hydrogel systems represents a critical next step. Finally, although surface chemistry was characterised, the influence of adsorbed protein layers remains an inherently variable factor *in vitro* and *in vivo*, and further work is needed to systematically understand the interplay of chemistry and mechanical properties to direct immune responses.

Taken together, this thesis demonstrates that both stiffness and viscoelasticity are powerful regulators of macrophage responses to biomaterials. It extends current understanding by showing that macrophage polarisation can be induced at physiologically relevant stiffnesses, and that stress relaxation alone modulates their phenotype independently of stiffness and chemistry. These insights are directly relevant for the design of immunomodulatory biomaterials, suggesting that engineering hydrogels with physiologically mimicking stiffness of soft tissues and matching biological relaxation timescales could

attenuate inflammatory activation and reduce FBR, eventually reducing implant rejections. While further work is required to translate these insights into 3D and long-term contexts, the advances presented here represent an important step toward the rational design of immunomodulatory biomaterials.

6.2 Future Work

Building on the findings of this thesis, a key direction for future research is the extension of hydrogel studies from 2D culture systems to 3D models that more accurately capture the structural and mechanical complexity of native tissues. While the present work systematically decoupled stiffness, viscoelasticity, and surface chemistry in 2D, macrophages *in vivo* encounter multidimensional environments with dynamic mechanical cues, extracellular matrix interactions, and the presence of other cell types. Developing 3D hydrogel systems with independently tuneable mechanical and biochemical properties, combined with co-culture models incorporating fibroblasts, would provide a more physiologically relevant platform to investigate how macrophages sense and integrate stiffness and viscoelasticity in three dimensions, as well as how crosstalk with fibroblasts influences their behaviour. Such approaches would also clarify whether the trends identified in 2D extend to more complex and tissue-like contexts.

Future studies should also address the role of the adsorbed protein layer, which remains highly variable and unknown. While the hydrogel surface chemistry was characterised, factors such as protein conformation and ligand presentation may critically influence how macrophages sense underlying material properties. Systematic investigations, combining controlled surface chemistry with protein adsorption analysis through approaches such as proteomic profiling, will be essential to elucidate

how protein identity, conformation, and surface density interact and regulate biological activities. Such insights will clarify the contribution of adsorbed proteins to macrophage–material interactions and guide the design of biomaterials with surfaces that actively promote favourable immune outcomes.

Another limitation of this work that should be addressed in future studies is that mechanical characterisation is primarily based on bulk rheological measurements, which do not fully capture the properties sensed by cells at the material interface. While bulk stiffness provides valuable insight into hydrogel mechanical properties, cell responses are also strongly influenced by surface mechanics, ligand presentation, and affinity of peptides and proteins in creating a “tight” or “loose” interactions with hydrogel surface, which together define the local microenvironment. Factors such as surface stiffness, pro-attachment motifs mobility like RGD, as well as their density and organisation can modulate integrin engagement and downstream mechanotrasduction pathways, ultimately affecting macrophage behaviour. Therefore, the observed cellular responses likely arise from a combination of bulk and interfacial properties, and future studies should aim to decouple these contributions using complementary techniques to achieve a more comprehensive understanding of cell-biomaterial interactions.

Finally, to bridge the gap between *in vitro* mechanistic studies and clinical relevance, optimised hydrogel formulations should be tested in animal models. Such studies would assess whether reduced pro-inflammatory activation *in vitro* corresponds to improved tissue integration, decreased fibrosis, and long-term biocompatibility *in vivo*. Insights gained from these investigations would inform the rational design of next-generation immunomodulatory biomaterials, enabling the development of implants that actively promote tissue homeostasis

and minimise chronic inflammation. Together, these efforts would provide a comprehensive framework for translating fundamental mechanobiology findings into practical biomaterial strategies for clinical applications.

Appendix

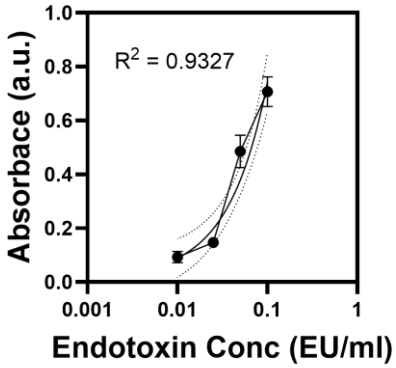

Figure S1 Endotoxin standard curve. Data is presented as mean of triplicates ± SD (n=3).

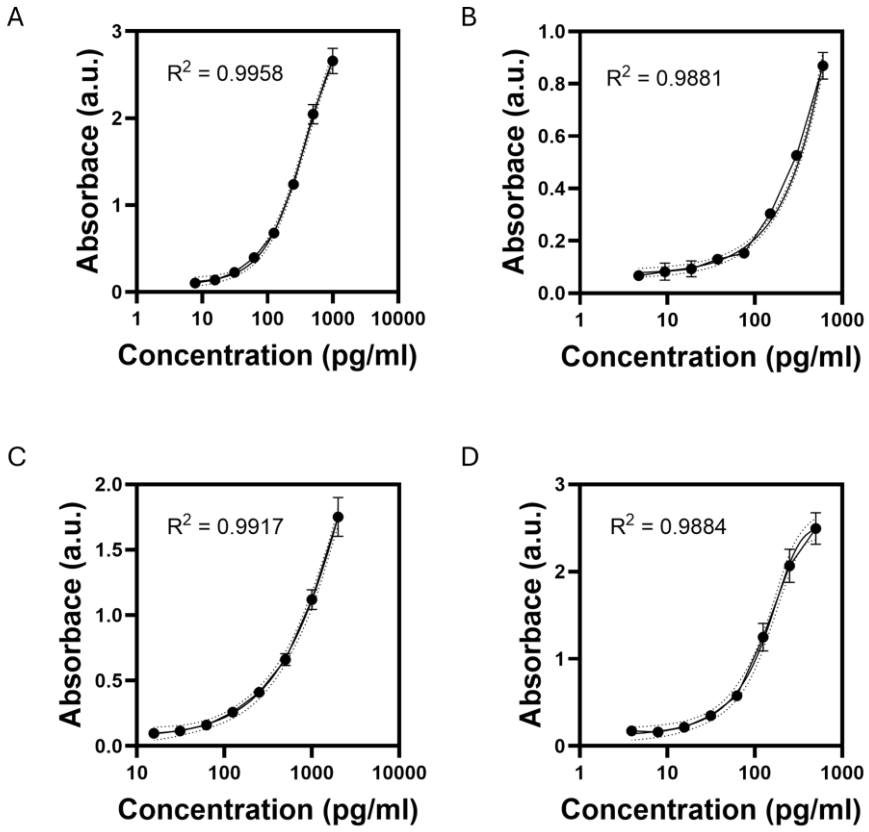

Figure S2 ELISA standard curves. (A) TNF-α, **(B)** IL-6, **(C)** IL-10, and **(D)** CCL18. Data is presented as mean of triplicates ± SD (n=3).

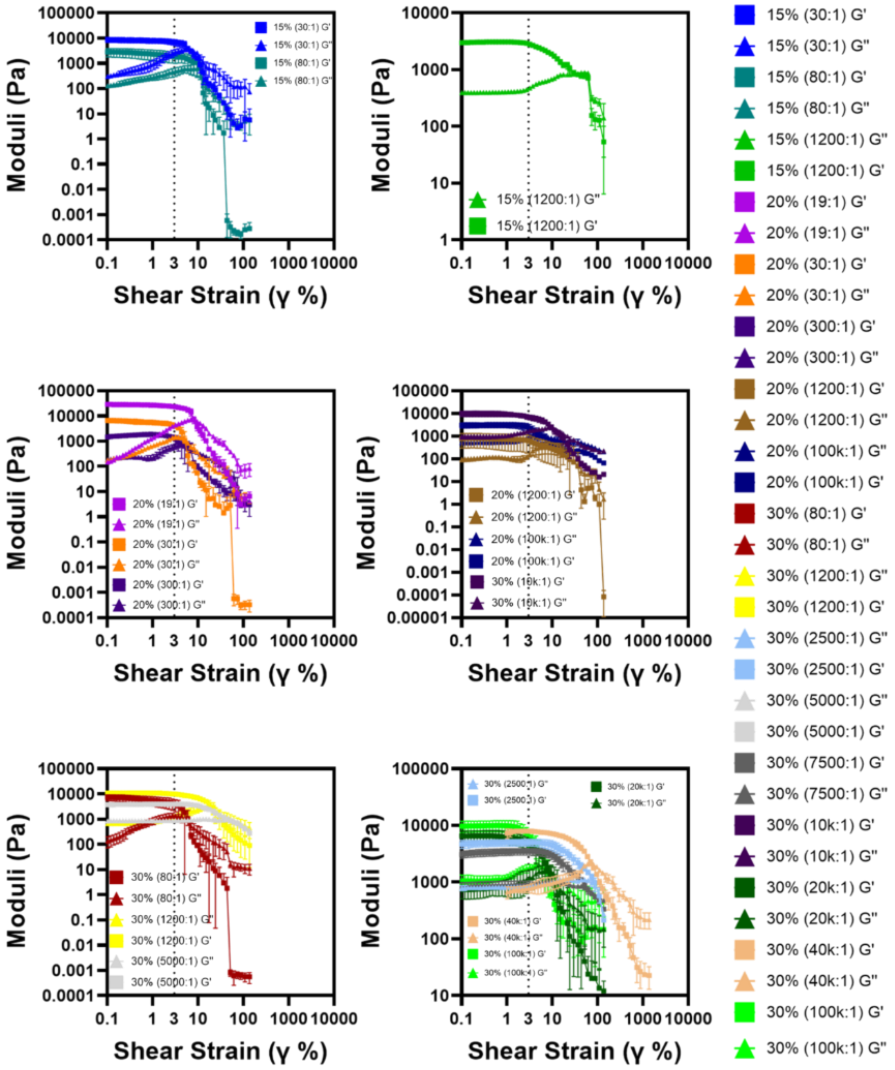

Figure S3 Amplitude sweeps of PAAm hydrogels. Data is presented as mean of triplicates ± SD (n=3).

References

1. Parkin J, Cohen B. An overview of the immune system. The Lancet (British edition). 2001;357(9270):1777-89.
2. Chaplin DDMDP. Overview of the immune response. Journal of allergy and clinical immunology. 2010;125(2):S3-S23.
3. Payne S. Viruses : From Understanding to Investigation. 1st ed. San Diego: Elsevier Science & Technology; 2017.
4. Rouse BT, Sehrawat S. Immunity and immunopathology to viruses: what decides the outcome? Nature reviews Immunology. 2010;10(7):514-26.
5. . HRG. Structure and Classification of Viruses. In: S B, editor. Medical Microbiology. 4th ed. The University of Texas Medical Branch at Galveston1996.
6. Zheng D, Liwinski T, Elinav E. Interaction between microbiota and immunity in health and disease. Cell research. 2020;30(6):492-506.
7. Murphy K, Weaver C, Berg L, Barton G. Janeway's immunobiology. Tenth edition. / Kenneth Murphy, Casey Weaver, Leslie J. Berg. ed. New York: W.W. Norton and Company; 2022.
8. Vivier E, Malissen B. Innate and adaptive immunity: specificities and signaling hierarchies revisited. Nature immunology. 2005;6(1):17-21.
9. Ahmed R, Gray D. Immunological memory and protective immunity: understanding their relation. Science. 1996;272(5258):54-60.
10. Anaya J-M, Shoenfeld Y, Rojas-Villarraga A, Levy RA, Cervera R. Autoimmunity: from bench to bedside [Internet]. 2013.

11. Huffaker A, Pearce G, Ryan CA. endogenous peptide signal in Arabidopsis activates components of the innate immune response. Proceedings of the National Academy of Sciences - PNAS. 2006;103(26):10098-103.

12. Pruitt RN, Schwessinger B, Joe A, Thomas N, Liu F, Albert M, et al. The rice immune receptor XA21 recognizes a tyrosine-sulfated protein from a Gram-negative bacterium. Science advances. 2015;1(6):e1500245-e.

13. Liu S, Liu H, Wang X, Shi L. The immune system of prokaryotes: potential applications and implications for gene editing. Biotechnology journal. 2024;19(2):e2300352-n/a.

14. Marshall JS, Warrington R, Watson W, Kim HL. An introduction to immunology and immunopathology. Allergy, asthma, and clinical immunology. 2018;14(Suppl 2):49-.

15. Proksch E, Brandner JM, Jensen J-M. The skin: an indispensable barrier. Experimental dermatology. 2008;17(12):1063-72.

16. Capaldo CT, Powell DN, Kalman D. Layered defense: how mucus and tight junctions seal the intestinal barrier. Journal of molecular medicine (Berlin, Germany). 2017;95(9):927-34.

17. Jiang Q, Cross AS, Singh IS, Chen TT, Viscardi RM, Hasday JD. Febrile Core Temperature Is Essential for Optimal Host Defense in Bacterial Peritonitis. Infection and Immunity. 2000;68(3):1265-70.

18. Foxman EF, Storer JA, Fitzgerald ME, Wasik BR, Hou L, Zhao H, et al. Temperature-dependent innate defense against the common cold virus limits viral replication at warm temperature in mouse airway cells. Proceedings of the National Academy of Sciences - PNAS. 2015;112(3):827-32.

19. Evans SS, Repasky EA, Fisher DT. Fever and the thermal regulation of immunity: the immune system feels the heat. Nature reviews Immunology. 2015;15(6):335-49.

20. Ostberg JR, Ertel BR, Lanphere JA. An Important Role for Granulocytes in the Thermal Regulation of Colon Tumor Growth. Immunological investigations. 2005;34(3):259-72.

21. Yu W-Z, Zhang Y, Liu X, Xiang Y, Li Z, Wu S. Synergistic antibacterial activity of multi components in lysozyme/chitosan/silver/hydroxyapatite hybrid coating. Materials & design. 2018;139:351-62.

22. Saurabh S, Sahoo PK. Lysozyme: an important defence molecule of fish innate immune system. Aquaculture research. 2008;39(3):223-39.

23. Yu Y-S, Lee J-Y, Woo J-W, Kim J-S, Bae Y-H, Cho S-J, et al. Identification and expression pattern of a new digestive invertebrate-type lysozyme from the earthworm. Genes & genomics. 2019;41(3):367-71.

24. **Silhavy TJ**, **Kahne D**, **W**alker S. The Bacterial Cell Envelope. *Cold Spring Harbor perspectives in biology*2010.

25. Merle NS, Noe R, Halbwachs-Mecarelli L, Fremeaux-Bacchi V, Roumenina LT. Complement system part II: Role in immunity. Frontiers in immunology. 2015;6(MAY):257-.

26. Walport MJ. Advances in immunology: Complement (first of two parts). The New England journal of medicine. 2001;344(14):1058-66.

27. Rodríguez de Córdoba S, Esparza-Gordillo J, Goicoechea de Jorge E, Lopez-Trascasa M, Sánchez-Corral P. The human complement factor H: functional roles, genetic variations and disease associations. Molecular Immunology. 2004;41(4):355-67.

28. Trouw LA, Daha MR. Role of complement in innate immunity and host defense. Immunology letters. 2011;138(1):35-7.

29. Sato MN, Pietrobon AJ, Yoshikawa FSY, Branco ACCC, Moustaïd-Moussa N. Role of Histamine in Modulating the Immune

Response and Inflammation. Mediators of inflammation. 2018;2018(2018):1-10.

30. White MV. The role of histamine in allergic diseases. Journal of allergy and clinical immunology. 1990;86(4):599-605.

31. Clark R, Gallin JI, Kaplan AP. The selective eosinophil chemotactic activity of histamine. The Journal of experimental medicine. 1975;142(6):1462-76.

32. Simon T, László V, Falus A. Impact of histamine on dendritic cell functions. Cell Biology International. 2011;35(10):997-1000.

33. Caron G, Delneste Y, Roelandts E, Duez C, Bonnefoy J-Y, Pestel J, et al. Histamine polarizes human dendritic cells into Th2 cell-promoting effector dendritic cells. The Journal of Immunology. 2001;167(7):3682-6.

34. Lichtenstein LM, Gillespie E. The effects of the H1 and H2 antihistamines on" allergic" histamine release and its inhibition by histamine. The Journal of Pharmacology and Experimental Therapeutics. 1975;192(2):441-50.

35. Jutel M, Akdis M, Akdis CA. Histamine, histamine receptors and their role in immune pathology. Clinical and experimental allergy. 2009;39(12):1786-800.

36. Swiecki M, Colonna M. Type I interferons: diversity of sources, production pathways and effects on immune responses. Current opinion in virology. 2011;1(6):463-75.

37. Kalliolias GD, Ivashkiv LB. Overview of the biology of type I interferons. Arthritis research & therapy. 2010;12:1-9.

38. Lee AJ, Ashkar AA. The dual nature of type I and type II interferons. Frontiers in immunology. 2018;9:2061.

39. Coleman JW. Nitric oxide in immunity and inflammation. International immunopharmacology. 2001;1(8):1397-406.

40. Lee WL, Harrison RE, Grinstein S. Phagocytosis by neutrophils. Microbes and infection. 2003;5(14):1299-306.

41. Banchereau J, Briere F, Caux C, Davoust J, Lebecque S, Liu Y-J, et al. Immunobiology of Dendritic Cells. Annual review of immunology. 2000;18(1):767-811.

42. Broz P, Monack DM. Newly described pattern recognition receptors team up against intracellular pathogens. Nature Reviews Immunology. 2013;13(8):551-65.

43. Borregaard N. Neutrophils, from Marrow to Microbes. Immunity (Cambridge, Mass). 2010;33(5):657-70.

44. Sheshachalam A, Srivastava N, Mitchell T, Lacy P, Eitzen G. Granule protein processing and regulated secretion in neutrophils. Frontiers in immunology. 2014;5:448.

45. Borregaard N, Lollike K, Kjeldsen L, Sengeløv H, Bastholm L, Nielsen MH, et al. Human neutrophil granules and secretory vesicles. European journal of haematology. 1993;51(4):187-98.

46. Cowland JB, Borregaard N. Granulopoiesis and granules of human neutrophils. Immunological reviews. 2016;273(1):11-28.

47. Van den Steen PE, Dubois B, Nelissen I, Rudd PM, Dwek RA, Opdenakker G. Biochemistry and molecular biology of gelatinase B or matrix metalloproteinase-9 (MMP-9). Critical reviews in biochemistry and molecular biology. 2002;37(6):375-536.

48. Faurschou M, Borregaard N. Neutrophil granules and secretory vesicles in inflammation. Microbes and infection. 2003;5(14):1317-27.

49. Witko-Sarsat V, Rieu P, Descamps-Latscha B, Lesavre P, Halbwachs-Mecarelli L. Neutrophils: molecules, functions and pathophysiological aspects. Laboratory investigation. 2000;80(5):617-53.

50. Guermonprez P, Valladeau J, Zitvogel L, Théry C, Amigorena S. ANTIGEN PRESENTATION AND T CELL STIMULATION BY

DENDRITIC CELLS. Annual review of immunology. 2002;20(1):621-67.

51. Savina A, Amigorena S. Phagocytosis and antigen presentation in dendritic cells. Immunological reviews. 2007;219(1):143-56.

52. Tacke F, Randolph GJ. Migratory fate and differentiation of blood monocyte subsets. Immunobiology. 2006;211(6-8):609-18.

53. Guilliams M, Mildner A, Yona S. Developmental and functional heterogeneity of monocytes. Immunity. 2018;49(4):595-613.

54. Ziegler-Heitbrock H. Definition of human blood monocytes. Journal of leukocyte biology. 2000;67(5):603-6.

55. Auffray C, Sieweke MH, Geissmann F. Blood monocytes: development, heterogeneity, and relationship with dendritic cells. Annual review of immunology. 2009;27(1):669-92.

56. Ziegler-Heitbrock L, Ancuta P, Crowe S, Dalod M, Grau V, Hart DN, et al. Nomenclature of monocytes and dendritic cells in blood. Blood, The Journal of the American Society of Hematology. 2010;116(16):e74-e80.

57. Ożańska A, Szymczak D, Rybka J. Pattern of human monocyte subpopulations in health and disease. Scandinavian journal of immunology. 2020;92(1):e12883.

58. Anbazhagan K, Duroux-Richard I, Jorgensen C, Apparailly F. Transcriptomic network support distinct roles of classical and non-classical monocytes in human. International reviews of immunology. 2014;33(6):470-89.

59. Yona S, Jung S. Monocytes: subsets, origins, fates and functions. Current opinion in hematology. 2010;17(1):53-9.

60. Shi C, Pamer EG. Monocyte recruitment during infection and inflammation. Nature reviews immunology. 2011;11(11):762-74.

61. Davies LC, Jenkins SJ, Allen JE, Taylor PR. Tissue-resident macrophages. Nature immunology. 2013;14(10):986-95.

62. Perdiguero EG, Geissmann F. The development and maintenance of resident macrophages. Nature immunology. 2016;17(1):2-8.

63. Hettinger J, Richards DM, Hansson J, Barra MM, Joschko A-C, Krijgsveld J, et al. Origin of monocytes and macrophages in a committed progenitor. Nature immunology. 2013;14(8):821-30.

64. Wu Y, Hirschi KK. Tissue-resident macrophage development and function. Frontiers in cell and developmental biology. 2021;8:617879.

65. Lazarov T, Juarez-Carreño S, Cox N, Geissmann F. Physiology and diseases of tissue-resident macrophages. Nature. 2023;618(7966):698-707.

66. Shapouri-Moghaddam A, Mohammadian S, Vazini H, Taghadosi M, Esmaeili SA, Mardani F, et al. Macrophage plasticity, polarization, and function in health and disease. Journal of cellular physiology. 2018;233(9):6425-40.

67. Huang X, Li Y, Fu M, Xin H-B. Polarizing Macrophages In Vitro. Macrophages. 2018;1784:119-26.

68. Sheikh Z, Brooks PJ, Barzilay O, Fine N, Glogauer M. Macrophages, foreign body giant cells and their response to implantable biomaterials. Materials. 2015;8(9):5671-701.

69. Jager NA, Wallis de Vries BM, Hillebrands J-L, Harlaar NJ, Tio RA, Slart RH, et al. Distribution of matrix metalloproteinases in human atherosclerotic carotid plaques and their production by smooth muscle cells and macrophage subsets. Molecular imaging and biology. 2016;18:283-91.

70. Orecchioni M, Ghosheh Y, Pramod AB, Ley K. Macrophage polarization: different gene signatures in M1 (LPS+) vs. classically and M2 (LPS–) vs. alternatively activated macrophages. Frontiers in immunology. 2019;10:1084.

71. Karlinsey K, Qu L, Matz AJ, Zhou B. A novel strategy to dissect multifaceted macrophage function in human diseases. Journal of Leukocyte Biology. 2022;112(6):1535-42.

72. Nahrendorf M, Swirski FK. Abandoning M1/M2 for a Network Model of Macrophage Function. Circ Res. 2016;119(3):414-7.

73. Fuchs AL, Costello SM, Schiller SM, Tripet BP, Copié V. Primary Human M2 Macrophage Subtypes Are Distinguishable by Aqueous Metabolite Profiles. International Journal of Molecular Sciences. 2024;25(4):2407.

74. Gharavi AT, Hanjani NA, Movahed E, Doroudian M. The role of macrophage subtypes and exosomes in immunomodulation. Cellular & molecular biology letters. 2022;27(1):83.

75. Majrashi M, Kotowska A, Scurr D, Hicks JM, Ghaemmaghami A, Yang J. Sustained Release of Dexamethasone from 3D-Printed Scaffolds Modulates Macrophage Activation and Enhances Osteogenic Differentiation. ACS Applied Materials & Interfaces. 2023;15(49):56623-38.

76. Chaintreuil P, Kerreneur E, Bourgoin M, Savy C, Favreau C, Robert G, et al. The generation, activation, and polarization of monocyte-derived macrophages in human malignancies. Frontiers in immunology. 2023;14:1178337.

77. Abaricia JO, Farzad N, Heath TJ, Simmons J, Morandini L, Olivares-Navarrete R. Control of innate immune response by biomaterial surface topography, energy, and stiffness. Acta biomaterialia. 2021;133:58-73.

78. Frank A-SJ, Larripa K, Ryu H, Röblitz S. Macrophage phenotype transitions in a stochastic gene-regulatory network model. Journal of Theoretical Biology. 2023;575:111634.

79. A ABJ, Lewis J ea. Innate Immunity. Molecular Biology of the Cell. New York: Garland Science2002.

80. Buchmann K. Evolution of innate immunity: clues from invertebrates via fish to mammals. Frontiers in immunology. 2014;5:459.

81. Sette A, Crotty S. Immunological memory to SARS-CoV-2 infection and COVID-19 vaccines. Immunological reviews. 2022;310(1):27-46.

82. Chi H, Pepper M, Thomas PG. Principles and therapeutic applications of adaptive immunity. Cell. 2024;187(9):2052-78.

83. Bonilla FA, Oettgen HC. Adaptive immunity. Journal of Allergy and Clinical Immunology. 2010;125(2):S33-S40.

84. Cooper MD. The early history of B cells. Nature Reviews Immunology. 2015;15(3):191-7.

85. Ryu W-S. Chapter 5 - Host Immune Response. In: Ryu W-S, editor. Molecular Virology of Human Pathogenic Viruses. Boston: Academic Press; 2017. p. 63-82.

86. LeBien TW, Tedder TF. B lymphocytes: how they develop and function. Blood. 2008;112(5):1570-80.

87. Nemazee D. Mechanisms of central tolerance for B cells. Nature Reviews Immunology. 2017;17(5):281-94.

88. Cheng S, Hsia CY, Feng B, Liou ML, Fang X, Pandolfi PP, et al. BCR-mediated apoptosis associated with negative selection of immature B cells is selectively dependent on Pten. Cell Res. 2009;19(2):196-207.

89. Bannish G, Fuentes-Pananá EM, Cambier JC, Pear WS, Monroe JG. Ligand-independent signaling functions for the B lymphocyte antigen receptor and their role in positive selection during B lymphopoiesis. J Exp Med. 2001;194(11):1583-96.

90. Janeway Jr CA, Travers P, Walport M, Shlomchik MJ. Generation of lymphocytes in bone marrow and thymus. Immunobiology: The Immune System in Health and Disease 5th edition: Garland Science; 2001.

91. Loder F, Mutschler B, Ray RJ, Paige CJ, Sideras P, Torres R, et al. B cell development in the spleen takes place in discrete steps and is determined by the quality of B cell receptor-derived signals. J Exp Med. 1999;190(1):75-89.

92. Yuan D, Witte PL. Transcriptional regulation of mu and delta gene expression in bone marrow pre-B and B lymphocytes. Journal of immunology (Baltimore, Md: 1950). 1988;140(8):2808-14.

93. Nutt SL, Hodgkin PD, Tarlinton DM, Corcoran LM. The generation of antibody-secreting plasma cells. Nature Reviews Immunology. 2015;15(3):160-71.

94. Hesslein DG, Aguila HL, Horowitz MC. 3 - The Adaptive Immune Response. In: Lorenzo J, Choi Y, Horowitz M, Takayanagi H, editors. Osteoimmunology. San Diego: Academic Press; 2011. p. 43-80.

95. Mauri C, Reddy V, Blair PA. Chapter 10 - B Cell Activation and B Cell Tolerance. In: Rose NR, Mackay IR, editors. The Autoimmune Diseases (Fifth Edition). Boston: Academic Press; 2014. p. 147-58.

96. Zou Y-R, Grimaldi C, Diamond B. Chapter 13 - B Cells. In: Firestein GS, Budd RC, Gabriel SE, McInnes IB, O'Dell JR, editors. Kelley and Firestein's Textbook of Rheumatology (Tenth Edition): Elsevier; 2017. p. 207-30.e3.

97. Cyster JG, Allen CDC. B Cell Responses: Cell Interaction Dynamics and Decisions. Cell. 2019;177(3):524-40.

98. Klein L, Kyewski B, Allen PM, Hogquist KA. Positive and negative selection of the T cell repertoire: what thymocytes see (and don't see). Nature Reviews Immunology. 2014;14(6):377-91.

99. Germain RN. T-cell development and the CD4–CD8 lineage decision. Nature reviews immunology. 2002;2(5):309-22.

100. Alberts B, Johnson A, Lewis J, Raff M, Roberts K, Walter P. Helper T cells and lymphocyte activation. Molecular biology of the cell 4th edition: Garland Science; 2002.

101. Rudd-Schmidt JA, Hodel AW, Noori T, Lopez JA, Cho H-J, Verschoor S, et al. Lipid order and charge protect killer T cells from accidental death. Nature Communications. 2019;10(1):5396.

102. Adu-Berchie K, Obuseh FO, Mooney DJ. T Cell Development and Function. Rejuvenation Res. 2023;26(4):126-38.

103. Chung L, Maestas Jr DR, Lebid A, Mageau A, Rosson GD, Wu X, et al. Interleukin 17 and senescent cells regulate the foreign body response to synthetic material implants in mice and humans. Science translational medicine. 2020;12(539):eaax3799.

104. Moore EM, Maestas Jr DR, Cherry CC, Garcia JA, Comeau HY, Davenport Huyer L, et al. Biomaterials direct functional B cell response in a material-specific manner. Science Advances. 2021;7(49):eabj5830.

105. Karkanitsa M, Fathi P, Ngo T, Sadtler K. Mobilizing Endogenous Repair Through Understanding Immune Reaction With Biomaterials. Frontiers in Bioengineering and Biotechnology. 2021;Volume 9 - 2021.

106. Lee JH, Shin SJ, Knowles JC, Lee HH, Kim HW. Adaptive immunity of materials: Implications for tissue healing and regeneration. Bioact Mater. 2024;41:499-522.

107. Olson NC, Sallam R, Doyle MF, Tracy RP, Huber SA. T helper cell polarization in healthy people: implications for cardiovascular disease. J Cardiovasc Transl Res. 2013;6(5):772-86.

108. Ramani K, Biswas PS. Interleukin-17: Friend or foe in organ fibrosis. Cytokine. 2019;120:282-8.

109. Zhang P, Wang J, Miao J, Zhu P. The dual role of tissue regulatory T cells in tissue repair: return to homeostasis or fibrosis. Front Immunol. 2025;16:1560578.

110. Chung L, Maestas DR, Housseau F, Elisseeff JH. Key players in the immune response to biomaterial scaffolds for regenerative medicine. Advanced drug delivery reviews. 2017;114:184-92.

111. Anderson JM, Rodriguez A, Chang DT. Foreign body reaction to biomaterials. Seminars in immunology. 2007;20(2):86-100.

112. Noskovicova N, Hinz B, Pakshir P. Implant Fibrosis and the Underappreciated Role of Myofibroblasts in the Foreign Body Reaction. Cells (Basel, Switzerland). 2021;10(7):1794.

113. Söhling N, Ondreka M, Kontradowitz K, Reichel T, Marzi I, Henrich D. Early Immune Response in Foreign Body Reaction Is Implant/Material Specific. Materials. 2022;15(6):2195.

114. Lemons Jack E, Hoffman Allan S, Schoen Frederick J, Ratner Buddy D. Section Host Reaction to Biomaterials and Their Evaluation. 3rd Edition ed: Elsevier; 2013. p. 2-.

115. Noh HH, Vogler EAEA. Volumetric Interpretation of Protein Adsorption: Competition from Mixtures and the Vroman Effect: A Contribution from the Hematology at Biomaterial Interfaces Research Group. Biomaterials. 2006;28(3):405-22.

116. Carnicer-Lombarte A, Chen ST, Malliaras GG, Barone DG. Foreign Body Reaction to Implanted Biomaterials and Its Impact in Nerve Neuroprosthetics. Frontiers in bioengineering and biotechnology. 2021;9:622524-.

117. Barker TH, Engler AJ. The provisional matrix: setting the stage for tissue repair outcomes. Matrix Biol. 2017;60-61:1-4.

118. Anderson JM, Jiang S. Implications of the Acute and Chronic Inflammatory Response and the Foreign Body Reaction to the Immune Response of Implanted Biomaterials. In: Corradetti B, editor. The Immune Response to Implanted Materials and Devices: The Impact of the Immune System on the Success of an Implant. Cham: Springer International Publishing; 2017. p. 15-36.

119. Zhou X, Wang Y, Ji J, Zhang P. Materials strategies to overcome the foreign body response. Advanced Healthcare Materials. 2024;13(18):2304478.

120. Chu C, Liu L, Rung S, Wang Y, Ma Y, Hu C, et al. Modulation of foreign body reaction and macrophage phenotypes concerning microenvironment. Journal of biomedical materials research Part A. 2020;108(1):127-35.

121. Parker JB, Griffin MF, Spielman AF, Wan DC, Longaker MT. Exploring the Overlooked Roles and Mechanisms of Fibroblasts in the Foreign Body Response. Adv Wound Care (New Rochelle). 2023;12(2):85-96.

122. Anderson J, Cramer S. Chapter 2 - Perspectives on the Inflammatory, Healing, and Foreign Body Responses to Biomaterials and Medical Devices. In: Badylak SF, editor. Host Response to Biomaterials. Oxford: Academic Press; 2015. p. 13-36.

123. Anderson JM. 40 - Biocompatibility and Bioresponse to Biomaterials. In: Atala A, Lanza R, Thomson JA, Nerem RM, editors. Principles of Regenerative Medicine. San Diego: Academic Press; 2008. p. 704-23.

124. Diegelmann RF, Evans MC. Wound healing: an overview of acute, fibrotic and delayed healing. Front Biosci. 2004;9:283-9.

125. Singh S, Young A, McNaught C-E. The physiology of wound healing. Surgery (Oxford). 2017;35(9):473-7.

126. Reinke JM, Sorg H. Wound repair and regeneration. Eur Surg Res. 2012;49(1):35-43.

127. Wallace HA, Basehore BM, Zito PM. Wound healing phases. 2017.

128. Eslami-Kaliji F, Hedayat Nia N, Lakey JRT, Smink AM, Mohammadi M. Mechanisms of Foreign Body Giant Cell Formation in Response to Implantable Biomaterials. Polymers. 2023;15(5):1313.

129. Kazi S, Raptis S, Abbaspour F, Zeng W. Foreign body-type giant cell reaction with extensive granulation tissue and intense inflammation

after chemotherapy mimicking residual lymphoma on FDG PET. Eur J Hybrid Imaging. 2022;6(1):18.

130. Cai F, Jiang B, He F. Formation and biological activities of foreign body giant cells in response to biomaterials. Acta Biomaterialia. 2024;188:1-26.

131. Lucke S, Walschus U, Hoene A, Schnabelrauch M, Nebe JB, Finke B, et al. The in vivo inflammatory and foreign body giant cell response against different poly(l-lactide-co-d/l-lactide) implants is primarily determined by material morphology rather than surface chemistry. Journal of biomedical materials research Part A. 2018;106(10):2726-34.

132. Jones JA, Chang DT, Meyerson H, Colton E, Kwon IK, Matsuda T, et al. Proteomic analysis and quantification of cytokines and chemokines from biomaterial surface-adherent macrophages and foreign body giant cells. Journal of Biomedical Materials Research Part A. 2007;83A(3):585-96.

133. Li JJ, Zreiqat H. Tissue Response to Biomaterials. In: Narayan R, editor. Encyclopedia of Biomedical Engineering. Oxford: Elsevier; 2019. p. 270-7.

134. Raghavendra GM, Varaprasad K, Jayaramudu T. Chapter 2 - Biomaterials: Design, Development and Biomedical Applications. In: Thomas S, Grohens Y, Ninan N, editors. Nanotechnology Applications for Tissue Engineering. Oxford: William Andrew Publishing; 2015. p. 21-44.

135. Todros S, Todesco M, Bagno A. Biomaterials and their biomedical applications: from replacement to regeneration. Processes. 2021;9(11):1949.

136. Bergmann CP, Stumpf A. Dental ceramics. Biomaterials. 2013:9-13.

137. The European Society for Biomaterials 9th European Conference on Biomaterials Chester, UK 9–11th September, 1991 in conjunction with 2nd Consensus Conference on Definitions in Biomaterials 7–8th September, 1991 and IUPAC working party on blood compatibility. Journal of Materials Science: Materials in Medicine. 1991;2(1):62-.

138. Lee EJ, Kasper FK, Mikos AG. Biomaterials for Tissue Engineering. Annals of biomedical engineering. 2014;42(2):323-37.

139. Al-Shalawi FD, Mohamed Ariff AH, Jung D-W, Mohd Ariffin MK, Seng Kim CL, Brabazon D, et al. Biomaterials as Implants in the Orthopedic Field for Regenerative Medicine: Metal versus Synthetic Polymers. Polymers [Internet]. 2023; 15(12).

140. Marin E. Forged to heal: The role of metallic cellular solids in bone tissue engineering. Materials Today Bio. 2023;23:100777.

141. Karunakar KK, Cheriyan BV, Nandhini J, Kataria K, Yabase L, Devan P, et al. Comprehensive Review of Biomedical Metals and Strategies for Advancing Regenerative Medicine. Biomedical Materials & Devices. 2025:1-33.

142. Zhou Z, Liu D. Mesenchymal stem cell-seeded porous tantalum-based biomaterial: A promising choice for promoting bone regeneration. Colloids and Surfaces B: Biointerfaces. 2022;215:112491.

143. Poh CK, Shi Z, Tan XW, Liang ZC, Foo XM, Tan HC, et al. Cobalt chromium alloy with immobilized BMP peptide for enhanced bone growth. Journal of Orthopaedic Research. 2011;29(9):1424-30.

144. Chen RJ, Lee VR. Cobalt Toxicity.[Updated 2022 Oct 26]. StatPearls [Internet] Treasure Island (FL): StatPearls Publishing. 2023.

145. Acheson JG, McKillop S, Lemoine P, Boyd AR, Meenan BJ. Control of magnesium alloy corrosion by bioactive calcium phosphate coating: Implications for resorbable orthopaedic implants. Materialia. 2019;6:100291.

146. Dykman L, Khlebtsov B, Khlebtsov N. Drug delivery using gold nanoparticles. Advanced Drug Delivery Reviews. 2025;216:115481.
147. Kanu GA, Parambath JBM, Abu Odeh RO, Mohamed AA. Gold Nanoparticle-Mediated Gene Therapy. Cancers (Basel). 2022;14(21).
148. Bohner M, Santoni BLG, Döbelin N. β-tricalcium phosphate for bone substitution: Synthesis and properties. Acta Biomaterialia. 2020;113:23-41.
149. Rahmati M, Mozafari M. Biocompatibility of alumina-based biomaterials–A review. Journal of cellular physiology. 2019;234(4):3321-35.
150. Budharaju H, Suresh S, Sekar MP, De Vega B, Sethuraman S, Sundaramurthi D, et al. Ceramic materials for 3D printing of biomimetic bone scaffolds – Current state-of-the-art & future perspectives. Materials & Design. 2023;231:112064.
151. Bhatia S. Natural polymers vs synthetic polymer. Natural polymer drug delivery systems: nanoparticles, plants, and algae: Springer; 2016. p. 95-118.
152. Saleh TA. Polymer science and polymerization methods toward hybrid materials. Polymer Hybrid Materials and Nanocomposites. 2021:59-103.
153. Rakowska PD, Tiddia M, Faruqui N, Bankier C, Pei Y, Pollard AJ, et al. Antiviral surfaces and coatings and their mechanisms of action. Communications Materials. 2021;2(1):53.
154. Hook AL, Chang C-Y, Yang J, Luckett J, Cockayne A, Atkinson S, et al. Combinatorial discovery of polymers resistant to bacterial attachment. Nature biotechnology. 2012;30(9):868-75.
155. Akbari A, Bigham A, Rahimkhoei V, Sharifi S, Jabbari E. Antiviral Polymers: A Review. Polymers [Internet]. 2022; 14(9).

156. Zhang Q, Zong Q, Feng X, Luo M, Sun W, Zhai Y. Antibacterial and antifouling materials for urinary catheter coatings. Acta Biomaterialia. 2025;192:28-47.

157. Kim P-H, Cho J-Y. Myocardial tissue engineering using electrospun nanofiber composites. BMB reports. 2016;49(1):26.

158. Almawash S, Osman SK, Mustafa G, El Hamd MA. Current and Future Prospective of Injectable Hydrogels—Design Challenges and Limitations. Pharmaceuticals [Internet]. 2022; 15(3).

159. Dabbaghi A, Ramazani A, Farshchi N, Rezaei A, Bodaghi A, Rezayati S. Synthesis, physical and mechanical properties of amphiphilic hydrogels based on polycaprolactone and polyethylene glycol for bioapplications: A review. Journal of Industrial and Engineering Chemistry. 2021;101:307-23.

160. Bhattarai N, Gunn J, Zhang M. Chitosan-based hydrogels for controlled, localized drug delivery. Advanced Drug Delivery Reviews. 2010;62(1):83-99.

161. Bashir S, Hina M, Iqbal J, Rajpar AH, Mujtaba MA, Alghamdi NA, et al. Fundamental Concepts of Hydrogels: Synthesis, Properties, and Their Applications. Polymers (Basel). 2020;12(11).

162. Yuan N, Xu L, Wang H, Fu Y, Zhang Z, Liu L, et al. Dual Physically Cross-Linked Double Network Hydrogels with High Mechanical Strength, Fatigue Resistance, Notch-Insensitivity, and Self-Healing Properties. ACS Applied Materials & Interfaces. 2016;8(49):34034-44.

163. Parhi R. Cross-Linked Hydrogel for Pharmaceutical Applications: A Review. Adv Pharm Bull. 2017;7(4):515-30.

164. Pruksawan S, Lim JWR, Lee YL, Lin Z, Chee HL, Chong YT, et al. Enhancing hydrogel toughness by uniform cross-linking using modified polyhedral oligomeric silsesquioxane. Communications Materials. 2023;4(1):75.

165. Hiemstra C, van der Aa LJ, Zhong Z, Dijkstra PJ, Feijen J. Novel in Situ Forming, Degradable Dextran Hydrogels by Michael Addition Chemistry: Synthesis, Rheology, and Degradation. Macromolecules. 2007;40(4):1165-73.

166. Dubey SK, Dheeraj, Hejmady S, Alexander A, Tiwari S, Singhvi G. Chapter 4 - Graft-modified polysaccharides in biomedical applications. In: Nayak A, Hasnain MS, Aminabhavi T, editors. Tailor-Made Polysaccharides in Biomedical Applications: Academic Press; 2020. p. 69-100.

167. Jacob LI, Pauer W, Schroeter B. Influence of redox initiator component ratios on the emulsion copolymerisation of vinyl acetate and neodecanoic acid vinyl ester. RSC advances. 2022;12(22):14197-208.

168. Schwalm R. Photoinitiators and Photopolymerization. In: Buschow KHJ, Cahn RW, Flemings MC, Ilschner B, Kramer EJ, Mahajan S, et al., editors. Encyclopedia of Materials: Science and Technology. Oxford: Elsevier; 2001. p. 6946-51.

169. Studer K, Nesvadba P, Jung T, Benkhoff J, Powell K, Lordelot C. Novel curing agents: Thermal radical initiators as viable alternatives to peroxides. Progress in Organic Coatings. 2008;61(2):119-25.

170. Moreira Teixeira LS, Feijen J, van Blitterswijk CA, Dijkstra PJ, Karperien M. Enzyme-catalyzed crosslinkable hydrogels: Emerging strategies for tissue engineering. Biomaterials. 2012;33(5):1281-90.

171. Alginates: IntechOpen; 2020.

172. Lee KY, Mooney DJ. Alginate: Properties and biomedical applications. Progress in polymer science. 2012;37(1):106-26.

173. Sanchez-Ballester NM, Bataille B, Soulairol I. Sodium alginate and alginic acid as pharmaceutical excipients for tablet formulation: Structure-function relationship. Carbohydrate polymers. 2021;270:118399-.

174. Hariyadi DM, Islam N. Current Status of Alginate in Drug Delivery. Advances in pharmacological and pharmaceutical sciences. 2020;2020:1-16.

175. Liu Q, Chiu A, Wang L-H, An D, Zhong M, Smink AM, et al. Zwitterionically modified alginates mitigate cellular overgrowth for cell encapsulation. Nature communications. 2019;10(1):5262-14.

176. Doloff JC, Veiseh O, Vegas AJ, Tam HH, Farah S, Ma M, et al. Colony stimulating factor-1 receptor is a central component of the foreign body response to biomaterial implants in rodents and non-human primates. Nature materials. 2017;16(6):671-80.

177. Cao L, Lu W, Mata A, Nishinari K, Fang Y. Egg-box model-based gelation of alginate and pectin: A review. Carbohydrate polymers. 2020;242:116389-.

178. Wang S, Tavakoli S, Parvathaneni RP, Nawale GN, Oommen OP, Hilborn J, et al. Dynamic covalent crosslinked hyaluronic acid hydrogels and nanomaterials for biomedical applications. Biomaterials science. 2022;1(22):6399-412.

179. Gao Y, Peng K, Mitragotri S. Covalently Crosslinked Hydrogels via Step-Growth Reactions: Crosslinking Chemistries, Polymers, and Clinical Impact. Advanced materials (Weinheim). 2021;33(25):e2006362-n/a.

180. Wang Y, Zhang R, Qiao Z, Dou B, Xu H, Meng F, et al. Polyacrylamide-Based Hydrogel with Biocompatibility and Tunable Stiffness for Three-Dimensional Cell Culture. ACS Applied Bio Materials. 2025;8(3):2356-64.

181. Charrier EE, Pogoda K, Li R, Park CY, Fredberg JJ, Janmey PA. A novel method to make viscoelastic polyacrylamide gels for cell culture and traction force microscopy. APL bioengineering. 2020;4(3).

182. Pérez-Calixto D, Amat-Shapiro S, Zamarrón-Hernández D, Vázquez-Victorio G, Puech P-H, Hautefeuille M. Determination by

Relaxation Tests of the Mechanical Properties of Soft Polyacrylamide Gels Made for Mechanobiology Studies. Polymers [Internet]. 2021; 13(4).

183. Denisin AK, Pruitt BL. Tuning the Range of Polyacrylamide Gel Stiffness for Mechanobiology Applications. ACS Applied Materials & Interfaces. 2016;8(34):21893-902.

184. Funaki M, Janmey PA. Chapter 23 - Technologies to Engineer Cell Substrate Mechanics in Hydrogels. In: Vishwakarma A, Karp JM, editors. Biology and Engineering of Stem Cell Niches. Boston: Academic Press; 2017. p. 363-73.

185. Zhang Y, Dai J, Hang R, Yao X, Bai L, Huang D, et al. Impact of surface biofunctionalization strategies on key effector cells response in polyacrylamide hydrogels for bone regeneration. Biomaterials Advances. 2024;158:213768.

186. LoPachin RM. The changing view of acrylamide neurotoxicity. Neurotoxicology. 2004;25(4):617-30.

187. Hayashi M, Tanii H, Horiguchi M, Hashimoto K. Cytotoxic effects of acrylamide and its related compounds assessed by protein content, LDH activity and cumulative glucose consumption of neuron-rich cultures in a chemically defined medium. Arch Toxicol. 1989;63(4):308-13.

188. Quasmi MN, Kumar D, Jangra A. Effects of dietary acrylamide on kidney and liver health: Molecular mechanisms and pharmacological implications. Toxicology Reports. 2025;14:101859.

189. Quatela VC, Chow J. Synthetic Facial Implants. Facial Plastic Surgery Clinics of North America. 2008;16(1):1-10.

190. Takahashi R, Tanaka A, Saito T, Ohashi S, Muto M, Yamaguchi M. Organ-On-A-Chip Platforms Created Through Buckled Microchannels of Porous Hydrogel Films. Advanced Materials Technologies. 2025;10(7):2401468.

191. Chakrapani G, Vijay Kumar V, Zare M. Next-Generation Biomaterials: Design Strategies, Clinical Translation, and the Rise of Intelligent Therapeutic Platforms. ACS Omega. 2025;10(40):46272-93.
192. Baker BM, Chen CS. Deconstructing the third dimension–how 3D culture microenvironments alter cellular cues. Journal of cell science. 2012;125(13):3015-24.
193. Sapudom J, Alatoom A, Mohamed WKE, Garcia-Sabaté A, McBain I, Nasser RA, et al. Dendritic cell immune potency on 2D and in 3D collagen matrices. Biomaterials Science. 2020;8(18):5106-20.
194. Bhattacharya A, Agarwal M, Mukherjee R, Sen P, Sinha DK. 3D micro-environment regulates NF-κβ dependent adhesion to induce monocyte differentiation. Cell Death & Disease. 2018;9(9):914.
195. Bu W, Wu Y, Ghaemmaghami AM, Sun H, Mata A. Rational design of hydrogels for immunomodulation. Regenerative biomaterials. 2022;9.
196. McWhorter FY, Davis CT, Liu WF. Physical and mechanical regulation of macrophage phenotype and function. Cellular and Molecular Life Sciences. 2015;72:1303-16.
197. Blakney AK, Swartzlander MD, Bryant SJ. The effects of substrate stiffness on the in vitro activation of macrophages and in vivo host response to poly(ethylene glycol)-based hydrogels. Journal of biomedical materials research Part A. 2012;100A(6):1375-86.
198. Sridharan R, Cavanagh B, Cameron AR, Kelly DJ, O'Brien FJ. Material stiffness influences the polarization state, function and migration mode of macrophages. Acta biomaterialia. 2019;89:47-59.
199. Zhuang Z, Zhang Y, Sun S, Li Q, Chen K, An C, et al. Control of Matrix Stiffness Using Methacrylate–Gelatin Hydrogels for a Macrophage-Mediated Inflammatory Response. ACS biomaterials science & engineering. 2020;6(5):3091-102.

200. Chen M, Zhang Y, Zhou P, Liu X, Zhao H, Zhou X, et al. Substrate stiffness modulates bone marrow-derived macrophage polarization through NF-κB signaling pathway. Bioactive materials. 2020;5(4):880-90.

201. Ni Y, Qi H, Zhang F, Jiang S, Tang Q, Cai W, et al. Macrophages modulate stiffness-related foreign body responses through plasma membrane deformation. Proceedings of the National Academy of Sciences - PNAS. 2023;120(3):e2213837120-e.

202. Camarero-Espinosa S, Carlos-Oliveira M, Liu H, Mano JF, Bouvy N, Moroni L. 3D Printed Dual-Porosity Scaffolds: The Combined Effect of Stiffness and Porosity in the Modulation of Macrophage Polarization. Advanced healthcare materials. 2022;11(1):e2101415-n/a.

203. Oftadeh R, Connizzo BK, Nia HT, Ortiz C, Grodzinsky AJ. Biological connective tissues exhibit viscoelastic and poroelastic behavior at different frequency regimes: Application to tendon and skin biophysics. Acta Biomaterialia. 2018;70:249-59.

204. Indana D, Agarwal P, Bhutani N, Chaudhuri O. Viscoelasticity and adhesion signaling in biomaterials control human pluripotent stem cell morphogenesis in 3D culture. Advanced Materials. 2021;33(43):2101966.

205. Cameron AR, Frith JE, Cooper-White JJ. The influence of substrate creep on mesenchymal stem cell behaviour and phenotype. Biomaterials. 2011;32(26):5979-93.

206. Cameron AR, Frith JE, Gomez GA, Yap AS, Cooper-White JJ. The effect of time-dependent deformation of viscoelastic hydrogels on myogenic induction and Rac1 activity in mesenchymal stem cells. Biomaterials. 2014;35(6):1857-68.

207. Chang T-L, Borelli AN, Cutler AA, Olwin BB, Anseth KS. Myofibers cultured in viscoelastic hydrogels reveal the effects of

integrin-binding and mechanosensing on muscle satellite cells. Acta Biomaterialia. 2025;192:48-60.

208. Bauer A, Gu L, Kwee B, Li WA, Dellacherie M, Celiz AD, et al. Hydrogel substrate stress-relaxation regulates the spreading and proliferation of mouse myoblasts. Acta Biomaterialia. 2017;62:82-90.

209. Hui E, Moretti L, Barker TH, Caliari SR. The Combined Influence of Viscoelastic and Adhesive Cues on Fibroblast Spreading and Focal Adhesion Organization. Cellular and Molecular Bioengineering. 2021;14(5):427-40.

210. Chester D, Kathard R, Nortey J, Nellenbach K, Brown AC. Viscoelastic properties of microgel thin films control fibroblast modes of migration and pro-fibrotic responses. Biomaterials. 2018;185:371-82.

211. Ciccone G, Azevedo Gonzalez-Oliva M, Versaevel M, Cantini M, Vassalli M, Salmeron-Sanchez M, et al. Epithelial Cell Mechanoresponse to Matrix Viscoelasticity and Confinement Within Micropatterned Viscoelastic Hydrogels. Advanced Science. 2025;12(18):2408635.

212. Mandal K, Gong Z, Rylander A, Shenoy VB, Janmey PA. Opposite responses of normal hepatocytes and hepatocellular carcinoma cells to substrate viscoelasticity. Biomaterials science. 2020;8(5):1316-28.

213. Fan W, Adebowale K, Váncza L, Li Y, Rabbi MF, Kunimoto K, et al. Matrix viscoelasticity promotes liver cancer progression in the pre-cirrhotic liver. Nature. 2024;626(7999):635-42.

214. Adebowale K, Gong Z, Hou JC, Wisdom KM, Garbett D, Lee H-p, et al. Enhanced substrate stress relaxation promotes filopodia-mediated cell migration. Nature Materials. 2021;20(9):1290-9.

215. Ansari S, Chen C, Hasani-Sadrabadi MM, Yu B, Zadeh HH, Wu BM, et al. Hydrogel elasticity and microarchitecture regulate dental-

derived mesenchymal stem cell-host immune system cross-talk. Acta Biomaterialia. 2017;60:181-9.

216. Del Campo A, Arzt E. Fabrication approaches for generating complex micro-and nanopatterns on polymeric surfaces. Chemical reviews. 2008;108(3):911-45.

217. Luu TU, Gott SC, Woo BWK, Rao MP, Liu WF. Micro- and Nanopatterned Topographical Cues for Regulating Macrophage Cell Shape and Phenotype. ACS Applied Materials & Interfaces. 2015;7(51):28665-72.

218. Cui L, Yao Y, Yim EKF. The effects of surface topography modification on hydrogel properties. APL bioengineering. 2021;5(3).

219. Visalakshan RM, MacGregor MN, Sasidharan S, Ghazaryan A, Mierczynska-Vasilev AM, Morsbach S, et al. Biomaterial Surface Hydrophobicity-Mediated Serum Protein Adsorption and Immune Responses. ACS Applied Materials & Interfaces. 2019;11(31):27615-23.

220. Lv L, Xie Y, Li K, Hu T, Lu X, Cao Y, et al. Unveiling the Mechanism of Surface Hydrophilicity-Modulated Macrophage Polarization. Advanced Healthcare Materials. 2018;7(19):1800675.

221. Roy Barman S, Jhunjhunwala S. Electrical Stimulation for Immunomodulation. ACS Omega. 2024;9(1):52-66.

222. Lee TT, García JR, Paez JI, Singh A, Phelps EA, Weis S, et al. Light-triggered in vivo activation of adhesive peptides regulates cell adhesion, inflammation and vascularization of biomaterials. Nature materials. 2015;14(3):352-60.

223. Vegas AJ, Veiseh O, Doloff JC, Ma M, Tam HH, Bratlie K, et al. Combinatorial hydrogel library enables identification of materials that mitigate the foreign body response in primates. Nature biotechnology. 2016;34(3):345-52.

224. Yadav TC, Bachhuka A. Tuning foreign body response with tailor-engineered nanoscale surface modifications: fundamentals to clinical applications. Journal of Materials Chemistry B. 2023;11(33):7834-54.

225. Dumbauld DW, Lee TT, Singh A, Scrimgeour J, Gersbach CA, Zamir EA, et al. How vinculin regulates force transmission. Proceedings of the National Academy of Sciences. 2013;110(24):9788-93.

226. Zhou H, Zhu Y, Yang B, Huo Y, Yin Y, Jiang X, et al. Stimuli-responsive peptide hydrogels for biomedical applications. Journal of Materials Chemistry B. 2024;12(7):1748-74.

227. Loxley GA, Coser C, Ghaemmaghami AM, Yang J. Long-term interleukin-4 release from 3D printable affinity hydrogels promotes M2-like macrophage polarisation in vitro. Biomaterials Science. 2025;13(9):2489-502.

228. Chen B, Wang J, Jin X, Wang X, Fan Z, Zhang Y, et al. Rapamycin incorporating hydrogel improves the progression of osteoarthritis by inducing synovial macrophages polarization and reducing intra-articular inflammation. Materials & Design. 2023;225:111542.

229. Shi G, Zhou Y, Liu W, Chen C, Wei Y, Yan X, et al. Bone-derived MSCs encapsulated in alginate hydrogel prevent collagen-induced arthritis in mice through the activation of adenosine A(2A/2B) receptors in tolerogenic dendritic cells. Acta Pharm Sin B. 2023;13(6):2778-94.

230. Fateh S, Alromaihi RA, Ghaemmaghami AM, Alexander MR. Unlocking Bio-Instructive Polymers: A Novel Multi-Well Screening Platform Based on Secretome Sampling. Bio-protocol. 2024;14(4):e4939.

231. Richterová V, Gjevik A, Vaculík O, Vejrosta J, Pekař M. Impact of Collagen on the Rheological and Transport Properties of Agarose Hydrogels. Gels. 2025;11(6).

232. Vassey M, Ma L, Kämmerling L, Mbadugha C, Trindade GF, Figueredo GP, et al. Innate immune cell instruction using micron-scale 3D objects of varied architecture and polymer chemistry: The ChemoArchiChip. Matter. 2023;6(3):887-906.

233. Vassey MJ, Figueredo GP, Scurr DJ, Vasilevich AS, Vermeulen S, Carlier A, et al. Immune Modulation by Design: Using Topography to Control Human Monocyte Attachment and Macrophage Differentiation. Advanced science. 2020;7(11):1903392-n/a.

234. Jeon O, Alsberg E. Photofunctionalization of alginate hydrogels to promote adhesion and proliferation of human mesenchymal stem cells. Tissue Eng Part A. 2013;19(11-12):1424-32.

235. Ruoslahti E. RGD AND OTHER RECOGNITION SEQUENCES FOR INTEGRINS. Annual review of cell and developmental biology. 1996;12(1):697-715.

236. Takada Y, Ye X, Simon S. The integrins. Genome Biology. 2007;8(5):215-.

237. Bellis SL. Advantages of RGD peptides for directing cell association with biomaterials. Biomaterials. 2011;32(18):4205-10.

238. Kumar VB, Tiwari OS, Finkelstein-Zuta G, Rencus-Lazar S, Gazit E. Design of Functional RGD Peptide-Based Biomaterials for Tissue Engineering. Pharmaceutics. 2023;15(2):345.

239. Zaveri TD, Lewis JS, Dolgova NV, Clare-Salzler MJ, Keselowsky BG. Integrin-directed modulation of macrophage responses to biomaterials. Biomaterials. 2014;35(11):3504-15.

240. Luo T, Tan B, Zhu L, Wang Y, Liao J. A Review on the Design of Hydrogels With Different Stiffness and Their Effects on Tissue Repair. Frontiers in bioengineering and biotechnology. 2022;10:817391-.

241. Adlerz KM, Aranda-Espinoza H, Hayenga HN. Substrate elasticity regulates the behavior of human monocyte-derived macrophages. European biophysics journal. 2016;45(4):301-9.

242. Alemie MN, Bright R, Nguyen NH, Truong VK, Palms D, Hayball JD, et al. Surface Chemistry Induced IgG Unfolding and Modulation of Immune Responses. ACS Applied Materials & Interfaces. 2024;16(38):50507-23.

243. Lee H, Li Y, Bao K, Lee SS, Kang H, Choi HS, et al. Zwitterionic alginate derivative as a new delivery platform for enhanced blood circulation. Journal of Pharmaceutical Investigation. 2025;55(1):143-54.

244. Rowley JA, Madlambayan G, Mooney DJ. Alginate hydrogels as synthetic extracellular matrix materials. Biomaterials. 1999;20(1):45-53.

245. Sandvig I, Karstensen K, Rokstad AM, Aachmann FL, Formo K, Sandvig A, et al. RGD-peptide modified alginate by a chemoenzymatic strategy for tissue engineering applications. Journal of Biomedical Materials Research Part A. 2015;103(3):896-906.

246. Denis FA, Hanarp P, Sutherland DS, Gold J, Mustin C, Rouxhet PG, et al. Protein Adsorption on Model Surfaces with Controlled Nanotopography and Chemistry. Langmuir. 2002;18(3):819-28.

247. Zhao L, Liu T, Li X, Cui Q, Wang X, Song K, et al. Protein adsorption on TiO2 nanostructures and its effects on surface topography and bactericidal performance. Applied Surface Science. 2022;576:151779.

248. Hautanen A, Gailit J, Mann DM, Ruoslahti E. Effects of Modifications of the RGD Sequence and Its Context on Recognition by the Fibronectin Receptor. The Journal of biological chemistry. 1989;264(3):1437-42.

249. To WS, Midwood KS. Plasma and cellular fibronectin: Distinct and independent functions during tissue repair. Fibrogenesis & tissue repair. 2011;4(1):21-.

250. Du Q, Wang W, Zeng X, Luo X. Antifouling zwitterionic peptide hydrogel based electrochemical biosensor for reliable detection of prostate specific antigen in human serum. Analytica Chimica Acta. 2023;1239:340674.

251. Liu S, Tang J, Ji F, Lin W, Chen S. Recent Advances in Zwitterionic Hydrogels: Preparation, Property, and Biomedical Application. Gels [Internet]. 2022; 8(1).

252. Sarker P, Lu T, Liu D, Wu G, Chen H, Jahan Sajib MS, et al. Hydration behaviors of nonfouling zwitterionic materials. Chemical Science. 2023;14(27):7500-11.

253. Molino PJ, Yang D, Penna M, Miyazawa K, Knowles BR, MacLaughlin S, et al. Hydration Layer Structure of Biofouling-Resistant Nanoparticles. ACS Nano. 2018;12(11):11610-24.

254. Ray S, Shard AG. Quantitative Analysis of Adsorbed Proteins by X-ray Photoelectron Spectroscopy. Analytical chemistry (Washington). 2011;83(22):8659-66.

255. Patel NR, Bole M, Chen C, Hardin CC, Kho AT, Mih J, et al. Cell elasticity determines macrophage function. 2012.

256. Rostam HM, Singh S, Salazar F, Magennis P, Hook A, Singh T, et al. The impact of surface chemistry modification on macrophage polarisation. Immunobiology. 2016;221(11):1237-46.

257. Shen M, Horbett TA. The effects of surface chemistry and adsorbed proteins on monocyte/macrophage adhesion to chemically modified polystyrene surfaces. Journal of Biomedical Materials Research: An Official Journal of The Society for Biomaterials, The Japanese Society for Biomaterials, and The Australian Society for

Biomaterials and the Korean Society for Biomaterials. 2001;57(3):336-45.

258. Diekjiirgen D, Astashkina A, Grainger DW, Holt D, Brooks AE. Cultured primary macrophage activation by lipopolysaccharide depends on adsorbed protein composition and substrate surface chemistry. J Biomater Sci Polym Ed. 2012;23(9):1231-54.

259. Buck E, Lee S, Stone LS, Cerruti M. Protein adsorption on surfaces functionalized with COOH groups promotes anti-inflammatory macrophage responses. ACS Applied Materials & Interfaces. 2021;13(6):7021-36.

260. Anderson JM, Ziats NP, Azeez A, Brunstedt MR, Stack S, Bonfield TL. Protein adsorption and macrophage activation on polydimethylsiloxane and silicone rubber. J Biomater Sci Polym Ed. 1995;7(2):159-69.

261. Previtera ML, Sengupta A. Substrate stiffness regulates proinflammatory mediator production through TLR4 activity in macrophages. PloS one. 2015;10(12):e0145813.

262. Xing X, Wang Y, Zhang X, Gao X, Li M, Wu S, et al. Matrix stiffness-mediated effects on macrophages polarization and their LOXL2 expression. The FEBS journal. 2021;288(11):3465-77.

263. Gruber E, Heyward C, Cameron J, Leifer C. Toll-like receptor signaling in macrophages is regulated by extracellular substrate stiffness and Rho-associated coiled-coil kinase (ROCK1/2). International immunology. 2018;30(6):267-78.

264. Taufalele PV, Wang W, Simmons AJ, Southard-Smith AN, Chen B, Greenlee JD, et al. Matrix stiffness enhances cancer-macrophage interactions and M2-like macrophage accumulation in the breast tumor microenvironment. Acta biomaterialia. 2023;163:365-77.

265. Guenther C. Stiffness regulates dendritic cell and macrophage subtype development and increased stiffness induces a tumor–

associated macrophage phenotype in cancer co–cultures. Frontiers in Immunology. 2024;15:1434030.

266. Scott RA, Kiick KL, Akins RE. Substrate stiffness directs the phenotype and polarization state of cord blood derived macrophages. Acta Biomaterialia. 2021;122:220-35.

267. Krombach F, Münzing S, Allmeling A-M, Gerlach JT, Behr J, Dörger M. Cell size of alveolar macrophages: an interspecies comparison. Environmental health perspectives. 1997;105(suppl 5):1261-3.

268. Patrick JH. Species differences in the structure and function of the immune system. Toxicology. 2003;188(1):49-71.

269. Mestas J, Hughes CC. Of mice and not men: differences between mouse and human immunology. The Journal of Immunology. 2004;172(5):2731-8.

270. Martinez FO, Helming L, Milde R, Varin A, Melgert BN, Draijer C, et al. Genetic programs expressed in resting and IL-4 alternatively activated mouse and human macrophages: similarities and differences. Blood, The Journal of the American Society of Hematology. 2013;121(9):e57-e69.

271. Daigneault M, Preston JA, Marriott HM, Whyte MK, Dockrell DH. The identification of markers of macrophage differentiation in PMA-stimulated THP-1 cells and monocyte-derived macrophages. PloS one. 2010;5(1):e8668.

272. Spiller KL, Wrona EA, Romero-Torres S, Pallotta I, Graney PL, Witherel CE, et al. Differential gene expression in human, murine, and cell line-derived macrophages upon polarization. Experimental cell research. 2016;347(1):1-13.

273. Guimarães CF, Gasperini L, Marques AP, Reis RL. The stiffness of living tissues and its implications for tissue engineering. Nature Reviews Materials. 2020;5(5):351-70.

274. Shi Y, Glaser KJ, Venkatesh SK, Ben-Abraham EI, Ehman RL. Feasibility of using 3D MR elastography to determine pancreatic stiffness in healthy volunteers. Journal of Magnetic Resonance Imaging. 2015;41(2):369-75.

275. Kolipaka A, Schroeder S, Mo X, Shah Z, Hart PA, Conwell DL. Magnetic resonance elastography of the pancreas: Measurement reproducibility and relationship with age. Magnetic resonance imaging. 2017;42:1-7.

276. An H, Shi Y, Guo Q, Liu Y. Test–retest reliability of 3D EPI MR elastography of the pancreas. Clinical radiology. 2016;71(10):1068. e7-. e12.

277. Pozzi R, Parzanese I, Baccarin A, Giunta M, Conti CB, Cantù P, et al. Point shear-wave elastography in chronic pancreatitis: A promising tool for staging disease severity. Pancreatology. 2017;17(6):905-10.

278. Rostam HM, Fisher LE, Hook AL, Burroughs L, Luckett JC, Figueredo GP, et al. Immune-instructive polymers control macrophage phenotype and modulate the foreign body response in vivo. Matter. 2020;2(6):1564-81.

279. Chen C, Chen Y, Lan Y-j, Tian M-n, Zhang Y-m, Lei Z-y, et al. Effects of substrate topography on the regulation of human fibroblasts and capsule formation via modulating macrophage polarization. Colloids and Surfaces B: Biointerfaces. 2023;222:113086.

280. Sovar A, Patrick MD, Annamalai RT. Substrate curvature influences cytoskeletal rearrangement and modulates macrophage phenotype. Frontiers in Immunology. 2025;Volume 15 - 2024.

281. Rehmann MS, Skeens KM, Kharkar PM, Ford EM, Maverakis E, Lee KH, et al. Tuning and Predicting Mesh Size and Protein Release from Step Growth Hydrogels. Biomacromolecules. 2017;18(10):3131-42.

282. Roca-Arroyo AF, Gutierrez-Rivera JA, Morton LD, Castilla-Casadiego DA. Hydrogel Network Architecture Design Space: Impact on Mechanical and Viscoelastic Properties. Gels. 2025;11(8).

283. Hasany M, Talebian S, Sadat S, Ranjbar N, Mehrali M, Wallace GG, et al. Synthesis, properties, and biomedical applications of alginate methacrylate (ALMA)-based hydrogels: Current advances and challenges. Applied Materials Today. 2021;24:101150.

284. Kalashnikov N, Moraes C. Substrate viscoelasticity affects human macrophage morphology and phagocytosis. Soft Matter. 2023;19(13):2438-45.

285. Tao D, Wang H, Chang S, Cheng J, Da N, Zhang L, et al. Matrix Viscoelasticity Orchestrates Osteogenesis via Mechanotransduction Mediated Metabolic Switch in Macrophages. Advanced Healthcare Materials. 2025;14(11):2405097.

286. Chaudhuri O, Cooper-White J, Janmey PA, Mooney DJ, Shenoy VB. Effects of extracellular matrix viscoelasticity on cellular behaviour. Nature. 2020;584(7822):535-46.

287. Zitzler L, Herminghaus S, Mugele F. Capillary forces in tapping mode atomic force microscopy. Physical Review B. 2002;66(15):155436.

288. Ondarçuhu T, Fabié L. Capillary forces in atomic force microscopy and liquid nanodispensing. Surface Tension in Microsystems: Engineering Below the Capillary Length: Springer; 2013. p. 279-305.

289. Heinrich MA, Heinrich L, Ankone MJK, Vergauwen B, Prakash J. Endotoxin contamination alters macrophage-cancer cell interaction and therapeutic efficacy in pre-clinical 3D in vitro models. Biomaterials Advances. 2023;144:213220.

290. Dede Eren A, Lucassen AWA, Tuvshindorj U, Truckenmüller R, Giselbrecht S, Eren ED, et al. Cells Dynamically Adapt to Surface

Geometry by Remodeling Their Focal Adhesions and Actin Cytoskeleton. Front Cell Dev Biol. 2022;10:863721.

291. Vaughan-Jackson A, Stodolak S, Ebrahimi KH, Johnson E, Reardon PK, Dupont M, et al. Density dependent regulation of inflammatory responses in macrophages. Frontiers in immunology. 2022;13:895488.

292. Wells RG. The role of matrix stiffness in regulating cell behavior. Hepatology. 2008;47(4):1394-400.

293. Santos A, Lagares D. Matrix stiffness: the conductor of organ fibrosis. Current rheumatology reports. 2018;20:1-13.

294. Vedadghavami A, Minooei F, Mohammadi MH, Khetani S, Kolahchi AR, Mashayekhan S, et al. Manufacturing of hydrogel biomaterials with controlled mechanical properties for tissue engineering applications. Acta biomaterialia. 2017;62:42-63.

295. Bartnikowski M, Wellard RM, Woodruff M, Klein T. Tailoring hydrogel viscoelasticity with physical and chemical crosslinking. Polymers. 2015;7(12):2650-69.

296. Elosegui-Artola A, Gupta A, Najibi AJ, Seo BR, Garry R, Tringides CM, et al. Matrix viscoelasticity controls spatiotemporal tissue organization. Nature Materials. 2023;22(1):117-27.

297. Chaudhuri O, Gu L, Darnell M, Klumpers D, Bencherif SA, Weaver JC, et al. Substrate stress relaxation regulates cell spreading. Nature Communications. 2015;6(1):6365.

298. Hui E, Gimeno KI, Guan G, Caliari SR. Spatiotemporal Control of Viscoelasticity in Phototunable Hyaluronic Acid Hydrogels. Biomacromolecules. 2019;20(11):4126-34.

299. Chen R-Q, Liu P-J, Li S, He H-P, Li D-M, Yuan G-X, et al. Healing of tendon-related diseases: insights from macrophage regulation. Military Medical Research. 2025;12(1):45.

300. Dabare PRL, Bachhuka A, Quek JY, Marsal LF, Hayball J, Vasilev K. Nano-Roughness-Mediated Macrophage Polarization for Desired Host Immune Response. Small Science. 2023;3(10):2300080.

301. Ferraz N, Hong J, Santin M, Karlsson Ott M. Nanoporosity of Alumina Surfaces Induces Different Patterns of Activation in Adhering Monocytes/Macrophages. International Journal of Biomaterials. 2010;2010(1):402715.

302. Veiseh O, Vegas AJ. Domesticating the foreign body response: Recent advances and applications. Adv Drug Deliv Rev. 2019;144:148-61.

303. Söderlund Z, Ibáñez-Fonseca A, Hajizadeh S, Rodríguez-Cabello JC, Liu J, Ye L, et al. Controlled release of growth factors using synthetic glycosaminoglycans in a modular macroporous scaffold for tissue regeneration. Communications Biology. 2022;5(1):1349.

304. Kim H-S, Kim S, Shin B-H, Heo C-Y, Faruq O, Van Anh LT, et al. Silicone Implants Immobilized with Interleukin-4 Promote the M2 Polarization of Macrophages and Inhibit the Formation of Fibrous Capsules. Polymers [Internet]. 2021; 13(16).

305. Moshayedi P, Ng G, Kwok JC, Yeo GS, Bryant CE, Fawcett JW, et al. The relationship between glial cell mechanosensitivity and foreign body reactions in the central nervous system. Biomaterials. 2014;35(13):3919-25.

306. Jain N, Vogel V. Spatial confinement downsizes the inflammatory response of macrophages. Nat Mater. 2018;17(12):1134-44.

307. Gupta M, Doss B, Lim CT, Voituriez R, Ladoux B. Single cell rigidity sensing: A complex relationship between focal adhesion dynamics and large-scale actin cytoskeleton remodeling. Cell Adh Migr. 2016;10(5):554-67.

308. Schiller HB, Fässler R. Mechanosensitivity and compositional dynamics of cell-matrix adhesions. EMBO Rep. 2013;14(6):509-19.

309. Lee M, Du H, Winer DA, Clemente-Casares X, Tsai S. Mechanosensing in macrophages and dendritic cells in steady-state and disease. Front Cell Dev Biol. 2022;10:1044729.

310. Atcha H, Jairaman A, Holt JR, Meli VS, Nagalla RR, Veerasubramanian PK, et al. Mechanically activated ion channel Piezo1 modulates macrophage polarization and stiffness sensing. Nat Commun. 2021;12(1):3256.

311. Dutta B, Goswami R, Rahaman SO. TRPV4 Plays a Role in Matrix Stiffness-Induced Macrophage Polarization. Front Immunol. 2020;11:570195.

312. Nasseri S, Bilston LE, Phan-Thien N. Viscoelastic properties of pig kidney in shear, experimental results and modelling. Rheologica Acta. 2002;41(1):180-92.

313. Su L, Wang M, Yin J, Ti F, Yang J, Ma C, et al. Distinguishing poroelasticity and viscoelasticity of brain tissue with time scale. Acta Biomaterialia. 2023;155:423-35.

314. Nicolle S, Noguer L, Palierne JF. Shear mechanical properties of the porcine pancreas: Experiment and analytical modelling. Journal of the Mechanical Behavior of Biomedical Materials. 2013;26:90-7.

315. Nam S, Hu KH, Butte MJ, Chaudhuri O. Strain-enhanced stress relaxation impacts nonlinear elasticity in collagen gels. Proceedings of the National Academy of Sciences. 2016;113(20):5492-7.

316. Elosegui-Artola A. The extracellular matrix viscoelasticity as a regulator of cell and tissue dynamics. Current Opinion in Cell Biology. 2021;72:10-8.

317. Zhou Y-W, Wu Y. Substrate Viscoelasticity Amplifies Distinctions between Transient and Persistent LPS-Induced Signals. Advanced Healthcare Materials. 2022;11(8):2102271.

318. Doyle AD, Nazari SS, Yamada KM. Cell–extracellular matrix dynamics. Physical Biology. 2022;19(2):021002.

319. Watanabe N, Mitchison TJ. Single-Molecule Speckle Analysis of Actin Filament Turnover in Lamellipodia. Science. 2002;295(5557):1083-6.

320. Milos F, del Campo A. Polyacrylamide Hydrogels as Versatile Biomimetic Platforms to Study Cell-Materials Interactions. Advanced Materials Interfaces. 2024;11(34):2400404.

321. Meli VS, Rowley AT, Veerasubramanian PK, Heedy SE, Liu WF, Wang S-W. Modulation of Stiffness-Dependent Macrophage Inflammatory Responses by Collagen Deposition. ACS Biomaterials Science & Engineering. 2024;10(4):2212-23.

322. Kandow CE, Georges PC, Janmey PA, Beningo KA. Polyacrylamide Hydrogels for Cell Mechanics: Steps Toward Optimization and Alternative Uses. Methods in Cell Biology. 83: Academic Press; 2007. p. 29-46.

323. Chaudhuri O, Gu L, Klumpers D, Darnell M, Bencherif SA, Weaver JC, et al. Hydrogels with tunable stress relaxation regulate stem cell fate and activity. Nature Materials. 2016;15(3):326-34.

324. Li N, Pan X-C. Controlled Radical Polymerization: from Oxygen Inhibition and Tolerance to Oxygen Initiation. Chinese Journal of Polymer Science. 2021;39(9):1084-92.

325. Caglio S, Righetti PG. On the pH dependence of polymerization efficiency, as investigated by capillary zone electrophoresis. Electrophoresis. 1993;14(5-6):554-8.

326. Ibata N, Terentjev EM. Development of Nascent Focal Adhesions in Spreading Cells. Biophysical Journal. 2020;119(10):2063-73.

327. Gardel ML, Sabass B, Ji L, Danuser G, Schwarz US, Waterman CM. Traction stress in focal adhesions correlates biphasically with actin retrograde flow speed. Journal of Cell Biology. 2008;183(6):999-1005.

328. Galbraith CG, Sheetz MP. A micromachined device provides a new bend on fibroblast traction forces. Proceedings of the National Academy of Sciences. 1997;94(17):9114-8.

329. Xiong JP, Stehle T, Diefenbach B, Zhang R, Dunker R, Scott DL, et al. Crystal structure of the extracellular segment of integrin alpha Vbeta3. Science. 2001;294(5541):339-45.

330. Dabare PRL, Bachhuka A, Quek JY, Marsal LF, Hayball J, Vasilev K. Nano-Roughness-Mediated Macrophage Polarization for Desired Host Immune Response. Small Science. 2023;3(10):2300080.

331. Taciak B, Białasek M, Braniewska A, Sas Z, Sawicka P, Kiraga Ł, et al. Evaluation of phenotypic and functional stability of RAW 264.7 cell line through serial passages. PLoS One. 2018;13(6):e0198943.

332. Vijayan V, Pradhan P, Braud L, Fuchs HR, Gueler F, Motterlini R, et al. Human and murine macrophages exhibit differential metabolic responses to lipopolysaccharide - A divergent role for glycolysis. Redox Biol. 2019;22:101147.

333. Zschaler J, Schlorke D, Arnhold J. Differences in innate immune response between man and mouse. Critical Reviews™ in Immunology. 2014;34(5).

334. Fang JY, Yang Z, Hu W, Hoang BX, Han B. Viscoelastic Hydrogel Modulates Phenotype of Macrophage-Derived Multinucleated Cells and Macrophage Differentiation in Foreign Body Reactions. Journal of Biomedical Materials Research Part A. 2025;113(1):e37814.

335. Keselowsky BG, Collard DM, García AJ. Surface chemistry modulates focal adhesion composition and signaling through changes in integrin binding. Biomaterials. 2004;25(28):5947-54.

336. Faucheux N, Tzoneva R, Nagel MD, Groth T. The dependence of fibrillar adhesions in human fibroblasts on substratum chemistry. Biomaterials. 2006;27(2):234-45.

337. du Roure O, Saez A, Buguin A, Austin RH, Chavrier P, Siberzan P, et al. Force mapping in epithelial cell migration. Proceedings of the National Academy of Sciences. 2005;102(7):2390-5.

338. Swaminathan V, Waterman CM. The molecular clutch model for mechanotransduction evolves. Nature Cell Biology. 2016;18(5):459-61.

339. Chan CE, Odde DJ. Traction Dynamics of Filopodia on Compliant Substrates. Science. 2008;322(5908):1687-91.

340. Vogel V, Sheetz M. Local force and geometry sensing regulate cell functions. Nature reviews Molecular cell biology. 2006;7(4):265-75.

341. Mooney DJ, Langer R, Ingber DE. Cytoskeletal filament assembly and the control of cell spreading and function by extracellular matrix. Journal of cell science. 1995;108(6):2311-20.